

**COMPUTATIONAL INVESTIGATIONS OF METAL ORGANIC  
FRAMEWORKS AND COVALENT ORGANIC  
FRAMEWORKS FOR GAS STORAGE AND GAS  
SEPARATION APPLICATIONS**

A Thesis

by

Ezgi GÜLÇAY

Submitted to the

Graduate School of Sciences and Engineering  
In Partial Fulfillment of the Requirements for  
the Degree of

Master of Science

in the  
Department of Mechanical Engineering

Özyeğin University  
July 2019

Copyright © 2019 by Ezgi Gülçay

**COMPUTATIONAL INVESTIGATIONS OF METAL  
ORGANIC FRAMEWORKS AND COVALENT ORGANIC  
FRAMEWORKS FOR GAS STORAGE AND GAS  
SEPARATION APPLICATIONS**

Approved by:

---

Asst. Prof. İlknur ERUÇAR FINDIKÇI, Advisor  
Department of Natural and Mathematical Sciences  
*Özyeğin University*

---

Asst. Prof. Hande ÖZTÜRK  
Department of Mechanical Engineering  
*Özyeğin University*

---

Asst. Prof. Benay UZER  
Department of Mechanical Engineering  
*Abdullah Gül University*

Date Approved: 9 July 2019

*My grateful thanks to,  
my beloved mother,  
who has always supported me with her encouragement and endless  
love and taught me how I could be strong and listen to my voice of  
conscience.*

## ABSTRACT

Ordered crystalline microporous materials including metal organic frameworks (MOFs), zeolite imidazolate frameworks (ZIFs), and covalent organic frameworks (COFs) have emerged as strong candidates for gas storage and gas separation applications due to their large surface areas, high pore volumes, tunable pore sizes and chemical stabilities. In this thesis, promising MOFs, ZIFs, and COFs were identified for various adsorption-based and membrane-based gas separation applications using molecular simulations. First, adsorption-based separation performances of 153 COFs, 14 IRMOFs and 8 ZIFs were assessed for efficient removal of carbon tetrachloride (CCl<sub>4</sub>) from the air. The top-performing three materials, namely, BLP-2H-AA, IRMOF-11 and ZIF-6 in each group were identified. Among the top three candidates, ZIF-6 gave the highest separation potential, suggesting that ZIF-6 can be used as an efficient adsorbent material in fixed bed units. In the second part of the thesis, all synthesized 309 COFs were evaluated for hydrogen (H<sub>2</sub>) storage at various temperatures and pressures. The effect of electrostatic interactions and the Feynman-Hibbs corrections on the ranking of the top COFs was also examined and results showed that coulombic interactions and the Feynman-Hibbs corrections do not affect the ranking of the COFs based on their working capacities. Among 296 COFs, COF-DL229-3fold outperformed the ultimate DOE targets for on board H<sub>2</sub> storage. The COFs which have high porosities ( $\geq 0.8$ ) and quite low densities (0.2-0.4 g/cm<sup>3</sup>) exhibited the promising performance for volumetric H<sub>2</sub> storage. In the final part of this thesis, a bio-compatible MOF library, including 1525 bio-MOFs which have endogenous

linkers and non-toxic metal centers, was developed. Oxygen (O<sub>2</sub>) storage and its separation from the air using bio-MOFs were examined. The methods used in this thesis guide both experimental and computational studies for the development of porous materials for various industrial applications.



## ÖZETÇE

Metal organik yapılar (MOF), zeolit imidazolat yapılar (ZIF) ve kovalent organik yapılar (COF) dahil olmak üzere kristal mikro gözenekli malzemeler, geniş yüzey alanları, yüksek gözenek hacimleri, ayarlanabilir gözenekleri boyutları ve kimyasal stabiliteyi nedeniyle gaz depolama ve gaz ayırma uygulamaları için güçlü adaylar olarak ortaya çıkmıştır. Bu tezde, moleküler simülasyonlar kullanarak çeşitli adsorpsiyon-bazlı ve membran-bazlı gaz ayırma uygulamaları için yüksek performans veren MOF, ZIF ve COF yapıları tanımlanmıştır. İlk olarak, 153 COF, 14 IRMOF ve 8 ZIF yapılarının adsorpsiyon-bazlı havadan karbon tetraklorürün ( $CCl_4$ ) ayırma performansları incelenmiştir. Her gruptan en iyi performans gösteren üç adsorban materyal (BLP-2H-AA, IRMOF-11 ve ZIF-6) belirlenmiştir. İlk üç aday arasında, ZIF-6 en yüksek ayırma potansiyelini vermiştir ve bu da ZIF-6'nın sabit yataklı birimlerde etkin bir adsorban malzeme olarak kullanılabileceğini göstermiştir. Tezin ikinci bölümünde, sentezlenen 309 COF yapıları çeşitli sıcaklıklarda ve basınçlarda hidrojen ( $H_2$ ) depolanması için değerlendirilmiştir. Elektrostatik etkileşimlerin ve Feynman-Hibbs düzeltmelerinin COF adsorbanlarının sıralaması üzerindeki etkileri de incelenmiş ve sonuçlar, Coulombic etkileşimlerinin ve Feynman-Hibbs düzeltmelerinin çalışma kapasitelerine göre COF adsorbanlarının sıralamasını etkilemediğini göstermiştir. 296 COF arasında, COF-DL229-3  $H_2$  depolaması için Amerika Birleşik Devletleri Enerji Bakanlığı (DOE) hedeflerini geçerek yüksek performans göstermiştir. Yüksek gözenekliliğe ( $\geq 0.8$ ) ve düşük yoğunluğa ( $0.2-0.4 \text{ g/cm}^3$ ) sahip COF yapıları

hacimsel H<sub>2</sub> depolaması için ümit verici performans sergilemiştir. Bu tezin son bölümünde, endojen bağlayıcılara ve toksin olmayan metal merkezlerine sahip 1525 biyo-uyumlu MOF kütüphanesi oluşturulmuştur. Oksijen (O<sub>2</sub>) depolanması ve havadan ayrılması biyo-MOF yapıları kullanılarak incelenmiştir. Bu tezde kullanılan yöntemler, çeşitli endüstriyel uygulamalar için hem deneysel hem de bilgisayarlı çalışmalara gözenekli malzemelerin geliştirilmesi için rehberdir.



## ACKNOWLEDGEMENTS

I am sure that this part is the most difficult part written in my thesis study. After my bachelor science graduation, life has not been easy for me. However, when I met İlknur Eruçar Fındıkçı, I felt that I gained not only an advisor, also a person who would affect my perspective on my life and to the academic world. I am very glad that our paths came across. I want to thank my advisor, Asst. Prof. İlknur Eruçar Fındıkçı, for her dedication and guidance throughout my master's degree. She has always been my inspiration. I want to express my gratitude to my committee members, Asst. Prof. Hande Öztürk and Asst. Prof. Benay Uzer for their valuable advice and time.

I owe one of the biggest thanks to my boyfriend, Berkay, for his care, love, endless support and understanding. He has always motivated me for my career. He was always there for me in hard times. I am sure that he will continue to be there after that. We will keep this togetherness, where we have learned to handle our ups and downs while growing up together, for the rest of our lives. I also want to thank you for my closest friend, Burcu, my sister who was born from another mother. Without her motivation, encouragement, support talks, I would not be in this point. I owe a special thanks to my dearest friend, Pelin. If she had not believed me, I would not have any chance to meet with Asst. Prof. İlknur Eruçar Fındıkçı. I want to thank my other friend from Istanbul Technical University, Melis for her hugs and lovely friendship. I also want to thank my friend, Memo, for his support and friendship. I am sure these people will always be with me whenever and wherever throughout my life.



Lastly, I also want to thank my yoga group for starting to teach me how to overcome my fears and how to be patient. Even though I am at the beginning of this path, I feel very fortunate to have met the miracle of now and awareness. A calming note to myself to be open to change: inhale and exhale.

I appreciate my beloved parents, Sevgi and Erdal for their unconditional support and endless love. They have always taught me how I could reach my goals and my dreams. I also want to thank my lovely aunt, Esin, for teaching that blood tie is not anything. I appreciate these two women, my mother and my aunt, who was from another mother, for being strong and realistic. I also want to thank my grandmother and grandfather for believing in me.

Finally, the financial support provided by the Scientific and Technological Research Council of Turkey (TUBITAK), the project no. 217M675, is acknowledged.

Ezgi Gülçay

09.07.2019

## TABLE OF CONTENTS

ABSTRACT.....	iv
ÖZETÇE .....	vi
ACKNOWLEDGEMENTS.....	viii
LIST OF TABLES .....	xii
LIST OF FIGURES.....	xiv
NOMENCLATURE .....	xvii
CHAPTER I.....	1
INTRODUCTION .....	1
CHAPTER II .....	10
LITERATURE REVIEW .....	10
2.1 Gas Storage.....	10
2.2 Gas Separation.....	20
2.2.1 Adsorption-based Gas Separation.....	20
2.2.2 Membrane Separation.....	26
2.3 Biomedical Applications .....	30
CHAPTER III.....	35
COMPUTATIONAL METHODOLOGY .....	35
3.1 Material Selection .....	35
3.2 Structural Characterization.....	37
3.3 Gas Adsorption Simulations of COFs and MOFs .....	39
3.3.1 Details of GCMC Simulations.....	45
3.4 Gas Diffusion Simulations of COFs and MOFs.....	47
3.4.1 Details of MD Simulations .....	50
3.5 Computational Screening of COFs and MOFs.....	50
3.5.1 Evaluation of Materials for Adsorption-based Gas Separation	50
3.5.2 Evaluation of Materials for Membrane-based Gas Separation.	53
CHAPTER IV .....	56
MOLECULAR SIMULATIONS OF COFs, IRMOFs AND ZIFs FOR ADSORPTION-BASED SEPARATION OF CARBON TETRACHLORIDE FROM AIR .....	56
4.1 Motivation .....	56
4.2 Simulation Details.....	57

4.3 Results and Discussion .....	61
4.3.1 Comparing Simulations with Experiments and Literature Data ....	61
4.3.2. Comparing Infinite Dilution Adsorption Selectivities of All Materials .....	62
4.3.3. Comparing Gas Adsorption Isotherms of Top Performing Materials .....	69
4.3.4 Comparing Gas Diffusion in ZIF-6 .....	77
CHAPTER V .....	80
COVALENT ORGANIC FRAMEWORKS FOR HYDROGEN STORAGE: A MOLECULAR SIMULATION STUDY .....	80
5.1 Motivation .....	80
5.2 Computational Details .....	81
5.3 Results and Discussion .....	81
5.3.1 Comparisons of Experiments with Simulations .....	81
5.3.2 Effect of Feynman-Hibbs Corrections on H <sub>2</sub> Working Capacities of COFs.....	85
5.3.3 Evaluation of the COFs Performances for H <sub>2</sub> Storage.....	87
CHAPTER VI.....	95
BIO-COMPATIBLE MOFs FOR STORAGE AND SEPARATION OF O <sub>2</sub> : A MOLECULAR SIMULATION STUDY .....	95
6.1 Motivation .....	95
6.2 Computational Details .....	96
6.3 Results and Discussion .....	97
6.3.1 Comparison of simulations with the available data .....	97
6.3.2 Adsorption-based O <sub>2</sub> /N <sub>2</sub> separation .....	99
6.3.3 O <sub>2</sub> Storage in 315 Bio-compatible MOFs.....	104
6.3.4 Membrane-based O <sub>2</sub> /N <sub>2</sub> Separation .....	111
CHAPTER VII .....	116
CONCLUSION.....	116
APPENDICES .....	121
APPENDIX A: Supplementary Information for Chapter IV .....	121
APPENDIX B: Supplementary Information for Chapter VI .....	132
BIBLIOGRAPHY.....	142
VITA.....	155

## LIST OF TABLES

<b>Table 3.1</b> Interaction parameters and partial charges used for adsorbate molecules.....	46
<b>Table 4.1</b> Top performing 15 materials ranked based on CCl <sub>4</sub> /Ar selectivity at 298 K and infinite dilution together with their $Q_{st}^0$ for Ar, CCl <sub>4</sub> , N <sub>2</sub> and O <sub>2</sub> . $Q_{st}^0$ values were given in kJ/mol. ....	66
<b>Table 4.2</b> Top performing 15 materials ranked based on CCl <sub>4</sub> /N <sub>2</sub> selectivity at 298 K and infinite dilution together with their $Q_{st}^0$ for Ar, CCl <sub>4</sub> , N <sub>2</sub> and O <sub>2</sub> . $Q_{st}^0$ values were given in kJ/mol. ....	66
<b>Table 4.3</b> Top performing 15 materials ranked based on CCl <sub>4</sub> /O <sub>2</sub> selectivity at 298 K and infinite dilution together with their $Q_{st}^0$ for Ar, CCl <sub>4</sub> , N <sub>2</sub> and O <sub>2</sub> . $Q_{st}^0$ values were given in kJ/mol. ....	67
<b>Table 4.4</b> The adsorption selectivities for binary mixtures at 10 bar and 298 K....	72
<b>Table 4.5</b> The adsorption selectivities for quaternary mixtures at 10 bar and 298 K. ....	74
<b>Table 4.6</b> Comparison between the gas uptakes obtained from quaternary mixture simulations and obtained from five-component mixture simulations under a relative humidity (RH) of 80% for ZIF-6. (The partial pressure of H <sub>2</sub> O is fixed at $3.28 \times 10^{-2}$ bar.).....	77
<b>Table 4.7</b> The initial loadings for single-component and quaternary mixture GCMC simulations, and the self-diffusivities of Ar, CCl <sub>4</sub> , N <sub>2</sub> and O <sub>2</sub> in ZIF-6 at 298 K and 10 bar. (u.c for unit cell).....	78
<b>Table 5.1</b> Data for comparison of simulations with the experiments for the saturated H <sub>2</sub> uptakes in 20 COFs. ....	84
<b>Table 5.2</b> Comparison of ranking of COFs based on volumetric H <sub>2</sub> working capacities .....	87
<b>Table 5.3</b> Top-performing 10 COFs ranked based on working capacities calculated at 100bar/77K for adsorption and 5bar/77K for desorption conditions. ....	88
<b>Table 5.4</b> Top-performing 10 COFs ranked based on working capacities calculated at 100bar/77K for adsorption and 5bar/160K for desorption conditions. ....	89
<b>Table 6.1</b> Top performing 15 MOFs identified for $S_{(O_2/N_2)}^0$ at infinite dilution and	

298 K with their calculated physical properties. ....	101
<b>Table 6.2</b> Top performing 15 MOFs identified for gravimetric $WC_{O_2}$ obtained at 140 bar storage and 5 bar desorption pressures at 298 K together with their calculated physical properties and $S^0_{(O_2/N_2)}$ .....	104
<b>Table 6.3</b> Top performing 15 MOFs identified for volumetric $WC_{O_2}$ obtained at 140 bar adsorption and 5 bar desorption pressures at 298 K together with their calculated physical properties and $S^0_{(O_2/N_2)}$ .....	107
<b>Table 6.4</b> Adsorption, diffusion and membrane selectivity data together with gas diffusivities and permeabilities for MOF membranes which surpass Robeson's 2008 upper bound for air separation. ....	112
<b>Table A.1</b> Structural properties of COFs, IRMOFs, ZIFs .....	121
<b>Table A.2</b> Data for comparison of our predicted gas uptake data with the experiments[97, 208] and other simulation data[96] available in the literature....	127
<b>Table A.3</b> The separation potentials (mol/L) of BLP-2H-AA, IRMOF-11 and ZIF-6 for binary and quaternary mixtures at 10 bar and 298 K. ....	131
<b>Table B.1</b> Crystal properties of the top 17 MOF membranes which surpass the Robeson's 2008 upper bound for $O_2/N_2$ separation together with their organic linkers and metals.....	136

## LIST OF FIGURES

<b>Figure 1.1</b> Number of papers featuring the term of “metal organic framework” in their titles. Accessed: 2019-03-27 from Web of Science ® A screenshot of Cu-BTC commonly known as HKUST-1 (HKUST for Hong Kong University of Science and Technology and BTC: benzene-1,3,5-tricarboxylate)[42] from CSD[31]. Red= oxygen, orange=copper, white=hydrogen and grey=carbon. ....	6
<b>Figure 1.2</b> Number of papers featuring the term of “covalent organic framework” in their titles. Accessed: 2019-03-27 from Web of Science ® A screenshot of COF-5[44] from CSD[31]. Red= oxygen, pink=boron, white=hydrogen and grey=carbon.....	8
<b>Figure 3.1</b> A representation for the LCD and PLD in a pore. ....	38
<b>Figure 3.2</b> Relations between permeability of the <i>i</i> component and <i>i/j</i> selectivity. Robeson’s upper bound[126] was also demonstrated. ....	55
<b>Figure 4.1.</b> Comparison of LCDs, pore volumes and surface areas of COFs, IRMOFs and ZIFs.....	58
<b>Figure 4.2</b> Comparison of experiments and molecular simulations for single-component adsorption isotherms of CCl <sub>4</sub> in CPL-11 at 298 K.....	61
<b>Figure 4.3</b> Comparison of our predictions with experiments[97] for CCl <sub>4</sub> in MIL-101, and simulation available in the literature[95] for Ar, CCl <sub>4</sub> , N <sub>2</sub> and O <sub>2</sub> adsorptions in Cu-BTC.....	62
<b>Figure 4.4</b> Relations between (a) $K_{\text{Henry}}$ of gas molecules and $Q_{\text{st}}^0$ , and (b) $S^0$ and LCDs of COFs, IRMOFs and ZIFs for CCl <sub>4</sub> /Ar, CCl <sub>4</sub> /N <sub>2</sub> and CCl <sub>4</sub> /O <sub>2</sub> separations at infinite dilution and 298 K. ....	64
<b>Figure 4.5</b> Single-component adsorption isotherms for (a) Ar, (b) CCl <sub>4</sub> , (c) N <sub>2</sub> and (d) O <sub>2</sub> in BLP-2H-AA, IRMOF-11 and ZIF-6 at 298 K. ....	69
<b>Figure 4.6</b> Binary mixture adsorption selectivities of BLP-2H-AA, IRMOF-11 and ZIF-6 for separation of CCl <sub>4</sub> /Ar, CCl <sub>4</sub> /N <sub>2</sub> and CCl <sub>4</sub> /O <sub>2</sub> mixtures at 298 K. ....	72
<b>Figure 4.7</b> Quaternary mixture adsorption isotherms for Ar, CCl <sub>4</sub> , N <sub>2</sub> and O <sub>2</sub> in BLP-2H-AA, IRMOF-11 and ZIF-6 at 298 K. The composition of the bulk gas mixture is Ar: 0.999%, CCl <sub>4</sub> : 0.1%, N <sub>2</sub> : 77.922% and O <sub>2</sub> : 20.979%.....	73

<b>Figure 4.8</b> Comparison of single-component and quaternary mixture self-diffusivities of (a)Ar, (b)CCl <sub>4</sub> , (c)N <sub>2</sub> and (d)O <sub>2</sub> in ZIF-6 at 298 K. Quaternary mixture composition of the bulk gas mixture is Ar: 0.999%, CCl <sub>4</sub> : 0.1%, N <sub>2</sub> : 77.922% and O <sub>2</sub> : 20.979%.....	79
<b>Figure 5.1</b> Comparison of simulations with the experiments[47] for single-component H <sub>2</sub> uptake in (a)COF-5, (b)COF-6, (c)COF-8, and (d)COF-10 at 77 K.....	83
<b>Figure 5.2</b> Comparison of experiments and our simulations for saturated H <sub>2</sub> uptakes in 20 COFs.....	84
<b>Figure 5.3</b> Effect of the Feynman-Hibbs corrections on our calculated H <sub>2</sub> uptake in 296 COFs. ....	86
<b>Figure 5.4</b> Comparison of volumetric H <sub>2</sub> working capacities of the most promising 10 COFs (closed symbols) and those of the top-performing MOFs reported in the literature (open spheres).[54] .....	91
<b>Figure 5.5</b> (a)R <sup>2</sup> values showing the relations between working capacities of H <sub>2</sub> (g/L) and several physical parameters. Relations between (b)density and H <sub>2</sub> working capacities (g/L), and (c)porosity and H <sub>2</sub> working capacity (g/L).....	93
<b>Figure 6.1</b> Comparison of our predictions with the literature for (a)N <sub>2</sub> uptake in Cu-BTC, IRMOF-1 and IRMOF-3 at 298 K, (b)O <sub>2</sub> working capacities of 10 MOFs at 298 K, (c)O <sub>2</sub> uptake in Cu-BTC, NU-125 and UiO-66 at 303 K. ....	98
<b>Figure 6.2</b> Relations between (a) K <sub>Henry</sub> of gas molecules and LCDs of MOFs, (b) K <sub>Henry</sub> of gases and Q <sub>st</sub> <sup>0</sup> , and (c) S <sup>0</sup> and LCDs of MOFs at 298 K. ....	100
<b>Figure 6.3</b> (a) Comparison of infinite dilution adsorption selectivities with mixture adsorption selectivities at 1, 5, 10, 100 and 140 bar and (b) Binary mixture adsorption selectivities of top 15 MOFs ranked based on S <sup>0</sup> <sub>(O<sub>2</sub>/N<sub>2</sub>) up to 140 bar at 298 K.....</sub>	103
<b>Figure 6.4</b> Relations between (a)pore volume and gravimetric wC <sub>O<sub>2</sub></sub> , (b)surface area and gravimetric wC <sub>O<sub>2</sub></sub> , (c)gravimetric wC <sub>O<sub>2</sub></sub> and S <sup>0</sup> <sub>(O<sub>2</sub>/N<sub>2</sub>)</sub> , (d)porosity and volumetric wC <sub>O<sub>2</sub></sub> , (e)surface area and volumetric wC <sub>O<sub>2</sub></sub> , (f)volumetric wC <sub>O<sub>2</sub></sub> and S <sup>0</sup> <sub>(O<sub>2</sub>/N<sub>2</sub>)</sub> of MOFs at 298 K. The data points in (c) and (f) graphs are color coded by infinite dilution isosteric heat of adsorption of O <sub>2</sub> . ....	109

<b>Figure 6.5</b> Membrane selectivity and O <sub>2</sub> permeability of promising MOF membranes for O <sub>2</sub> /N <sub>2</sub> separation.....	112
<b>Figure A.1</b> Henry's constants of (a)Ar, (b)CCl <sub>4</sub> , (c)N <sub>2</sub> and (d)O <sub>2</sub> as a function of LCDs of COFs, IRMOFs and ZIFs .....	128
<b>Figure A.2</b> Binary mixture adsorption isotherms for (a)CCl <sub>4</sub> /Ar, (b)CCl <sub>4</sub> /N <sub>2</sub> and (c)CCl <sub>4</sub> /O <sub>2</sub> in BLP-2H-AA at 298 K. The composition of the bulk gas mixtures are CCl <sub>4</sub> /Ar: 1/99, CCl <sub>4</sub> /N <sub>2</sub> : 1/99 and CCl <sub>4</sub> /O <sub>2</sub> : 1/99.....	129
<b>Figure A.3</b> Binary mixture adsorption isotherms for (a)CCl <sub>4</sub> /Ar, (b)CCl <sub>4</sub> /N <sub>2</sub> and (c)CCl <sub>4</sub> /O <sub>2</sub> in IRMOF-11 at 298 K. The composition of the bulk gas mixtures are CCl <sub>4</sub> /Ar: 1/99, CCl <sub>4</sub> /N <sub>2</sub> : 1/99 and CCl <sub>4</sub> /O <sub>2</sub> : 1/99.....	129
<b>Figure A.4</b> Binary mixture adsorption isotherms for (a)CCl <sub>4</sub> /Ar, (b)CCl <sub>4</sub> /N <sub>2</sub> and (c)CCl <sub>4</sub> /O <sub>2</sub> in ZIF-6 at 298 K. The composition of the bulk gas mixtures are CCl <sub>4</sub> /Ar: 1/99, CCl <sub>4</sub> /N <sub>2</sub> : 1/99 and CCl <sub>4</sub> /O <sub>2</sub> : 1/99.....	130
<b>Figure A.5</b> Pore size distributions of BLP-2H-AA, IRMOF-11 and ZIF-6. ....	131
<b>Figure A.6</b> GCMC screenshots of Ar (purple spheres), CCl <sub>4</sub> (green), N <sub>2</sub> (blue) and O <sub>2</sub> (red) adsorption in ZIF-6. Dark blue: Zn, blue: N, dark grey: C, white: H .....	131
<b>Figure B.1</b> Adsorption isotherms of O <sub>2</sub> and N <sub>2</sub> in their binary mixture (O <sub>2</sub> :N <sub>2</sub> is 21:79) in WIWHUG and XACZEH at 298 K up to 140 bar.....	132
<b>Figure B.2</b> GCMC Screenshots of O <sub>2</sub> (red spheres) and N <sub>2</sub> (blue spheres) adsorption in WIWHUG and XACZEH. Red = O, dark blue = N, orange = Cu, dark grey = C, light grey = H .....	133
<b>Figure B.3</b> Gravimetric and volumetric O <sub>2</sub> working capacities of 315 MOFs at 298 K (at 140 bar storage and 5 bar release pressures). The data points are color mapped by porosities. ....	134
<b>Figure B.4</b> R <sup>2</sup> values showing the relations between (a)gravimetric working capacity of O <sub>2</sub> (mol/kg) and several parameters, (b)volumetric working capacity of O <sub>2</sub> (cm <sup>3</sup> (STP)/cm <sup>3</sup> ) and several parameters. ....	135



## NOMENCLATURE

Al	: Aluminium
AlPO <sub>4</sub>	: Aluminophosphates
ANG	: Adsorbed natural gas
Ar	: Argon
B	: Boron
BEA	: Zeolite beta
Bio-MOF	: Bio-compatible MOF
BTC	: Benzene-1,3,5-tricarboxylate
C	: Carbon
c	: Concentration
C <sub>2</sub> H <sub>4</sub>	: Ethylene
C <sub>2</sub> H <sub>6</sub>	: Ethane
Ca	: Calcium
CCl <sub>4</sub>	: Carbon tetrachloride
CD	: Cyclodextrin
Cd	: Cadmium
CH <sub>4</sub>	: Methane
CNG	: Compressed natural gas
Co	: Cobalt
CO	: Carbon monoxide
CO <sub>2</sub>	: Carbon dioxide
COF	: Covalent organic framework
COM	: Center of mass
CoRE	: Computational-ready experiment
CPO	: Coordination polymer of Oslo
Cr	: Chromium

CSD	: Cambridge Structural Database
Cu	: Copper
CUK	: Cambridge University-KRICT
CWA	: Chemical warfare agent
$D_0$	: Corrected diffusivity
DFT	: Density-functional theory
DOE	: The U.S. Department of Energy
$D_t$	: Transport diffusivity
E	: Electrostatic energy
EMD	: Equilibrium molecular dynamics
EOS	: Equation of state
F	: Force
FAU	: Faujasite
Fe	: Iron
GCMC	: Grand canonical Monte Carlo
$H_2$	: Hydrogen
$H_2S$	: Hydrogen sulfide
HKUST	: Hong Kong University of Science and Technology
HSECoE	: Hydrogen Storage Engineering Center of Excellence
IAST	: Ideal adsorption solution theory
IRMOF	: Isorecticular MOF
J	: Flux
K	: Potassium
k	: Boltzmann constant
$K_{Henry}$	: Henry's constant
KOH	: Potassium hydroxide
Kr	: Krypton
LCD	: Largest cavity diameter

LD <sub>50</sub>	: Oral lethal dose
LJ	: Lennard-Jones
MD	: Molecular dynamics
Mg	: Magnesium
MIL	: Materials of Institut Lavoisier
MMM	: Mixed matrix membranes
Mn	: Manganese
MOF	: Metal organic framework
N <sub>2</sub>	: Nitrogen
n <sub>abs</sub>	: Absolute adsorbed gas amount
N <sub>ads</sub>	: Adsorption amount of gas component
N <sub>des</sub>	: Desorption amount of gas component
n <sub>ex</sub>	: Excess adsorption
NH	: Nose-Hoover
NH <sub>3</sub>	: Ammonia
Ni	: Nickel
NO	: Nitric oxide
NOTT	: University of Nottingham
NU	: Northwestern University
O <sub>2</sub>	: Oxygen
OH	: Hydroxy
P	: Phosphate
P	: Pressure
P	: Permeability
P	: Probability
PCN	: Porous coordination network
PCP	: Porous coordination polymer
PIM	: Polymer of intrinsic microporosity

PLD	: Pore limiting diameter
PU	: Polyurethane
PV	: Pore volume
q	: Partial atomic charge
Q <sub>st</sub>	: Isosteric heat of adsorption
r	: Separation distance
R	: Ideal gas constant
r <sub>i</sub>	: Position of the i <sup>th</sup> particle
RPM3-Zn	: Zn <sub>2</sub> (4,4'-biphenyldicarboxylate) <sub>2</sub> (1,2-bipyridylethene)
S	: Selectivity
SA	: Surface area
SAPO	: Silicoaluminophosphate
SB	: Stony Brook
SBF	: Simulated body fluid
SBU	: Secondary building unit
Si	: Silicon
STA	: St. Andrews microporous material
STP	: Standard temperature and pressure
T	: Temperature
TIC	: Toxic industrial chemical
U	: Potential energy
UFF	: Universal Force Field
UiO	: University of Oslo
UMCM	: University of Michigan Crystalline Material
V	: Volume
V	: Vanadium
VOC	: Volatile organic compound
Xe	: Xenon

ZIF	: Zeolitic imidazolate framework
Zn	: Zinc
Zr	: Zirconium
$\Delta N$	: Working capacity
$\Delta Q$	: Separation potential
$\mu$	: Chemical potential
$\varepsilon$	: Well depth
$\hbar$	: Planck constant
f	: Fugacity
$\Lambda$	: Broglie thermal wavelength
v	: Velocity
$\rho$	: Density
$\sigma$	: Molecular length
$\phi$	: Porosity
$\chi$	: Atomic electronegativity

## CHAPTER I

### INTRODUCTION

Crystalline solids have been widely investigated in the literature and remarkable progress has been made in research areas of crystal engineering. Traditional materials were initially defined as micro- to mesoporous materials (pore diameters 5-20 Å and 20-500 Å, respectively). Microporous materials are divided into two different groups, such as inorganic and carbon-based structures. Microporous inorganic materials have also two subclasses including aluminophosphates and aluminosilicates. Aluminophosphates (AlPO<sub>4</sub>) are three dimensional structures with Al<sup>3+</sup> (aluminium) and P<sup>5+</sup> (phosphate) ions.[1] The first microporous crystalline structure was synthesized in the class of aluminophosphate in 1982 by Wilson et al.[2] for size- and shape selective adsorption of large molecules including 2,2-dimethylpropane (6.2 Å). Aluminosilicates are also three-dimensional materials composed of Al, silicon (Si), oxygen (O), and various types of cations (such as sodium). Zeolites are well-known three-dimensional materials in aluminosilicates with building units consisting of AlO<sub>4</sub> and/or SiO<sub>4</sub> tetrahedral clusters. Zeolites have tunnels or cages where metal ions and water molecules can accommodate. There are almost 40 natural, and more than 150 synthetic zeolite structures.[3]

Microporous inorganic materials have been extensively studied in different gas adsorption applications for separation technology, and pollution control. Adsorption, a surface phenomenon, can be defined as the enrichment of one or more species in the region between two bulk phases (the surface and

## CHAPTER I: Introduction

the components) at an equilibrium condition. This process occurs between a solid material (adsorbent) and a gas to be adsorbed (adsorbate). Depending on the interaction between adsorbate and adsorbent, adsorption is classified as physisorption (adsorption with only Van der Waals electrostatic interaction) and chemisorption (adsorption with chemical bonding). Adsorption isotherms, which is the relation between the amount of adsorbate and the equilibrium pressure at a fixed temperature, are generally measured or computed in the literature.[4] For an efficient gas adsorption application, the identity of an adsorbent material is important. Many studies have been conducted so far to identify efficient adsorbents for various gas adsorption applications such as methane (CH<sub>4</sub>), hydrogen (H<sub>2</sub>), nitrogen (N<sub>2</sub>) and O<sub>2</sub>. The adsorption of CH<sub>4</sub>, which is the main component of natural gas, and H<sub>2</sub> has significant commercial applications in energy-related areas and has been widely studied in the literature. For example, Martin and coworkers[5] investigated CH<sub>4</sub> adsorption in two different adsorbent materials, AlPO<sub>4</sub>-5 and SAPO-5 (SAPO for silicoaluminophosphate). In a different study, Langmi et al.[6] tested H<sub>2</sub> uptake in various zeolites as NaA (Linde Type A structure type), NaX and NaY (faujasite structure type) and NaCsRHO and their ion-exchanged forms (cadmium and magnesium ions). Besides small gas molecules, zeolites have also been studied for adsorption of large molecules such as hexane. For example, Rioland and coworkers[7] studied adsorption of n-hexane and cyclohexane in two different zeolites, BEA (zeolite beta) and FAU-type (faujasite zeolite) for decontamination in satellites. The excellent reviews about studies of adsorption of various gas molecules in zeolites were referred to the readers.[8, 9]

The other class of traditional materials is carbon-based materials and among these materials activated carbons have been widely examined in different adsorption studies in the literature. Activated carbons can be produced from different carbonaceous precursors such as coal, petroleum and then activated by treatment with chemicals (such as acids or bases), or oxidation with carbon dioxide (CO<sub>2</sub>) and they have microcrystalline structures. Adsorption-based gas separation performance of activated carbons have been tested so far due to their large surface areas (up to 2500 m<sup>2</sup>/g) and their attractive characteristics such as size-selective pores. Activated carbons have highly disordered structures due to the defects by heteroatoms (such as O, and H) and vacant lattice sites in their structures.[10] However, the presence of O atoms on their surface plays a significant role in their adsorption capacities of especially polar gases and water. Lozano-Castello et al.[11] prepared four types of activated carbons using different ratios of KOH (potassium hydroxide)/anthracite to demonstrate the effect of pore sizes on CH<sub>4</sub> storage. This study showed that even activated carbons have enormously large channels, they are not efficient for CH<sub>4</sub> adsorption due to their useless large voids. Excellent reviews have been published on gas adsorption in activated carbons.[12, 13] Besides microporous materials, mesoporous structures have also been investigated for gas adsorption in the literature. [14, 15]

In the early 1990s, the term of porous coordination polymers (PCPs) appeared and this term has been taken a significant interest in crystal engineering due to their large cavity sizes and designable structural properties. The term of CP is defined as a compound with repeating units in existing all coordination in one-, two- or three-dimensions. PCPs contain two different



## CHAPTER I: Introduction

central components as linkers (can be halides), and connectors (generally transition metals).[16, 17] Furthermore, PCPs have also been investigated for gas adsorption due to their tunable chemical and physical properties, and structural flexibility. For example, Hijikata et al.[18] designed a series of four PCPs with different pore sizes (ranging from 5.6 Å to 14.3 Å) to control their adsorption behavior depending on different kinetic diameters of adsorbates such as CO<sub>2</sub>, (3.3 Å), CH<sub>4</sub>, (3.8 Å), ethane (C<sub>2</sub>H<sub>6</sub>, 4.4 Å) and ethylene (C<sub>2</sub>H<sub>4</sub>, 4.2 Å). There are many studies about adsorption of various gas molecules including argon (Ar), CH<sub>4</sub>, N<sub>2</sub>, and O<sub>2</sub> in PCPs in the literature.[19-21]

As a new class of crystalline materials, metal-organic frameworks (MOFs) were discovered as PCPs and these structures were named as MOFs by Yaghi et al.[22] in 1995. MOFs have become one of the fastest growing class of porous materials due to their high thermal stability, high porosity (0.3-0.9), large surface areas (1000-10,000 m<sup>2</sup>/g), and tunable physical and chemical properties.[23, 24] MOFs are built from metal ions or clusters, termed as secondary building units (SBUs), and organic ligands to create strong coordinative bonds.[24] In MOF synthesis, almost all cations including alkaline earth, transition metals and lanthanides are used as metal sites, whereas phosphonates, carboxylates, pyridyl, polyamines (benzene, imidazole, oxalic acid) and cyano groups can be commonly used as organic ligands.[25] MOF synthesis is based on a systematic approach known as reticular synthesis. In this concept, the same SBUs are used to construct ordered frameworks with different physical properties. Yaghi et al.[26] first used the reticular design concept and synthesized IRMOF-1 (IRMOF for isoreticular MOF, also known as MOF-5) using zinc-oxygen-carbon (Zn-O-C) motif. Then, the same

group[27] used the same topology of IRMOF-1 to construct a family of sixteen IRMOFs with benzene links and octahedral  $Zn_4O$  clusters. Although they have the same three-dimensional cubic lattices, their pore apertures are ranged from 3.8 Å to 28.8 Å because of the different types of organic linkers. In contrast to traditional materials, such as zeolites, and activated carbons, MOFs have more controllable pore sizes and shapes, and chemical functionalities. Additionally, MOFs have much more flexibility than zeolites, which might allow an easier surface modification by a chemical reaction or a guest exchange without losing their overall crystallinity.[28] These highly crystalline materials have generally three-dimensional structures due to their strong interatomic bonds between the atoms. Recently, amorphization process, in which a structural change occurs in the presence of an external stimuli such as pressure and temperature, has been used in the field of MOFs to enhance their mechanical strength. In the literature, ZIFs (zeolitic imidazolate frameworks), as a sub group of MOFs, have been tested for amorphization due to their structural similarity with zeolitic silica materials for reversible gas adsorption applications.[29, 30] Therefore, both crystalline and amorphous MOFs can be currently synthesized using different experimental techniques in the literature.

All synthesized MOFs are stored with a unique 'refcode', which consists of 6 letters, in the Cambridge Structural Database (CSD).[31] CSD is a database which includes the properties of synthesized crystal structures including crystallographic parameters, atomic coordinates and space groups. Moghadam et al.[23] recently reported 86,673 MOFs available in this database. Theoretically, an infinite number of MOFs can be synthesized due to the numerous types of metal cations and organic ligands. Throughout the last two

decades, thousands of MOFs have been both experimentally and computationally studied due to their permanent porosity and tunable properties which make them suitable for various applications including gas separation[32] and gas storage[33], carbon capture[34], catalysis[35, 36], drug delivery[37], biomolecule encapsulation[38], optical and luminescent applications[39], sensing, and imaging[40, 41]. Figure 1.1 illustrates the increase in the number of published papers on MOFs from 2005 to 2019. As shown in Figure 1.1, there has been a growing interest in this research area of MOFs from 2008 (a total number of publications: 373) to 2018 (a total number of publications: 4061).

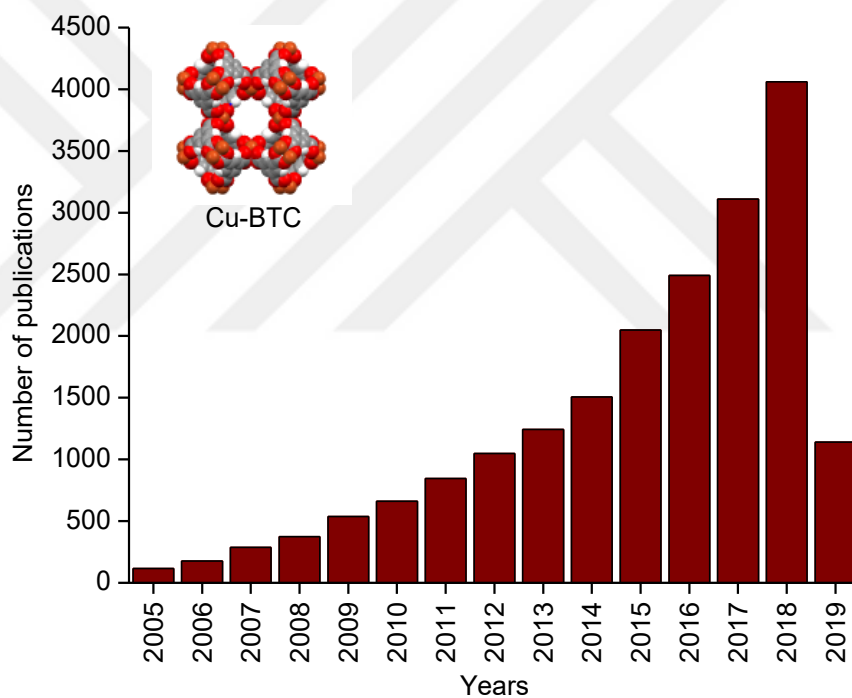


**Figure 1.1** Number of papers featuring the term of “metal organic framework” in their titles. Accessed: 2019-03-27 from Web of Science ® A screenshot of Cu-BTC commonly known as HKUST-1 (HKUST for Hong Kong University of Science and Technology and BTC: benzene-1,3,5-tricarboxylate)[42] from CSD[31]. Red= oxygen, orange=copper, white=hydrogen and grey=carbon.

Covalent-organic frameworks (COFs) are an emerging class of MOFs, that contains strong covalent bonds between atoms such as H, boron (B), C, N

and O. Since COFs are built up by solely light elements, they have lower densities than MOFs. Depending on their building units, these structures can be classified as two- or three-dimensional COFs. In two-dimensional COFs, atoms are covalently bonded to form a layered periodic structure.[43] In 2005, Yaghi et al.[44] first demonstrated their topological design principle and synthesized successful two-dimensional COFs, which were named as COF-1 and COF-5, with pore sizes ranging from 7 Å to 27 Å, respectively. These two materials exhibit high thermal stabilities (up to ~850 K) and high surface areas (711 and 1590 m<sup>2</sup>/g for COF-1 and COF-5, respectively). In 2007, Yaghi and coworkers[45] synthesized the first three-dimensional COFs, COF-102 and COF-103, based on triangular and tetrahedral nodes. Compared with their previous study, these COFs have higher surface areas (3472 and 4210 m<sup>2</sup>/g for COF-102 and COF-103, respectively) and extremely low densities (0.17 g/cm<sup>3</sup>). Currently, experimental COF structures are deposited in a database named as CoRE (computation-ready, experiment) COF and there are totally 309 structures including 41 three-dimensional COFs and 268 two-dimensional COFs.[46] COFs can also be great candidates for gas storage[47], gas separation[48], catalysis[49], photoelectricity[50] and thin-films[51] applications due to their high surface areas (ranged from 260.8 m<sup>2</sup>/g to 25,917.1 m<sup>2</sup>/g), high porosity (0.25-0.96), and tunable chemical/physical properties. Figure 1.2 shows the number of publications on COFs from 2005 to 2019. Similar to Figure 1.1, there is a rapidly growing interest in this area. However, comparison with the available number of MOFs (a total of publications in 2018: 4061), there are less papers about COFs (a total of publications in 2018: 168) due their less available structures.

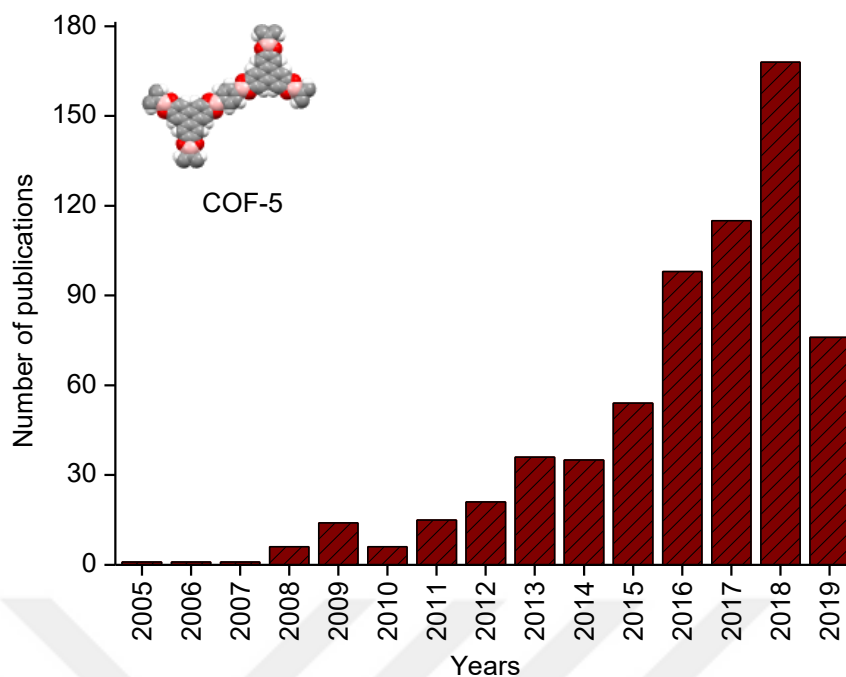


**Figure 1.2** Number of papers featuring the term of “covalent organic framework” in their titles. Accessed: 2019-03-27 from Web of Science ® A screenshot of COF-5[44] from CSD[31]. Red= oxygen, pink=boron, white=hydrogen and grey=carbon.

The objective of this thesis is to identify promising MOFs and COFs for adsorption-based and membrane-based gas separation applications including volatile organic compound separation, hydrogen storage and air separation using high-throughput computational screening methods. In Chapter II, both experimental and computational studies on potential applications of MOFs and COFs were reviewed. Adsorption-based and membrane-based gas adsorption studies and biomedical applications of MOFs and COFs were briefly discussed. In Chapter III, the computational methodology used in this study was discussed in detail. In Chapter IV, separation performances of COFs, IRMOFs and ZIFs were assessed for efficient removal of carbon tetrachloride ( $\text{CCl}_4$ ) from the air. The top-performing three materials in each group were identified and

## CHAPTER I: Introduction

investigated in detail. In Chapter V, all synthesized COFs were evaluated for H<sub>2</sub> storage at 77 K/160 K and various pressures (2, 5, and 100 bar) and deliverable volumetric capacities were calculated using different H<sub>2</sub> models. In Chapter VI, a bio-compatible MOF library was developed, and bio-MOFs were further examined for O<sub>2</sub> storage and O<sub>2</sub> separation from the air. Finally, the results of these three studies were discussed in Chapter VII. In this thesis, we emphasize that molecular simulations will provide an insight into the gas separation and/or gas storage mechanisms of MOFs. The methods used in this thesis guide both experimental and computational studies for the development of porous materials for various industrial applications. The biocompatible MOF library was created in this thesis will be also highly useful for future studies on biomedical applications of MOFs.

## CHAPTER II

### LITERATURE REVIEW

The domain of COFs and MOFs have rapidly expanded, and these materials have been tested in various research areas including gas storage, gas separation, and biomedical applications such as drug encapsulation and drug delivery, biomedical gas storage, sensing and imaging. Although there are many potential applications for these materials, very few of them have been used for industrial scale production due to their high-cost synthesis.[52] In this chapter, the recent experimental and computational studies on gas storage and gas separation, and biomedical applications of MOFs and COFs are summarized.

#### *2.1 Gas Storage*

In recent years, the storage of energy-relevant gases, such as H<sub>2</sub> and CH<sub>4</sub>, is a major focus of research in the development of portable electronics and gas-fueled vehicles. Comparison with the products of fuel gases such as CO<sub>2</sub>, the products of H<sub>2</sub> storage systems such as water are environmentally friendly and non-toxic. For hydrogen-powered vehicles, H<sub>2</sub> can be stored at room temperature (298 K), however at very high pressure (~700 bar), which brings safety issues to design critical equipment. To avoid this issue, liquefaction process has been investigated for on-board H<sub>2</sub> storage at low temperatures (77 K, the liquid nitrogen temperature). As an alternative to this method, cryo-adsorption process has been used to store H<sub>2</sub> at 100 bar and 77 K and desorb H<sub>2</sub> at 5 bar and 160 K conditions based on the tank design criteria

proposed by Hydrogen Storage Engineering Center of Excellence (HSECoE).[53] However, storage tanks have limitations depending on their volumetric capacities. H<sub>2</sub> has a lower energy density (8 MJ/L) than that of gasoline (32 MJ/L). To solve this issue, porous adsorbent materials are proposed. Thus, for volume basis applications, when H<sub>2</sub> molecules are adsorbed within a porous material, capacity of on-board H<sub>2</sub> storage systems can be increased at moderate pressures and temperatures. Herein, the identity of the porous adsorbent material is important for efficient H<sub>2</sub> storage. Promising adsorbents should have high H<sub>2</sub> working capacity. Working capacity is defined as the difference between the amount of adsorbate molecules at a storage pressure and the amount of adsorbate molecules at a desorption pressure. To evaluate the performance of porous adsorbent materials for H<sub>2</sub> storage, The U.S. Department of Energy (DOE) targets have been used in the literature. The DOE target for on-board H<sub>2</sub> storage has been set at 30 g/L (~4.5 wt%) for 2020 and at 40 g/L (~5.5 wt%) for 2025 at 233K/333K and a pressure range between 3 bar to 12 bar.[54] MOFs are great alternatives for on-board H<sub>2</sub> storage systems due to their highly porous structures providing high volumetric and gravimetric H<sub>2</sub> working capacities. For example, in 2003, IRMOF-1 was first tested for H<sub>2</sub> adsorption at 78 K and 298 K by Rosi et al.[55] and they reported that IRMOF-1 gives higher H<sub>2</sub> uptake (4.5 wt%) at 78 K and 0.7 bar than that measured at 298 K and 20 bar (1.0 wt%). It should be also noted that IRMOF-1 could not reach the saturated H<sub>2</sub> uptake at 298 K. This study showed that MOFs can provide high H<sub>2</sub> uptakes at cryogenic temperatures (77 K). In 2007, H<sub>2</sub> uptakes in IRMOF-1 and ZIF-8 were reported as 10.3 wt% and 4.4 wt% , respectively at 30 K and ~5 bar by Yildirim's group.[56] Furukawa et al.[57]



## CHAPTER II: Literature Review

tested MOF-177, which was built from Zn ions and benzenetribenzoate ligands, for high-pressure H<sub>2</sub> storage at 77 K up to 70 bar. MOF-177 exhibited a very high H<sub>2</sub> uptake as 7.5 wt % at 70 bar and 77 K. Gómez-Gualdrón et al.[58] tested the isorecticular series of zirconium-based MOFs including NU-n (NU: Northwestern University, n:1101-1103). Among these series, NU-1101 gave the maximum volumetric H<sub>2</sub> working capacity as ~47 g/L (~9 wt%) and NU-1103 gave the highest gravimetric H<sub>2</sub> working capacity as ~13 wt% (~43 g/L) at 100 bar/77 K for adsorption and 5 bar/160 K for desorption conditions.

Besides experimental efforts, molecular simulations have been also performed to identify promising MOFs for efficient H<sub>2</sub> storage. In 2016, Snurr's group[59] investigated H<sub>2</sub> delivery performance of 137,953 hypothetical MOFs at 77 K and at 100 bar (for adsorption) and 2 bar (for desorption) using computational methodology. MOFs which have mediocre pore sizes (~14 Å) and high void fraction (0.9) exhibited high H<sub>2</sub> volumetric working capacities (around 50 g/L), exceeding the DOE target. The same group[60] then screened 54,776 MOFs for H<sub>2</sub> storage under the same operating condition. Among these MOFs, MFU-4l(Zn) (refcode: UPOZAB) gave the highest deliverable H<sub>2</sub> uptake as 36 g/L which was also validated by experiments. COFs including COF-1, COF-5, COF-102, COF-103, COF-105, and COF-108 were also tested for H<sub>2</sub> storage at 77 K up to 100 bar by Han et al.[61] due to their large surface areas (up to ~4000 m<sup>2</sup>/g). Among these six COFs, COF-108 gave the maximum gravimetric H<sub>2</sub> uptake (~19 wt%), whereas COF-102 gave the highest volumetric H<sub>2</sub> uptake (~40 g/L). All these pioneer experimental and computational studies showed that MOFs can be promising adsorbents for H<sub>2</sub> storage.

## CHAPTER II: Literature Review

CH<sub>4</sub>, which is the major component of natural gas, is a cleaner burning fuel than that of gasoline or diesel. Therefore, it can be used as an alternative fuel in both heavy and light vehicles. Traditionally, CH<sub>4</sub> is stored in a compressed natural gas fuel tank, also known as CNG. Whereas CNG is an easy method for natural gas storage, the usage of these vessels has a drawback. The CNG fuel tank should be almost three times larger than a traditional gasoline tank due to lower energy density of CH<sub>4</sub> (~11 MJ/L) than that of gasoline (~32 MJ/L). For this reason, adsorbed natural gas fuel tanks (ANG) is widely used for conventional CH<sub>4</sub> storage. ANG provides high volumetric H<sub>2</sub> capacities at lower pressures than CNG technology and at room temperature unlike liquefaction. Porous materials have been widely examined and enhanced for natural gas storage. The DOE target has also been used to evaluate the performance of adsorbents for CH<sub>4</sub> storage. For ANG fuel tanks, the target has been set at 180 cm<sup>3</sup>(STP)/cm<sup>3</sup> (STP for standard temperature and pressure) at 35 bar and 298 K.[62]

MOFs offer high performance for CH<sub>4</sub> storage. For example, CH<sub>4</sub> uptake in a MOF, CuSiF<sub>6</sub>(4,4'-bipyridine)<sub>2</sub>, was first examined by Kitagawa et al.[63] in 2000 and 6.5 mol of CH<sub>4</sub> per 1 kg of the MOF at 36 bar and 298 K was reported. In a different study, Yaghi and coworkers[27] reported the CH<sub>4</sub> uptake in IRMOF-6 as 240 cm<sup>3</sup>(STP)/g at 36 bar and 298 K due to its suitable pore aperture (~6 Å) for CH<sub>4</sub> uptake. Furukawa et al.[47] examined the CH<sub>4</sub> storage performances of seven COFs including COF-1, 5, 6, 8, 10, 102, and 103 at 298 K and high-pressure (up to 70 bar). In gravimetric units, they found that saturated CH<sub>4</sub> of these COFs are range from 4 wt% to 18.7 wt%. Among seven COFs, COF-102 gave the highest volumetric CH<sub>4</sub> uptake as almost 136

## CHAPTER II: Literature Review

and  $193 \text{ cm}^3(\text{STP})/\text{cm}^3$  at 35 bar and 70 bar, respectively. The results in  $\text{cm}^3(\text{STP})/\text{cm}^3$  for COF-102 were well within the DOE target ( $180 \text{ cm}^3(\text{STP})/\text{cm}^3$ ) at 35 bar. Besides experimental studies, molecular simulations play a significant role to identify the best-performing porous materials for  $\text{CH}_4$  uptake. Wilmer et al.[64] computed  $\text{CH}_4$  adsorption in 137,953 hypothetical MOFs at 35 bar and 298 K by using molecular simulations. Among all these MOFs, NOTT-107 (NOTT: University of Nottingham) gave the highest  $\text{CH}_4$  uptake as  $213 \text{ cm}^3(\text{STP})/\text{cm}^3$ , which was also validated by experiments. In a different study, Gómez-Gualdrón et al.[65] performed simulations of 122,835 hypothetical MOFs to understand the maximum volumetric  $\text{CH}_4$  at 298 K and at 65 bar (adsorption) and 5.8 bar (desorption). The observed range of  $\text{CH}_4$  storage in the top-performing materials which have large volumetric surface areas ( $2100\text{-}2300 \text{ m}^2/\text{cm}^3$ ) and mediocre pore sizes ( $10 \text{ \AA}$  to  $12 \text{ \AA}$ ), was found to be almost  $100\text{-}206 \text{ cm}^3(\text{STP})/\text{cm}^3$ . According to these recent studies, MOFs and COFs can be great adsorbents for natural gas storage.

The research on carbon capture and sequestration has gained momentum to reduce the effects of global warming. As the concentration of  $\text{CO}_2$  increases in the atmosphere, the average global temperature increases. For example, from the beginning of the 1900s, the average global temperature increased ( $\sim 2 \text{ }^\circ\text{C}$ ). This increase in temperature has some impacts on health and environment such as extreme weather events, and sea level rise.[66] Therefore, the elimination of  $\text{CO}_2$  emission is highly important for all human being and environment. MOFs can be excellent candidates for carbon capture applications since they can provide strong adsorption sites for  $\text{CO}_2$  due to their open (unsaturated) metal sites. For example, Dietzel et al.[67] tested two different MOFs with open metal

## CHAPTER II: Literature Review

sites, CPO-27-n (n: nickel (Ni), magnesium (Mg), and CPO for Coordination Polymer of Oslo), for CO<sub>2</sub> capture and reported the highest CO<sub>2</sub> uptake as 51 wt% and 63 wt%, respectively at 50 bar and 298 K. In a different study, Millward et al.[68] tested nine different MOFs including Cu-BTC, IRMOF-1, IRMOF-3, IRMOF-6, IRMOF-11, MOF-2, MOF-74, MOF-177, and MOF-505 for CO<sub>2</sub> uptake at 298 K and up to 42 bar. The saturated CO<sub>2</sub> uptake of nine MOFs was ranged of 2.5 mol/kg to 33.5 mol/kg. Among these MOFs, MOF-177, which have the highest surface area (4508 m<sup>2</sup>/g) gave the highest CO<sub>2</sub> uptake (33.5 mol/kg). This study showed that MOFs without open metal sites, which have high surface areas, can also exhibit high CO<sub>2</sub> uptake. There are excellent reviews about carbon capture applications of MOFs in the literature.[34, 69]

High-pressure O<sub>2</sub> storage has various applications from medical to aerospace such as photodynamic therapy in which high O<sub>2</sub> loading efficiency is desired[70] and control system of the spacecraft cabin O<sub>2</sub> concentration[71]. It is also required for the enrichment of air during the catalyst regeneration in industrial catalytic units.[72] To the best of our knowledge, there are only a few studies on O<sub>2</sub> uptake in MOFs. For example, Piscopo et al.[73] built up two series of fluorine-containing UiO-66 (UiO for University of Oslo), and observed that O<sub>2</sub> adsorption capacity can be increased by using fluorine-containing UiO-66 series due to favorable interaction between oxygen and fluorine. Gallagher et al.[74, 75] studied two different MOFs with porphyrin ligand, such as PCN-224-Co (PCN for porous coordination network, and Co for cobalt) and PCN-224-Fe (Fe: iron). These two MOFs with different metal sites were reported as promising materials for biological O<sub>2</sub> storage and transport due to enhanced interactions between O<sub>2</sub> and

## CHAPTER II: Literature Review

framework atoms. These studies showed that MOFs can exhibit high performance for O<sub>2</sub> storage and separation. Computational studies also play a critical role to choose the best candidates prior to experiments due to the enormous number of MOFs in the current CSD.[31] For example, DeCoste et al.[76] screened 10,000 hypothetical MOFs to identify the promising MOFs for O<sub>2</sub> storage. They reported that Cu-BTC and NU-125 give the highest O<sub>2</sub> uptake as 13.2 mol/kg and 17.4 mol/kg, respectively at 140 bar and 298 K. They also validated their predictions by performing experiments. Similarly, Fairen-Jimenez and coworkers[77] performed molecular simulations to compute O<sub>2</sub> uptake in 2932 existing MOFs and validated their simulation results with experiments for UMCM-152 (UMCM: University of Michigan Crystalline Material), which gave the maximum volumetric O<sub>2</sub> working capacity (249 cm<sup>3</sup> (STP)/cm<sup>-3</sup>). They reported that UMCM-152 can deliver 22.5% more O<sub>2</sub> than NU-125, which was known as the best material for O<sub>2</sub> storage to date. They also reported that DIDDOK gives the highest gravimetric O<sub>2</sub> working capacity as 20.4 mol/kg. In another study, McIntyre et al.[78] performed molecular simulations of IRMOFs-n (n=1:16), MOF-177 and UiO-66 and showed that O<sub>2</sub>/N<sub>2</sub> selectivities of these MOFs based on ideal adsorption solution theory (IAST) are found to be between 1-1.3 at 298 K. These pioneering experimental and computational studies showed that MOFs exhibit promising performance for O<sub>2</sub> adsorption.

Gas storage studies on MOFs have also been extended to the harmful and toxic chemicals, which are released by burning fossil fuels and/or human activities. Ammonia (NH<sub>3</sub>), hydrogen sulfide (H<sub>2</sub>S), and volatile organic compounds (such as CCl<sub>4</sub> and benzene) are examples of the most common hazardous gas molecules in the outdoor and indoor environments.[25] Toxic

## CHAPTER II: Literature Review

chemicals lead to harmful effects on the environment such as ozone depletion and global climate change. The huge number of available MOFs can provide opportunities for decontamination of these chemicals.[79] For example, Glover and coworkers[80] tested  $\text{NH}_3$  adsorption in a series of MOF-74 with four different metal centers including Co, Mg, Ni, and Zn at 298 K. Among these MOFs, Co-MOF-74 exhibited the highest gravimetric  $\text{NH}_3$  uptake as 6.7 mol/kg and 4.3 mol/kg under the dry and high humid conditions (relative humidity 0%, and 80%, respectively). In a different study, Katz and coworkers[81] studied  $\text{NH}_3$  uptake in Cu-CPO-27, also known as Cu-MOF-74, at 298 K under the 0%, and 80% relative humidity. Cu-CPO-27 gave higher  $\text{NH}_3$  uptake (7.6 mol/kg) under the 80% relative humidity than that under the 0% relative humidity (3.4 mol/kg). This result was attributed to high density of  $\text{Cu}^{2+}$  metal sites per unit cell resulting in the highest  $\text{NH}_3$  uptake under the humid conditions.  $\text{H}_2\text{S}$  is the other toxic chemical, which commonly encountered in the natural gas and petroleum industries.  $\text{H}_2\text{S}$  was used as a chemical warfare agent (CWA) during World War I by Great Britain. MOFs can also be great alternative for  $\text{H}_2\text{S}$  storage. For example, Maurin and coworkers[82] examined  $\text{H}_2\text{S}$  adsorption in MIL-47(V), and MIL-53(Cr) (MIL: Materials of Institut Lavoisier, and V: vanadium) at 303 K and at a wide range of pressure (up to 18 bar) by using both experimental and computational methods. MIL-47-V gave slightly higher saturated  $\text{H}_2\text{S}$  uptake (14 mol/kg) than MIL-53-Cr (12 mol/kg). This can be explained by the flexible structure of MIL-53(Cr). As the pressure increased, the structure of MIL-47(V) remained rigid whereas the pore apertures of MIL-53(Cr) became narrower resulting in lower gas adsorption. In a recent study, Mg-CUK-1 (CUK for Cambridge University-

## CHAPTER II: Literature Review

KRICT) was synthesized and tested for H<sub>2</sub>S adsorption by Sanchez-Gonzalez et al.[83] and they reported that Mg-CUK-1 gives H<sub>2</sub>S uptake as 3.1 mol/kg in the presence of high relative humidity (95 %). Many studies on various toxic gas adsorption in MOFs can be found in the literature.[84]

Storage of VOCs such as CCl<sub>4</sub>, benzene etc., has received attention due to their serious harmful risks on human health and environment. As a consequence of 2<sup>nd</sup> Montreal Protocol, CCl<sub>4</sub> was phased out in 1992. Until 1992, CCl<sub>4</sub> had been widely preferred in dry cleaning processes as a replacement for petroleum distillates especially dissolving nonpolar compounds as fats, and oils. Although the maximum emissions were identified as 8 Gg of CCl<sub>4</sub>/year by Montreal Protocol, a recent study[85] showed that CCl<sub>4</sub> has been observed in the air as 35 Gg/year. This result showed that CCl<sub>4</sub> has been still used as a solvent in chemical industries because of the lack of replacement of compounds. CCl<sub>4</sub> removal from air has become an important issue since it is a strong ozone-depleting gas, and hazardous for health. Anand et al.[86] showed that CCl<sub>4</sub> can cause serious damage in the brain, liver, and kidney of male Wistar rats. Various methods; such as catalysis-assisted plasma technology[87], non-thermal plasma processing[88], photocatalytic degradation[89], absorption[90], bio-filtration[91], membrane separation, oxidation,[92] and adsorption[93] have been investigated for removal of CCl<sub>4</sub> from air. Among all these different destruction and recovery methods, adsorption has been widely used due to its low cost, simple design, and high efficiency.

Researches on capture of VOCs, toxic industrial chemicals (TICs) including NH<sub>3</sub>, and H<sub>2</sub>S and various CWAs such as sarin, chlorine, and mustard

## CHAPTER II: Literature Review

gas have been potential applications of MOFs. Adsorption of toxic chemicals have some challenges due to presence of water. However, MOFs, especially hydrophobic MOFs, can give higher adsorption capacities than traditional materials such as activated carbons.[79, 94] Although MOFs have been studied for removal of toxic chemicals in the literature, there are only a few studies on  $\text{CCl}_4$  adsorption. Calero's group[95] predicted  $\text{CCl}_4$  adsorption isotherms in Cu-BTC by using molecular simulations.  $\text{CCl}_4$  adsorption in Cu-BTC was reported as 6.2 mol/kg at 298 K and 0.1 bar. The same group[96] then investigated the effect of humidity on the  $\text{CCl}_4$  removal from air in Cu-BTC by performing molecular simulations. They showed that  $\text{CCl}_4$  uptake in Cu-BTC decreases in the presence of water. For example,  $\text{CCl}_4$  adsorption in Cu-BTC decreased from 56 to 37 molecules per unit cell in the presence of 10% air humidity, since water molecules were preferentially adsorbed at the central cages of Cu-BTC. Up to date, there are only a few experimental studies on  $\text{CCl}_4$  adsorption in MOFs. For example, Zheng et al.[97] reported that 13 mol  $\text{CCl}_4$ /kg MOF is adsorbed within the pores of MIL-101 at 303 K. In a different study, Jafari et al.[98] studied  $\text{CCl}_4$  adsorption in ZIF-8 and reported the  $\text{CCl}_4$  uptake as 98.31 mg/g at 273 K and under the atmospheric pressure. Various studies on adsorption of VOCs in MOFs have been reported in excellent reviews.[99, 100]

The recent experimental and computational studies on storage of several gases including  $\text{H}_2$ ,  $\text{CH}_4$ ,  $\text{CO}_2$ ,  $\text{O}_2$ , toxic gases and VOCs such as  $\text{NH}_3$ ,  $\text{H}_2\text{S}$ , benzene, acetone, toluene,  $\text{CCl}_4$  in MOFs were discussed. All these studies play a significant role to provide novel synthesized materials and develop new techniques for gas adsorption applications of MOFs.



## ***2.2 Gas Separation***

Separation is a process which is used to purify a mixture of substances into more than one product. Efficient gas separation processes can save natural resources and decrease the required energy. Separation processes, such as crystallization, distillation, extraction, adsorption, and membrane separation, have been used in industry for purification. Among them, distillation has been widely preferred for separation. However, this process requires high energy and high cost.[101] Adsorption-based and membrane-based methods can be alternatives for various gas separation processes due to their less complex infrastructure, lower operating cost, and lower energy consumption. MOFs can be promising candidates for adsorption-based and membrane-based gas separations. Mechanism of gas separation process in MOFs is primarily based on molecular sieving effect and adsorbate-adsorbent interactions. MOFs have been studied for separation of various gases, especially light gas molecules, such as CH<sub>4</sub>, H<sub>2</sub>, O<sub>2</sub>, Kr (krypton), N<sub>2</sub>, and Xe (xenon). Many excellent reviews on gas separation applications of MOFs exist in the literature.[102, 103]

### **2.2.1 Adsorption-based Gas Separation**

Adsorption-based, also known as equilibrium-based, gas separation is based on the adsorption equilibrium of gas mixtures. The performance of this process depends on the characteristic of an adsorbent material. Both high gas selectivity and high gas working capacity are desired for an ideal adsorbent material. MOF based gas separation has gained momentum and have shown great promise, especially for the separation of CO<sub>2</sub> from flue gas and natural gas. As we discussed before, as the concentration of CO<sub>2</sub> in the air increases, it causes average global temperature rise. Therefore, developing energy-efficient

## CHAPTER II: Literature Review

CO<sub>2</sub> capture technologies is essential. Flue gas separation, which is mainly separation CO<sub>2</sub> from N<sub>2</sub>, and landfill gas separation, which is defined as CO<sub>2</sub> capture from CH<sub>4</sub> are two important industrial processes.[69] MOFs can be great candidates to achieve high CO<sub>2</sub> separation. For example, Garcia et al.[104] studied the separation of equimolar mixture of CO<sub>2</sub>/CH<sub>4</sub> in four MOFs including CPO-27-n (n: Ni, Co, Zn) and STA-12-Ni (STA-12: St. Andrews microporous material no.12) at 303 K and 1 bar using both experimental and computational methods. CO<sub>2</sub>/CH<sub>4</sub> selectivities of these MOFs were reported to be in a range between 6 to 15. Among them, CPO-27-Ni exhibited the highest CO<sub>2</sub> selectivity over CH<sub>4</sub> (15) due to its high affinity towards CO<sub>2</sub>. In a different study, Xian et al.[105] examined CO<sub>2</sub> separation from equimolar CO<sub>2</sub>/CH<sub>4</sub> and CO<sub>2</sub>/N<sub>2</sub> mixtures in two MOFs, MIL-100(Fe) and MIL-100(Cr) at 303 K and 1 bar. They reported that Fe-based MIL-100 gives higher CO<sub>2</sub> selectivity (5.3 for CO<sub>2</sub>/CH<sub>4</sub>, and 8.6 for CO<sub>2</sub>/N<sub>2</sub>) than that of Cr-based MIL-100 (4.5 for CO<sub>2</sub>/CH<sub>4</sub>, and 6.7 for CO<sub>2</sub>/N<sub>2</sub>). They also tested CO<sub>2</sub> selectivity over CH<sub>4</sub> under the 50% relative humidity and reported CO<sub>2</sub>/CH<sub>4</sub> selectivity of MIL-100(Fe) and MIL-100(Cr) as 16.3 and 3.7, respectively. In the presence of water molecules, CO<sub>2</sub> selectivity of MIL-100(Fe) was enhanced. When water molecules were adsorbed in Fe metal surface of MIL-100, alkaline active site of this MOF's surface increased. Thus, higher CO<sub>2</sub> uptake in MIL-100(Fe) was obtained than that of Cr-based MIL-100 due to the acidity of CO<sub>2</sub>. In a computational study, Altintas et al.[106] performed molecular simulations for 3816 MOFs to identify top-performing materials for CO<sub>2</sub>/N<sub>2</sub> (flue gas, bulk phase 15:85) and CO<sub>2</sub>/CH<sub>4</sub> (landfill gas, 50:50) separations at 298 K and at two different pressures (1 bar and 0.1 bar). Among 3816 MOFs, 30 MOFs, which

## CHAPTER II: Literature Review

were the best candidates for selective CO<sub>2</sub> separation, were further investigated for ternary mixture adsorption, CO<sub>2</sub>/N<sub>2</sub>/CH<sub>4</sub> (5:90:5), at 10 bar and 298 K for suggesting a more realistic adsorbent evaluation assessment. CO<sub>2</sub> selectivities of 30 MOFs were calculated as 29.8-516.6 for CO<sub>2</sub>/N<sub>2</sub> mixture and 8.5-339 for CO<sub>2</sub>/CH<sub>4</sub> mixture. They reported that MOFs, which exhibited high CO<sub>2</sub> selectivities over both CH<sub>4</sub> and N<sub>2</sub>, have mediocre pore sizes ( $3.8 \times 5 \text{ \AA} - 5 \times 7.5 \text{ \AA}$ ) and surface area ( $< 1000 \text{ m}^2/\text{g}$ ) at this operating condition. This study can lead the experimental MOF design for efficient CO<sub>2</sub> separation. With these pioneering studies, CO<sub>2</sub> separation using MOFs has been widely tested in the literature and several reviews have published to evaluate MOF-based gas separation.[107, 108]

Another important industrial gas separation process is air separation and/or purification. Air mixture contains N<sub>2</sub> (78 %), O<sub>2</sub> (20.9 %), Ar (1 %) and the other gas components (0.1 %) such as air pollutants. In order to produce pure O<sub>2</sub>, air separation has been widely used which purifies O<sub>2</sub> and N<sub>2</sub>. [78] Cryogenic distillation, which requires high pressure (from 6.5 bar to 13.2 bar) and ultra-low temperature (88 K), is a traditional method to separate air mixtures based on the boiling point differences of gas molecules. Although this technology has been used since the early 1900s, it is complex, energy intensive, and also expensive.[109] Adsorption-based gas separation has also become an alternative method for O<sub>2</sub>/N<sub>2</sub> separations. Most adsorbent materials used for air separation are either N<sub>2</sub> selective or non-selective.[110, 111] Achieving high selectivity towards O<sub>2</sub> with high O<sub>2</sub> working capacity is highly required for an efficient adsorbent material for O<sub>2</sub> separation. To the best of our knowledge, there are only a few experimental studies on O<sub>2</sub> storage and separation with using

## CHAPTER II: Literature Review

MOFs. Wang et al.[112] used a three-dimensional MOF, RPM3-Zn,  $Zn_2(4,4'$ -biphenyldicarboxylate) $_2(1,2$ -bipyridylethene), for  $O_2/N_2$  separation and reported selectivity of  $O_2$  over  $N_2$  as 5 at 1 bar and at both 77 K and 87 K.  $O_2$  selectivity of this MOF was explained by its metal sites and gate-opening process of RPM3-Zn at low temperatures. In a different study, Wang et al.[113] examined the effect of metal ions on  $O_2$  adsorption capacity of  $M_3(BTC)_2$  type materials (M= Co, Cr, Cu, Fe, Mn and Ni) and found out that  $Ni_3(BTC)_2$  can be a promising material for  $O_2/N_2$  separation. Parkes et al.[114] examined  $M_2(dobdc)$  (M for Cr, Fe and Mn) MOF series for pure gas and competitive gas adsorption of  $O_2$  and  $N_2$  by performing simulations. They showed that unsaturated metal sites enhance  $O_2$  selectivity due to strong interactions between  $O_2$  and the MOFs' metal centers. In a recent study, Demir et al.[115] performed molecular simulations for  $O_2/N_2$  separation in ~2867 CoRE MOFs at 1 bar 298 K. Among them, totally 210 MOFs, which exhibited  $O_2/N_2$  selectivity  $>1$ , were identified as  $O_2$  selective adsorbents. Four MOFs, such as IRMOF-1, IRMOF-14, Ce-UiO-66, and UiO-66(Zr) were chosen to further investigate their binding affinity towards frameworks' metal sites. Metal catecholates including cadmium (Cd), Co, Mg, Ni, and Zn were added to four MOFs by using molecular simulations. Cd-catecholates showed big difference between single-component  $O_2$  adsorption (80-95 kJ/mol) and single-component  $N_2$  adsorption (3-20 kJ/mol). They elucidated that this difference might enhance high  $O_2/N_2$  selectivity of MOFs. These pioneering studies showed that MOFs with functional units, such as porphyrin ligand and fluorine moieties, and/or MOFs with unsaturated metal sites exhibit enhanced  $O_2$  adsorption.

$H_2$  separation is also important to use  $H_2$  in vehicles as a replacement of fossil fuels.  $H_2$  can be purified from synthetic gas (syngas), which contains  $CH_4$

and CO<sub>2</sub>, obtained from steam reforming of natural gas. For example, Altintas et al.[32] performed molecular simulations for 4350 MOFs to assess these MOFs for adsorption-based CH<sub>4</sub>/H<sub>2</sub> separation at two different pressures (1 and 10 bar). All selectivity values were reported to be greater than one. This was explained that CH<sub>4</sub> is more preferred than H<sub>2</sub> in all these MOFs due to its stronger interaction with the framework atoms. They reported that 8 MOFs, namely as FEHCOM, JOVXUP, KEWZOD, KINNEC, PIBXOP, ROHKAC, RORVAX, and SIKGEA, were found to be the best performing materials for CH<sub>4</sub>/H<sub>2</sub> separation. Also, 1647 MOFs gave higher CH<sub>4</sub>/H<sub>2</sub> selectivities (~60) than the traditional materials including zeolites (~13) and carbonaceous based structures (~58.3).

MOFs also have the potential to capture noble gases such as Kr and Xe to prevent their emission into the air. Xe has been widely used in many applications, ranging from electronics to the medical industry. Therefore, separation Xe from Kr process is very important to reuse them and reduce the nuclear wastes.[116] MOFs have also been tested for noble gas separation. For example, Mueller et al.[117] first tested adsorption-based separation Xe/Kr (bulk phase: 6/94) in Cu-BTC at 40 bar and 328 K by using experimental methods. Cu-BTC was found to be Xe selective and Xe uptake in this MOF was almost 60 wt%. Chen et al.[118] synthesized a MOF, SBMOF-2 (SB for Stony Brook) and reported that SBMOF-2 has high Xe selectivity over Kr (10) at 298 K and 1 bar. Xe selectivity of SBMOF-2 was attributed to the framework's cages constructed by phenyl rings and enriched with -OH (hydroxy) polar groups. Banerjee et al.[119] performed simulations for ~125,000 MOFs, including ~5000 existing MOFs and ~120,000 hypothetical

## CHAPTER II: Literature Review

MOFs, to identify a promising material for Xe/Kr separation under ambient conditions. Among them, SBMOF-1 (refcode: KAXQIL) was found to be a Xe selective material (70.6), that was also validated by experiments, due to its favorable binding sites for Xe molecules. Simon et al.[120] combined a machine learning algorithm with the molecular simulations for identifying the best-performing materials for Xe/Kr separation. Totally 10,981 MOFs, including 7341 hypothetical and 3640 existing MOFs, were studied for Xe/Kr separation at 1 bar and 298 K. They reported that JAVTAC, which was constructed by aluminophosphate, gives the highest Xe selectivity (86.6). As shown in these studies, MOFs are great alternatives for Xe/Kr separation due to their highly selective binding sites for Xe.

MOFs are also great candidates to capture toxic gases from the environment. For example, Zhao et al.[121] studied benzene separation from water using Cu-BTC at 308 K and  $1.5 \times 10^{-3}$  bar under 34% relative humidity and reported that Cu-BTC gives high benzene selectivity over water as 17.6. In a different computational study, Matito-Martos et al.[122] performed molecular simulations of 1647 MOFs, whose pore sizes are  $> 3.72 \text{ \AA}$ , to capture CWAs including sarin, soman and mustard gas under humidity conditions. They elucidated that MOFs should have high surface areas ( $> 2000 \text{ m}^2/\text{g}$ ) and mediocre pore sizes ( $> 12 \text{ \AA}$ ) to be used for these separation applications.

The studies on different gas storage and/or separation applications including  $\text{CO}_2$  capture,  $\text{O}_2/\text{N}_2$  separation,  $\text{H}_2$  separation, Xe/Kr separation and some toxic gas adsorption were discussed in this section. All these experimental and computational studies are very important for identifying the best performing MOFs and the development of novel technologies for gas

separation applications.

### 2.2.2 Membrane Separation

Membranes are widely used as separating agents for sustainable industrial growth due to their usable equipment size, waste generation, cost-efficiency and energy utilization. Membrane-based gas separation is a pressure-driven process.[123] A mixture is fed across the membrane, and then one or more components, that give high transport rate, can be separated from the mixture. Membranes can be categorized into three different groups as polymeric membranes, inorganic membranes and composite membranes. They can also be used as a combination of the first two categories (porous inorganic membranes). Different transport mechanisms such as Knudsen diffusion, and molecular sieving are observed in porous membranes. Knudsen separation is based on the different molecular weights of the gases. This mechanism can be enhanced with membranes, whose pore apertures are smaller than 500 Å. The molecular sieving mechanism is also based on pore diameters of the membranes and those of the gases to be separated. This mechanism can be achieved in a balance between pore size and porosity. Porous inorganic membranes are also governed by molecular sieve mechanism.[124] A detailed discussion about gas transport mechanism in membranes can be found in the literature.[125]

Polymeric (non-porous) membranes are governed by solution-diffusion mechanism since gas molecules can diffuse through the membrane due to the concentration or pressure gradient. This mechanism is based on both solubility and transport of gas molecules. Polymeric membranes, such as polyimide and polysulfone, are easy to synthesize and widely used in gas separation processes.

## CHAPTER II: Literature Review

The efficiency of a polymeric membrane is dependent on both high selectivity and high permeability. High selectivity is required for high purity, and high gas permeability is required to decrease the surface area of the membrane resulting in low capital cost. Polymer membranes have a trade-off between selectivity and permeability. This trade off is commonly expressed with the Robeson's upper bound and used for different gas separations including  $H_2/CH_4$ ,  $O_2/N_2$ , and  $H_2/CO_2$ . [126] Polymeric membranes are widely used for air separation due to ease of scale-up and low cost. Although these membranes have low  $O_2$  permeabilities (0.05-370 Barrer), they generally exhibit moderate  $O_2/N_2$  selectivities (3.3-10.5). [127] Jeazet et al. [128] studied polysulfone (PSF) for  $O_2$  separation and reported its  $O_2$  permeability as 1.5 Barrer and selectivity of  $O_2$  over  $N_2$  as 5.9 at 303 K and 3 bar. Another pure polyurethane (PU) membrane was tested by Rodrigues et al. [129] for  $O_2/N_2$  separation and reported that it exhibits low  $O_2$  permeability (2.8 Barrer) and selectivity (4) at 298 K and 4 bar.

Many carbon molecular sieves and zeolites have been fabricated as membranes and tested for different gas separation applications. For example, Singh et al. [130] studied three different membranes including carbon molecular sieve, zeolite 4A and polypyrrolone for  $O_2/N_2$  separation. Carbon molecular sieve and zeolite 4A gave high  $O_2$  selectivity than polypyrrolone due to their strong size-sieving properties and selective pore apertures. Inorganic membranes generally exhibit higher gas selectivity than polymeric membranes. However, using inorganic membranes in gas separation applications has some challenges due to their high operational cost and the defects in their structures. [131, 132]

Composite membranes also known as mixed matrix membranes



(MMMs), in which inorganic particles are embedded into a polymer matrix, have been developed to solve this permeability-selectivity trade-off. MMMs consisted of various inorganic fillers have been tested for various gas separation applications. For example, Vu et al.[133] prepared MMMs consisting of carbon molecular sieves embedded into a pure polymer membrane and tested them for O<sub>2</sub>/N<sub>2</sub> separation. MMMs (36 v% of CMS and polymer) exhibited high O<sub>2</sub> selectivity (7.9) and permeability (3 Barrer) at 308 K. A detailed discussion about inorganic and composite membranes can be found in the literature.[134]

MOFs have also been tested as filler particles in polymeric membranes to increase the gas permeabilities and selectivities of pure polymers. For example, Zornoza et al.[135] prepared two different MMMs (Cu-BTC and ZIF-8 in a PSF matrix) and compared their O<sub>2</sub>/N<sub>2</sub> separation performances, such as O<sub>2</sub> permeabilities, with pure polymer membranes' performances. ZIF-8 gave higher selectivity due to its smaller pore sizes (3.4 Å) than Cu-BTC (6 Å). Similarly, ZIF-8 were incorporated into the PIM-1 (polymer of intrinsic microporosity) by Bushell et al.[136] This MMM surpassed the Robeson's 2008 upper bound established for O<sub>2</sub>/N<sub>2</sub> separation, when 43 vol% ZIF-8 was embedded into the pure PIM-1. Cu-BTC and MIL-101(Cr) were also used as fillers in polymers and O<sub>2</sub> permeabilities of MMMs increased without any significant change in selectivities.[128, 137] However, performing the membrane-based gas separation with high O<sub>2</sub> permeability and selectivity has been still required for industrial air separation applications.

Besides traditional materials, thin-film MOF membranes can be fascinating alternative for membrane-based separation technology due to their wide range of pore sizes (micro- to meso-), high porosities and permanent

pores. A large number of MOFs is found to surpass the Robeson's upper bound for various gas separation applications in the literature. For example, Huang et al.[138] synthesised ZIF-95 membrane and examined its separation performance for H<sub>2</sub>/CO<sub>2</sub>:50/50 mixture at 603 K and 1 bar. ZIF-95 membrane exceeded the upper bound and gave high H<sub>2</sub> selectivity over CO<sub>2</sub> as 25.7. This membrane has also high potential for H<sub>2</sub> purification due to its high thermal stability. Bux et al.[139] investigated ZIF-8 membrane for H<sub>2</sub> separation from CO<sub>2</sub>, N<sub>2</sub>, O<sub>2</sub>, and CH<sub>4</sub>. H<sub>2</sub> permeance ( $\sim 0.6 \text{ m}^3 \text{ (STP)/m}^2 \cdot \text{h} \cdot \text{bar}$ ) were found to be higher than the other gases ( $\sim 0.1 \text{ m}^3 \text{ (STP)/m}^2 \cdot \text{h} \cdot \text{bar}$ ) due to its smaller pore sizes compared to other gas molecules. Similarly, Huang et al.[140] studied H<sub>2</sub> separation from equimolar four different mixtures including H<sub>2</sub>/CH<sub>4</sub>, H<sub>2</sub>/CO<sub>2</sub>, H<sub>2</sub>/N<sub>2</sub>, and H<sub>2</sub>/O<sub>2</sub> using ZIF-22 membranes at 1 bar and 323 K. ZIF-22 membranes gave H<sub>2</sub> selectivities over CH<sub>4</sub>, CO<sub>2</sub>, N<sub>2</sub>, and O<sub>2</sub> as 1.72, 1.66, 1.88, and 1.89, respectively. In a different study, Zhao et al.[141] tested IRMOF-1 membranes for CO<sub>2</sub>/H<sub>2</sub> (bulk phase: 82/18) and CO<sub>2</sub>/N<sub>2</sub> (88/12) separations at 3.5 bar and 380 K and reported that CO<sub>2</sub> selectivities in these mixtures are found to be 1.5 and 6, respectively. In a recent computational study, Altintas et al.[142] performed simulations of 4240 MOF membranes for H<sub>2</sub>/CH<sub>4</sub> separation at infinite dilution and 298 K. Among all these MOF membranes, 1545 MOFs were found to outperform polymeric membranes exceeding the upper bound due to their high H<sub>2</sub> membrane selectivities (0.1-96.95) and/or high H<sub>2</sub> permeabilities ( $\sim 10^3$ - $10^5$  Barrer). They also reported that MOFs membranes, which have small surface areas ( $<1000 \text{ m}^2/\text{g}$ ), mediocre porosities ( $0.5 < \phi < 0.75$ ) and densities ( $1 < \rho < 1.5 \text{ g/cm}^3$ ), exhibit enhanced H<sub>2</sub> selectivities and permeabilities. Also, MOFs with Cd, Cu and Zn metal sites are promising for H<sub>2</sub> separation. Comparison with other gases, H<sub>2</sub> has the smallest

molecular sizes (2.89 Å). Thus molecular sieving effects play a significant role in H<sub>2</sub> separation process.[143] These results can be useful to guide further experiments for MOFs with high H<sub>2</sub> selectivity.

As we discussed above, both thin-film MOF membranes and MMMs are great candidates for high performance gas separation applications. There are many studies on gas separation applications of MOF membranes in the literature.[144-146]

### ***2.3 Biomedical Applications***

MOFs can be used for different biological applications including biomedical gas storage, and drug storage and/or drug delivery. In the design of MOFs for biomedical applications, the basic criteria as toxicology, stability in physical condition and metal daily requirement in humans should be considered. Non-toxic metal cations and endogenous organic linkers, which are biomolecules as constitutive ingredients of body composition, have been used to synthesize biocompatible MOFs.[147] To detect toxicity, oral lethal dose 50 (LD<sub>50</sub>)[148], which is the amount of a component that kills half the members in a given population after a certain test period, is considered. Cations such as calcium (Ca<sup>2+</sup>), Fe<sup>3+</sup>, Mg<sup>2+</sup>, Zn<sup>2+</sup> have high LD<sub>50</sub> (range from 100 to 5000 mg/Kg) and high daily requirements (range from 11 to 1200 mg/day). Thus, MOFs with these metal sites are the best candidates for biological applications. Bioactive metals such as zirconium (Zr<sup>4+</sup>, LD<sub>50</sub>=4100 mg/kg and requirement=3.5 mg/day) or paramagnetic metal ions such as manganese (Mn<sup>2+</sup>, LD<sub>50</sub>=3730 mg/kg and requirement=4.5-8.2 mg/day) can be used to synthesize biocompatible MOFs. Amino acids, cyclodextrin, citrates, fumarates, nucleobases, peptides, and porphyrins have been used as

endogenous linkers.[149] In the literature, various biocompatible MOFs based on endogenous linkers have been synthesized. For example, the first anionic bio-MOF, namely as bio-MOF-1, was synthesized by Rosi et al.[150] using  $Zn^{2+}$  ions and adenine for encapsulation of a cationic drug, procainamide. The same research group[151] then synthesized bio-MOF-11 using  $Co^{2+}$  ions with adenine linkers as a paddle-wheel cluster. Bio-MOFs-n (n:12-14) were also synthesized as bio-MOF-11 analogues by using different aliphatic monocarboxylates.[152] The same group[153, 154] also synthesized another bio-MOF-n (n:100-103) series, which have the high surface areas (2704-4410  $m^2/g$ ), with using  $Zn^{2+}$  ions. Another biocompatible MOF series are edible MOFs, namely as CD-MOFs (CD for cyclodextrin), which were built up from  $\gamma$ -cyclodextrin building units and potassium ( $K^+$ ) cations by Smaldone et al.[155] It should be noted that while synthesizing CD-MOF-n (n:1-3), suitable food ingredients, which are renewable and natural components, can be preferred.

An alternative approach is coupling bioactive molecules with cations to design MOFs whose linkers are active molecules. This approach avoids the necessity for high surface area and/or large pore apertures to achieve high drug encapsulation. While the biodegradation of the MOFs carries on, active biomolecule can be released. For example, the first bioactive MOF, BioMIL-1, was built up  $Fe^{3+}$  and nicotinic acid and investigated for the delivery of nicotinate molecules by Serre and coworkers.[156] Another interesting example is that Miller et al.[157] synthesized BioMIL-3 consisting of Ca cations and 3,3',5,5'-azobenzenetetracarboxylate organic linkers and tested this MOF for the delivery of a biomedical gas, nitric oxide (NO). Tamames-Tabar et al.[158] synthesized another Zn- and azelate-based BioMIL-5 for the

## CHAPTER II: Literature Review

treatment of skin disorders. These pioneering studies showed that the use of endogenous linkers and non-toxic metal sites of MOFs makes bio-MOFs possible candidates for biological applications.

Regarding the toxicity of ligands, few MOFs with exogenous linkers, including MIL series, UiO series, ZIF-8, and Cu-BTC, have been tested for various biomedical applications. For example, the first study on drug storage and drug delivery of MOFs was carried by Horcajada et al.[159] Two chromium (Cr)-based MOFs, MIL-100 and MIL-101, were tested to deliver an analgesic and anti-inflammatory drug, ibuprofen. These two MOFs were found to be higher drug ibuprofen loadings (0.35 g/g and 1.38 g/g, respectively) than that of a traditional material, mesoporous silica, (0.35 g/g) due to their large pore apertures (25-34 Å), and high surface areas (3100-5900 m<sup>2</sup>/g). Release of ibuprofen from MIL-100 and -101 were then investigated in simulated body fluid (SBF, pH=7.4) at 310 K and it occurred within 3 days and 6 days, respectively. Interactions between ibuprofen molecules and the Lewis acid metal sites of MIL series can be driving force of the drug delivery process. In the literature, there are many excellent reviews based on storage and/or delivery of different biocomponents including anticancer drugs, enzymes, hormones, and cosmetic molecules using MOFs.[148, 160, 161]

Besides experimental methods, molecular simulations can also be used to better understand drug delivery mechanisms of MOFs at the atomistic level. For example, Babarao et al.[162] performed molecular simulations for the first drug, ibuprofen, encapsulation in MIL-101 and used density-functional theory (DFT) to examine drug-host interactions. MIL-101 gave the saturated ibuprofen loading as 1.11 g/g which was consistent with the experimental

## CHAPTER II: Literature Review

measurements (1.38 g/g). This small difference might be explained by the remaining solvent molecules in experimental measurements. Similarly, Erucar et al.[163] studied storage of ibuprofen and two various cosmetic molecules, caffeine (also known as lipo-reducer), and urea (hydrating agent), in 24 various biocompatible MOFs by using molecular simulations. They reported that seven biocompatible MOFs, including Bio-MOF-100 (~1.5 g/g), Bio-MOF-102 (~2.0 g/g), RAVWIW (~1.6 g/g), RAVWUI (~1.8 g/g), RAVXAP (~2.0 g/g), RAVXET (~1.6 g/g), and RAVXIX (~2.5 g/g) outperformed the Cr-based MIL-101 (~1.4 g/g). Encapsulation of caffeine and urea in these 24 MOFs was also examined. Similarly, Bio-MOF-100 series and MOF-74 series (such as RAVVUH, RAVXIX) were found to be the best-performing MOFs for caffeine and urea adsorption. This computational study showed that properties of MOFs including chemical topologies, pore sizes and pore volumes affect their ibuprofen adsorption capacities. There are a few reviews on drug delivery in MOFs.[164-166]

MOFs have also been tested for storage of biomedical gases, which can be produced endogenously in the human body and vital for life, such as carbon monoxide (CO), NO, H<sub>2</sub>S, and O<sub>2</sub>. NO, which is a biological signaling (also known as gasotransmitter) molecule, has been used in various biomedical applications for antibacterial, antithrombotic and wound healing purposes.[167] Hinks et al.[168] tested NO storage in two different Ni- and Co-based MOFs and reported that their uptakes as almost 7 mol NO/1 kg of MOFs at 1 bar and 310 K. As we discussed above, BioMIL-3 was tested for NO storage and its adsorption capacity was reported as 0.08 mol/kg at 1 bar by Miller et al.[157] Although BioMIL-3 adsorbed low NO molecule, this MOF

## CHAPTER II: Literature Review

could be a promising candidate due to its slow NO release profile without any burst effect. Another gas transmitter molecules, CO, can bind the iron metal sites in hemoglobin and play a significant role to deliver O<sub>2</sub> in the human body.[169] Ni-based CPO-27, was tested for CO storage at 303 K by Chavan et al.[170] CO was reported to bond strongly to Ni<sup>2+</sup> ions due to strong electrostatic interactions. H<sub>2</sub>S, the third gas transmitter gas, has also been used for the treatments of diabetes, cardiovascular diseases because of its anti-inflammatory effects.[171] MOFs have great potential for H<sub>2</sub>S storage and delivery.[171] For example, Allan et al.[172] studied H<sub>2</sub>S uptake in two MOFs, CPO-27-M (M: Ni and Zn), at 1 bar and 303 K and reported their uptake as almost 12 mol/kg, and 10 mol/kg, respectively. After 30 minutes, the amount of H<sub>2</sub>S delivery from Ni-CPO-27 (1.8 mol/kg) was also found to be higher than Zn-CPO-27 (0.5 mol/kg) due to strong interaction between Ni atoms and H<sub>2</sub>S molecules. O<sub>2</sub> has been another medical gas and used for various activity of humans' cells, organs and tissues. O<sub>2</sub> has been supplied by inhalation mask for the treatment of CO poisoning and/or respiratory insufficiency.[72] As discussed above, MOFs can be widely tested for O<sub>2</sub> storage.[76, 77]

In the last decades, MOFs have been widely studied for gas storage, gas separation and biological applications. To guide the experimental studies and identify promising candidates for different applications, computational studies especially have importance. Details of molecular simulations are mentioned in the following chapter.

## CHAPTER III

### COMPUTATIONAL METHODOLOGY

Molecular simulations are used to provide reasonable predictions about adsorption or diffusion mechanisms of a material. Simulations provide an insight into the transport phenomena at the molecular scale which cannot easily be accessible by using experimental methods. This chapter introduces our material datasets, structural analysis of materials, and the computational methodology used in this thesis to estimate adsorption and diffusion coefficients of gas molecules in MOFs. Grand canonical Monte Carlo (GCMC) and equilibrium molecular dynamics (EMD) simulation methods are introduced to predict equilibrium adsorption properties of adsorbates (gas molecules) and their diffusion coefficients.

#### *3.1 Material Selection*

This thesis provides three different studies. In Chapter IV, 225 different materials including 166 COFs, 16 IRMOFs, and 43 ZIFs were studied for  $\text{CCl}_4$  adsorption. COFs and ZIFs were chosen because of their highly robust structures.[44, 173] IRMOFs were also selected since a considerable amount of research has been done on these materials because of their functional groups in the pores, exhibiting favorable adsorption sites for gas molecules.[27] The crystal structures of COFs were taken from the solvent-free COF database constructed by Tong et al.[48] The crystal structure of IRMOFs and ZIFs were also taken from CSD.[31] Solvent in these materials were cleaned by using an algorithm developed by Moghadam et al.[23] In Chapter V, 309 COFs in the



### CHAPTER III: Computational Methodology

recent CoRE-COF database[46] were considered to investigate H<sub>2</sub> storage.

In Chapter VI, bio-compatible MOF library was created to investigate their performances for various biomedical applications. As discussed above, MOFs with endogenous linkers are biologically friendly, non-toxic and bio-compatible and can be used for different biological studies. The current MOF database (69,699 MOFs) and a search algorithm available in CSD[31] with the keywords as follows: acetamide, acetate, adamantane, adenine, amino, aspartate, citrate, cyclodextrin, dicyanamide, formadide, formate, fumarate, gallate, glutamate, glutarate, glycine, guanine, maleato, malonate, metalloporphyrin, muconate, oxalate, penicillin, peptide, porphyrin, proline, succinate and thymine were used. These 28 different endogenous linkers were previously defined in the literature.[148, 174] After using a search algorithm, 1472 MOFs with these linkers were found. Various MOFs, which were tested in the previous study for biomedical applications, were also added. These MOFs included 9 MIL series, 10 MOF-74 series and 34 well-known MOFs, such as Cu-BTC, UiO-66, and ZIF-8.[148, 159, 175-177] MIL series were reported that they gave high performance for drug encapsulation applications due to their large surface areas (ranged from 200 to 3000 m<sup>2</sup>/g).[159, 175, 176] MOF-74 series were also used as drug carriers because of their non-toxic metal sites (Mg<sup>2+</sup> and Zn<sup>2+</sup> cations) and large pore sizes (ranging from 11 to 54 Å).[177] At the end of this selection criteria, total of 1525 MOFs with endogenous linkers were found. To investigate these MOFs for any biomedical applications, metal toxicity, which is evaluated by the oral lethal dose parameter (LD<sub>50</sub>), should be considered. Therefore, metals such as Cu, Fe, Mg, Mn (manganese) and Zn, are commonly preferred based on their LD<sub>50</sub>. [148] For this reason, these MOFs were also considered based on their metal sites. Among 1525

## CHAPTER III: Computational Methodology

MOFs, the common metal sites are as follows: Co (165 MOFs), Cu (227 MOFs), Fe (76 MOFs), Mg (37 MOFs), Mn (221 MOFs), Zn (260 MOFs), and Zr (18 MOFs). However, a few MOFs (122) in this library may have toxicity in metals, such as mercury (Hg), Cd, lead (Pb), and ruthenium (Ru). The crystal structures of 1525 MOFs were taken from CSD.[31] The same modified crystal structures of bio-MOF-1, -100, -101, and -102, which were studied for ibuprofen, caffeine and urea encapsulation[163], were used. Prior to molecular simulations, a Python code developed by Moghadam et al.[23] were used to clean solvent molecules in these MOFs.

### ***3.2 Structural Characterization***

Calculation of the structural properties of MOFs such as pore sizes is highly required in computational studies to classify materials with their geometrical characteristics. Zeo++[178], based on Voronoi decomposition, is a useful tool for structure analysis of a material. Voronoi decomposition is a graphical shown method for void space of the structure. While using Voronoi decomposition, the void space of a material is divided points and built a Voronoi network to provide information about geometry and topology of the material. Detailed discussion of structural analysis for crystalline materials and membranes by performing Voronoi decomposition can be found in the literature.[179, 180]

The largest cavity diameter (LCD), and pore limiting diameter (PLD) are used to give information about pore geometry. LCD is defined as the largest cavity in a framework, whereas PLD is a minimum limiting pore aperture on the diffusion path through the framework. Figure 3.1 shows an illustration for these diameters. The other important structural parameters are surface area

(SA), and pore volume (PV) of a material. SA is defined as the accessible surface in which a sphere with a probe radius can be contacted on each pair of the atomic surface of the framework without any penetration between probe and framework's atoms. Accessible SA helps us to understand the performances of materials for adsorption applications. PV is described as the reachable total volume by the framework's atoms. This calculation is obtained by different methods as using zero probe size (helium probe size) to determine the maximum free volume (accessible PV). In Zeo ++ code[178], both SA and PV are determined using a Monte Carlo sampling approach.

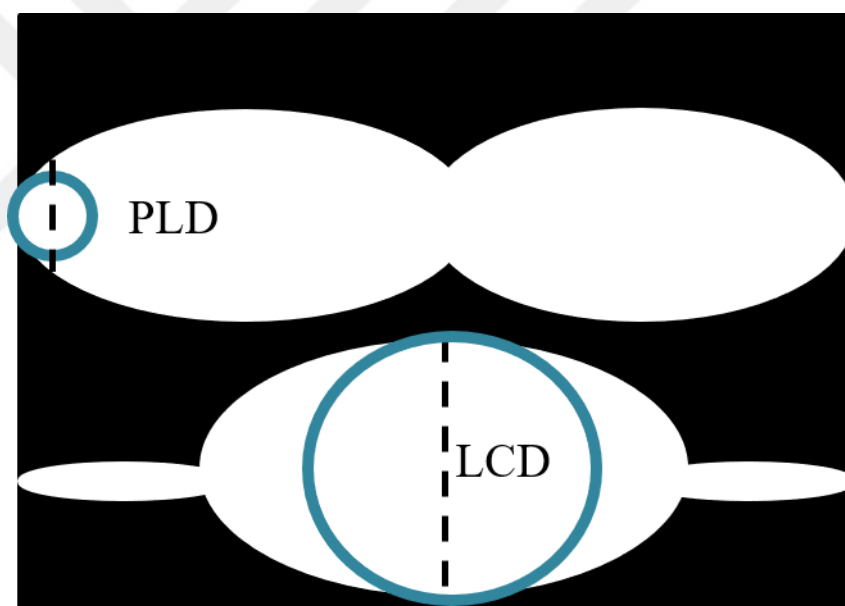


**Figure 3.1** A representation for the LCD and PLD in a pore.

All LCDs, PLDs, SAs, and PVs of MOFs and COFs were calculated by Zeo++ software.[178] SA calculations were performed by using nitrogen kinetic diameter as 1.86 Å and the trial number was set to 2000. For free volume calculations, zero probe size was used, and the number of trials was set to 50,000. Accessible PVs and porosities were also calculated using the helium probe (1.29 Å). Finally, open (unsaturated) metal sites in the frameworks, which give

information about the binding site of MOFs, were also identified by Zeo++[178].

### 3.3 Gas Adsorption Simulations of COFs and MOFs

Monte Carlo (MC) technique provides information to determine the equilibrium properties of materials using a stochastic approach (non-time dependent). This simulation technique can be described as machine experiments for nanoporous materials. In MC simulations, different ensembles are assumed in a desired system. For example, the canonical ensemble ( $N, V, T$ ), isobaric- isothermal ensemble ( $N, p, T$ ), and grand canonical ensemble ( $\mu, V, T$ ) have been employed for the types of adsorption. A detail methodology of these ensembles can be found in the literature.[181] Depending on the type of ensemble, several random moves such as insertion, swap, rotation should be identified. The corresponding moves create various fluctuations in energy. An acceptance or a rejection criterion is defined for the terminal step.

To determine the number of adsorbed gas molecules in simulations, the grand canonical ensemble ( $\mu, V, T$ ) where volume ( $V$ ), temperature ( $T$ ), and chemical potential ( $\mu$ ) are kept constant is commonly used to be consistent with the gas adsorption experiments. While these parameters are constant, the energy of the system and the number of adsorbed molecules ( $N$ ) fluctuate. In a typical experimental system, chemical potential and temperature of the gas molecules to be adsorbed and gas molecules in the outside of the adsorbent are equal at the equilibrium. In this ensemble, pressure is not directly involved. However, chemical potential is related to the pressure and/or fugacity with an equation of state (EOS). In the equilibrium stage, the amount of adsorbed gas molecules is determined by using a statistical average approach in GCMC simulation. These results obtained from GCMC simulations can be compared

## CHAPTER III: Computational Methodology

with the available experimental data obtained from gravimetric and/or volumetric measurements.

In statistical thermodynamics, Boltzmann factor is described as  $\exp[-\beta U]$ .  $U$  is the total energy. Additionally, molecular partition function is shown with  $Q$  and defined as the summation of Boltzmann factors, as follows:

$$Q = \sum_{k=0}^{\infty} \exp[-\beta U] \quad (3.1)$$

Statistical thermodynamics should be used to better understand the GCMC simulations. First, the partition function is expressed for canonical ensemble as follows:

$$Q(N, V, T) = \frac{V^N}{\Lambda^{3N} N!} \int ds^N \exp[-\beta U(s^N)] \quad (3.2)$$

where  $s^N$  shows the fractional (reduced) coordinates.  $\Lambda$  represents the Broglie thermal wavelength which is calculated by  $\sqrt{\hbar^2 / (2\pi \cdot m \cdot k_B \cdot T)}$ .  $\hbar$ ,  $m$  and  $k_B$  show Planck constant, molecular mass of the particle, and Boltzmann constant, respectively.

Then, our system is coupled a gas reservoir that contains  $N$  number of particles and volume as  $V$ . The total volume of this reservoir equals to  $V_0 - V$ , where  $V_0$  is the initial volume. The number of particles obtained in the reservoir equals to  $M - N$  where  $M$  is the total number of particles in the whole system. Our total partition function is equal to the product of Equation 3.2 as follows:

$$\begin{aligned}
 & Q(M, V, V_0, T) \\
 &= \sum_{N=0}^M \left[ \frac{(V_0 - V)^{M-N}}{\Lambda^{3(M-N)} (M-N)!} \int ds^{M-N} \right] \times \left[ \frac{V^N}{\Lambda^{3N} N!} \int ds^N \exp[-\beta U(s^N)] \right] \\
 &= \sum_{N=0}^M \frac{V^N (V_0 - V)^{M-N}}{\Lambda^{3M} (M-N)! N!} \int ds^{M-N} \int ds^N \exp[-\beta U(s^N)] \quad (3.3)
 \end{aligned}$$

Assuming our selected reservoir is much larger than the system, the limit of  $M$  goes to infinity. Particle density ( $\rho$ ) equals to  $M/V$  and the chemical potential can be calculated by  $\mu = k_B T \ln \Lambda^3 \rho$ . If the limit of  $M$  goes to infinity:

$$Q(\mu, V, T) = \sum_{N=0}^{\infty} \frac{\exp(\beta \mu N) V^N}{\Lambda^{3N} N!} \int ds^N \exp[-\beta U(s^N)] \quad (3.4)$$

In GCMC simulations, Equation 3.4 is the main partition function.

As discussed above, the random moves used in grand canonical ensemble are rotation or translation displacement, insertion and deletion for single-gas components. An acceptance criterion for translation/rotational displacement of the particles with a probability ( $P$ ) can be written as follows:

$$P = \min\{1, \exp(-\beta \Delta U)\} \quad (3.5)$$

where  $\Delta U$  shows the change in total energy. While  $\Delta U$  is lower than zero or the magnitude of  $\Delta U$  is lower than randomly number (0-1), the move is accepted.

For the insertion criterion, the particle is randomly placed at a position in the system and this move can be accepted with a probability as follows:

$$P = \min\left\{1, \frac{\beta f V}{N+1} \exp(-\beta \Delta U)\right\} \quad (3.6)$$

where  $f$  represents the fugacity.

Deletion is the move for removing of the random particles and an acceptance probability can be written as:

$$P = \min \left\{ 1, \frac{N}{\beta fV} \exp(-\beta \Delta U) \right\} \quad (3.7)$$

For mixture GCMC simulations, an identity change move should be used for different molecules in the mixture. Probability of acceptance criterion can be given as:

$$P = \min \left\{ 1, \frac{f_j N_i}{f_i (N_j + 1)} \exp(-\beta \Delta U) \right\} \quad (3.8)$$

where  $i$  and  $j$  shows two different components obtained in the mixture.

Acceptance rate is commonly fixed in a ranged between 0.4 to 0.5.

Molecular simulations are performed using three common cycles including initialization, equilibration and production. These cycles used in GCMC simulations should be controlled to evaluate the total energy and to obtain accurate results.

In GCMC simulations, models for adsorbents (COFs or MOFs) and for the adsorbates including  $H_2$ ,  $CCl_4$ ,  $O_2$ ,  $N_2$  are used to compute the energetic interactions between their two atoms. For describing energetic interactions between adsorbent and adsorbate, various interatomic potentials, also known as force fields, are described in the literature. To model interatomic interactions (non-bonded) between two atoms, Lennard-Jones (LJ) 12-6 potentials and Coulombic interactions are used to predict repulsion/dispersion forces, and electrostatic interactions, respectively using Equation 3.9 as follows:

$$U_{ij}(r) = 4\varepsilon_{ij} \left( \left( \frac{\sigma_{ij}}{r} \right)^{12} - \left( \frac{\sigma_{ij}}{r} \right)^6 \right) + \frac{q_i q_j}{4\pi \varepsilon_0 r} \quad (3.9)$$

where  $U_{ij}$  is the potential energy between atoms  $i$  and  $j$ ,  $\varepsilon_{ij}$  is the well depth,  $r$  shows the separation distance from the center of one particle to that of other particle,  $\sigma_{ij}$  represents the molecular length scale based on the particle diameter.

## CHAPTER III: Computational Methodology

Moreover, the term of  $r^{12}$  represents the repulsive forces and the term of  $r^6$  shows the attractive long-range forces. To save the computational cost, a cut-off radius is used in LJ 12-6. This means that the long-range interactions between far away atoms are ignored. Periodic boundary conditions are commonly applied in all simulations to avoid surface effects. The Lennard-Jones parameters of the individual frameworks' atoms are generally taken from generic force fields such as Universal Force Field (UFF)[182] and DREIDING[183]. All the atoms in the periodic table are defined in these generic force fields. UFF[182] parameters are described based on the hybridization and connectivity of the elements. DREIDING[183] parameters are defined for organic compounds based on their crystal structures. The Lorentz-Berthelot combining rules are used for cross interactions between adsorbate/adsorbent or adsorbate/adsorbate.[184, 185] The Lorentz rule[184] is performed by using arithmetic mean of molecular lengths ( $\sigma_{ij} = (\sigma_{ii} + \sigma_{jj})/2$ ). The Berthelot rule[185] is performed by using geometric mean of well depths ( $\epsilon_{ij} = \sqrt{\epsilon_{ii} \cdot \epsilon_{jj}}$ ).

To calculate electrostatic interactions, Coulomb potential (the second part of the Equation 3.1) are used where  $q_i$ ,  $q_j$ , and  $\epsilon_0$  represent partial atomic charges of  $i$  and  $j$ , and the electric constant. The partial charges of the frameworks' atoms can be estimated from the quantum chemical calculations such as DFT and approximate methods such as charge equilibration (Qeq). Qeq, the first charge equilibration method, were reported by Rappe et al.[186] This method assigns frameworks' atoms based on the available ionization potential, electron affinity, and atomic radius. The molecular system electrostatic energy ( $E$ ) composed of  $N$  number of atoms is expressed as:



$$\begin{aligned}
E(q_1, q_2, \dots, q_N) &= \sum_{A=1}^N \left[ E_{A0} + \chi_A^0 q_A + \frac{1}{2} J_{AA}^0 q_A^0 \right] \\
&+ \frac{1}{2} \sum_{A=1}^N \sum_{B=1, B \neq A}^N J_{AB} q_A q_B
\end{aligned} \tag{3.10}$$

where the first summation term is for each charged atom and the second term is for interatomic Coulombic interactions.  $E_{A0}$  is the ground state energy,  $\chi_A^0$  is atomic electronegativity and  $J_{AA}^0$  shows the self-Coulomb integral of atom A. Ewald summation is used to calculate long-range electrostatic calculations.[187]

The quantum effects of small gas molecules, such as  $H_2$ , should be considered at low temperatures because of their low molecular masses. In molecular simulations, the Feynman-Hibbs corrections (Equation 3.11) are used for  $H_2$  storage in COFs to include the quantum effects at 77 K.

$$U_{FH}(r) = U_{LJ}(r) + U_{coul}(r) + \frac{\hbar^2}{24\mu kT} \nabla^2 U_{LJ}(r) \tag{3.11}$$

Herein,  $\hbar$  shows the Planck constant divided by  $2\pi$ . The terms of  $\mu$ ,  $k$  and  $T$  are the reduced mass, the Boltzmann constant, and absolute temperature, respectively.

To compare the results of GCMC simulations with experimental values, absolute adsorbed gas amount ( $n_{abs}$ ), which cannot be directly measured, is converted to the excess adsorption ( $n_{ex}$ ). The excess adsorption can be explained by the difference between the amount of the absolute adsorbed gas and the amount of bulk gas in the adsorbed region and calculated from:

$$n_{ex} = n_{abs} - V_p \rho_{bulk}(P, T) \tag{3.12}$$

where,  $V_p$  shows the pore volume ( $cm^3/g$ ), and  $\rho_{bulk}$  is the density of the gas in the bulk phase ( $g/cm^3$ ) calculated with Peng-Robinson EOS at temperature ( $T$ )

and pressure (P).

Isosteric heat of adsorption ( $Q_{st}$ ) is also computed in GCMC simulations to identify favorable interactions between frameworks' atoms and gas molecules using the ensemble average fluctuations[188]:

$$Q_{st} = RT - \left( \frac{\langle U_{ads} \times N_{ads} \rangle - \langle U_{ads} \rangle \times \langle N_{ads} \rangle}{\langle N_{ads}^2 \rangle - \langle N_{ads} \rangle \times \langle N_{ads} \rangle} \right) \quad (3.13)$$

where R and T are ideal gas constant, and temperature, respectively.  $\langle U_{ads} \rangle$  and  $\langle N_{ads} \rangle$  represent the average potential energy for adsorbed phase, and the average amount of adsorbate molecules in frameworks. In GCMC, these brackets  $\langle \dots \rangle$  symbolize for an average of a quantity.

### 3.3.1 Details of GCMC Simulations

In this thesis, all GCMC simulations were performed as implemented in RASPA [189] to calculate the number of adsorbed gas molecules in a specified temperature and pressure. To compute the chemical potential, Widom particle insertion method[188] was used. Peng-Robinson EOS[190] was also used to convert the bulk pressure to the corresponding fugacity. For single-component gas simulations, three types of trial moves including translation, reinsertion and swap of the molecules were considered. For gas molecules with quadrupole moments, rotation move was also considered. This move is used for rotating a molecule that selected randomly. In gas mixture simulations, identity change move was used for exchanging of different gas molecules that is chosen randomly. The truncated distance was assumed as 13 Å. The simulation cell lengths were increased to at least 26 Å along each dimension and periodic boundary conditions were applied in all simulations. GCMC simulations to compute  $CCl_4$  adsorption in COFs, IRMOFs, and ZIFs (Chapter IV) and  $O_2/N_2$

adsorption-based and membrane-based separation in MOFs (Chapter VI) were carried out for a total of  $1 \times 10^4$  cycles with the first  $5 \times 10^3$  cycles for initialization and the last  $5 \times 10^3$  cycles for taking ensemble averages. To obtain  $H_2$  storage in COFs (Chapter V), simulations were carried out for a total of  $1 \times 10^4$  cycles with  $3 \times 10^3$  cycles for the equilibration. Rigid frameworks were assumed for COFs and MOFs to save a significant amount of computational time.

The LJ parameters of the frameworks' atoms were taken from UFF and DREIDING. All interaction parameters for the adsorbate molecules, Ar,  $H_2$ ,  $CCl_4$ ,  $O_2$ ,  $N_2$  were given in Table 3.1. Single-site spherical LJ model was used to model for Ar[191] and  $CCl_4$ [95] molecules.  $N_2$  and  $O_2$  were modeled as three-site linear molecules with three charged LJ interaction sites located at each atom. Two sites were located at two  $N_2$  and  $O_2$  atoms and the third sites were located at their center of mass (COM) with partial point charges.[192, 193] As shown in Table 3.1,  $O_2$  molecules were modeled using two different sets of parameters.  $H_2$  molecules were modeled using two different models as (i) a single-site model,[194] and (ii) three-site linear molecule with two located at two atoms and the third one located at its center of mass.[195]

**Table 3.1** Interaction parameters and partial charges used for adsorbate molecules

Molecule	Site	$\epsilon/kB$ (K)	$\sigma$ (Å)	$q(e)$
Ar	Single site	124.070	3.380	0.000
$CCl_4$	Single site	519.730	5.140	0.000
$H_2$	COM	36.700	2.958	-0.936
	H	0.000	0.000	0.468
$H_2$	Single site	34.200	2.960	0.000

N <sub>2</sub>	COM	38.298	3.306	-0.405
	N	0.000	0.000	0.810
O <sub>2</sub>	COM	53.023	3.045	-0.112
	O	0.000	0.000	0.224
O <sub>2</sub>	COM	49.0	3.02	-0.113
	O	0.000	0.000	0.226

### 3.4 Gas Diffusion Simulations of COFs and MOFs

Diffusion is a process based on the movement of the guest molecules in a fluid. The term of self-diffusivity helps us to understand the motion of a particle. Molecular dynamics (MD) simulations are performed to calculate self-diffusivities of each adsorbates in MOFs and COFs. MD technique provides information about the motion of a particle using a time-dependent approach, unlike MC method.

MD simulations are performed in several steps such as initialization, equilibration, and production. In the initialization step, a MC simulation with an NVT ensemble, in which number of molecules, volume, and temperature are fixed, is performed to locate the adsorbate molecules within the framework. Initial velocities of the particles can be assigned using the Maxwell-Boltzmann distribution.[196, 197] There is a simple relation between the kinetic energy of the molecule and T as  $k_B T = m \langle v_i^2 \rangle$ , where  $v_i$  shows the velocity of the  $i^{\text{th}}$  particle. However, constant T is not equivalent with the constant kinetic energy of the particle. Thus, in canonical ensemble (NVT), kinetic temperature can fluctuate. The velocities are calculated until the total momentum is equal to zero. Then, in equilibration step, MD simulation is also performed at NVT ensemble. In the final step, production, ensemble and properties that requested are calculated. Newton's equations of motion are solved numerically to

## CHAPTER III: Computational Methodology

determine the velocities in each step as follows:

$$F_i = m_i \ddot{r}_i \quad (3.14)$$

where,  $F_i$ ,  $m_i$ , and  $r_i$  show force, mass, and position of the  $i^{\text{th}}$  particle, respectively. The force on the particles is calculated by using the derivative of the potential which is defined by LJ 12-6 and Coulombic interactions. To solve Newton's equation of motion, Verlet algorithm is used. This algorithm is based on the position of the particle at different time ( $t$ ) period and acceleration as follows:

$$r(t + \Delta t) = r(t) + \dot{r}(t)\Delta t + \frac{1}{2}\ddot{r}(t)\Delta t^2 + \frac{\partial^3 r}{\partial t^3} \frac{\Delta t^3}{3!} + \dots \quad (3.15)$$

and

$$r(t - \Delta t) = r(t) - \dot{r}(t)\Delta t + \frac{1}{2}\ddot{r}(t)\Delta t^2 - \frac{\partial^3 r}{\partial t^3} \frac{\Delta t^3}{3!} + \dots \quad (3.16)$$

These two equations are summed and:

$$r(t + \Delta t) = 2r(t) - r(t - \Delta t) + \ddot{r}(t)\Delta t^2 + \dots \quad (3.17)$$

the term of  $v$  (velocity) disappears. Position of the particles can be determined without the  $v$  of the components. Thus, Verlet algorithm cannot be directly used to determine the  $v$  of the particle in a new position. However,  $v$  can be accurately estimated from the trajectory with the order  $\Delta t^2$  as follows:

$$\dot{r}(t) = v(t) = \frac{r(t + \Delta t) - r(t - \Delta t)}{2\Delta t} \quad (3.18)$$

Also, this equation can be used for the estimation of the kinetic energy of the components and the total energy.

During MD simulations, new velocity, position and acceleration of the particle are predicted at  $t+\Delta t$ . Using Equation 3.14, the force on the particle is repredicted at time  $t+\Delta t$ . This loop is repeated until the final time step for the total simulation.

Nose-Hoover (NH) thermostat[198, 199] is used to keep the temperature constant during the simulation. The self-diffusivities of gas molecules in the structures' pores are calculated from the MD trajectories in a defined simulation time and estimated from the Einstein relation[200] using the mean-squared displacement (MSD) of individual particles as follows:

$$D_{\text{self},i} = \lim_{t \rightarrow \infty} \frac{1}{dNt} \left\langle \sum_{i=1}^N [\vec{r}_i(t) - \vec{r}_i(0)]^2 \right\rangle \quad (3.19)$$

where,  $d$  is the number of spatial dimensions ( $d=2, 4$  or  $6$  for 1-, 2-, and 3-dimensions) for diffusion,  $N$  represents the number of molecules,  $\vec{r}(t)$  shows the position of the particle at time  $t$ , which is generally preferred as nanosecond. The angular brackets show the average of ensemble.

Single-component corrected diffusivity ( $D_0$ ) describes the total diffusivity of adsorbed molecules and is calculated as follows:

$$D_{0,i} = \lim_{t \rightarrow \infty} \frac{1}{dNt} \left\langle \left( \sum_{i=1}^{N_i} [r_{il}(t) - r_{il}(0)] \right)^2 \right\rangle \quad (3.20)$$

where,  $r_{il}(t)$  and  $r_{il}(0)$  are the 3-dimensional position vectors  $i^{\text{th}}$  molecule of component  $i$  at time  $t$  and initial, respectively.

The transport diffusivity ( $D_t$ ) of a single-component gas is also calculated by considering the corrected diffusivity and thermodynamic correction factor[201]:

$$D_{t,i}(c) = D_{0,i}(c) \cdot \frac{\partial \ln f_i}{\partial \ln c_i} \quad (3.21)$$

where,  $c$  and  $f$  represent the adsorbate concentration, and bulk phase fugacity, respectively.

### 3.4.1 Details of MD Simulations

In this study, GCMC simulations were first performed to examine gas adsorption in MOFs. MD simulations were then computed using the number of adsorbed gas molecules obtained from GCMC simulations. MD simulations were performed with a step size of 1 fs up to a total of 10 ns at 298 K. For each structure, MD simulations were carried out for a total of  $1 \times 10^7$  cycles with the first  $5 \times 10^4$  cycles for initialization and  $1 \times 10^5$  cycles for equilibration. Three types of moves including translation, reinsertion and rotation of molecules were considered for MD simulations. In Chapter IV, self-diffusivities of gas molecules were calculated from the slope of MSD (Equation 3.19) in the time limit (1-7 ns) of simulations. In Chapter VI, self-diffusivities of gas molecules were also calculated from the slope of MSD in the computation time limit from 1 to 5 ns.

### 3.5 Computational Screening of COFs and MOFs

Considering the large of number of COFs and MOFs, screening methods provide an opportunity for the discovery of useful adsorbent materials for adsorption-based and membrane-based gas separations. The methodology described below is used to identify the promising adsorbents and membranes studied in this thesis.

#### 3.5.1 Evaluation of Materials for Adsorption-based Gas Separation

To evaluate the adsorption-based gas separation performance of materials, several metrics including adsorption selectivity ( $S^0$ ), isosteric heat of adsorption at infinite dilution ( $Q_{st}^0$ ), adsorption selectivity ( $S_{ads}$ ), working capacity ( $\Delta N$ ), and separation potential ( $\Delta Q$ ) were considered in this thesis.

In the literature, most of the gas selectivities of MOFs were computed

at zero-coverage (infinite dilution). Selectivities performed at infinite dilution can give a quick idea for the separation performances of adsorbents.[202] At infinite dilution, adsorption selectivity is defined as the ratio of the predicted Henry's constants ( $K_{\text{Henry}}$ ) of gas species as follows:

$$S_{(i/j)}^0 = \frac{K_{\text{Henry},i}}{K_{\text{Henry},j}} \quad (3.22)$$

where,  $K_{\text{Henry}}$  shows the Henry's constants of gas species,  $i$  and  $j$ .

$Q_{\text{st}}^0$ , that is defined as difference in the partial molar enthalpy of adsorbate between the bulk and adsorbed phases is calculated at infinite dilution using Widom particle insertion method[188], as follows:

$$Q_{\text{st}}^0 = RT - (U_{\text{total}}^0) \quad (3.23)$$

where,  $R$  is the ideal gas constant (kJ/mol K),  $T$  is the temperature (K), and  $U_{\text{total}}^0$  is the total adsorption energy (kJ/mol) calculated at infinite dilution. At zero-coverage, molecular simulations were carried out  $1 \times 10^5$  MC cycles to compute Henry's constants of gas species and isosteric heat of adsorption values.

$S_{\text{ads}(i/j)}$  is the most widely used metric for evaluation of adsorbents and is described as the ratio of compositions of adsorbed gases in the adsorbent normalized by the ratio of the bulk phase compositions of components in a mixture:

$$S_{\text{ads}(i/j)} = \frac{(x_i/x_j)}{(y_i/y_j)} \quad (3.24)$$

where,  $x$  is the molar fraction of the adsorbed species and  $y$  is the molar fraction of the bulk phase. The subscripts,  $i$  and  $j$  represent the adsorbed components. Equation 3.24 defines the adsorbent selectivity for component  $i$  over  $j$ . The bulk phase compositions of mixtures are determined by industrial operating



## CHAPTER III: Computational Methodology

conditions. Comparison with  $S_{(i/j)}^0$ ,  $S_{\text{ads}(i/j)}$  is generally found to be lower since  $S_{(i/j)}^0$  do not consider the bulk composition effect. To assess the real gas separation performances of materials, performing mixture GCMC simulations is highly required.

Performances of adsorbents can also be ranked by their working capacities. Working capacity is described as the difference between the number of adsorbate molecules at a storage pressure and the number of adsorbate molecules at a desorption pressure. Equation 3.25 is used to calculate working capacity.

$$\Delta N = N_{\text{ads}} - N_{\text{des}} \quad (3.25)$$

Herein,  $N_{\text{ads}}$  is the adsorption amount and  $N_{\text{des}}$  is the desorption amount of a gas component.

A convenient metric, separation potential ( $\Delta Q$ ), is used to assess the separation potential of materials in fixed bed units.[203, 204]  $\Delta Q$ , which combines the effect of gas uptake, selectivity and composition on gas separations, can be easily used to analyze the achievable productivities in a fixed bed unit. The value of  $\Delta Q$  demonstrates the same hierarchy of gas productivities which are obtained from breakthrough simulations. The productivities of pure gases in their mixtures were predicted by using the gas uptakes obtained from binary mixture GCMC simulations as follows:

$$\Delta Q_{(j/i)} = Q_i \frac{y_j}{1-y_j} - Q_j \quad (3.26)$$

where  $\Delta Q_{(j/i)}$  is the productivity of pure  $j$  (mol of gas/ L of adsorbent in the packed bed).  $Q_i$  and  $Q_j$  are the volumetric gas uptake capacities (mol/L) which are estimated by using the framework density (kg/L) and the gravimetric gas uptake capacity (mol/kg) of the adsorbent. For separation of a quaternary mixture ( $i/j/k/l$ ),

the separation potential for  $l/ijk$  separation is given as:

$$\Delta Q_{(l/ijk)} = (Q_i + Q_j + Q_k) \frac{y_l}{1 - y_l} - Q_l \quad (3.27)$$

Here, component  $l$  is the weakest adsorbed gas within the adsorbent, which is purely recovered from the exiting gas stream from the fixed bed unit.

### 3.5.2 Evaluation of Materials for Membrane-based Gas Separation

A membrane should have both high gas selectivity and high gas permeability for an efficient separation application. A membrane with high selectivity, however low permeability, can be undesirable due to high surface area required and also, high capital cost. On the other hand, high gas permeability can be useless with low gas selectivity, since gas separation cannot be achieved with high purity.

Shell model[201] is used to calculate the single-component gas permeability through a MOF membrane. This model assumes that the diffusivity of component to be adsorbed are constant through the membrane at the average feed concentration ( $\nabla c_i$ , Equation 3.29) and permeate site. Steady-state flux ( $J$ ) is calculated based on Fick's law[201]:

$$J_i = -D_t(c_i^{ave}) \cdot \nabla c_i \quad (3.28)$$

where  $D_t$  is the transport diffusivity,  $c_i$  is the single-component gas adsorption amount and  $\nabla c_i$  is the adsorbed gas concentration gradient, that is based on the difference between permeate pressure and the feed of the membrane.

$$\nabla c_i = (c_i^{permeate} - c_i^{feed})/L \quad (3.29)$$

Steady-state flux ( $J$ ) is converted to single-component gas permeability ( $P$ ) using:

$$P_i^{pure} = J/\Delta p/L \quad (3.30)$$

where  $\Delta p$  is pressure drop and  $L$  is membrane thickness.[205]

Permeabilities of gas species in their binary mixture,  $P_i$  (also  $P_j$ , mol/m/s/Pa) is determined by using the following equation that was suggested by Krishna et al.[206]

$$P_i^{\text{mix}} = \frac{\phi \times D_{i,\text{self}} \times c_i}{f_i} \quad (3.31)$$

where,  $\phi$  is the fractional pore volume (porosity),  $c_i$  is the concentration of the component at the upstream of the membrane (mol of gas/m<sup>3</sup> of accessible pore volume of materials). This concentration is the amount of adsorbed gas obtained from binary mixture GCMC simulations and defined in terms of accessible pore volume of materials.  $D_{i,\text{self}}$  is the self-diffusivities of gas species (m<sup>2</sup>/s),  $f_i$  is the bulk phase fugacity (Pa) of the component. To compute the accessible pore volume per unit cell of a material and the porosity in Equation 3.32, helium probe is used. In the literature results for permeability are commonly reported as Barrer (1 Barrer=3.348 × 10<sup>-16</sup> mol/(m<sup>2</sup>·s·Pa)). [126]

Mixture gas selectivity of membranes is determined as the ratio of gas permeabilities of the (as represented by  $i$  and  $j$ ) components in mixture:

$$S_{\text{mem}(i/j)} = \frac{P_i}{P_j} \quad (3.32)$$

To predict the membrane-based gas separation performances of materials, both mixture adsorption and diffusion data are used. Keskin et al.[207] also showed a valid approximation to predict membrane selectivity,  $S_{\text{mem}(i/j)}$ , of MOFs for a desired gas separation as follows:

$$S_{\text{mem}(i/j)} = S_{\text{ads}(i/j)} \times S_{\text{diff}(i/j)} \quad (3.33)$$

where,  $S_{\text{diff}(i/j)}$  is self-diffusivity for gas mixtures and is estimated as the ratio of self-diffusivities of gas species at the adsorbed initial loadings ( $c_i / c_j$ ) in the

mixture.

$$S_{\text{diff (i/j)}} = \frac{D_{i,\text{self}}(c_i/c_j)}{D_{j,\text{self}}(c_i/c_j)} \quad (3.34)$$

Figure 3.2 shows a trade-off between gas permeability and gas selectivity of various membranes for a separation application.  $i$  and  $j$  represents the gas components in the mixture.

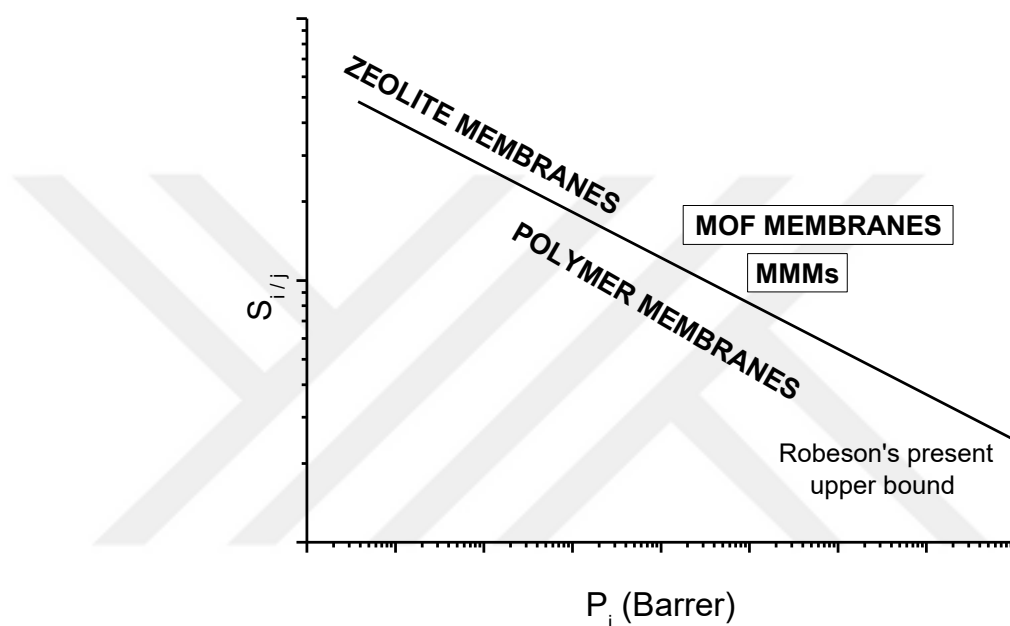


**Figure 3.2** Relations between permeability of the  $i$  component and  $i/j$  selectivity. Robeson's upper bound[126] was also demonstrated.

As shown in Figure 3.2, materials that surpass Robeson's upper bound, can be promising membranes for desired applications. For example, polymeric membranes exhibit generally high selectivity whereas low permeability. However, a large number of available MOF membranes can exhibit high performance. [140, 202]

## CHAPTER IV

# MOLECULAR SIMULATIONS OF COFs, IRMOFs AND ZIFs FOR ADSORPTION-BASED SEPARATION OF CARBON TETRACHLORIDE FROM AIR<sup>1</sup>

### 4.1 Motivation

In this chapter, separation performances of 153 COFs, 14 IRMOFs, and 8 ZIFs were assessed for adsorption-based separation of CCl<sub>4</sub> from binary mixtures, including CCl<sub>4</sub>/Ar, CCl<sub>4</sub>/N<sub>2</sub>, and CCl<sub>4</sub>/O<sub>2</sub> at infinite dilution and 298 K by using GCMC simulation methods. Single-component, binary mixture and quaternary mixture adsorption isotherms in the top performing materials, which gave the highest adsorption selectivity towards CCl<sub>4</sub>, were examined at 298 K and a various pressure range. Quaternary mixture adsorption isotherms were then computed at 298 K considering air mixture as Ar (0.999%), CCl<sub>4</sub> (0.1%), N<sub>2</sub> (77.922%) and O<sub>2</sub> (20.979%). Adsorption selectivities and separation potentials of the best candidates were also estimated. MD simulations were finally performed to examine diffusion of Ar, CCl<sub>4</sub>, N<sub>2</sub> and O<sub>2</sub> as single-component and air mixtures in the most promising material. So far, there are only two different types of MOFs which were tested for CCl<sub>4</sub> uptake. Considering the large number of synthesized MOFs in the literature, it is highly required to examine the potential of various MOFs which have different physical and chemical properties for efficient CCl<sub>4</sub> removal from air. Results of this computational study will give information to identify the best performing materials for CCl<sub>4</sub> removal from air.

---

<sup>1</sup>The results given in this chapter were published in Journal of Molecular Graphics and Modelling with following reference: Gulcay, E., & Erucar, I. (2019). Molecular simulations of COFs, IRMOFs and ZIFs for adsorption-based separation of carbon tetrachloride from air. *Journal Molecular Graphics and Modelling*. 86. 84-94.

## 4.2 Simulation Details

In this chapter, our GCMC simulation results were compared with the available experimental data of Kitagawa's group[208] and Chen's group[97], and computational data of Calero's group[95, 96] for single-component adsorption in CPL-11, Cu-BTC and MIL-101(Cr). Single-component adsorption of Ar, N<sub>2</sub> and O<sub>2</sub> and their quaternary mixture adsorption in Cu-BTC were also studied. The crystal structure of CPL-11, which has a one-dimensional porous coordination pillared layer structure with large pore sizes (10 Å×6 Å), was taken from the study of Kitagawa's group.[208] Molecular simulations were performed under the same conditions with the experiments (at 298 K and a ranged pressure from 1×10<sup>-3</sup> to 0.1 bar). Cu-BTC, which has Cu-Cu dimers with a three-dimensional network giving pore sizes range from 7 to 9 Å, with a refcode FIQCEN[42] was taken from CSD.[31] CCl<sub>4</sub> uptakes in Cu-BTC were computed at 298 K and up to 0.1 bar. The crystal structure of MIL-101[209], which has large pore sizes (30 Å×34 Å) and high surface area (5900 m<sup>2</sup>/g), was taken from the structure database of RASPA[189] simulation package. CCl<sub>4</sub> uptake in MIL-101(Cr) was computed at 303 K to be consistent with the experiments.[97]

225 different materials including 166 COFs, 16 IRMOFs, and 43 ZIFs were studied. Figure 4.1 illustrates the relation between PVs and SAs for 225 materials and the color dots represent the distribution of LCDs. The complete list of all these materials with their common names and structural properties were given in Table A.1.

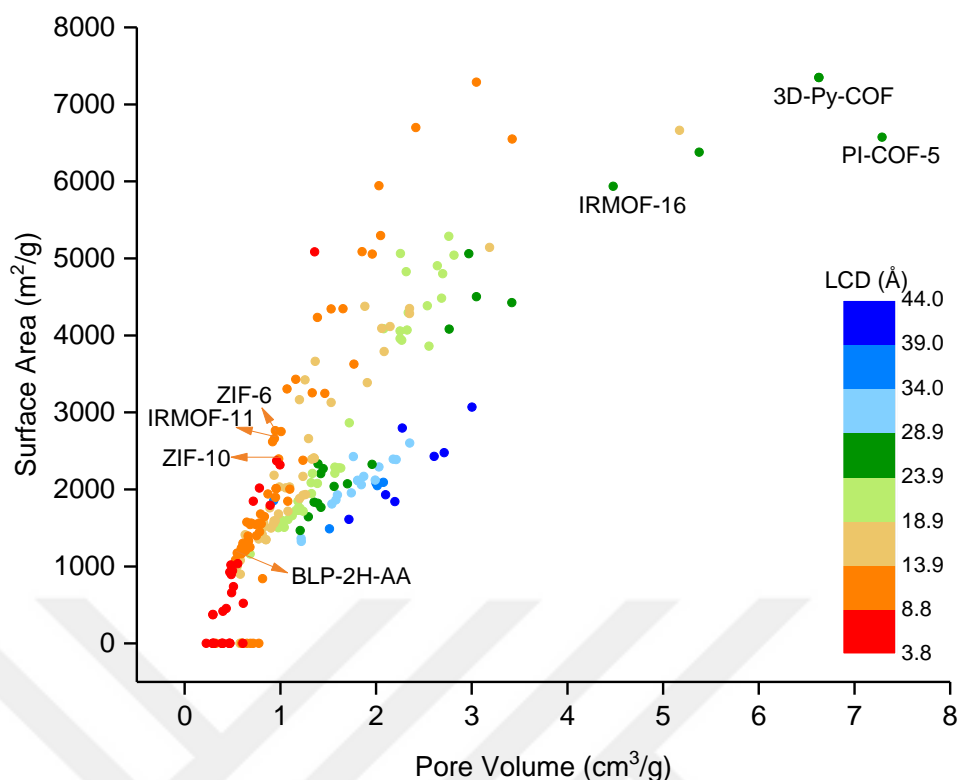


**Figure 4.1.** Comparison of LCDs, pore volumes and surface areas of COFs, IRMOFs and ZIFs.

Among 225 materials, COFs have higher LCD values (from 4.9 to 43.9 Å) than IRMOFs (10.1-25.4Å) and ZIFs (3.9-35.6Å). Moreover, LCD/PLD ratios of these materials were determined to identify the uniformity among channels or windows. The calculated LCD/PLD ratio ranged from 1.0 to 1.8 for COFs, 1.3 to 6.1 for IRMOFs, and 1.1 to 7.2 for ZIFs. This structural analysis showed that channels within COFs have almost the same size as the large cavities, indicating that COFs have more uniform structures than IRMOFs and ZIFs. The calculated SAs (PVs) of all materials ranged from 372 m<sup>2</sup>/g (0.2 cm<sup>3</sup>/g) to 7346.9 m<sup>2</sup>/g (7.3 cm<sup>3</sup>/g), respectively. Among the materials we considered, 3D-Py-COF (Py: pyrene-based) has the largest SA (7346.9 m<sup>2</sup>/g) and a very high PV (6.6 cm<sup>3</sup>/g). Similar to 3D-Py-COF, PI-COF-5 (PI: polyimide) has a very large SA (6574.3 m<sup>2</sup>/g) and the highest PV (7.3 cm<sup>3</sup>/g). 3D-Py-COF has square-like pores and pts

## CHAPTER IV: Molecular Simulations of COFs, IRMOFs and ZIFs for Adsorption-based Separation of Carbon Tetrachloride from Air

topology whereas PI-COF-5 has diamond-like pores. Among IRMOF series, IRMOF-16 has the highest PV ( $4.5 \text{ cm}^3/\text{g}$ ) and a very large SA ( $5935.6 \text{ m}^2/\text{g}$ ). ZIFs have generally lower LCDs, PVs and SAs than COFs and IRMOFs. Among ZIFs, ZIF-10 has the highest PV ( $\sim 1.0 \text{ cm}^3/\text{g}$ ) and a very large SA ( $2395.0 \text{ m}^2/\text{g}$ ), but a mediocre LCD ( $12.5 \text{ \AA}$ ). Our results showed that 24 materials (1 COF, 2 IRMOFs and 21 ZIFs) have almost zero accessible SAs as shown in Figure 4.1 and these materials were excluded from further analysis. Therefore, a total of 201 materials that have non-zero accessible SAs was considered for GCMC simulations. The adsorption selectivities of 201 materials for  $\text{CCl}_4$  separation from  $\text{CCl}_4/\text{Ar}$ ,  $\text{CCl}_4/\text{N}_2$ ,  $\text{CCl}_4/\text{O}_2$  mixtures were computed at 298 K and infinite dilution and 26 materials (12 COFs and 14 ZIFs) which gave infinite selectivities were excluded. Finally, a total of 175 materials (153 COFs, 14 IRMOFs and 8 ZIFs) was considered for adsorption-based  $\text{CCl}_4$  separation.

Initially, these 175 materials were computed for Henry's constants and isosteric heats of Ar,  $\text{CCl}_4$ ,  $\text{N}_2$ , and  $\text{O}_2$  at 298 K and infinite dilution. Then the most promising three materials in each group of COFs, IRMOFs and ZIFs, which gave the highest  $\text{CCl}_4$  selectivity at infinite dilution and 298 K, were selected. Single-component adsorption isotherms of Ar,  $\text{CCl}_4$ ,  $\text{N}_2$ , and  $\text{O}_2$  in these three materials were computed at 298 K and a wide range of pressure ( $1 \times 10^{-5}$  - 10 bar). Herein, it is important to note that we initially performed our simulations at infinite dilution using a screening approach to identify the best candidates for  $\text{CCl}_4$  separation at 298 K. To investigate the potential of the promising adsorbents in detail, we considered the saturated vapor pressure of  $\text{CCl}_4$  as almost 15 kPa at 298 K. Binary mixture simulations were considered as follows:  $\text{CCl}_4/\text{Ar}$ ,  $\text{CCl}_4/\text{N}_2$  and  $\text{CCl}_4/\text{O}_2$  at 298 K up to 15 bar and a bulk



## CHAPTER IV: Molecular Simulations of COFs, IRMOFs and ZIFs for Adsorption-based Separation of Carbon Tetrachloride from Air

ratio of 1:99. We finally computed quaternary mixture adsorption isotherms of Ar (0.999%), CCl<sub>4</sub> (0.1%), N<sub>2</sub> (77.922%) and O<sub>2</sub> (20.979%) in the top three candidates by mimicking the air compositions[96] at 298 K up to 150 bar. To analyze the effect of water vapor, the molar ratio of five component mixture of Ar/CCl<sub>4</sub>/N<sub>2</sub>/O<sub>2</sub>/H<sub>2</sub>O was fixed at Ar:CCl<sub>4</sub>:N<sub>2</sub>:O<sub>2</sub>:H<sub>2</sub>O=0.0097/0.00097/0.7537/0.2029/0.0328. In order to keep the relative humidity of the system constant, the partial pressure of water was kept at  $3.28 \times 10^{-2}$  bar, which is the 80% of the vapor pressure of the TIP4P water model.[210]

The potential parameters of all frameworks' atoms were taken from the Dreiding Force Field.[183] However, the Universal Force Field (UFF)[182] LJ parameters were used for the atoms whose parameters were not included in Dreiding. These force fields were selected based on the results of previous simulation studies in which good agreements between predicted gas uptakes and experimental measurements of different MOFs and ZIFs were demonstrated.[211, 212] It is also important to note that although CCl<sub>4</sub> is a non-polar molecule overall, it has an octupole moment due to highly electronegative chlorine (Cl) atoms. Considering its tetrahedral shape, using five-site models for CCl<sub>4</sub> may affect the adsorption results due to packing effects. However, a single-site LJ potential for CCl<sub>4</sub> was used due to its the computational cost and the good agreement between experimental and predicted vapor-liquid equilibrium curve for CCl<sub>4</sub>. [96]

MD simulations were finally performed to examine single-component and quaternary mixture diffusion of Ar, CCl<sub>4</sub>, N<sub>2</sub> and O<sub>2</sub> in the top performing material. In MD simulations, the initial loadings were taken from the results of single-component and quaternary mixture GCMC simulations computed at 10 bar and 298

K to compute the self-diffusivity of the less adsorbed components with a high statistical accuracy.

### 4.3 Results and Discussion

#### 4.3.1 Comparing Simulations with Experiments and Literature Data

We first compared our simulation results with the available experimental data of Kitagawa's group[208] for single-component  $\text{CCl}_4$  adsorption in CPL-11. As shown in Figure 4.2, our predictions are in a good agreement with the experimental measurements of  $\text{CCl}_4$  adsorption in CPL-11.

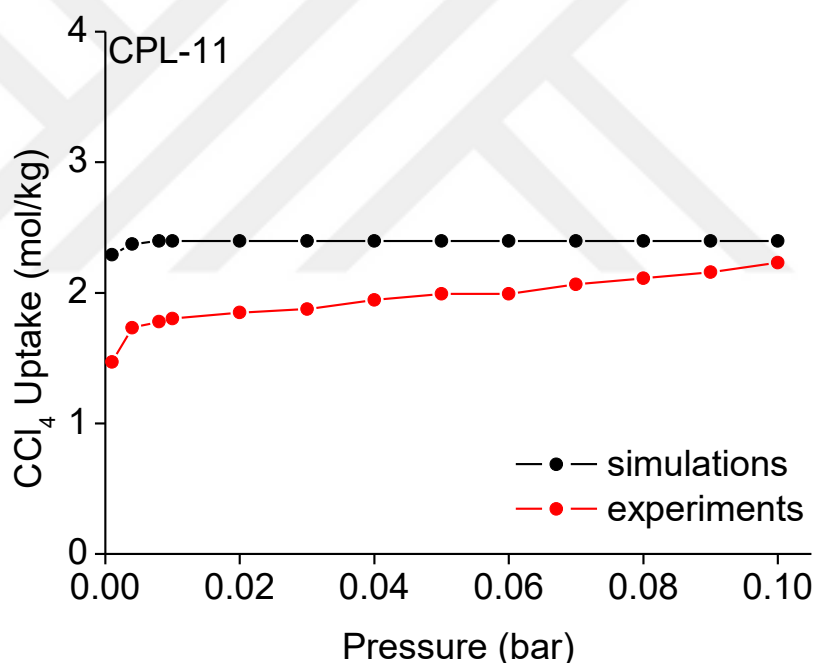


**Figure 4.2** Comparison of experiments and molecular simulations for single-component adsorption isotherms of  $\text{CCl}_4$  in CPL-11 at 298 K.

Figure 4.3 shows the comparison of 16 data points (3 data points for single-component  $\text{CCl}_4$  adsorption in MIL-101(Cr); 10 data points for single-component adsorption of Ar,  $\text{CCl}_4$ ,  $\text{N}_2$  and  $\text{O}_2$  in Cu-BTC and 3 data points for quaternary mixture adsorption in Cu-BTC) at various pressures and temperatures (shown in

Table A.2). Figure 4.3 shows that our simulation results agreed with the predictions of Calero's group[95] for single-component Ar, CCl<sub>4</sub>, N<sub>2</sub> and O<sub>2</sub> uptakes and quaternary air mixture uptakes in Cu-BTC and also with the experiments of Chen's group[97] for single-component CCl<sub>4</sub> uptake in MIL-101(Cr). Chen's group[97] reported that the maximum CCl<sub>4</sub> uptake in MIL-101(Cr) was 13 mol/kg at 303 K. However, our results showed that the maximum CCl<sub>4</sub> adsorption in MIL-101(Cr) was around 15 mol/kg under the same conditions. This difference was attributed to smaller SA (~1832 m<sup>2</sup>/g) of the synthesized MIL-101(Cr) than that of used in molecular simulation (~2991 m<sup>2</sup>/g). Overall, there is a good agreement between our simulation results and the literature data.

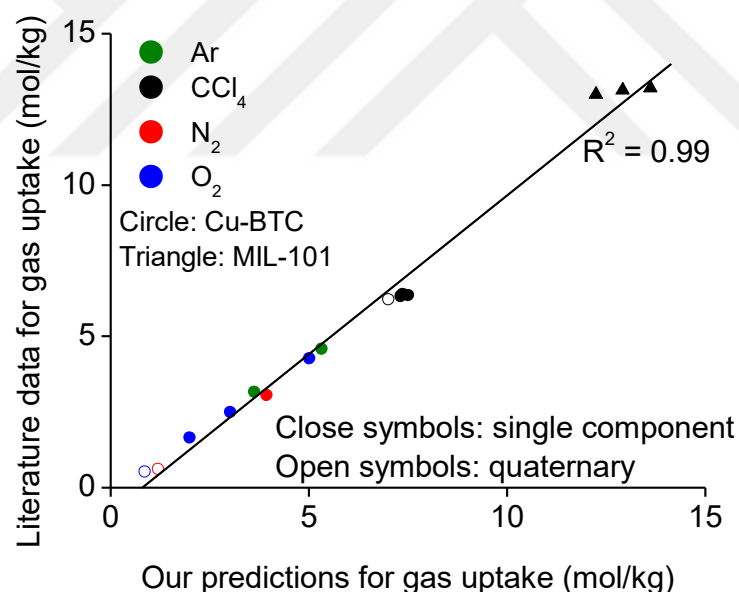


**Figure 4.3** Comparison of our predictions with experiments[97] for CCl<sub>4</sub> in MIL-101, and simulation available in the literature[95] for Ar, CCl<sub>4</sub>, N<sub>2</sub> and O<sub>2</sub> adsorptions in Cu-BTC.

### 4.3.2. Comparing Infinite Dilution Adsorption Selectivities of All Materials

$Q_{st}^0$  is a thermodynamic variable and widely used to evaluate the

## CHAPTER IV: Molecular Simulations of COFs, IRMOFs and ZIFs for Adsorption-based Separation of Carbon Tetrachloride from Air

performance of materials for adsorption-based gas separation processes. Since infinite dilution adsorption selectivities were determined from the ratios of  $K_{\text{Henry}}$  values of each competing gas molecules, the relations between  $K_{\text{Henry}}$  values of four gas molecules and  $Q_{\text{st}}^0$  values were initially examined. As shown in Figure 4.4,  $K_{\text{Henry}}$  values of gas molecules increase,  $Q_{\text{st}}^0$  values also increase.  $Q_{\text{st}}^0$  of  $\text{CCl}_4$  (from 22 to 56 kJ/mol) were found to be much higher than those of Ar (from 5.1 to 23 kJ/mol),  $\text{N}_2$  (from 5.0 to 23 kJ/mol) and  $\text{O}_2$  (from 5.4 to 24 kJ/mol), indicating stronger adsorption of  $\text{CCl}_4$  molecules within the pores of materials.  $K_{\text{Henry}}$  values of  $\text{CCl}_4$  molecules ( $6 \times 10^{-5}$ - $3 \times 10^{-1}$  mol/kg·Pa) were higher than those for Ar ( $5 \times 10^{-7}$ - $1 \times 10^{-5}$  mol/kg·Pa),  $\text{N}_2$  ( $3 \times 10^{-7}$ - $9 \times 10^{-6}$  mol/kg·Pa) and  $\text{O}_2$  ( $5 \times 10^{-7}$ - $1 \times 10^{-5}$  mol/kg·Pa), adsorption selectivity strongly favored  $\text{CCl}_4$  over the other gas molecules in all materials. The calculated adsorption selectivities of COFs for  $\text{CCl}_4/\text{Ar}$ ,  $\text{CCl}_4/\text{N}_2$  and  $\text{CCl}_4/\text{O}_2$  mixtures ranged from 50 to  $2 \times 10^5$  at 298 K and infinite dilution. For IRMOFs, the infinite dilution adsorption selectivities ranged between almost 400 and  $4 \times 10^4$ . The selectivity values of IRMOFs were intermediate in magnitude between those for COFs and ZIFs. Overall, ZIFs exhibited high adsorption selectivities (from  $\sim 1 \times 10^4$  to  $1 \times 10^5$ ) for  $\text{CCl}_4$  under the same conditions.

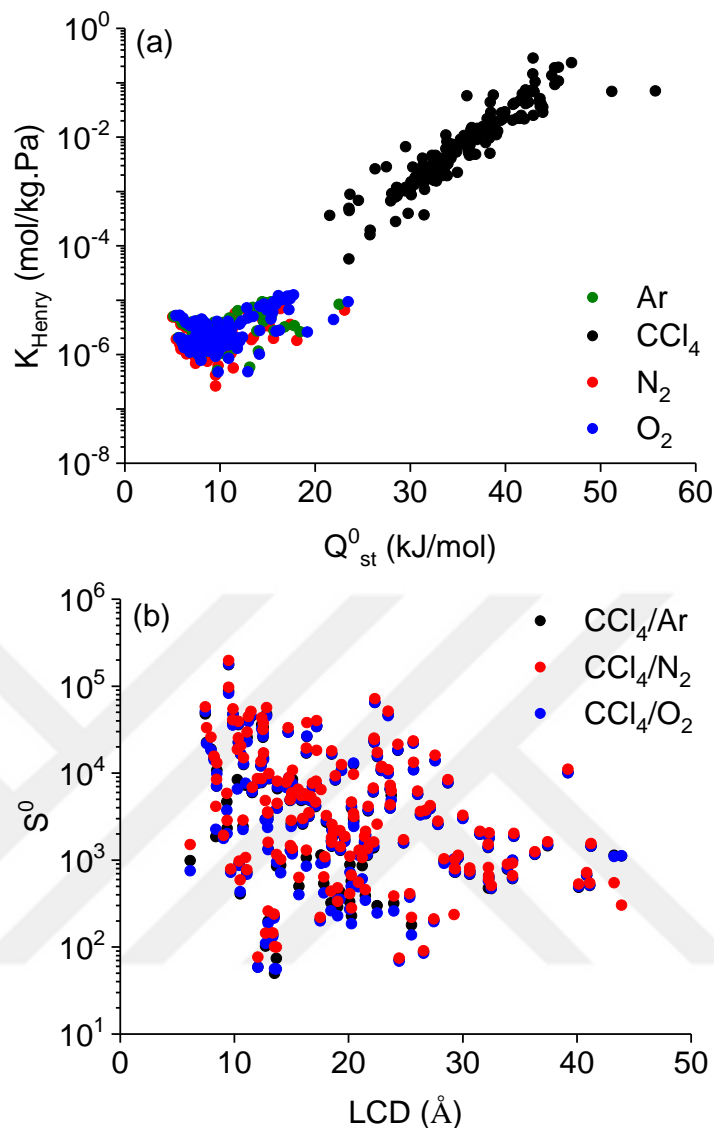


**Figure 4.4** Relations between (a)  $K_{\text{Henry}}$  of gas molecules and  $Q_{\text{st}}^0$ , and (b)  $S^0$  and LCDs of COFs, IRMOFs and ZIFs for  $\text{CCl}_4/\text{Ar}$ ,  $\text{CCl}_4/\text{N}_2$  and  $\text{CCl}_4/\text{O}_2$  separations at infinite dilution and 298 K.

Adsorption selectivity is generally governed by the pore textures of the materials. For this reason, the relations between LCDs of 175 frameworks and their adsorption selectivities were also studied. Figure 4.4(b) shows that adsorption selectivities for  $\text{CCl}_4/\text{Ar}$ ,  $\text{CCl}_4/\text{N}_2$  and  $\text{CCl}_4/\text{O}_2$  separations generally decrease with increasing LCDs (especially  $>24$  Å). This result is expected since small cavities can be more favorable adsorption sites, indicating strong confinement of  $\text{CCl}_4$  gas molecules within the pores of materials. The correlations between  $K_{\text{Henry}}$  of gases

in COFs, IRMOFs and ZIFs and their LCDs were also investigated in Figure A.1. There is no clear correlation between LCDs (ranged from 3.8 to 45 Å) of materials and  $K_{\text{Henry}}$  of Ar, N<sub>2</sub> and O<sub>2</sub> as shown in Figure A.1(a), (c) and (d). However, as the LCDs of frameworks increase from 24 to 45 Å, a slight decrease in  $K_{\text{Henry}}$  values can be seen. In Figure A.1(b), it is clear that  $K_{\text{Henry}}$  of CCl<sub>4</sub> generally decreases with increasing LCDs. In accordance with adsorption selectivities computed at infinite dilution, materials which have large LCDs (larger than 24 Å) may not be promising candidates for removal of CCl<sub>4</sub> from Ar, N<sub>2</sub> and O<sub>2</sub>. Understanding this type of correlations is significant to design materials for efficient CCl<sub>4</sub> separation applications.

The best performing 15 materials which exhibited very high adsorption selectivities for CCl<sub>4</sub> over Ar, N<sub>2</sub> and O<sub>2</sub> at infinite dilution and 298K were listed in Table 4.1-4.3. Among the top materials, 13 materials are common for each separation: BLP-2H-AA (a borazine-linked polymer COF), ZIF-6, Ph-An-COF (a photoresponsive COF with anthracene units), iPrTAPB-TFP (1,3,5-tris(4'-amino-3',5'-isopropylphenyl) benzene-1,3,5-triformylphloroglucinol), ZIF-60-MER, HAT-COF (HAT for hexaazatriphenylene), BDT-OEt-COF (BDT-OEt: benzodithiophene-ethoxy), TpPA-NO<sub>2</sub> (1,3,5-triformylphloroglucinol-2-nitro-1,4-phenylenediamine), ZIF-65-SOD, COF-202, COF-JLU2 (JLU for Jilin University), IRMOF-11 and COF-42-bnn. These materials have mediocre LCDs (7.5-23.5 Å), SAs (656.5-4232.3 m<sup>2</sup>/g) and PVs (0.5-1.4 cm<sup>3</sup>/g). Among the top promising COFs, only COF-202 is a three-dimensional material[213], other COFs are two-dimensional.  $Q_{\text{st}}^0$  values of Ar, CCl<sub>4</sub>, N<sub>2</sub> and O<sub>2</sub> at 298 K were also given in Tables 4.1-4.3. The top promising materials have generally similar  $Q_{\text{st}}^0$  values for Ar (~10 kJ/mol), CCl<sub>4</sub> (~40 kJ/mol), N<sub>2</sub> (~10 kJ/mol) and O<sub>2</sub> (~10 kJ/mol).

**Table 4.1** Top performing 15 materials ranked based on CCl<sub>4</sub>/Ar selectivity at 298 K and infinite dilution together with their  $Q_{st}^0$  for Ar, CCl<sub>4</sub>, N<sub>2</sub> and O<sub>2</sub>.  $Q_{st}^0$  values were given in kJ/mol.

Material	$Q_{st,Ar}^0$	$Q_{st,CCl_4}^0$	$Q_{st,N_2}^0$	$Q_{st,O_2}^0$	$S_{CCl_4/Ar}^0$	$S_{CCl_4/N_2}^0$	$S_{CCl_4/O_2}^0$
BLP-2H-AA	10.62	42.91	10.55	10.79	$1.8 \times 10^5$	$2.0 \times 10^5$	$1.8 \times 10^5$
ZIF-6	10.71	46.95	10.75	11.17	$8.8 \times 10^4$	$9.7 \times 10^4$	$8.2 \times 10^4$
Ph-An-COF	9.77	44.88	9.63	10.02	$6.5 \times 10^4$	$7.2 \times 10^4$	$6.5 \times 10^4$
iPrTAPB-TFP	9.73	39.87	9.55	9.81	$4.8 \times 10^4$	$5.8 \times 10^4$	$5.1 \times 10^4$
HAT-COF	9.75	42.86	9.60	10.05	$4.8 \times 10^4$	$5.5 \times 10^4$	$4.7 \times 10^4$
ZIF-60-MER	11.26	45.21	11.07	11.76	$4.7 \times 10^4$	$5.7 \times 10^4$	$4.5 \times 10^4$
BDT-OEt-COF	10.26	43.14	10.19	10.64	$4.7 \times 10^4$	$5.2 \times 10^4$	$4.6 \times 10^4$
TpPA-NO <sub>2</sub>	10.78	43.02	10.52	10.90	$4.4 \times 10^4$	$5.1 \times 10^4$	$4.6 \times 10^4$
ZIF-65-SOD	11.00	42.39	11.09	11.38	$4.0 \times 10^4$	$4.5 \times 10^4$	$3.9 \times 10^4$
COF-202	10.40	42.90	10.48	10.85	$3.7 \times 10^4$	$4.1 \times 10^4$	$3.6 \times 10^4$
COF-JLU2	9.99	38.73	10.00	10.16	$3.6 \times 10^4$	$3.9 \times 10^4$	$3.7 \times 10^4$
IRMOF-11	14.68	45.58	14.47	15.55	$3.6 \times 10^4$	$4.3 \times 10^4$	$3.2 \times 10^4$
ICOF-2	9.21	42.31	17.39	9.61	$3.5 \times 10^4$	$1.8 \times 10^4$	$3.4 \times 10^4$
COF-42-bnn	10.03	42.14	9.70	10.16	$3.4 \times 10^4$	$4.0 \times 10^4$	$3.5 \times 10^4$
IRMOF-13	14.31	45.17	14.34	15.21	$3.3 \times 10^4$	$3.7 \times 10^4$	$2.9 \times 10^4$

**Table 4.2** Top performing 15 materials ranked based on CCl<sub>4</sub>/N<sub>2</sub> selectivity at 298 K and infinite dilution together with their  $Q_{st}^0$  for Ar, CCl<sub>4</sub>, N<sub>2</sub> and O<sub>2</sub>.  $Q_{st}^0$  values were given in kJ/mol.

Material	$Q_{st,Ar}^0$	$Q_{st,CCl_4}^0$	$Q_{st,N_2}^0$	$Q_{st,O_2}^0$	$S_{CCl_4/Ar}^0$	$S_{CCl_4/N_2}^0$	$S_{CCl_4/O_2}^0$
BLP-2H-AA	10.62	42.91	10.55	10.79	$1.8 \times 10^5$	$2.0 \times 10^5$	$1.8 \times 10^5$
ZIF-6	10.71	46.95	10.75	11.17	$8.8 \times 10^4$	$9.7 \times 10^4$	$8.2 \times 10^4$
Ph-An-COF	9.77	44.88	9.63	10.02	$6.5 \times 10^4$	$7.2 \times 10^4$	$6.5 \times 10^4$
iPrTAPB-TFP	9.73	39.87	9.55	9.81	$4.8 \times 10^4$	$5.8 \times 10^4$	$5.1 \times 10^4$
ZIF-60-MER	11.26	45.21	11.07	11.76	$4.7 \times 10^4$	$5.7 \times 10^4$	$4.5 \times 10^4$
HAT-COF	9.75	42.86	9.60	10.05	$4.8 \times 10^4$	$5.5 \times 10^4$	$4.7 \times 10^4$
BDT-OEt-COF	10.26	43.14	10.19	10.64	$4.7 \times 10^4$	$5.2 \times 10^4$	$4.6 \times 10^4$
TpPA-NO <sub>2</sub>	10.78	43.02	10.52	10.90	$4.4 \times 10^4$	$5.1 \times 10^4$	$4.6 \times 10^4$

CHAPTER IV: Molecular Simulations of COFs, IRMOFs and ZIFs for Adsorption-based Separation of Carbon Tetrachloride from Air

ZIF-65-SOD	11.00	42.39	11.09	11.38	$4.0 \times 10^4$	$4.5 \times 10^4$	$3.9 \times 10^4$
IRMOF-11	14.68	45.58	14.47	15.55	$3.6 \times 10^4$	$4.3 \times 10^4$	$3.2 \times 10^4$
COF-202	10.40	42.90	10.48	10.85	$3.7 \times 10^4$	$4.1 \times 10^4$	$3.6 \times 10^4$
COF-42-bnn	10.03	42.14	9.70	10.16	$3.4 \times 10^4$	$4.0 \times 10^4$	$3.5 \times 10^4$
COF-JLU2	9.99	38.73	10.00	10.16	$3.6 \times 10^4$	$3.9 \times 10^4$	$3.7 \times 10^4$
ZIF-97	18.43	51.20	18.08	19.18	$2.6 \times 10^4$	$3.8 \times 10^4$	$2.7 \times 10^4$
IRMOF-13	14.31	45.17	14.34	15.21	$3.3 \times 10^4$	$3.7 \times 10^4$	$2.9 \times 10^4$

**Table 4.3** Top performing 15 materials ranked based on  $\text{CCl}_4/\text{O}_2$  selectivity at 298 K and infinite dilution together with their  $Q_{\text{st}}^0$  for Ar,  $\text{CCl}_4$ ,  $\text{N}_2$  and  $\text{O}_2$ .  $Q_{\text{st}}^0$  values were given in kJ/mol.

Material	$Q_{\text{st,Ar}}^0$	$Q_{\text{st,CCl}_4}^0$	$Q_{\text{st,N}_2}^0$	$Q_{\text{st,O}_2}^0$	$S_{\text{CCl}_4/\text{Ar}}^0$	$S_{\text{CCl}_4/\text{N}_2}^0$	$S_{\text{CCl}_4/\text{O}_2}^0$
BLP-2H-AA	10.62	42.91	10.55	10.79	$1.8 \times 10^5$	$2.0 \times 10^5$	$1.8 \times 10^5$
ZIF-6	10.71	46.95	10.75	11.17	$8.8 \times 10^4$	$9.7 \times 10^4$	$8.2 \times 10^4$
Ph-An-COF	9.77	44.88	9.63	10.02	$6.5 \times 10^4$	$7.2 \times 10^4$	$6.5 \times 10^4$
iPrTAPB-TFP	9.73	39.87	9.55	9.81	$4.8 \times 10^4$	$5.8 \times 10^4$	$5.1 \times 10^4$
HAT-COF	9.75	42.86	9.60	10.05	$4.8 \times 10^4$	$5.5 \times 10^4$	$4.7 \times 10^4$
BDT-OEt-COF	10.26	43.14	10.19	10.64	$4.7 \times 10^4$	$5.2 \times 10^4$	$4.6 \times 10^4$
TpPA-NO <sub>2</sub>	10.78	43.02	10.52	10.90	$4.4 \times 10^4$	$5.1 \times 10^4$	$4.6 \times 10^4$
ZIF-60-MER	11.26	45.21	11.07	11.76	$4.7 \times 10^4$	$5.7 \times 10^4$	$4.5 \times 10^4$
ZIF-65-SOD	11.00	42.39	11.09	11.38	$4.0 \times 10^4$	$4.5 \times 10^4$	$3.9 \times 10^4$
COF-JLU2	9.99	38.73	10.00	10.16	$3.6 \times 10^4$	$3.9 \times 10^4$	$3.7 \times 10^4$
COF-202	10.40	42.90	10.48	10.85	$3.7 \times 10^4$	$4.1 \times 10^4$	$3.6 \times 10^4$
COF-42-bnn	10.03	42.14	9.70	10.16	$3.4 \times 10^4$	$4.0 \times 10^4$	$3.5 \times 10^4$
ICOF-2	9.21	42.31	17.39	9.61	$3.5 \times 10^4$	$1.8 \times 10^4$	$3.4 \times 10^4$
IRMOF-11	14.68	45.58	14.47	15.55	$3.6 \times 10^4$	$4.3 \times 10^4$	$3.2 \times 10^4$
COF-18Å	10.32	41.78	10.26	10.63	$3.0 \times 10^4$	$3.3 \times 10^4$	$2.9 \times 10^4$

IRMOF-11, IRMOF-13 and ZIF-97 exhibited slightly higher  $Q_{\text{st}}^0$  for Ar,  $\text{N}_2$  and  $\text{O}_2$  than the remaining materials. Among these three structures, IRMOF-11 and IRMOF-13 gave similar performances resulting in an enhanced selectivity towards  $\text{CCl}_4$ . These two materials are catenated which means that two different



## CHAPTER IV: Molecular Simulations of COFs, IRMOFs and ZIFs for Adsorption-based Separation of Carbon Tetrachloride from Air

frameworks interpenetrate into each other.[27] The catenation of IRMOF-11 and IRMOF-13 enabled different types of pores with different sizes which enhanced adsorbate-adsorbent interactions. Another material which gave high  $Q_{st}^0$  values for Ar, CCl<sub>4</sub>, N<sub>2</sub> and O<sub>2</sub> was ZIF-97. This can be explained by the strong confinement of Ar, CCl<sub>4</sub>, N<sub>2</sub> and O<sub>2</sub> within the narrow pores (3.7 Å) of ZIF-97. Another interesting example is ICOF-2 (ICOF: ionic COF). This material also showed high  $Q_{st}^0$  for N<sub>2</sub> adsorption (~17 kJ/mol) which was attributed to its ionic structure.[214] Although ICOF-2 has an ionic property,  $Q_{st}^0$  for O<sub>2</sub> (9.6 kJ/mol) is not as high as  $Q_{st}^0$  for N<sub>2</sub>. This can be explained by larger quadrupole moment of N<sub>2</sub> ( $0.27e \times 10^{-16}$  electrostatic units (esu)) than that of O<sub>2</sub> ( $<0.09e \times 10^{-16}$  esu), resulting in a strong interaction between N<sub>2</sub> molecules and the framework.[215] Then the top promising three materials in each group of COFs, IRMOFs and ZIFs were identified namely as BLP-2H-AA, IRMOF-11 and ZIF-6, respectively. Among these three materials, BLP-2H-AA has the maximum CCl<sub>4</sub> selectivity over Ar ( $1.8 \times 10^5$ ), N<sub>2</sub> ( $2 \times 10^5$ ) and O<sub>2</sub> ( $1.8 \times 10^5$ ) at 298 K and infinite dilution. ZIF-6 has also CCl<sub>4</sub> selectivity over Ar ( $8.8 \times 10^4$ ), N<sub>2</sub> ( $9.7 \times 10^4$ ) and O<sub>2</sub> ( $8.2 \times 10^4$ ) and IRMOF-11 has CCl<sub>4</sub> selectivity over Ar ( $3.6 \times 10^4$ ), N<sub>2</sub> ( $4.3 \times 10^4$ ) and O<sub>2</sub> ( $3.2 \times 10^4$ ) under the same conditions. BLP-2H-AA has smaller surface area (~1200 m<sup>2</sup>/g) and lower pore volume (0.6 cm<sup>3</sup>/g) than ZIF-6 (~2800 m<sup>2</sup>/g, and 0.9 cm<sup>3</sup>/g) and IRMOF-11 (~2700 m<sup>2</sup>/g, and 0.9 cm<sup>3</sup>/g). Pore sizes of BLP-2H-AA (9Å × 9.5Å) are intermediate in magnitude between those for ZIF-6 (5.7Å × 9.5Å) and IRMOF-11 (6.9Å × 12.4Å). The best performing materials for CCl<sub>4</sub> separations were identified based on infinite dilution conditions. Their single-component, binary and quaternary mixture gas adsorption in these top promising materials were discussed below.

### 4.3.3. Comparing Gas Adsorption Isotherms of Top Performing Materials

The top three candidates for  $\text{CCl}_4$  separation from air were identified in each group of COFs (namely as BLP-2H-AA), IRMOFs (IRMOF-11) and ZIFs (ZIF-6). Single-component adsorption isotherms of Ar,  $\text{CCl}_4$ ,  $\text{N}_2$  and  $\text{O}_2$  in BLP-2H-AA, IRMOF-11 and ZIF-6 were computed at 298 K and a pressure ranged from  $10^{-5}$  to 10 bar. However,  $\text{CCl}_4$  adsorption isotherms were computed until 0.15 bar due to its saturation vapor pressure at 298 K. Figure 4.5 shows that  $\text{CCl}_4$  is more strongly adsorbed than Ar,  $\text{N}_2$  and  $\text{O}_2$  in BLP-2H-AA, IRMOF-11 and ZIF-6.

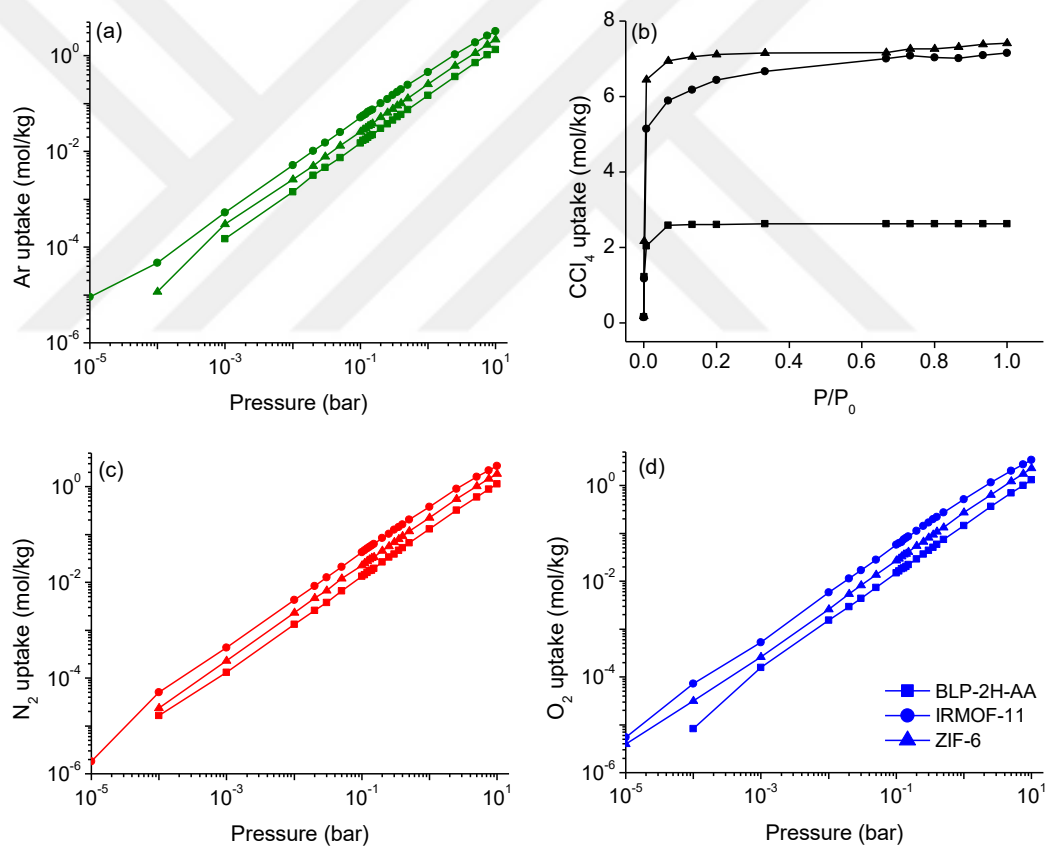


**Figure 4.5** Single-component adsorption isotherms for (a) Ar, (b)  $\text{CCl}_4$ , (c)  $\text{N}_2$  and (d)  $\text{O}_2$  in BLP-2H-AA, IRMOF-11 and ZIF-6 at 298 K.

As shown in Figure 4.5, single-component  $\text{CCl}_4$  adsorption was close to saturation whereas single-component adsorptions of Ar,  $\text{N}_2$  and  $\text{O}_2$  were far from

saturation. Since the kinetic diameters of Ar (3.38 Å), N<sub>2</sub> (3.64 Å) and O<sub>2</sub> (3.46 Å) are smaller than the CCl<sub>4</sub> size (5.77 Å), they can still find space in these three materials at high pressure. Figure 4.5(b) shows that the saturation pressure for single-component CCl<sub>4</sub> adsorption in IRMOF-11 (~0.1 bar) was much higher than those of BLP-2H-AA and ZIF-6 (~10<sup>-2</sup> bar). The CCl<sub>4</sub> saturation uptakes were almost 2.5 mol/kg in BLP-2H-AA, 7 mol/kg in both IRMOF-11 and ZIF-6. BLP-2H-AA exhibited the lowest adsorption capacity due to its small SA (1168.1 m<sup>2</sup>/g) and PV (0.6 cm<sup>3</sup>/g). IRMOF-11 and ZIF-6 have almost the same structural properties such as LCDs (9.5 Å), SAs (~2700 m<sup>2</sup>/g) and PVs (0.9 cm<sup>3</sup>/g), therefore similar trend was observed for their single-component adsorption isotherms.

Binary mixture adsorption isotherms of CCl<sub>4</sub>/Ar, CCl<sub>4</sub>/N<sub>2</sub> and CCl<sub>4</sub>/O<sub>2</sub> in these three materials were computed at 298 K and at a bulk composition of 1:99. Their simulation results were shown in Figure A.2-A.4. CCl<sub>4</sub> was preferred over Ar, N<sub>2</sub> and O<sub>2</sub> in binary mixtures in BLP-2H-AA, IRMOF-11 and ZIF-6. This result was expected from single-component adsorption isotherms. The adsorbed amounts of CCl<sub>4</sub> molecules in these materials for CCl<sub>4</sub>/Ar, CCl<sub>4</sub>/N<sub>2</sub> and CCl<sub>4</sub>/O<sub>2</sub> mixtures did not significantly changed. Adsorption strongly favored CCl<sub>4</sub> over Ar, N<sub>2</sub> and O<sub>2</sub> in mixtures and also CCl<sub>4</sub> adsorption was close to saturation in all mixtures. However, IRMOF-11 has a different trend for adsorption mechanism than BLP-2H-AA and ZIF-6. The stepwise behavior of gas adsorption in IRMOF-11 may be attributed to its cubic and catenated structure, leading to various pore size distribution. Figure A.5 shows pore size distribution of BLP-2H-AA, IRMOF-11 and ZIF-6. As shown in this Figure A.5, BLP-2H-AA and ZIF-6 have common one wide peak around 9.5 Å whereas IRMOF-11 has a wide range of pore size distribution (4.7, 7.5, 8.5, 8.9, 11.5 and 12.3 Å).

In order to assess the performance of these top materials for adsorption-based gas separation, binary mixture adsorption selectivity is generally considered. Figure 4.6 shows that adsorption selectivities of BLP-2H-AA, IRMOF-11 and ZIF-6 for  $\text{CCl}_4/\text{Ar}$ ,  $\text{CCl}_4/\text{N}_2$  and  $\text{CCl}_4/\text{O}_2$  separations. As shown in Figure 4.6, adsorption selectivity favored  $\text{CCl}_4$  in all mixtures, following a decreasing trend with increasing pressure. Adsorption selectivities for  $\text{CCl}_4$  over Ar were determined as  $4.6 \times 10^2$ ,  $3.7 \times 10^2$  and  $8.4 \times 10^3$  for BLP-2H-AA, IRMOF-11 and ZIF-6 at 10 bar, respectively. Adsorption selectivity for  $\text{CCl}_4$  over  $\text{N}_2$  ( $\text{O}_2$ ) at same pressure was estimated as  $9.0 \times 10^2$  ( $4.2 \times 10^2$ ) for BLP-2H-AA,  $4.8 \times 10^2$  ( $3.2 \times 10^2$ ) for IRMOF-11 and  $1.5 \times 10^4$  ( $4.2 \times 10^3$ ) for ZIF-6, respectively. Among these three materials, ZIF-6 is the most promising material for adsorption-based separation of  $\text{CCl}_4$  from Ar,  $\text{N}_2$  or  $\text{O}_2$ . Pores of ZIF-6 ( $5.7 \times 9.5 \text{ \AA}$ ) are narrower than the pores of BLP-2H-AA ( $6.9 \times 12.4 \text{ \AA}$ ) and IRMOF-11 ( $9.0 \times 9.5 \text{ \AA}$ ), indicating a much stronger confinement of  $\text{CCl}_4$  molecules in ZIF-6. Due to strong adsorption of  $\text{CCl}_4$  molecules in ZIF-6, it exhibited high selectivity towards  $\text{CCl}_4$ .

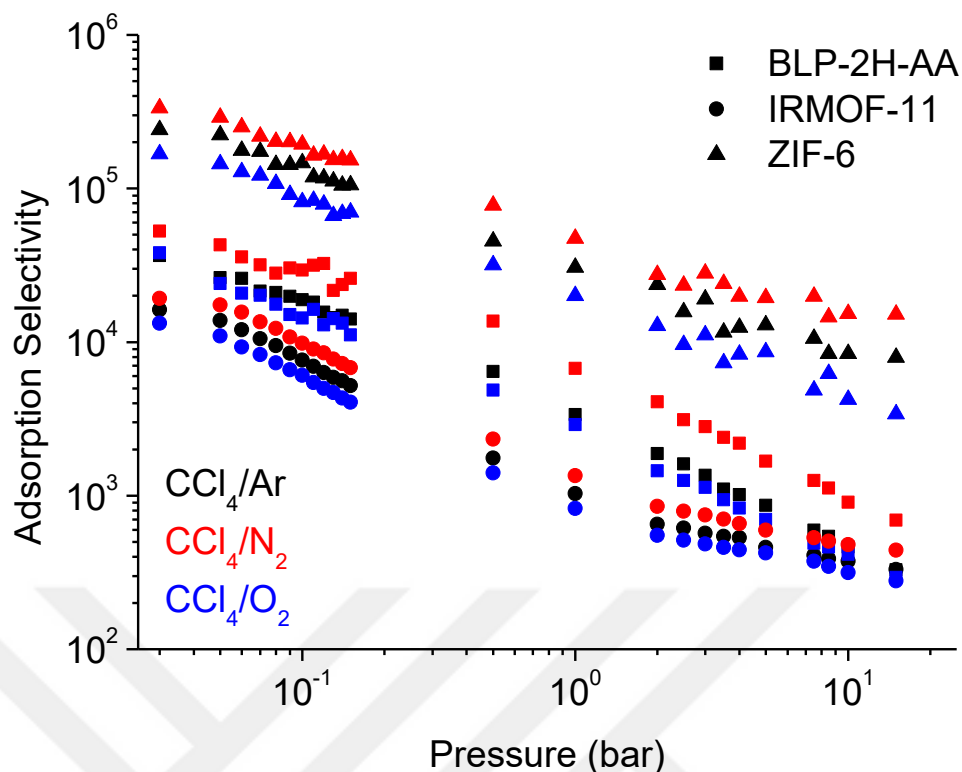


**Figure 4.6** Binary mixture adsorption selectivities of BLP-2H-AA, IRMOF-11 and ZIF-6 for separation of  $\text{CCl}_4/\text{Ar}$ ,  $\text{CCl}_4/\text{N}_2$  and  $\text{CCl}_4/\text{O}_2$  mixtures at 298 K.

Table 4.4 shows  $\text{CCl}_4/\text{Ar}$ ,  $\text{CCl}_4/\text{N}_2$  and  $\text{CCl}_4/\text{O}_2$  adsorption selectivities obtained from binary mixture simulations at 10 bar and 298 K. Results showed that binary mixture adsorption selectivities for  $\text{CCl}_4$  over Ar,  $\text{N}_2$  and  $\text{O}_2$  are lower than infinite dilution selectivities. This result is expected because infinite dilution adsorption selectivities do not consider the composition effect. Overall, these results suggested that using infinite dilution adsorption selectivities can give a quick idea about the performance of materials but performing mixture simulations is important to assess the realistic performance of materials for  $\text{CCl}_4$  separation.

**Table 4.4** The adsorption selectivities for binary mixtures at 10 bar and 298 K.

Material	$S_{\text{binary,CCl}_4/\text{Ar}}$	$S_{\text{binary,CCl}_4/\text{N}_2}$	$S_{\text{binary,CCl}_4/\text{O}_2}$
BLP-2H-AA	$4.6 \times 10^2$	$9.0 \times 10^2$	$4.2 \times 10^2$
IRMOF-11	$3.7 \times 10^2$	$4.8 \times 10^2$	$3.2 \times 10^2$

ZIF-6	$8.4 \times 10^3$	$1.5 \times 10^4$	$4.2 \times 10^3$
-------	-------------------	-------------------	-------------------

Gas separations are generally examined as binary mixtures in the literature because performing four-component or five-component simulations can be highly costly. However, simulating air compositions is important to evaluate gas separation performance of materials for industrial applications. To mimic the air compositions, a quaternary gas mixture was considered with a bulk composition of 0.999% Ar, 0.1% CCl<sub>4</sub>, 77.922% N<sub>2</sub> and 20.979% O<sub>2</sub>. Figure 4.7 shows the quaternary mixture adsorption isotherms in BLP-2H-AA, IRMOF-11 and ZIF-6 at 298 K and up to 50 bar. As expected from binary mixture adsorption isotherms, CCl<sub>4</sub> was preferred over other gas molecules in air mixture in these three different materials. Although the bulk composition of CCl<sub>4</sub> is very low (0.1%) in the quaternary mixture, adsorption performance of CCl<sub>4</sub> in these materials did not dramatically change.

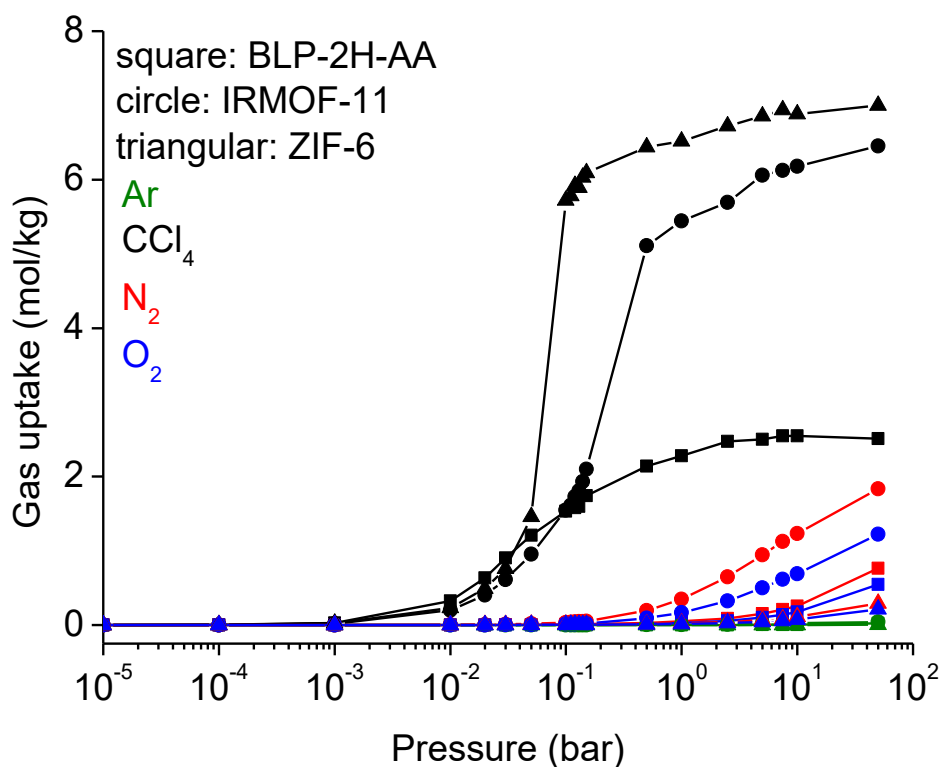


**Figure 4.7** Quaternary mixture adsorption isotherms for Ar, CCl<sub>4</sub>, N<sub>2</sub> and O<sub>2</sub> in

CHAPTER IV: Molecular Simulations of COFs, IRMOFs and ZIFs for Adsorption-based Separation of Carbon Tetrachloride from Air

BLP-2H-AA, IRMOF-11 and ZIF-6 at 298 K. The composition of the bulk gas mixture is Ar: 0.999%, CCl<sub>4</sub>: 0.1%, N<sub>2</sub>: 77.922% and O<sub>2</sub>: 20.979%.

Quaternary mixture adsorption selectivities for CCl<sub>4</sub> over Ar were calculated as  $4.1 \times 10^3$ ,  $2.5 \times 10^3$  and  $3.0 \times 10^4$  at 298 K and 10 bar for BLP-2H-AA, IRMOF-11 and ZIF-6, respectively. Similarly, quaternary mixture adsorption selectivity for CCl<sub>4</sub> over N<sub>2</sub> (O<sub>2</sub>) at 10 bar was estimated as  $7.8 \times 10^3$  ( $3.1 \times 10^3$ ) for BLP-2H-AA,  $3.9 \times 10^3$  ( $1.9 \times 10^3$ ) for IRMOF-11 and  $4.8 \times 10^4$  ( $2.0 \times 10^4$ ) for ZIF-6.

**Table 4.5** The adsorption selectivities for quaternary mixtures at 10 bar and 298 K.

Material	$S_{\text{quaternary,CCl}_4/\text{Ar}}$	$S_{\text{quaternary,CCl}_4/\text{N}_2}$	$S_{\text{quaternary,CCl}_4/\text{O}_2}$
BLP-2H-AA	$4.1 \times 10^3$	$7.8 \times 10^3$	$3.1 \times 10^3$
IRMOF-11	$2.5 \times 10^3$	$3.9 \times 10^3$	$1.9 \times 10^3$
ZIF-6	$3.0 \times 10^4$	$4.8 \times 10^4$	$2.0 \times 10^4$

Results of quaternary mixture adsorption selectivities at 298 K and 10 bar were listed in Table 4.5. Quaternary mixture adsorption selectivities were found to be one order of magnitude higher than binary mixture adsorption selectivities due to decreasing bulk composition of CCl<sub>4</sub> from 1% (binary mixture) to 0.1% (quaternary mixture). Based on both binary and quaternary mixture simulations, ZIF-6 exhibited the best performance for CCl<sub>4</sub> separation. GCMC snapshots of Ar, CCl<sub>4</sub>, N<sub>2</sub> and O<sub>2</sub> adsorption in this material at 298 K up to 50 bar were given in Figure A.6. As shown in Figure A.6, CCl<sub>4</sub> molecules were preferentially adsorbed within the pores of ZIF-6 at low pressures. The number of Ar, N<sub>2</sub> and O<sub>2</sub> molecules were less than CCl<sub>4</sub> molecules in all pressures, indicating favorable adsorption of CCl<sub>4</sub> molecules within the framework. The ranking of the top materials based on adsorption selectivity (ZIF-6 > BLP-2H-AA > IRMOF-11) did not change as we

considered quaternary mixture simulations. This analysis showed that considering binary mixture simulations may be adequate to evaluate the separation performance of materials for adsorption-based  $\text{CCl}_4$  separations. However, it is important to note that mimicking air composition is important to understand the real performance of materials for industrial applications.

Krishna[203, 204] recently used a simple metric, shown as  $\Delta Q$ , as a separation potential to rank the materials for efficient gas separation in fixed bed units and discussed that  $\Delta Q$  gave the same hierarchy of productivities which were obtained from breakthrough simulations. The calculated  $\Delta Q$  for binary and quaternary mixture separations at 10 bar and 298 K were given in Table A.3.  $\Delta Q$  followed the similar trend with adsorption selectivities for  $\text{CCl}_4/\text{N}_2$  separation for the best performing material, ZIF-6. However, although BLP-2H-AA gave higher  $\text{CCl}_4/\text{N}_2$  selectivity ( $9.0 \times 10^2$ ) than IRMOF-11 ( $4.8 \times 10^2$ ), its separation potential ( $\sim 232$ ) was found to be lower than the latter ( $\sim 523$ ). For quaternary mixtures, defining adsorption selectivity is challenging, therefore  $\Delta Q$  is a useful metric to analyze the separation performance of materials for quaternary mixtures. Although BLP-2H-AA exhibited high adsorption selectivities for  $\text{CCl}_4/\text{N}_2$  separations, and high productivities for  $\text{N}_2$  in binary mixture, its separation potential in quaternary mixture was found to be very low ( $\sim 8.5$ ), indicating that this material may not be promising for air separations. Among these three materials, ZIF-6 gave the highest  $\Delta Q$  ( $\sim 19$ ) for  $\text{N}_2$  in quaternary mixtures, resulting in a high productivity of  $\text{N}_2$  in the exiting stream of a fixed bed unit. Similarly, IRMOF-11 exhibited high  $\Delta Q$  ( $\sim 18$ ) for  $\text{N}_2$  in quaternary mixtures. This analysis showed that investigation of  $\Delta Q$  is crucial for identifying the best candidate for air separations rather than considering only mixture selectivities. It is also important to discuss structural



stabilities of these top performing three candidates for long-term adsorption-based gas separations. BLP-2H-AA has high thermal stability up to almost 700 K.[216] IRMOF-11 has also high thermal stability up to nearly 800 K.[27] ZIF-6 has one of the most stable topologies in ZIFs (up to almost 800 K) due to its pure imidazole linker.[173]

The presence of humidity in the air may affect  $\text{CCl}_4$  uptake in adsorbents due to the competition for the same adsorption sites. Therefore,  $\text{CCl}_4$  adsorption in ZIF-6, which gave the best performance among 201 materials, was also investigated under a relative humidity of 80% at 298 K. Five-component (Ar,  $\text{CCl}_4$ ,  $\text{N}_2$ ,  $\text{O}_2$  and  $\text{H}_2\text{O}$ ) GCMC simulations were performed at 1 bar and 10 bar. Comparison between five-component and quaternary mixture simulation results were given in Table 4.6. Results showed that the presence of water did not affect the adsorption of Ar,  $\text{N}_2$  and  $\text{O}_2$  in ZIF-6 at 1 bar.  $\text{CCl}_4$  adsorption slightly increased from 6.5 mol/kg to 6.6 mol/kg under a relative humidity of 80% at 1 bar. On the other hand, the presence of water at 10 bar affected the adsorption of Ar,  $\text{CCl}_4$ ,  $\text{N}_2$  and  $\text{O}_2$ . Ar ( $\text{CCl}_4$ ) uptake decreased from 0.002 mol/kg to 0.001 mol/kg (from 6.9 mol/kg to 5.9 mol/kg). Adsorption of  $\text{N}_2$  ( $\text{O}_2$ ) also decreased by almost half from 0.1 mol/kg to 0.06 mol/kg (from 0.07 mol/kg to 0.04 mol/kg). This can be explained by strong adsorption of  $\text{H}_2\text{O}$  molecules in ZIF-6 at relatively high pressures. Due to the competition between gas molecules and water vapor, gas uptakes under relative humidity decreased. However, overall performance of ZI-6 did not change in the presence of  $\text{H}_2\text{O}$  vapor. ZIF-6 still exhibited high selectivity towards  $\text{CCl}_4$  in  $\text{CCl}_4/\text{Ar}$ ,  $\text{CCl}_4/\text{N}_2$  and  $\text{CCl}_4/\text{O}_2$  mixtures at 80% relative humidity. Similar results were also found for Cu-BTC in the previous computational study of Calero's group.[96]

**Table 4.6** Comparison between the gas uptakes obtained from quaternary mixture simulations and obtained from five-component mixture simulations under a relative humidity (RH) of 80% for ZIF-6. (The partial pressure of H<sub>2</sub>O is fixed at  $3.28 \times 10^{-2}$  bar.)

		RH%							
		0%	80%	0%	80%	0%	80%	0%	80%
	<b>P bar</b>	<b>N<sub>Ar</sub> (mol/kg)</b>		<b>N<sub>CCl<sub>4</sub></sub> (mol/kg)</b>		<b>N<sub>N<sub>2</sub></sub> (mol/kg)</b>		<b>N<sub>O<sub>2</sub></sub> (mol/kg)</b>	
ZIF-	1	0.0005	0.0004	6.518	6.594	0.025	0.023	0.015	0.013
6	10	0.002	0.001	6.886	5.974	0.112	0.065	0.074	0.043

#### 4.3.4 Comparing Gas Diffusion in ZIF-6

Computational investigation of gas transport mechanism is important to understand the interactions between gas molecules and adsorbent materials. Therefore, single-component and quaternary mixture gas diffusion in ZIF-6, which gave the best performance, were examined. The initial loadings of MD simulations for both single-component and quaternary mixture were taken from GCMC simulation results at 298 K and 10 bar. Figure 4.8 shows single-component and quaternary mixture self-diffusivities of Ar, CCl<sub>4</sub>, N<sub>2</sub> and O<sub>2</sub> in ZIF-6. Diffusion did not favor CCl<sub>4</sub> over other gas molecules in this material because heavier and strongly adsorbed CCl<sub>4</sub> molecules diffused much slower than the lighter, smaller and weakly adsorbed gas molecules. Initial loadings (molecules/unit cell) and the self-diffusivities (cm<sup>2</sup>/s) of gases in ZIF-6 were listed in Table 4.7. The self-diffusivity of CCl<sub>4</sub> in ZIF-6 ( $3.6 \times 10^{-7}$  cm<sup>2</sup>/s) was much lower than the self-diffusivities of Ar ( $7.6 \times 10^{-5}$  cm<sup>2</sup>/s), N<sub>2</sub> ( $8.6 \times 10^{-5}$  cm<sup>2</sup>/s) and O<sub>2</sub> ( $8.0 \times 10^{-5}$  cm<sup>2</sup>/s).

**Table 4.7** The initial loadings for single-component and quaternary mixture GCMC simulations, and the self-diffusivities of Ar, CCl<sub>4</sub>, N<sub>2</sub> and O<sub>2</sub> in ZIF-6 at 298 K and 10 bar. (u.c for unit cell)

Gas	Loadings (m/u.c)	D <sub>self</sub> (cm <sup>2</sup> /s)	
Ar	single	56	$7.6 \times 10^{-5}$
	mixture	1	$1.3 \times 10^{-6}$
CCl <sub>4</sub>	single	191	$3.6 \times 10^{-7}$
	mixture	175	$1.3 \times 10^{-6}$
N <sub>2</sub>	single	48	$8.6 \times 10^{-5}$
	mixture	3	$5.2 \times 10^{-5}$
O <sub>2</sub>	single	59	$8.0 \times 10^{-5}$
	mixture	2	$2.1 \times 10^{-6}$

Erucar et al.[163] showed that the interaction strength between guest molecules and the host material affects the diffusion behavior of adsorbates. Strong interaction between guest molecules and the host material caused slow diffusion of guest molecules. Therefore, ZIF-6 exhibited high isosteric heat of adsorption for CCl<sub>4</sub> (~47 kJ/mol), leading slow diffusion of the gas molecules. Self-diffusivities of Ar ( $1.3 \times 10^{-6}$  cm<sup>2</sup>/s), N<sub>2</sub> ( $5.2 \times 10^{-6}$  cm<sup>2</sup>/s) and O<sub>2</sub> ( $2.1 \times 10^{-6}$  cm<sup>2</sup>/s) in quaternary mixture were found to be one order lower in magnitude than single-component self-diffusivities of these gases. However, CCl<sub>4</sub> diffusion slightly increased in ZIF-6 when the quaternary mixture was considered in molecular simulations.

CHAPTER IV: Molecular Simulations of COFs, IRMOFs and ZIFs for Adsorption-based Separation of Carbon Tetrachloride from Air

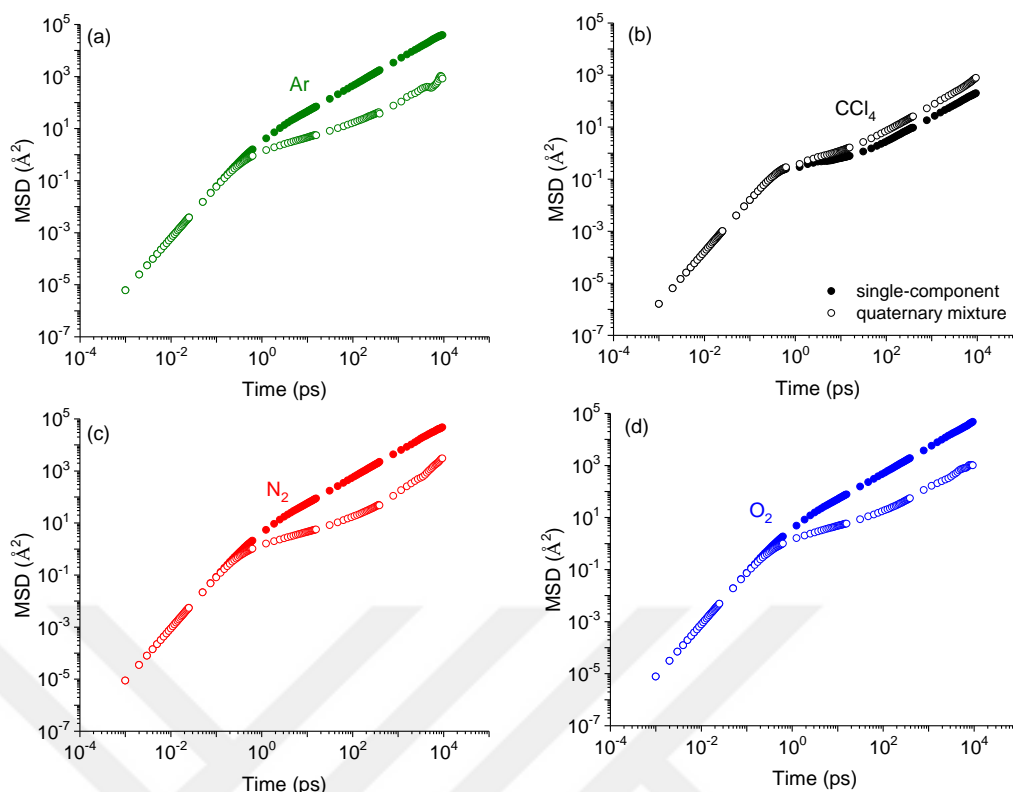


**Figure 4.8** Comparison of single-component and quaternary mixture self-diffusivities of (a)Ar, (b)CCl<sub>4</sub>, (c)N<sub>2</sub> and (d)O<sub>2</sub> in ZIF-6 at 298 K. Quaternary mixture composition of the bulk gas mixture is Ar: 0.999%, CCl<sub>4</sub>: 0.1%, N<sub>2</sub>: 77.922% and O<sub>2</sub>: 20.979%.

For example, the self-diffusivity of CCl<sub>4</sub> in quaternary mixture ( $1.3 \times 10^{-6}$  cm<sup>2</sup>/s) was higher than the single-component self-diffusivity of CCl<sub>4</sub> ( $3.6 \times 10^{-7}$  cm<sup>2</sup>/s) in ZIF-6. This can be explained by the number of gas molecules in the pores. In a unit cell of ZIF-6, the number of slowly diffusing CCl<sub>4</sub> decreased from 191 to 175 molecules/unit cell as quaternary mixture was considered and steric hindrance effects decreased. 175 CCl<sub>4</sub> molecules slowly diffusing were present in the pores of ZIF-6, the diffusion of Ar, N<sub>2</sub> and O<sub>2</sub> molecules slightly decreased. Comparison of single-component and mixture diffusivities showed that the adsorbed number of molecules and the interaction strength between adsorbates and the host affect diffusion behavior of gas molecules within the pores of ZIF-6.

## CHAPTER V

# COVALENT ORGANIC FRAMEWORKS FOR HYDROGEN STORAGE: A MOLECULAR SIMULATION STUDY<sup>2</sup>

### *5.1 Motivation*

In this chapter, high-throughput molecular simulations were computed to screen the recent CoRE-COF database for H<sub>2</sub> storage. The effect of Feynman-Hibbs correction on calculated H<sub>2</sub> isotherms were also examined to consider quantum effects at low temperatures. GCMC simulations were performed to compute volumetric H<sub>2</sub> storage of 296 COFs at three different operating conditions: (i) at 100 bar/77K → 2 bar/77 K, (ii) at 100 bar/77 K → 5 bar/77 K, and (iii) at 100 bar/77 K → 5 bar/160K. The best performing candidates, which exhibited high performance for H<sub>2</sub> uptake, were identified. The best performing materials were then compared with the top performing MOFs which were previously identified in the literature. The relations between structural properties of COFs including pore sizes, densities, porosities, and their H<sub>2</sub> working capacities were finally examined to better understand structure-performance relationships.

---

<sup>2</sup>The results given in this chapter were submitted to Journal of the Turkish Chemical Society, Section A: Chemistry with following title: Gulcay, E., & Erucar, I. (2019). Computational screening of covalent organic frameworks for hydrogen storage.

## 5.2 Computational Details

To validate our computational methodology, our predictions with the available experimental data of Furukawa et al.[47] for single-component H<sub>2</sub> adsorption isotherm were compared. Adsorption isotherms of H<sub>2</sub> in four COFs (COF-5, COF-6, COF-8, and COF-10) were computed at 77 K and up to 80 bar to be consistent with the study of Furukawa et al.[47]. We also computed saturated H<sub>2</sub> uptake in several COFs reported in the literature by Li et al.[217] (ACOF-1), Stegbauer et al.[218] (ATFG-COF), Furukawa et al.[47] (COF-1, COF-5, COF-6, COF-8, COF-10, COF-102, and COF-103), Li et al.[219] (COF-JLU2), Ge et al.[220] (COF-TpAzo), Neti et al.[221] (CoPc-PorDBA), Kaleeswaran et al.[222] (iPrTAPB-TFP, iPrTAPB-TFPB, TAPB-TFP, and TAPB-TFPB), Kang et al.[223] (NUS-3), Bhunia et al.[224] (PCTF-1 and PCTF-2), and Kahveci et al.[225] (TD-COF-5).

Among 309 COFs, 13 COFs have almost zero accessible SAs and these frameworks were excluded from further H<sub>2</sub> adsorption analysis.

## 5.3 Results and Discussion

### 5.3.1 Comparisons of Experiments with Simulations

The comparison of our predictions with the experimental measurements of COFs, including COF-n (n: 5, 6, 8, 10) for single-component H<sub>2</sub> uptake at 77 K were given in Figure 5.1. Simulations were computed by considering three various scenarios: (i) all electrostatic interactions are on, (ii) H<sub>2</sub>-H<sub>2</sub> electrostatic interactions are on, and (iii) all electrostatic interactions are off. For the first case, H<sub>2</sub>-H<sub>2</sub> electrostatic interactions using the Darkrim and Levesque potential and H<sub>2</sub>-framework electrostatic interactions were computed during GCMC simulations and the Feynman-Hibbs correction was added into the potential

energy. For the second case, only H<sub>2</sub>-H<sub>2</sub> electrostatic interactions were considered using the Darkrim and Levesque potential and the Feynman–Hibbs correction was applied during simulations. For the last case, a simple single-site LJ potential for H<sub>2</sub> was used and the Feynman–Hibbs correction was not applied in these simulations. As shown in Figure 5.1, simulations computed using the Feynman–Hibbs corrections agreed well with the reported experimental data. Simulations performed using the single-site H<sub>2</sub> model overestimated H<sub>2</sub> uptake in all these four COFs. For example, Furukawa et al.[47] reported 35.1 mg/g in COF-5, and our prediction of H<sub>2</sub> adsorption in COF-5 using the single-site model as 41.2 mg/g at 77 K and 80 bar. The calculated H<sub>2</sub> adsorption in COF-5 obtained from the simulations with the Feynman-Hibbs corrections were as 37.0 mg/g (H<sub>2</sub>-H<sub>2</sub> electrostatic interactions were on) and 38.0 mg/g (all electrostatic interactions were on) at the same conditions. The results from computed Feynman-Hibbs corrections were found to be similar. Results showed that only H<sub>2</sub>-H<sub>2</sub> electrostatic interactions can be considered to perform H<sub>2</sub> uptake in COFs at cryogenic conditions due to low computation cost. Similar results for coulombic interaction between H<sub>2</sub>-H<sub>2</sub> gas molecules and COFs were also reported that not affect the H<sub>2</sub> uptake at both 77 K and 298 K by Assfour et al.[226]

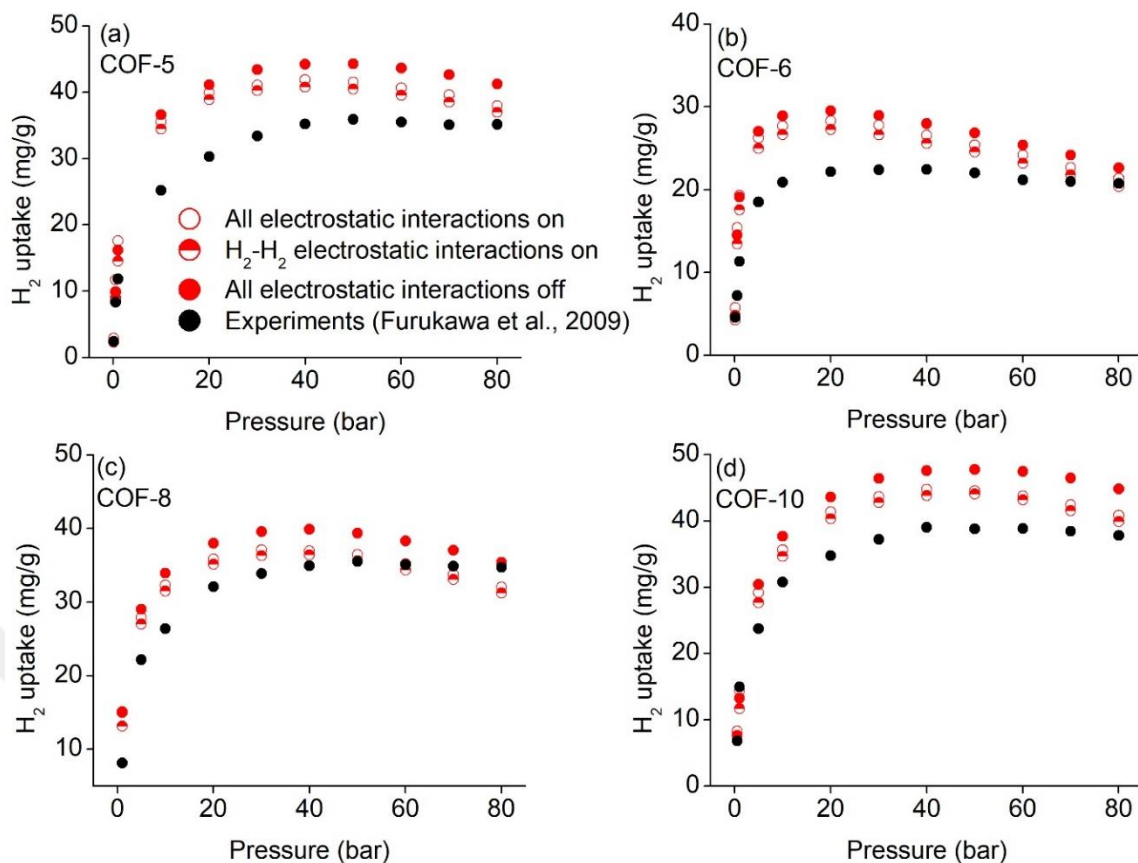


**Figure 5.1** Comparison of simulations with the experiments[47] for single-component H<sub>2</sub> uptake in (a)COF-5, (b)COF-6, (c)COF-8, and (d)COF-10 at 77 K.

Figure 5.2 shows our simulation results with the available experiments for the saturated H<sub>2</sub> adsorption capacities of 20 COFs. Simulated H<sub>2</sub> adsorption were obtained from the GCMC simulations with the Feynman-Hibbs corrections using the Darkrim and Levesque potential for H<sub>2</sub> (H<sub>2</sub>-H<sub>2</sub> electrostatic interactions were on). There is a good agreement between our predictions and available experimental data for saturated H<sub>2</sub> uptakes in 20 COFs.



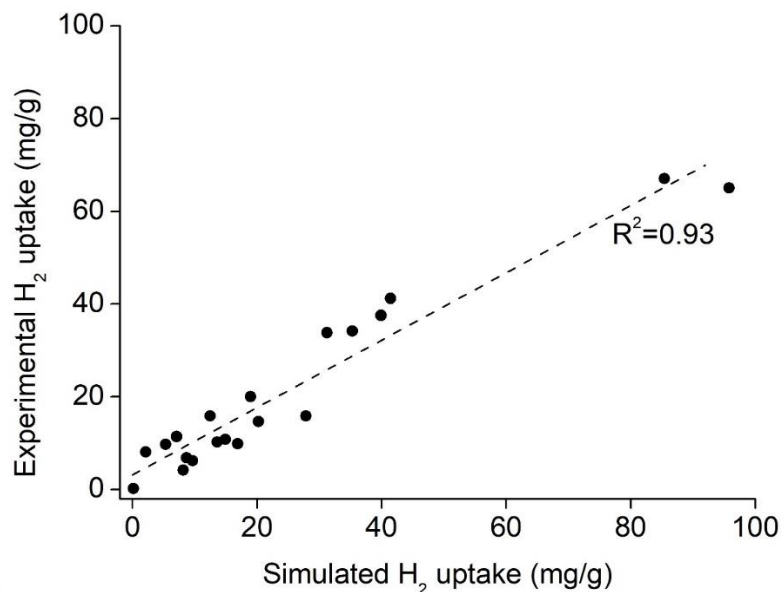


**Figure 5.2** Comparison of experiments and our simulations for saturated H<sub>2</sub> uptakes in 20 COFs.

COFs' names together with our predictions and measured H<sub>2</sub> uptakes at the different temperatures and pressures were given in Table 5.1. Among 20 COFs, COF-102 and COF-103 are only 3-dimensional and the remaining COFs are all 2-dimensional. The large discrepancy was observed between simulated H<sub>2</sub> uptake and experimental measurements for only 3-dimensional COFs, COF-102, and COF-103. Simulations dramatically overestimated H<sub>2</sub> uptake in these two COFs. These results might be attributed to the remaining solvent molecules and defects inside COFs. Overall, the good agreement between our predictions and experimental data motivated us to compute H<sub>2</sub> working capacities of 296 COFs.

**Table 5.1** Data for comparison of simulations with the experiments for the saturated H<sub>2</sub> uptakes in 20 COFs.

COF Name	P (bar)	T (K)	Our data (mg/g)	Literature Data (mg/g)	Reference

ACOF-1 <sup>[1]</sup>	1	77	16.89	9.89	[217]
ATFG-COF <sup>[2]</sup>	30	308	2.14	8.12	[218]
COF-1	90	77	20.24	14.68	[47]
COF-5	90	77	35.30	34.19	[47]
COF-6	90	77	18.97	20.04	[47]
COF-8	80	77	31.23	33.85	[47]
COF-10	80	77	39.91	37.58	[47]
COF-102	90	77	85.41	67.07	[47]
COF-103	90	77	95.79	65.05	[47]
COF-JLU2 <sup>[3]</sup>	1	77	12.48	15.86	[219]
COF-TpAzo <sup>[4]</sup>	1	77	13.61	10.29	[220]
CoPc-PorDBA <sup>[5]</sup>	1	77	41.43	41.24	[221]
iPrTAPB-TFP <sup>[6]</sup>	1	77	7.09	11.42	[222]
iPrTAPB-TFPB <sup>[7]</sup>	1	77	8.15	4.18	[222]
TAPB-TFP	1	77	14.90	10.82	[222]
TAPB-TFPB	1	77	9.63	6.26	[222]
NUS-3 <sup>[8]</sup>	1	273	0.14	0.24	[223]
PCTF-1 <sup>[9]</sup>	0.25	77	5.31	9.75	[224]
PCTF-2	0.5	77	8.67	6.86	[224]
TD-COF-5 <sup>[10]</sup>	1	77	27.88	15.89	[225]

[1]ACOF: azine-based COF; [2]ATFG: 1,3,5-triformylphloroglucinol; [3]JLU: Jilin University; [4]TpAzo: triformylphloroglucinol 4,4'-azodianiline; [5]CoPc-PorDBA: cobalt-based phthalocyanine-porphyrin dehydrobenzoannulenes; [6]iPrTAPB-TFP: 1,3,5-tris(4-aminophenyl)benzene - 1,3,5-triformylphloroglucinol; [7] TFPB: 1,3,5-tris(4'-formylphenyl)benzene; [8]NUS: National University of Singapore; [9]PCTF: porous covalent triazine-based organic frameworks [10]TD: triptycene-derived

### 5.3.2 Effect of Feynman-Hibbs Corrections on H<sub>2</sub> Working Capacities

Working capacity is a useful metric for evaluation of adsorbents to use in gas separation applications. In the literature, a simple spherical H<sub>2</sub> model and classical LJ potential are widely used in molecular simulations to compute H<sub>2</sub>

working capacities at cryogenic temperature. However, quantum effects at low temperature can have influence for small molecules uptakes. Thus, the Feynman-Hibbs corrections can be used to consider quantum effects at low temperature. Comparison of working capacities of 296 COFs computed at three different operating conditions (i) from 100 bar/77K to 2 bar/77 K, (b) from 100 bar/77 K to 5 bar/77 K, and (c) from 100 bar/77 K to 5 bar/160K were given in Figure 5.3. In this figure, the results obtained from the simulations using the Feynman-Hibbs corrections were found almost similar with the results obtained from the simulations using the single-site H<sub>2</sub> model at three various operating conditions.

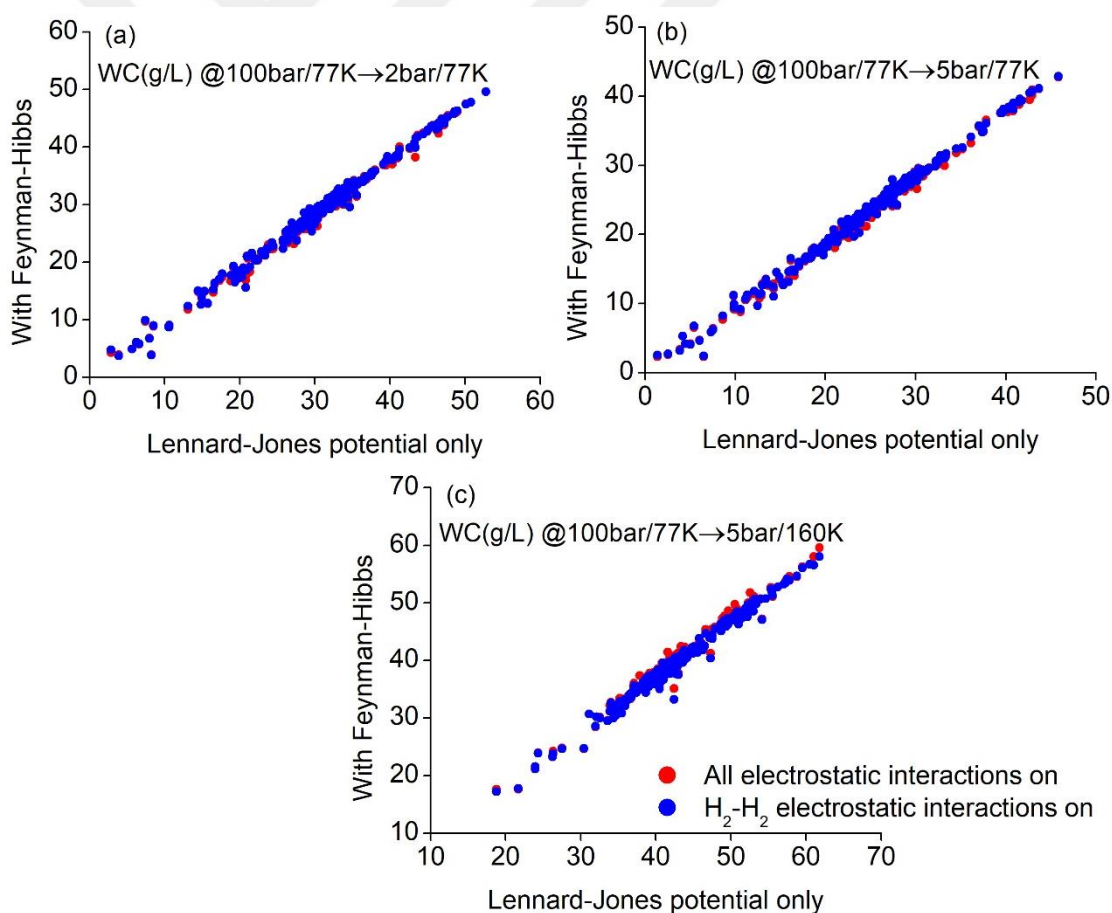


**Figure 5.3** Effect of the Feynman-Hibbs corrections on our calculated H<sub>2</sub> uptake in 296 COFs.

There are obvious relationships between results obtained from only LJ potential and that of LJ potential with the Feynman-Hibbs corrections. The best performing COFs based on their working capacities calculated from three different scenarios were ranked and the Spearman rank correlation coefficient (SRCC,  $-1 \leq \text{SRCC} \leq 1$ ) were estimated. When SRCC is found to be 1, there is a perfect correlation between two rankings. The comparison of ranking of COFs based on volumetric H<sub>2</sub> working capacities obtained from GCMC simulations using different potentials was given in Table 5.2. As shown in Table 5.2, the ranking of COFs is highly correlated, and the Feynman-Hibbs corrections and adsorbate-adsorbent electrostatic interactions do not actually affect the ranking of materials. Therefore, predictions using only LJ potential with the single-site H<sub>2</sub> model can give quick and precise information about the volumetric H<sub>2</sub> working capacities of COFs.

**Table 5.2** Comparison of ranking of COFs based on volumetric H<sub>2</sub> working capacities

Adsorption/desorption conditions	LJ vs LJ with the FH <sup>‡</sup> (all electrostatic interactions)	LJ vs LJ with the FH (only H <sub>2</sub> -H <sub>2</sub> electrostatic interactions)
100bar/77K → 2bar/77K	0.96	0.97
100bar/77K → 5bar/77K	0.96	0.99
100bar/77K → 5bar/160K	0.99	0.98

‡: the Feynman-Hibbs corrections

### 5.3.3 Evaluation of the COFs Performances for H<sub>2</sub> Storage

The top performing COFs for H<sub>2</sub> storage were identified and ranked based on their H<sub>2</sub> working capacities obtained from single-component GCMC simulations at 100bar/77K adsorption and 5bar/77K/160K desorption conditions. The top performing 10 COFs, that exhibited the highest volumetric H<sub>2</sub> working capacities (38.9-42.9 g/L) at 100bar/77K adsorption and 5bar/77K

desorption conditions, were given in Table 5.3. As shown in this table, the results were obtained from GCMC simulations with the Feynman-Hibbs corrections using the Darkrim and Levesque potential for H<sub>2</sub> (only H<sub>2</sub>-H<sub>2</sub> electrostatic interactions were on). The porosities (densities) of the most promising 10 COFs were ranged from 0.87 to 0.92 (0.16-0.24 g/cm<sup>3</sup>). Among these COFs, only IISERP-COF3 has 2-dimensional. The remaining of COFs have 3-dimensional. COF-DL-229-3fold gave the highest working capacity (42.9 g/L) among 296 COFs which could be attributed to its high porosity (0.87) and large surface area (~8462 m<sup>2</sup>/g). COF-DL-229-3fold has also smaller pore apertures (10.72×10.15 Å) compared to remaining 9 COFs which enhance H<sub>2</sub>-COF interactions. Bucior et al. also reported that highly porous materials exhibit weak interactions between H<sub>2</sub> and adsorbent to bind H<sub>2</sub> molecules.

**Table 5.3** Top-performing 10 COFs ranked based on working capacities calculated at 100bar/77K for adsorption and 5bar/77K for desorption conditions.

COF	LCD-PLD (Å)	$\rho$ (g/cm <sup>3</sup> )	$\phi$	WC (g/L)
COF-DL <sup>[1]</sup> 229-3fold	10.72-10.15	0.24	0.87	42.92
PI <sup>[2]</sup> -COF-5-2P <sup>[3]</sup>	13.35-10.52	0.26	0.88	41.14
COF-DL229-2fold	17.57-14.36	0.16	0.92	40.78
DL-COF-1-ctn	16.21-14.26	0.19	0.90	40.67
DL-COF-2-ctn	16.19-14.24	0.21	0.90	40.47
COF-105	18.80-16.12	0.18	0.91	39.63
DL-COF-1-bor	22.72-16.03	0.17	0.91	39.41
IISERP <sup>[4]</sup> -COF3	22.16-19.77	0.22	0.90	39.15
Ni-DBA <sup>[5]</sup> -3D-COF-ctn	20.96-17.60	0.17	0.92	39.04
DL-COF-2-bor	25.15-15.94	0.19	0.91	38.87

[1] DL: dual linkage; [2] PI: polyimide; [3] 2P: biphenyl-4,4'-dicarboxaldehyde; [4]

IISERP: Indian Institute of Science Education and Research Pune; [5] DBA: dehydrobenzoannulenes.

10 COFs were also ranked based on their volumetric working capacities calculated at 100bar/77K for adsorption and 5bar/160K for desorption conditions and given in Table 5.4. Among these COFs, COF-103 gave the highest volumetric working capacity as 58.0 g/L at 100 bar/77K adsorption and 5bar/160K desorption conditions. The best performing materials given in Table 5.4 have higher densities (0.24-0.47 g/cm<sup>3</sup>) compared to the top candidates listed in Table 5.3 whereas they have narrower pore apertures and lower porosities than the latter. ILCOF-1-AB has only 2-dimensional structures whereas the remaining COFs have 3-dimensional. Among all these 20 materials, COF-DL229-3fold is the common COF that gives high performance at two different adsorption/desorption conditions. Results showed that the most performing materials should be chosen considering different operating conditions.

**Table 5.4** Top-performing 10 COFs ranked based on working capacities calculated at 100bar/77K for adsorption and 5bar/160K for desorption conditions.

COF	LCD-PLD (Å)	$\rho$ (g/cm <sup>3</sup> )	$\phi$	WC (g/L)
COF-103	9.68-8.50	0.39	0.80	58.04
ILCOF[1]-1-AB	11.09-9.41	0.34	0.82	56.71
COF-102	9.04-7.99	0.42	0.78	56.52
3D-Py[2]-COF-2P	13.47-12.29	0.28	0.85	56.06
BF[3]-COF-1	13.26-8.62	0.40	0.79	54.63
COF-DL229-3fold	10.72-10.15	0.24	0.87	54.13
BF-COF-2	13.28-7.58	0.47	0.78	53.87
3D-CuPor-COF	16.46-13.64	0.33	0.84	53.47
3D-Por[4]-COF	16.31-13.66	0.31	0.84	53.26

## CHAPTER V: Covalent Organic Frameworks for Hydrogen Storage: A Molecular Simulation Study

COF-DL229-5fold	11.25-11.20	0.37	0.80	52.73
-----------------	-------------	------	------	-------

[1] ILCOF: imine-linked; [2] Py: pyrene-based; [3] BF: base-functionalized; [4] Por: porphyrin.

Figure 5.4 shows the comparison of volumetric H<sub>2</sub> working capacities of the most promising 10 COFs (given in Table 5.4) performed under various temperature and pressure conditions with those of the most promising MOFs at the same conditions. As shown in Figure 5.4, COFs outperformed the most promising 10 MOFs including Cu-BTC, NU-125, NU-1000, NU-1101, NU-1102, NU-1103, NOTT-112, anthracene -based UiO-68, UiO-67 and CYCU-3-Al (CYCU: Chung-Yuan Christian University) at 100bar/77K adsorption and 5bar/160K desorption conditions. Among 10 COFs, COF-DL229-3fold exhibited high performance for H<sub>2</sub> storage at two various operating conditions, exceeding the DOE 2020 and 2025 targets. This result may be attributed to optimal pore apertures (10.72 Å × 10.15 Å), density (0.24 g/cm<sup>3</sup>), and adequate porosity (0.87) of COF. Bobbitt et al.[59] also reported that the materials, that have optimal pore apertures (~12 Å) and porosity (~0.9), tend to bind stronger with H<sub>2</sub> molecules and enhance for H<sub>2</sub> uptake capacity.

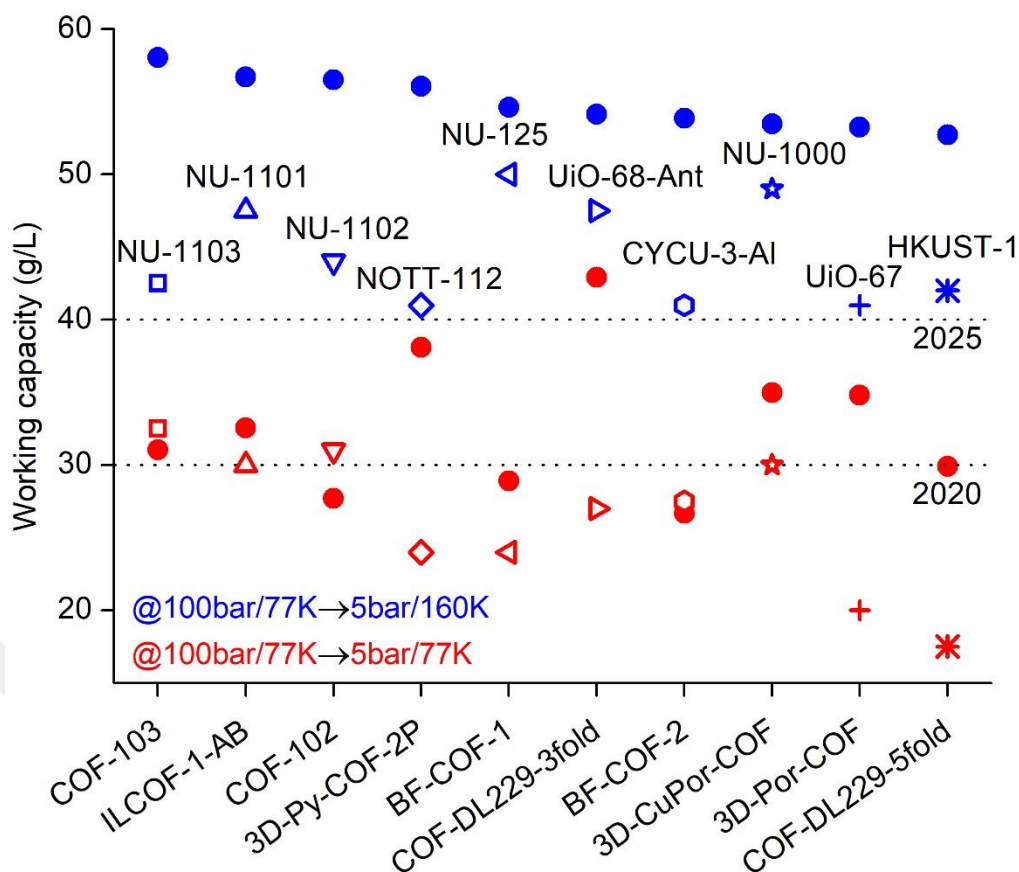


**Figure 5.4** Comparison of volumetric H<sub>2</sub> working capacities of the most promising 10 COFs (closed symbols) and those of the top-performing MOFs reported in the literature (open spheres).[54]

As shown in Figure 5.4, NU-1103 (32.5 g/L) outperformed BF-COF-1, BF-COF-2, COF-102, COF-103, and COF-DL229-5fold at 100bar/77K adsorption and 5bar/77K desorption conditions. This was attributed to its higher porosity (0.88) and lower density (0.29 g/cm<sup>3</sup>) than these 5 COFs, in which porosities were ~0.8, and densities ~0.4 g/cm<sup>3</sup>. Moreover, NU-1000, NU-1101, and NU-1102 have slightly higher porosities (~ 0.8) than BF-COF-1, BF-COF-2, and COF-102 (~0.78). Thus, these 3 MOFs (~30.5 g/L) also outperformed 3 COFs at the same operating conditions. At 100bar/77K adsorption and 5bar/77K desorption conditions, BF-COF-2 exhibited almost similar H<sub>2</sub> working capacity with CYCU-3-Al due to their almost similar densities (0.45 g/cm<sup>3</sup>). The other



## CHAPTER V: Covalent Organic Frameworks for Hydrogen Storage: A Molecular Simulation Study

4 COFs, namely as ILCOF-1-AB, 3D-Py-COF-2P, 3D-CuPor-COF, and 3D-Por-COF exhibited higher H<sub>2</sub> working capacities than MOFs at the two operating conditions. Overall, COFs can exceed the DOE 2020 and 2025 targets for on board H<sub>2</sub> storage.

Relationship between structural characteristics and performances of materials is important to give an insight the behavior of candidates and to synthesize promising materials for desired gas storage applications. Therefore, the structure-performance relations for 296 COFs were finally examined. The relations between volumetric H<sub>2</sub> working capacities of COFs and their structural properties as LCD, PLD, SA, density ( $\rho$ ), unit cell volume (UV), PV, porosity ( $\phi$ ) in Figure 5.5. Figure 5.5(a) showed that R<sup>2</sup> were found to be higher than 0.8 for the relations between volumetric working capacities and  $\rho$ , and  $\phi$  of COFs at two operating conditions at 100bar/77K adsorption and 2bar/77K (also 5bar/77K) desorption. For the third case (100bar/77K  $\rightarrow$  5bar/160 K), there is no strong correlation (R<sup>2</sup>=0.5) between volumetric working capacities of COFs and their LCDs, PLDs, SAs, UVs, PVs for each three operating conditions.

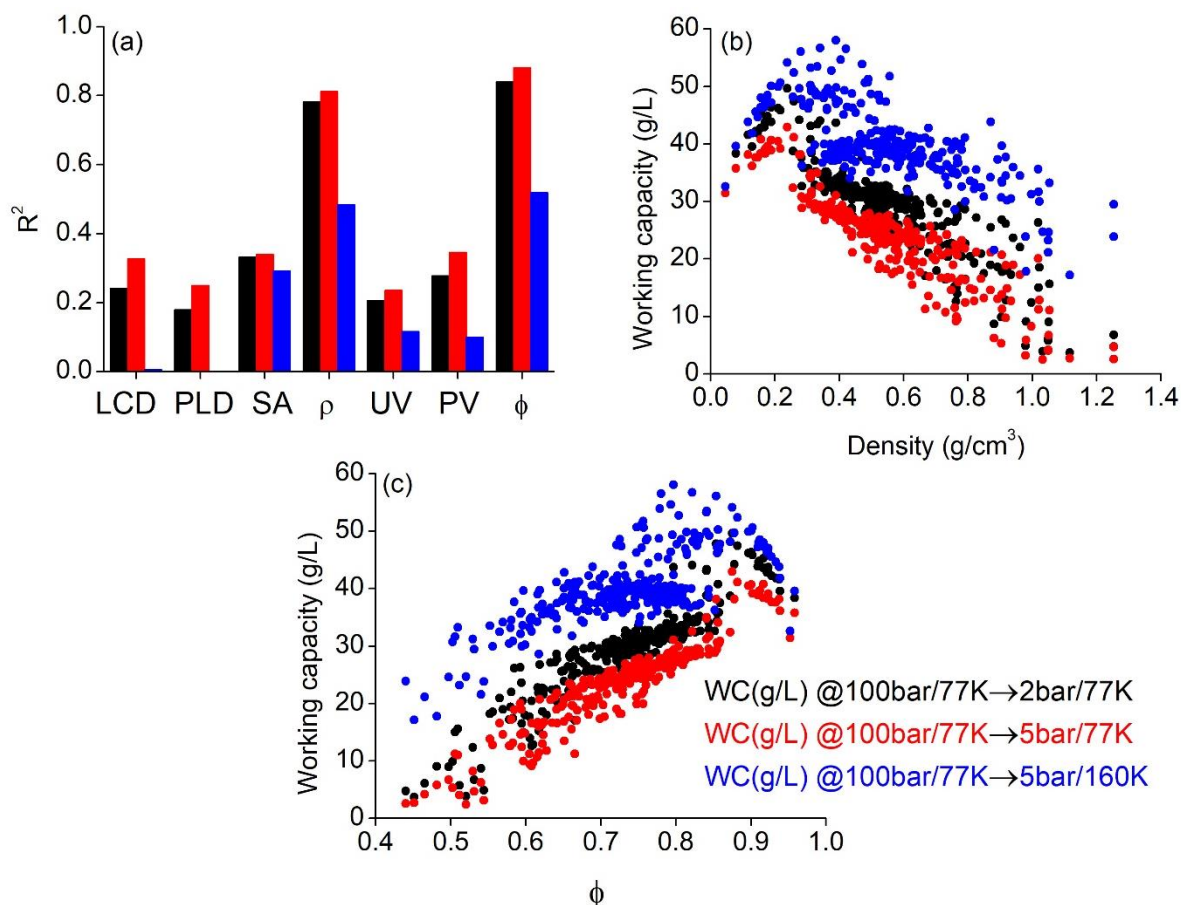


**Figure 5.5** (a) $R^2$  values showing the relations between working capacities of  $H_2$  (g/L) and several physical parameters. Relations between (b)density and  $H_2$  working capacities (g/L), and (c)porosity and  $H_2$  working capacity (g/L).

As shown in Figure 5.5(b), the relations between volumetric  $H_2$  working capacities of COFs and their densities (0.05-1.25 g/cm<sup>3</sup>) at three operational conditions.  $H_2$  working capacities of COFs are negatively correlated with densities, especially higher than 0.3 g/cm<sup>3</sup>, at these conditions. COFs, whose densities are in the ranged from 0.12 g/cm<sup>3</sup> to 0.26 g/cm<sup>3</sup>, gave generally high  $H_2$  working capacities (32.4-54.1 g/L). For example, COF-DL229-3fold exhibited the highest  $H_2$  working capacities as 49.62 g/L (42.92 g/L) at 100 bar/77K adsorption and 2 bar/77 K desorption (at 100 bar/77K adsorption and 5 bar/77 K desorption) due to its optimal density (0.24 g/cm<sup>3</sup>) and high porosity

(0.87). Figure 5.5(c) shows that there is a linear relationship between H<sub>2</sub> working capacities of COFs and their porosities (0.44-0.96). COFs, which have high porosities ( $\geq 0.8$ ) and quite low densities (0.2-0.4 g/cm<sup>3</sup>), generally give high volumetric H<sub>2</sub> working capacities. For example, COF-103, which exhibited the maximum H<sub>2</sub> working capacity at 100 bar/77 K adsorption and 5bar/160K desorption, has high porosity (0.8) and quite low density (~0.4 g/cm<sup>3</sup>). On the other hand, COF-DL229-0fold has the highest porosity (0.96), however gave an average performance for H<sub>2</sub> working capacities (~35 g/L) at three operating conditions due to its extremely low density (0.08 g/cm<sup>3</sup>) and very large pore apertures (24.6×31.9 Å). Results emphasized that volumetric H<sub>2</sub> storage in COFs can be positively (negatively) correlated with the porosities (densities) of COFs, like MOFs. It should also be noted that among 296 COFs, 257 COFs have 2-dimensional structures, and the remaining 39 COFs which commonly exhibit high performance for H<sub>2</sub> storage are 3-dimensional.

## CHAPTER VI

# BIO-COMPATIBLE MOFs FOR STORAGE AND SEPARATION OF O<sub>2</sub>: A MOLECULAR SIMULATION STUDY<sup>3</sup>

### *6.1 Motivation*

In this chapter, the recent MOF database (69,699 MOFs) was screened and identified 1525 MOFs, which have biocompatible properties due to their endogenous organic linkers such as amino acids, cyclodextrins, nucleobases, and porphyrins and metal centers.[227] These endogenous linkers have various functional groups in their units which may enhance interactions between O<sub>2</sub> gas molecules and framework atoms. Up to date, the performance of MOFs with endogenous linkers has not been studied for separation and storage of O<sub>2</sub>. The performance of bio-compatible MOFs was examined for adsorption-based and membrane-based O<sub>2</sub> separation and also for high-pressure O<sub>2</sub> storage. Binary mixture (O<sub>2</sub>/N<sub>2</sub>:21/79) adsorption selectivities were estimated at a wide range of pressure (up to 140 bar) and compared with those calculated from results of infinite dilution. On the other hand, high-pressure O<sub>2</sub> storage is highly required for different medical and industrial applications including the treatment of respiratory insufficiency, the hyperbaric oxygen treatment for carbon monoxide poisoning and air enrichment in the catalytic units.[72] For this reason, gravimetric and volumetric O<sub>2</sub> working capacities of 315 bio-compatible MOFs were estimated at 298 K and 140 bar (storage) and 5 bar (release), considering the conventional

---

<sup>3</sup>The results given in this chapter were published in Industrial & Engineering Chemistry Research with following reference: Gulcay, E., & Erucar, I. (2019). Bio-compatible MOFs for storage and separation of O<sub>2</sub>: A molecular simulation study. Industrial & Engineering Chemistry Research, 58(8), 3225-3237.

## CHAPTER VI: Bio-compatible MOFs for Storage and Separation of O<sub>2</sub>: A Molecular Simulation Study

pressures used in medical O<sub>2</sub> tanks. For promising MOFs, MD simulations were performed to estimate O<sub>2</sub> permeabilities. Bio-compatible MOF membranes, which exhibited high O<sub>2</sub> permeabilities and selectivities towards O<sub>2</sub>, were identified.

### 6.2 Computational Details

In order to validate our computational methodology, our predictions were compared with the available experimental and computational data of DeCoste et al.[76] for single component O<sub>2</sub> adsorption and Moghadam et al.[77] for O<sub>2</sub> working capacity. DeCoste et al.[76] examined single-component O<sub>2</sub> uptake in Cu-BTC, NU-125 and UiO-66 at 310 K and various pressures (up to 140 bar). Cu-BTC with a refcode FIQCEN was used in our simulations. As discussed in the previous chapter, Cu-BTC has Cu-Cu dimers with a 3-dimensional network and mediocre pore sizes (13.7 Å×6.7 Å) and also, large surface area (~2130 m<sup>2</sup>/g).[42] NU-125 (refcode: REWNEO) has a large surface area (~3335 m<sup>2</sup>/g) and high pore volume (1.3 cm<sup>3</sup>/g).[228] UiO-66 (refcode: RUBTAK) is a Zr-based MOF with 1,4-benzene dicarboxylate (BDC) linkers and has smaller pore sizes (8.6 Å×4.0 Å) and surface area (~1070 m<sup>2</sup>/g) than the other two structures.[229] O<sub>2</sub> working capacities of 10 different MOFs (ANUGIA, ANUGUM, BICDAU, DIDDOK, HIGRIA, HIHNUJ, ICALOP, KEFBEE, MOCKAR and WEBKOF) were also calculated at 298 K, 5 bar and 140 bar to be consistent with the study of Moghadam et al.[77] Predictions for the single-component N<sub>2</sub> adsorption in Cu-BTC, IRMOF-1 and IRMOF-3 were also compared with the experimental data of Siberio-Perez et al.[230] and computational data of Karra et al.[231] IRMOF-1 and IRMOF-3 have cubis structures with large cavities (~15 Å) and surface areas (~3500 m<sup>2</sup>/g). N<sub>2</sub> uptakes in Cu-BTC, IRMOF-1 and IRMOF-3 were computed at 298 K up to 90 bar to be consistent with the literature.

## CHAPTER VI: Bio-compatible MOFs for Storage and Separation of O<sub>2</sub>: A Molecular Simulation Study

1525 bio-compatible MOFs have various PLDs (0.4-53.3 Å), accessible SAs (from 0 to 5537.3 m<sup>2</sup>/g), and PVs (0.03-7.9 cm<sup>3</sup>/g). 315 MOFs which have SAs > 0 m<sup>2</sup>/g and PLDs > 3.4 Å were used for the O<sub>2</sub>/N<sub>2</sub> separation investigation. The potential parameters of MOFs were taken from the Universal Force Field (UFF).[182] This forcefield was chosen based on the results of previous simulation studies that were in a good agreement with the experiments for various applications.[37, 212]

### *6.3 Results and Discussion*

#### **6.3.1 Comparison of simulations with the available data**

Comparison between our simulation results and the available experimental and computational data for single-component O<sub>2</sub> and N<sub>2</sub> adsorption in different MOFs was given in Figure 6.1. Our predictions with the experimental measurements of Siberio-Perez et al.[230] and the simulation results of Karra et al.[231] were first compared for N<sub>2</sub> adsorption in Cu-BTC, IRMOF-1 and IRMOF-3 at 298 K. As shown in Figure 6.1(a), there is a good agreement between our predictions and experimental measurements for N<sub>2</sub> uptake. Siberio-Perez et al.[230] measured N<sub>2</sub> adsorption in IRMOF-1 as 6.86 mol/kg at 90 bar and 298 K. Under the same conditions, N<sub>2</sub> uptake in this material were predicted as 6.76 mol/kg by computationally. Similarly, Karra et al.[231] reported N<sub>2</sub> uptake in Cu-BTC (IRMOF-3) as 5.22 mol/kg (4.78 mol/kg) at 298 K and 42 bar. Our prediction for N<sub>2</sub> adsorption in Cu-BTC (IRMOF-3) was 5.02 mol/kg (4.95 mol/kg). O<sub>2</sub> working capacities ( $WC_{O_2}$ ) of 10 MOFs (ANUGIA, ANUGUM, BICDAU, DIDDOK, HIGRIA, HIHNUJ, ICALOP, KEFBEE, MOCKAR and WEBKOF) were compared with the predictions of Moghadam et al.[77] in Figure 6.1(b). It is important to note that Moghadam et al.[77] used density derived electrostatic and

## CHAPTER VI: Bio-compatible MOFs for Storage and Separation of O<sub>2</sub>: A Molecular Simulation Study

chemical (DDEC) charge method for partial charges of MOFs' atoms. Although in our simulations, a quick charge equilibration method was used to assign partial charges of MOFs' atom, our results were consistent with the literature.[77] This result may be attributed to weak coulombic interactions between gas molecules and the frameworks at high pressure (140 bar for adsorption and 5 bar for desorption). In Figure 6.1(c), a good agreement between our predictions and the data of DeCoste et al.[76] was shown for the single-component O<sub>2</sub> uptake in Cu-BTC, NU-125 and UiO-66. Simulations slightly underestimated O<sub>2</sub> adsorption in Cu-BTC at 303 K and 140 bar. Our predictions for O<sub>2</sub> uptake in NU-125 were in a better agreement with the experimental data than those reported in the literature.[76]

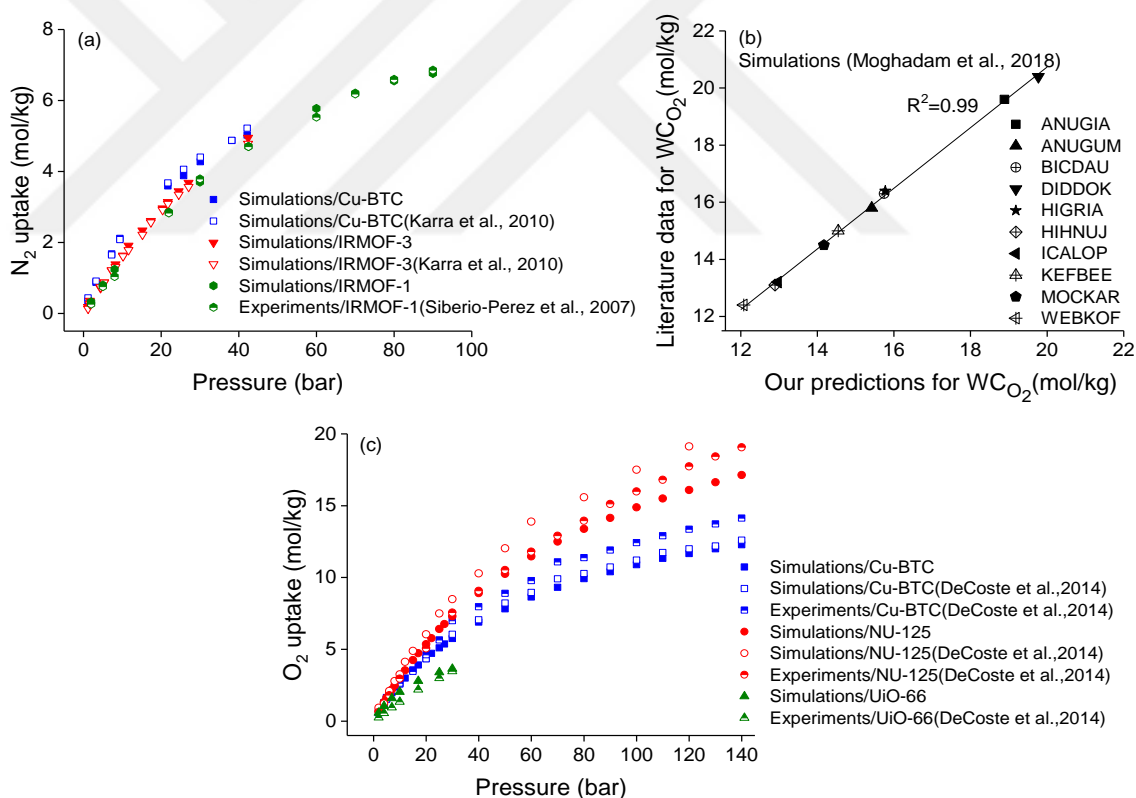


**Figure 6.1** Comparison of our predictions with the literature for (a)N<sub>2</sub> uptake in Cu-BTC, IRMOF-1 and IRMOF-3 at 298 K, (b)O<sub>2</sub> working capacities of 10 MOFs at 298 K, (c)O<sub>2</sub> uptake in Cu-BTC, NU-125 and UiO-66 at 303 K.

### 6.3.2 Adsorption-based O<sub>2</sub>/N<sub>2</sub> separation

After validating the accuracy of our computational methodology,  $K_{\text{Henry}}$  values of O<sub>2</sub> and N<sub>2</sub> for 315 MOFs, which have non-zero SAa and PLDs > 3.4 Å, were computed at 298 K and infinite dilution.  $K_{\text{Henry}}$  values of O<sub>2</sub> and N<sub>2</sub> were ranged from  $4.04 \times 10^{-7}$  to  $5.4 \times 10^{-5}$  mol/kg/Pa and from  $4.28 \times 10^{-7}$  to  $7.75 \times 10^{-3}$  mol/kg/Pa, respectively. As shown in Figure 6.2(a), while increasing LCDs of MOFs,  $K_{\text{Henry}}$  values of O<sub>2</sub> and N<sub>2</sub> generally decrease. The majority of MOFs exhibited similar  $K_{\text{Henry}}$  values in magnitude for O<sub>2</sub> and N<sub>2</sub>, indicating that equilibrium-based O<sub>2</sub> separation from N<sub>2</sub> is difficult. 21 MOFs gave higher  $K_{\text{Henry}}$  values for N<sub>2</sub> than O<sub>2</sub>. Figure 6.2(b) shows that  $Q_{\text{st}}^0$  values for N<sub>2</sub> (from 5.4 to 59.4 kJ/mol) were much higher than those for O<sub>2</sub> (from 5.6 to 24.5 kJ/mol), indicating stronger adsorption of N<sub>2</sub> molecules within these frameworks. This can be attributed to higher quadrupolar moment of N<sub>2</sub> molecules (almost 4 times) than that of O<sub>2</sub>. [110] The relation between LCDs of MOFs and their adsorption selectivities calculated at 298 K and infinite dilution was given in Figure 6.2(c).  $S^0_{(\text{O}_2/\text{N}_2)}$  of MOFs was in the range of  $5 \times 10^{-4}$  and 1.51. Their infinite dilution adsorption selectivities were calculated between 1 and 0.5, since 257 MOFs gave similar  $K_{\text{Henry}}$  values of O<sub>2</sub> and N<sub>2</sub>. These MOFs can not be promising materials for adsorption-based O<sub>2</sub>/N<sub>2</sub> separation. 37 MOFs were identified as O<sub>2</sub> selective adsorbents due to their  $S^0_{(\text{O}_2/\text{N}_2)}$  values ranged from 1.0 to 1.51. On the other hand, 21 MOFs were identified as N<sub>2</sub> selective adsorbents because of their  $S^0_{(\text{O}_2/\text{N}_2)}$  values smaller than 0.5. In all these MOFs,  $Q_{\text{st}}^0$  values for N<sub>2</sub> were much higher than those for O<sub>2</sub>, indicating stronger adsorption of N<sub>2</sub> molecules because of the enhanced electrostatic interactions between N<sub>2</sub> gas molecules and the free cations.



## CHAPTER VI: Bio-compatible MOFs for Storage and Separation of O<sub>2</sub>: A Molecular Simulation Study

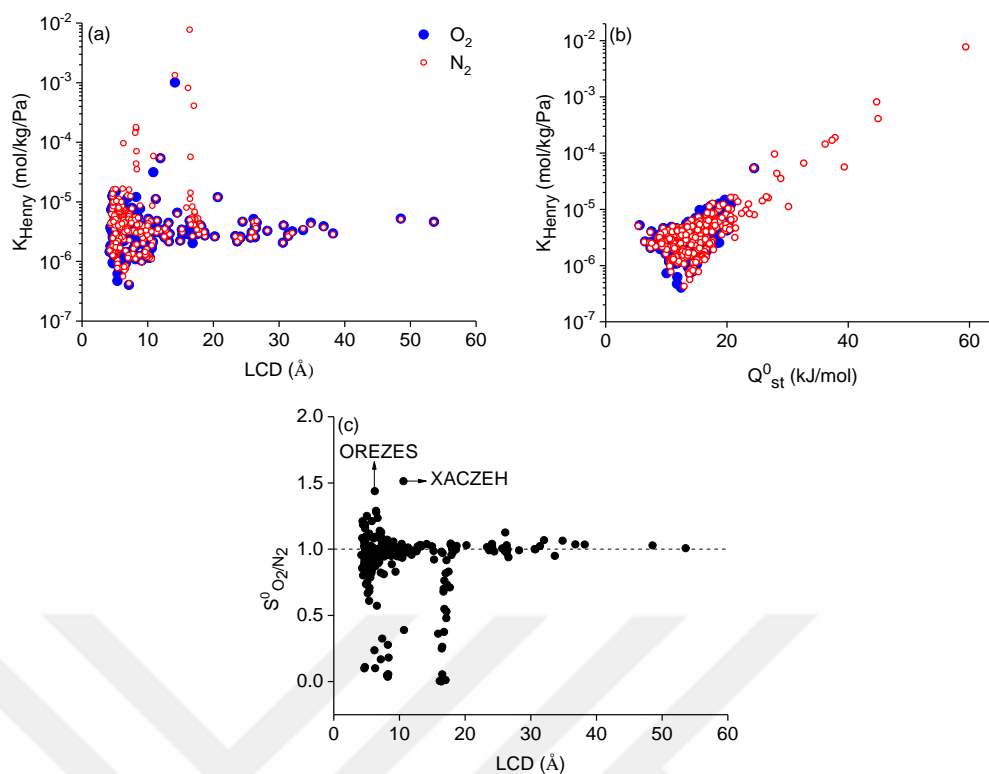


**Figure 6.2** Relations between (a)  $K_{\text{Henry}}$  of gas molecules and LCDs of MOFs, (b)  $K_{\text{Henry}}$  of gases and  $Q_{\text{st}}^0$ , and (c)  $S^0$  and LCDs of MOFs at 298 K.

The top performing 15 MOFs ranked based on their  $S^0_{(\text{O}_2/\text{N}_2)}$  were given in Table 6.1. Among 315 MOFs, OREZES and XACZEH were identified as the top two candidates having the highest  $S^0_{(\text{O}_2/\text{N}_2)}$  (1.4 and 1.5, respectively). These MOFs gave much higher  $Q_{\text{st}}^0$  values for O<sub>2</sub> adsorption (14.6 and 16.5 kJ/mol, respectively) than those for N<sub>2</sub> adsorption (13.9 and 14.5 kJ/mol, respectively) which can be explained by their open metal sites including Ca (calcium) in OREZES and Cu in XACZEH. McIntyre et al.[78] also elucidated that MOFs with open metal sites can be great candidates as adsorbents for O<sub>2</sub> separation from air. CATDEH, CATDIL, CAYRIE and CAYROK have almost same pore volumes ( $\sim 0.4 \text{ cm}^3/\text{g}$ ) and pore sizes ( $\sim 6.5 \text{ \AA} \times 5 \text{ \AA}$ ) due to their common Zn-porphyrin based structures. Thus, these MOFs gave almost the similar  $S^0_{(\text{O}_2/\text{N}_2)}$  ( $\sim 1.3$ ). SADZUV, which is a peptide-based MOF

## CHAPTER VI: Bio-compatible MOFs for Storage and Separation of O<sub>2</sub>: A Molecular Simulation Study

with Cu metal sites, and DEPJIR02, which is a formate-based MOF with Zn metal sites, have the highest pore volume ( $\sim 0.6 \text{ cm}^3/\text{g}$ ) in these 15 MOFs, also they have similar  $S^0_{(\text{O}_2/\text{N}_2)}$  (1.2). FIFNUE, FIFNUE01, FIFPAM and FIFPAM01, which have formate-linkers, gave similar performances due to their common structural properties, such as pore sizes ( $\sim 5 \text{ \AA} \times 4 \text{ \AA}$ ) and pore volumes ( $\sim 0.4 \text{ cm}^3/\text{g}$ ). CAYSIE, which has a porphyrin organic linkers with Co metal sites, gave the lowest adsorption selectivity of O<sub>2</sub> over N<sub>2</sub> as 1.1 at infinite dilution.

**Table 6.1** Top performing 15 MOFs identified for  $S^0_{(\text{O}_2/\text{N}_2)}$  at infinite dilution and 298 K with their calculated physical properties.

MOFs	LCD - PLD (Å)	PV (cm <sup>3</sup> /g)	$S^0_{(\text{O}_2/\text{N}_2)}$
XACZEH	10.61 – 7.24	0.50	1.51
OREZES	6.25 – 4.66	0.22	1.44
CATDEH	6.43 – 4.83	0.40	1.29
CAYROK	6.46 – 4.90	0.39	1.28
MIXJOU	5.04 – 3.82	0.48	1.25
CAYRIE	6.67 – 5.10	0.41	1.23
CATDIL	6.68 – 5.04	0.40	1.23
SADZUV	5.80 – 4.08	0.63	1.21
DEPJIR02	4.39 – 3.81	0.58	1.21
FIFPAM	4.70 – 3.85	0.40	1.19
WIWHUG	4.44 – 3.92	0.30	1.18
FIFPAM01	4.72 – 3.78	0.41	1.18
FIFNUE01	4.77 – 3.93	0.41	1.18
FIFNUE	4.78 – 3.96	0.41	1.16
CAYSIE	7.01 – 4.99	0.39	1.14

The adsorption-based gas separation performance of MOFs has been generally investigated at infinite dilution conditions due to lower computational time. To better understand real separation performances of MOFs for industrial applications, mixture adsorption selectivities should also be considered for the top promising candidates. For this reason, binary mixture GCMC simulations for the

## CHAPTER VI: Bio-compatible MOFs for Storage and Separation of O<sub>2</sub>: A Molecular Simulation Study

top 15 candidates were performed at five various pressures (1, 5, 10, 100 and 140 bar) and 298 K. Bulk composition of binary mixture was assumed as O<sub>2</sub>/N<sub>2</sub>:21/79 to mimic air concentration. Comparison between mixture adsorption selectivities and those obtained from infinite dilution conditions was given in Figure 6.3. Figure 6.3(a) shows the relation between  $S^0_{(O_2/N_2)}$  and binary mixture adsorption selectivities up to 140 bar. Binary mixture adsorption selectivities for O<sub>2</sub>/N<sub>2</sub> separation were ranged from 1.1 to 1.5 for these MOFs at 1, 5 and 10 bar. Results showed that predictions at infinite dilution conditions can give a precise description about the adsorption-based air separation performance of MOFs up to 10 bar. Selectivity is not dependent on the bulk gas composition at low pressures. However, while increasing the pressure up to 100 bar, mixture adsorption selectivities for O<sub>2</sub> over N<sub>2</sub> differed (1.2-1.8) from those obtained at infinite dilution. This was attributed to packing effects occurred at high pressures. The distribution of binary mixture adsorption selectivities of the top 15 MOFs computed from binary mixture GCMC simulations was given in Figure 6.3(b). As shown in this figure, adsorption selectivities at low pressures is almost constant. When the pressure increased up to 10 bar, mixture adsorption selectivities showed a general tendency to increase while increasing pressure. Only for XACZEH, mixture adsorption selectivities followed a decreasing trend with increasing pressure.

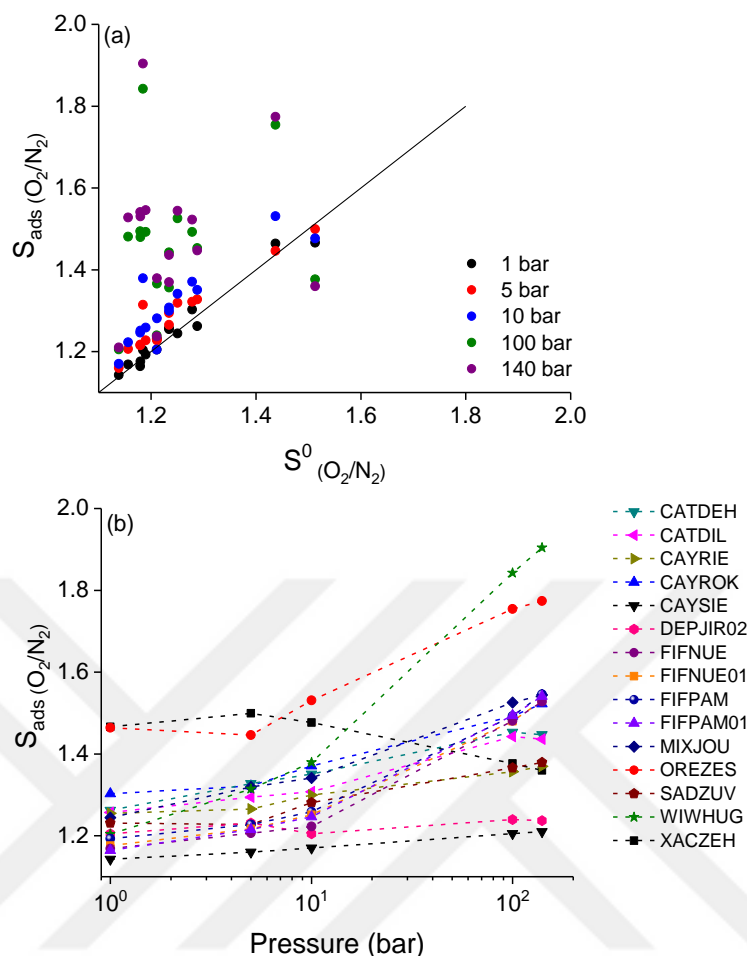


**Figure 6.3** (a) Comparison of infinite dilution adsorption selectivities with mixture adsorption selectivities at 1, 5, 10, 100 and 140 bar and (b) Binary mixture adsorption selectivities of top 15 MOFs ranked based on  $S^0_{(O_2/N_2)}$  up to 140 bar at 298 K.

In order to better understand the adsorption mechanism at high pressures, adsorption isotherms of O<sub>2</sub> and N<sub>2</sub> in two MOFs, WIWHUG and XACZEH, were computed because of their different trends in binary mixture selectivities. WIWHUG showed a sharp increase with increasing pressure, whereas XACZEH showed a sharp decrease with increasing pressure. Figure B.1 (B.2) shows adsorption isotherms (screenshots) of O<sub>2</sub> and N<sub>2</sub> in these MOFs up 140 bar and 298

## CHAPTER VI: Bio-compatible MOFs for Storage and Separation of O<sub>2</sub>: A Molecular Simulation Study

K. As shown in Figure B.1, O<sub>2</sub> and N<sub>2</sub> adsorptions in WIWHUG were close to saturation at low pressures due to its smaller pore volume (0.3 cm<sup>3</sup>/g) than XACZEH (0.5 cm<sup>3</sup>/g). Since WIWHUG has narrow pore windows (4.4 Å×3.9 Å), small O<sub>2</sub> molecules (3.46 Å) could find space at high pressures as shown in Figure B.2. Therefore, O<sub>2</sub>/N<sub>2</sub> selectivity increased. On the other hand, both N<sub>2</sub> and O<sub>2</sub> molecules were adsorbed in XACZEH with increasing pressure due to larger spherical-type pore apertures (10.6 Å× 7.2 Å) and its higher pore volume. Since N<sub>2</sub> uptake in XACZEH was almost three times higher than O<sub>2</sub> uptake at high pressures, O<sub>2</sub>/N<sub>2</sub> selectivity decreased. Overall, our results showed that adsorption-based air separation using bio-compatible MOFs can be challenging due to similar interaction energies of gas molecules with the frameworks' atoms, however MOFs which have non-saturated metal sites can be used as adsorbents due to their higher adsorption selectivities for O<sub>2</sub>/N<sub>2</sub> binary mixture.

### 6.3.3 O<sub>2</sub> Storage in 315 Bio-compatible MOFs

After adsorbent-separation of O<sub>2</sub> over N<sub>2</sub>, the capacity of MOFs were tested for high pressure O<sub>2</sub> storage. Since conventional compressed O<sub>2</sub> adsorption (desorption) pressure is 140 (5) bar for high-pressure tanks, O<sub>2</sub> working capacities of 315 bio-compatible MOFs were calculated at 140 bar storage and 5 bar desorption pressures at 298 K. Table 6.2 shows the best performing 15 MOFs ranked based on their gravimetric O<sub>2</sub> working capacities.

**Table 6.2** Top performing 15 MOFs identified for gravimetric WC<sub>O<sub>2</sub></sub> obtained at 140 bar storage and 5 bar desorption pressures at 298 K together with their calculated physical properties and S<sup>0</sup><sub>(O<sub>2</sub>/N<sub>2</sub>)</sub>.

MOF	LCD – PLD (Å)	PV (cm <sup>3</sup> /g)	S <sup>0</sup> <sub>(O<sub>2</sub>/N<sub>2</sub>)</sub>	WC <sub>O<sub>2</sub></sub> (mol/kg)
MOSDIJ	48.55 – 29.10	7.96	1.03	52.85
ADATEG	26.34 – 13.79	3.18	1.03	32.99

CHAPTER VI: Bio-compatible MOFs for Storage and Separation of O<sub>2</sub>: A Molecular Simulation Study

RAVXIX	53.58 – 53.26	3.85	1.01	29.42
TOCJEC	31.40 – 26.28	3.21	1.02	24.72
RAVXAP	34.86 – 34.36	2.95	1.06	24.40
MERLED	26.46 – 25.19	2.44	1.00	22.70
RAVWUI	36.79 – 36.43	2.54	1.04	21.63
SAPBIW	20.23 – 14.72	2.64	1.03	21.61
BIPSUQ	18.61 – 16.93	1.92	1.00	20.78
BORYOY	18.18 – 14.41	2.08	0.98	20.69
RAVWIW	30.70 – 30.15	2.28	1.00	20.25
BEWCUD	10.59 – 8.54	1.61	1.01	19.87
ADUROI	25.67 – 17.11	2.08	1.01	19.71
DOGBEI	26.04 – 14.54	1.98	0.99	19.66
RAVWOC	28.22 – 27.56	2.10	0.99	17.97

The best performing MOFs exhibited generally high pore volumes (from 2 to 8 cm<sup>3</sup>/g) and large pore apertures (9-15 Å). As shown in Table 6.2, MOSDIJ (PCN-332(Fe)) gave the highest gravimetric O<sub>2</sub> working capacity as 52.9 mol/kg due to its highest pore volume (7.9 cm<sup>3</sup>/g) and the largest surface area (5668.9 m<sup>2</sup>/g). ADATEG and RAVXIX exhibited similar working capacities for O<sub>2</sub> as ~30 mol/kg due to their similar pore volumes (3.2 and 3.9 cm<sup>3</sup>/g, respectively). MOF-74 series including RAVWIW, RAVWOC, RAVWUI, RAVXAP and RAVXIX gave high O<sub>2</sub> working capacities (18-29 mol/kg) due to their large pore volumes and open-metal sites. SAPBIW (also known as bio-MOF-100) and TOCJEC (also known as bio-MOF-102), which have adenine as organic linkers, also exhibited high O<sub>2</sub> working capacities (22-25 mol/kg) due to their high pore volumes (~3 cm<sup>3</sup>/g). This may also be explained by free dimethylammonium (DMA) cations, which enhanced adsorbate-adsorbate interactions. BEWCUD, BIPSUQ, BORYOY, DOGBEI (also known as PCN-224-Ni) and MERLED were synthesized by porphyrins as building units, showed almost similar working capacities of O<sub>2</sub> (20-23 mol/kg). Among these 5 MOFs, MERLED gave the highest O<sub>2</sub> working capacity (23 mol/kg) because of highest pore volume and largest pore size. It should be noted

## CHAPTER VI: Bio-compatible MOFs for Storage and Separation of O<sub>2</sub>: A Molecular Simulation Study

that these top performing MOFs outperformed the previously reported promising materials, including NU-125 (15.7 mol/kg), Cu-BTC (11.9 mol/kg)[76] and UMCM-152 (19.6 mol/kg)[77] also traditional adsorbent materials such as activated carbon (8 mol/kg) and NaX zeolite (6.6 mol/kg) in terms of gravimetric O<sub>2</sub> working capacity. The top performing MOFs identified for adsorption-based O<sub>2</sub>/N<sub>2</sub> separation (given in Table 6.1) are not the same those identified for O<sub>2</sub> storage. As discussed in the literature[78], the pore geometry and/or pore sizes have a significant affect on O<sub>2</sub>/N<sub>2</sub> adsorption selectivity. Since pore volume has a more pronounced effect on O<sub>2</sub> storage, the best performing MOFs which have the highest O<sub>2</sub> working capacities are not the best candidates for adsorbent-based air separation. For adsorbent-based O<sub>2</sub>/N<sub>2</sub> separation, MOFs which have mediocre pore volumes such as XACZEH can be selective adsorbents with moderate O<sub>2</sub> working capacities.

Volumetric O<sub>2</sub> working capacities of 315 MOFs were also calculated since volumetric capacities were required to determine the size of the tank. Figure B.3 shows the relation between gravimetric and volumetric O<sub>2</sub> working capacities of 315 MOFs together with their porosities. The MOFs with high gravimetric capacities generally exhibited low volumetric capacities. For example, MOSDIJ has the highest gravimetric O<sub>2</sub> working capacity among 315 MOFs, but its volumetric deliverable capacity is moderate (141.8 cm<sup>3</sup> (STP)/cm<sup>3</sup>) due to its low density (0.12 g/cm<sup>3</sup>). Large surface area and high pore volume increased the gravimetric O<sub>2</sub> working capacities, but low framework density decreased the volumetric O<sub>2</sub> working capacities. Similar results were reported in the literature.[77] The best performing 15 MOFs ranked based on their volumetric O<sub>2</sub> working capacities were given in Table 6.3.

**Table 6.3** Top performing 15 MOFs identified for volumetric WC<sub>O<sub>2</sub></sub> obtained at 140 bar adsorption and 5 bar desorption pressures at 298 K together with their calculated physical properties and S<sup>0</sup><sub>(O<sub>2</sub>/N<sub>2</sub>)</sub>.

MOF	LCD – PLD (Å)	PV (cm <sup>3</sup> /g)	S <sup>0</sup> <sub>(O<sub>2</sub>/N<sub>2</sub>)</sub>	WC <sub>O<sub>2</sub></sub> (cm <sup>3</sup> (STP)/cm <sup>3</sup> )
ADASOP	18.04 – 6.69	1.22	1.00	231.85
HIKSIF	16.57 – 4.85	0.97	0.97	226.17
LEPKEZ	10.10 – 5.73	0.99	0.95	225.71
BEWCUD	10.59 – 8.54	1.61	1.01	222.52
LEPKOJ	10.45 – 5.89	0.93	0.93	221.69
ZEZFIV	10.69 – 9.42	1.36	0.39	218.87
DUPVER	9.93 – 6.47	0.92	0.98	216.16
CUBBEI	11.32 – 8.35	1.12	1.01	215.02
SAHYIK	14.95 - 7.84	1.33	1.02	214.27
ADUWON	16.38 – 6.00	1.48	0.98	213.76
PICZAE	8.79 – 4.97	0.97	0.95	212.95
FIQCEN	13.19 – 6.67	0.82	1.03	212.02
RAVVUH	17.18 – 16.38	1.23	0.92	211.82
ADUWIH	9.28 – 6.55	0.99	1.02	210.25
AGAXIP	8.05 – 6.78	0.84	0.99	209.65

The best MOFs exhibited generally mediocre pore volumes (0.8-1.6 cm<sup>3</sup>/g) and pore apertures (8-18 Å). As shown in Table 6.3, ADASOP gave the highest volumetric O<sub>2</sub> working capacity (231.9 cm<sup>3</sup> (STP)/cm<sup>3</sup>) due to its high porosity (0.8). Following ADASOP, HIKSIF (also known as Zr-PCN-221(Cu)), LEPKEZ and LEPKOJ gave almost the same working capacities (~225 cm<sup>3</sup> (STP)/cm<sup>3</sup>) because of their large surface areas (~2800 m<sup>2</sup>/g) and high porosities (~0.7). ZEZFIV, DUPVER, CUBBEI, SAHYIK, ADUWON, PICZAE and FIQCEN (common name as Cu-BTC) gave similar volumetric O<sub>2</sub> working capacities (212-218.8 cm<sup>3</sup> (STP)/cm<sup>3</sup>) due to their similar porosities (~0.7). Among these 7 MOFs, ZEZFIV exhibited the highest O<sub>2</sub> working capacity because of its free DMA cations which enhanced adsorbate-adsorbate interactions. RAVVUH, ADUWIH and



## CHAPTER VI: Bio-compatible MOFs for Storage and Separation of O<sub>2</sub>: A Molecular Simulation Study

AGAXIP gave similar volumetric O<sub>2</sub> working capacities as almost 210 cm<sup>3</sup> (STP)/cm<sup>3</sup>.

Establishing structure-performance relationships is important to better understand materials' behaviour and to synthesize materials with desired properties. Therefore, the relations between gravimetric and volumetric O<sub>2</sub> working capacities of MOFs and their physical/chemical structural properties including LCD, PLD, density, PV, SA, porosity ( $\phi$ ) and  $Q_{st}^0$  in Figure B.4. As shown in Figure B.4(a), correlation coefficients ( $R^2 > 0.8$ ) were found to be very high for the relations between gravimetric working capacities and PVs, SAs and porosities of MOFs. Since the framework density is an important parameter for volumetric capacities[77], instead of PV and porosity gave a high correlation coefficient ( $R^2 = 0.7$ ) for the volumetric capacity. Weak correlations between volumetric capacities of MOFs and their LCDs, PLDs, PVs and  $Q_{st}^0$  values were given in Figure B.4(b).

CHAPTER VI: Bio-compatible MOFs for Storage and Separation of O<sub>2</sub>: A Molecular Simulation Study

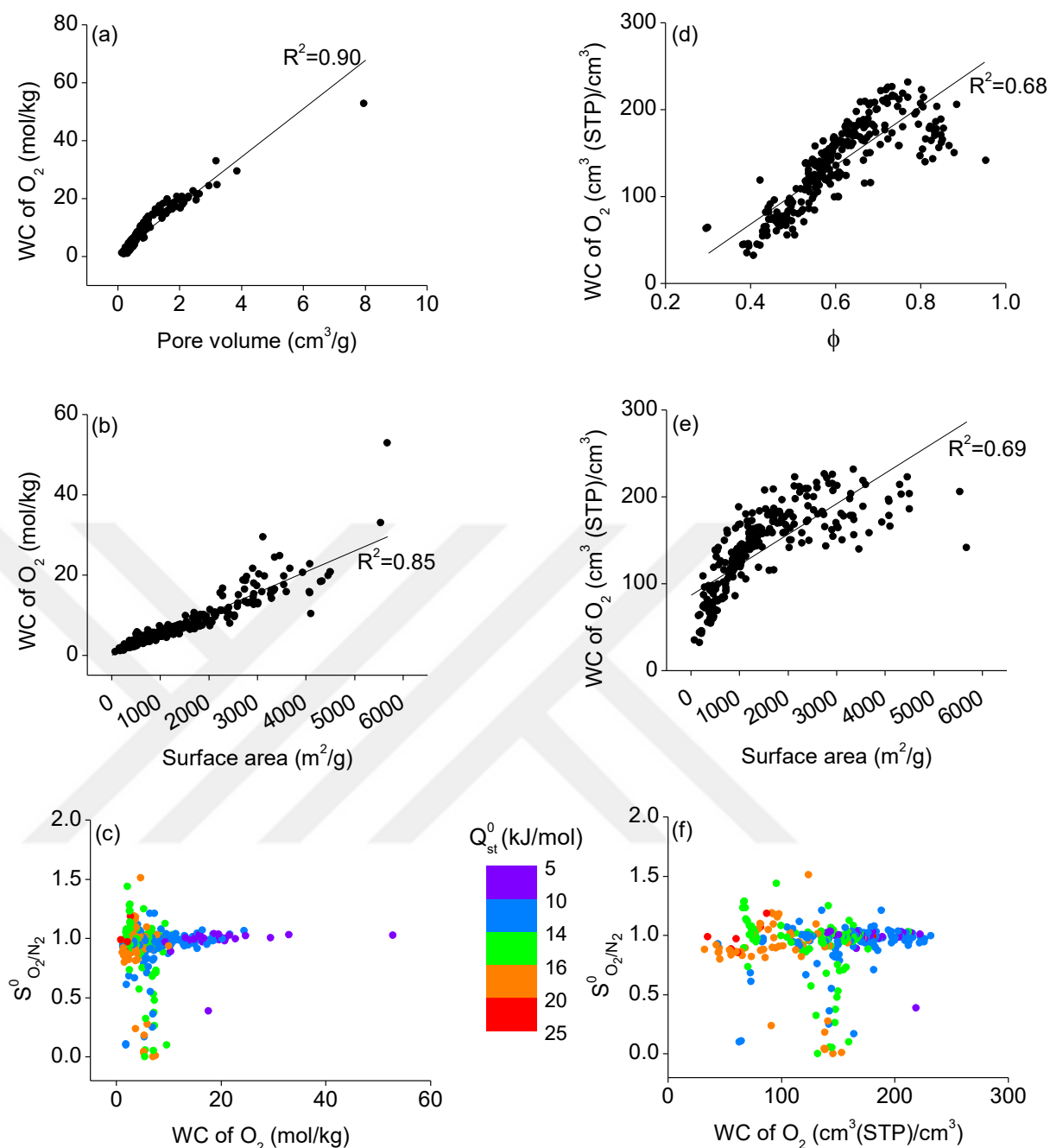


**Figure 6.4** Relations between (a)pore volume and gravimetric  $w_{C_{O_2}}$ , (b)surface area and gravimetric  $w_{C_{O_2}}$ , (c)gravimetric  $w_{C_{O_2}}$  and  $S_{(O_2/N_2)}^0$ , (d)porosity and volumetric  $w_{C_{O_2}}$ , (e)surface area and volumetric  $w_{C_{O_2}}$ , (f)volumetric  $w_{C_{O_2}}$  and  $S_{(O_2/N_2)}^0$  of MOFs at 298 K. The data points in (c) and (f) graphs are color coded by infinite dilution isosteric heat of adsorption of O<sub>2</sub>.

As shown in Figure 6.4(a) and (b), there is an obvious linear relationship between gravimetric O<sub>2</sub> working capacities of MOFs and their PVs and/or SAs. O<sub>2</sub> working

## CHAPTER VI: Bio-compatible MOFs for Storage and Separation of O<sub>2</sub>: A Molecular Simulation Study

capacities of MOFs increased from 0.8 mol/kg to 52.9 mol/kg, as the PVs (0.1-7.9 cm<sup>3</sup>/g) and SAs (74.7-5668.9 m<sup>2</sup>/g) of MOFs increased. Figure 6.4(c) shows that the relation between gravimetric O<sub>2</sub> working capacities, infinite dilution adsorption selectivities and heat of adsorption of O<sub>2</sub> values. As O<sub>2</sub> working capacities of MOFs increased, their adsorption selectivities and heats of adsorption generally decreased. The highest O<sub>2</sub> gravimetric capacity was obtained for MOFs with heats of adsorption (~7 kJ/mol), whose O<sub>2</sub>/N<sub>2</sub> selectivities were around 1 due to their large PVs. Figure 6.4(d) and (e) show relations between volumetric O<sub>2</sub> working capacities of 315 MOFs (32.2-230 cm<sup>3</sup> (STP)/cm<sup>3</sup>) and their porosities (0.3-0.9) and SAs (74.7-5668.9 m<sup>2</sup>/g). No obvious correlation was found between volumetric capacities, adsorption selectivities and O<sub>2</sub> heats of adsorption as shown in Figure 6.4(f). The highest O<sub>2</sub> volumetric working capacity was obtained for MOFs with heats of adsorption between 11-12 kJ/mol, whose O<sub>2</sub>/N<sub>2</sub> selectivities was around 1 due to their high porosities between 0.7-0.8. The high heats of adsorption of O<sub>2</sub> (20-25 kJ/mol) were observed for MOFs with porosities between 0.4-0.6, resulting in low volumetric capacities.

It is important to discuss structural stabilities of these promising 45 MOFs, which were ranked based on their  $S^0_{(O_2/N_2)}$ , gravimetric and volumetric O<sub>2</sub> working capacities. Porphyrin-based materials such as CAYSIE[232], DOGBEI[233] and MERLED (common name: PCN-600-Fe)[234] have the highest thermal stabilities almost up to 620 K. Similarly, 6 materials in MOF-74 series (RAVVUH, RAVWIW, RAVWOC, RAVWUI, RAVXAP and RAVXIX)[235] and SAHYIK (also known as IRMOF-1)[26] have high thermal stabilities up to 570 K. These top performing materials have generally high thermal stabilities up to 470 K except ADUWIH and ADUWON (family structures and common name as MOF-1 and MOF-2,

## CHAPTER VI: Bio-compatible MOFs for Storage and Separation of O<sub>2</sub>: A Molecular Simulation Study

respectively)[236], BIPSUQ[237], BORYOY[238], DUPVER[239], FIFNUE01 and FIFPAM01 (family structures)[240], LEPKEZ and LEPKOJ (family structures)[241], PICZAE[242] and XACZEH[243] which have thermal stabilities up to almost 320 K. Chemical and physical stabilities of these MOFs after solvent removal should be also investigated prior to industrial applications. It is also important to note that among all the top performing materials, 35 MOFs have open metal sites except BEWCUD, CAYSIE, CUBBEI, MIXJOU, MOSDIJ, PICZAE, SAHYIK (IRMOF-1), SAPBIW (bio-MOF-100) and TOCJEC (bio-MOF-102).

### 6.3.4 Membrane-based O<sub>2</sub>/N<sub>2</sub> Separation

Equilibrium-based air separation is challenging because of the similar interactions of O<sub>2</sub> and N<sub>2</sub> gas molecules with the atoms of the frameworks. Thus, kinetic-based separation performances of the top performing 44 materials (BEWCUD is common among the MOFs with the highest gravimetric and volumetric O<sub>2</sub> working capacities) were also examined. For the kinetic-based gas separation, both the investigation of adsorption and diffusion of gas molecules are important to better assess. In order to understand gas transport in these materials, binary mixture MD simulations were performed by using adsorbed O<sub>2</sub> and N<sub>2</sub> amounts obtained from binary mixture GCMC simulations at 1 bar and 298 K. Figure 6.5 shows O<sub>2</sub> permeabilities (ranged from  $4.0 \times 10^3$  to  $1.8 \times 10^6$  Barrer) and O<sub>2</sub>/N<sub>2</sub> membrane selectivities (0.2-11) of these 44 materials together with the Robeson's 1991 and 2008 upper bounds. Since a few MOFs gave high O<sub>2</sub> permeabilities, the Robeson's upper bounds were extrapolated and represented high permeability region with a dash line.

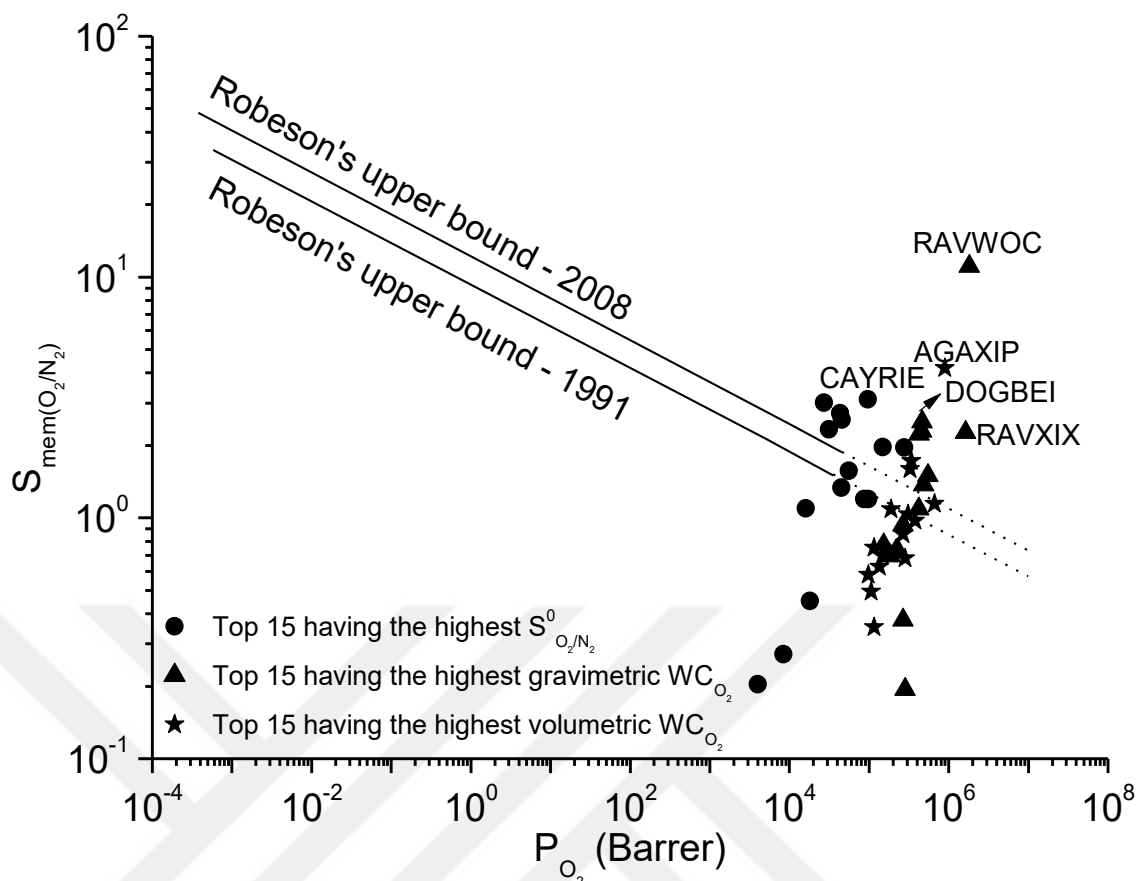


**Figure 6.5** Membrane selectivity and O<sub>2</sub> permeability of promising MOF membranes for O<sub>2</sub>/N<sub>2</sub> separation.

Table 6.4 shows the best promising 17 materials which surpass the Robeson's upper bound. Structural properties of these materials including linkers, metal centers and crystal types were given in Table B.1. In all these MOFs, smaller O<sub>2</sub> gas molecules (3.46 Å) diffused faster than N<sub>2</sub> gas molecules (3.64 Å) through the pores of MOFs and diffusion selectivity favored O<sub>2</sub>.

**Table 6.4** Adsorption, diffusion and membrane selectivity data together with gas diffusivities and permeabilities for MOF membranes which surpass Robeson's 2008 upper bound for air separation.

MOF	$D_{O_2, self}$	$D_{N_2, self}$	$P_{O_2}$	$P_{N_2}$	$S_{ads}(O_2/N_2)$	$S_{diff}(O_2/N_2)$	$S_{mem}(O_2/N_2)$
-----	-----------------	-----------------	-----------	-----------	--------------------	---------------------	--------------------

CHAPTER VI: Bio-compatible MOFs for Storage and Separation of O<sub>2</sub>: A Molecular Simulation Study

AGAXIP	$7.21 \times 10^{-4}$	$1.70 \times 10^{-4}$	$8.94 \times 10^5$	$2.14 \times 10^5$	0.99	4.23	4.19
BIPSUQ	$1.40 \times 10^{-3}$	$9.29 \times 10^{-4}$	$5.47 \times 10^5$	$3.65 \times 10^5$	1.00	1.50	1.50
BORYOY	$1.02 \times 10^{-3}$	$4.38 \times 10^{-4}$	$4.59 \times 10^5$	$2.00 \times 10^5$	0.98	2.34	2.29
CATDIL	$1.34 \times 10^{-4}$	$6.19 \times 10^{-5}$	$4.35 \times 10^4$	$1.61 \times 10^4$	1.26	2.16	2.72
CAYRIE	$2.68 \times 10^{-4}$	$1.08 \times 10^{-4}$	$9.63 \times 10^4$	$3.10 \times 10^4$	1.25	2.48	3.10
CUBBEI	$5.60 \times 10^{-4}$	$3.27 \times 10^{-4}$	$3.38 \times 10^5$	$1.97 \times 10^5$	1.00	1.71	1.71
DEPJRO2	$2.34 \times 10^{-4}$	$1.43 \times 10^{-4}$	$1.49 \times 10^5$	$7.56 \times 10^4$	1.20	1.63	1.96
DOGBEI	$1.20 \times 10^{-3}$	$4.75 \times 10^{-4}$	$4.64 \times 10^5$	$1.85 \times 10^5$	0.99	2.53	2.50
FIFNUE	$4.49 \times 10^{-5}$	$2.05 \times 10^{-5}$	$4.57 \times 10^4$	$1.79 \times 10^4$	1.17	2.19	2.56
FIFPAM	$2.71 \times 10^{-5}$	$1.08 \times 10^{-5}$	$2.71 \times 10^4$	$9.01 \times 10^3$	1.19	2.52	3.00
HIKSIF	$3.63 \times 10^{-4}$	$2.23 \times 10^{-4}$	$3.29 \times 10^5$	$2.06 \times 10^5$	0.98	1.63	1.60
RAVWOC	$4.88 \times 10^{-3}$	$4.44 \times 10^{-4}$	$1.82 \times 10^6$	$1.64 \times 10^5$	1.01	10.99	11.10
RAVXAP	$1.31 \times 10^{-3}$	$1.01 \times 10^{-3}$	$4.85 \times 10^5$	$3.53 \times 10^5$	1.06	1.30	1.38
RAVXIX	$5.60 \times 10^{-3}$	$2.48 \times 10^{-3}$	$1.62 \times 10^6$	$7.15 \times 10^5$	1.00	2.25	2.25
SADZUV	$5.32 \times 10^{-5}$	$2.81 \times 10^{-5}$	$3.13 \times 10^4$	$1.34 \times 10^4$	1.23	1.90	2.34
SAPBIW	$1.67 \times 10^{-3}$	$7.89 \times 10^{-4}$	$4.25 \times 10^5$	$1.91 \times 10^5$	1.05	2.12	2.23
WIWHUG	$1.09 \times 10^{-4}$	$6.72 \times 10^{-5}$	$2.77 \times 10^5$	$1.42 \times 10^5$	1.20	1.62	1.94

Since adsorption selectivities were almost unity in these MOFs membrane selectivities were governed by diffusion selectivities. RAVWOC is the most promising membrane for O<sub>2</sub>/N<sub>2</sub> separation among 44 MOFs due to its very high O<sub>2</sub> permeability ( $1.8 \times 10^6$  Barrer) and high membrane selectivity (11). High membrane selectivity of RAVWOC was driven by high diffusion selectivity (11) towards O<sub>2</sub>, since O<sub>2</sub> diffusion ( $4.9 \times 10^{-3}$  cm<sup>2</sup>/s) was one order of magnitude higher than N<sub>2</sub> diffusion ( $4.4 \times 10^{-4}$  cm<sup>2</sup>/s) in this MOF. Following RAVWOC, AGAXIP showed

## CHAPTER VI: Bio-compatible MOFs for Storage and Separation of O<sub>2</sub>: A Molecular Simulation Study

high O<sub>2</sub> permeability ( $8.9 \times 10^5$  Barrer) and moderate membrane selectivity (4.2). Among these MOFs, BIPSUQ, BORYOY, CUBBEI, DOGBEI, HIKSIF, RAVXAP, RAVXIX and SAPBIW (common name bio-MOF-100) gave high O<sub>2</sub> permeabilities (from  $3.3 \times 10^5$  to  $1.6 \times 10^6$  Barrer) however low membrane selectivities (a range from 1.4 to 2.5). The high O<sub>2</sub> permeabilities in these MOFs were attributed to their high pore volumes (0.6-2.9 cm<sup>3</sup>/g). Among these MOFs, RAVXAP and RAVXIX have isorecticular structures with RAVWOC. However, membrane selectivities of RAVXAP (1.4) and RAVXIX (2.3) were much lower than the membrane selectivity of RAVWOC (11.1). Self-diffusion coefficients of O<sub>2</sub> and N<sub>2</sub> have the same order of magnitude in these MOFs, resulting in low diffusion selectivities (1.3-2.3). Self-diffusion coefficients of O<sub>2</sub> ( $1.3 \times 10^{-3}$  cm<sup>2</sup>/s) and N<sub>2</sub> ( $1 \times 10^{-3}$  cm<sup>2</sup>/s) in RAVXAP were almost the same, indicating a non-selective diffusion. This may be attributed to slightly higher isosteric heat of adsorption value of O<sub>2</sub> (11 kJ/mol) than that of N<sub>2</sub> (10 kJ/mol) in this MOF. DEPJIR02 and WIWHUG exhibited similar performances due to their similar adsorption (1.2) and diffusion (1.6) selectivities. CATDIL, CAYRIE, FIFNUE, FIFPAM and SADZUV gave similar mediocre O<sub>2</sub> permeabilities ( $2.7 \times 10^4$ - $9.6 \times 10^4$  Barrer) and membrane selectivities (2.3-3.1) due to their similar structural properties including pore volumes (0.05-0.14 cm<sup>3</sup>/g) and pore sizes (3.9-6.7 Å). Results showed that 17 bio-compatible MOFs outperformed traditional polymeric membranes in terms of O<sub>2</sub> permeability and O<sub>2</sub> selectivity over N<sub>2</sub>. However, it should be noted that our simulations do not give any information about the stabilities of these MOF membranes. The permeabilities and selectivities reported in this chapter were estimated by assuming defect-free and ideal membranes. For real synthesis, cracks and/or defects may be occurred at the interface which can

## CHAPTER VI: Bio-compatible MOFs for Storage and Separation of O<sub>2</sub>: A Molecular Simulation Study

effect the flux of gas molecules through the pores of MOF membranes. Moreover, industrial-scale synthesis of these MOFs requires large-scale production in which the cost and the rapid availability of reactants, a high-yield synthesis procedure and purity of the compounds should be considered.[52] Among the promising materials, RAVWOC, RAVXAP and RAVXIX are isorecticular series of MOF-74, which is commercially produced.[52] Non-toxic metal sources and/or bio-compatible linkers offer a tremendous opportunity for environmentally-friendly MOF synthesis.[244] However, future experimental work is required to address the challenges related to scalable synthesis of these MOFs.



## CHAPTER VII

### CONCLUSION

The development of efficient adsorbents and membranes is required for volatile organic compound separation, hydrogen storage and air separation. MOFs and COFs have great potential in various gas storage and gas separation applications as discussed throughout this thesis. MOFs, which have non-toxic metal sites and endogenous linkers, also are great candidates for biomedical applications. However, identifying promising MOFs using only experimental methods is difficult due to the large number of available COFs and MOFs in the literature. Herein, molecular simulations play a key role to identify the top performing materials providing quick and reliable information about the gas separation and/or gas storage mechanisms of MOFs and COFs. In this thesis, the potential of MOFs and COFs for various gas storage and separation applications was studied using molecular simulations.

In the first chapter of this thesis, the performances of 153 COFs, 14 IRMOFs and 8 ZIFs were assessed for adsorption-based separation of  $\text{CCl}_4$  from air at 298 K. The top three materials in each group, namely as BLP-2H-AA, IRMOF-11 and ZIF-6, were identified based on their results of adsorption selectivities for  $\text{CCl}_4/\text{Ar}$ ,  $\text{CCl}_4/\text{N}_2$  and  $\text{CCl}_4/\text{O}_2$  mixtures at infinite dilution conditions and 298 K. Single-component adsorption for these four different gas molecules, binary mixture ( $\text{CCl}_4/\text{Ar}$ ,  $\text{CCl}_4/\text{N}_2$  and  $\text{CCl}_4/\text{O}_2$ ) and quaternary air mixture (0.1%  $\text{CCl}_4$ , 0.999%  $\text{Ar}$ , 77.922%  $\text{N}_2$  and 20.979%  $\text{O}_2$ ) adsorption isotherms in these three top promising materials were then computed at 298 K.

## CHAPTER VII: Conclusion

Based on the results of binary mixture ( $\text{CCl}_4/\text{Ar}$ ,  $\text{CCl}_4/\text{N}_2$  and  $\text{CCl}_4/\text{O}_2$ ) adsorption selectivities, ZIF-6 outperformed BLP-2H-AA and IRMOF-11. Separation potentials of these frameworks were also calculated for binary and quaternary mixtures at 298 K and we observed similar trends with the binary adsorption selectivities. Among the top three candidates, ZIF-6 gave the highest separation potential, indicating that ZIF-6 can be used as an efficient adsorbent material in fixed bed units. The effect of relative humidity (80%) on adsorption-based  $\text{CCl}_4$  separation performance of ZIF-6 was also considered. Based on simulation results, ZIF-6 exhibited high selectivity towards  $\text{CCl}_4$  in  $\text{CCl}_4/\text{Ar}$ ,  $\text{CCl}_4/\text{N}_2$  and  $\text{CCl}_4/\text{O}_2$  binary mixtures at 80% relative humidity. It should be also emphasized that ZIF-6 has no open metal sites. Comparison with MOFs with no open metal sites, the adsorbents with open metal sites may have lower selectivity. To better understand this, investigation of adsorption of VOCs in a high number of materials is required at a wide range of relative humidity in further works. Single-component and quaternary mixture diffusivities of Ar,  $\text{CCl}_4$ ,  $\text{N}_2$  and  $\text{O}_2$  in ZIF-6 were finally computed. Results showed that the adsorbed number of gas molecules and the interaction strength between gas molecules and the host material affect diffusion of gas molecules. Results of this chapter will serve as a guide for experimental studies, particularly in the design and synthesis of promising COF, IRMOF and ZIF adsorbents to achieve high separation performance for removal of  $\text{CCl}_4$  from air.

In the second part of this work,  $\text{H}_2$  storage performance of 296 COFs was assessed at various temperatures and pressures. The top performing 10 COFs, which exhibited the maximum volumetric  $\text{H}_2$  working capacities were identified at different operating conditions. The effect of electrostatic interactions and the Feynman-Hibbs corrections on the ranking of the top

## CHAPTER VII: Conclusion

materials was also examined and results showed that coulombic interactions and the Feynman-Hibbs corrections do not actually affect the ranking of the COFs based on their working capacities. Among 296 COFs, COF-DL229-3fold outperformed the ultimate DOE 2020 and DOE 2025 technical targets for on board H<sub>2</sub> storage. The COFs which have high porosities ( $\geq 0.8$ ) and quite low densities (0.2-0.4 g/cm<sup>3</sup>) gave the promising performance for volumetric H<sub>2</sub> storage. Results of this study will be helpful for experimental studies to design and synthesize novel COFs to achieve efficient H<sub>2</sub> capture.

In the third part of this thesis, 1525 bio-compatible MOFs were initially identified, and their structural properties were estimated. Both adsorption-based and membrane-based separation of O<sub>2</sub> from N<sub>2</sub> using these MOFs were assessed at 298 K. O<sub>2</sub> working capacities of 315 MOFs which have SAs  $> 0$  m<sup>2</sup>/g and PLDs  $> 3.4$  Å, were also computed at adsorption (140 bar) and desorption pressures (5 bar). Top 45 MOFs, which gave the best adsorption selectivities, the highest gravimetric and volumetric O<sub>2</sub> working capacities at 298 K were identified. Results showed that XACZEH gave the highest adsorption selectivity (1.5) at infinite dilution and 298 K, due to its open Cu sites. Infinite dilution adsorption selectivities were also compared with the binary mixture adsorption selectivities. Results showed that infinite dilution adsorption selectivities can give quick and reasonable predictions about the adsorption-based air separation performances of MOFs at low pressures, but mixture GCMC simulations should be performed for more realistic performance predictions of MOFs at high pressures. Among 315 bio-compatible MOFs, MOSDIJ and ADASOP exhibited the highest gravimetric (52.9 mol/kg) and volumetric (231.9 cm<sup>3</sup> (STP)/cm<sup>3</sup>) O<sub>2</sub> working capacities, respectively due to their high porosities and large surface areas. Binary-mixture MD simulations were

## CHAPTER VII: Conclusion

performed to investigate the membrane-based air separation performances of the top promising MOFs. Among these MOFs, RAVWOC gave the highest membrane selectivity (11) due to its high O<sub>2</sub> permeability and high O<sub>2</sub> selectivity. 17 MOFs outperformed polymeric membranes by surpassing the Robeson's 2008 upper bound for O<sub>2</sub>/N<sub>2</sub> separation. This computational study will be helpful for identifying the promising bio-compatible MOFs for air separation and O<sub>2</sub> capture. The bio-compatible MOF library constructed in this work will also guide both experiments and computational studies, particularly in design and development of bio-compatible MOFs for various biomedical applications in future work. However, further studies are highly required to examine the stability and toxicity of linkers and metals in these materials for medical applications.

It should be important to note our assumptions used during molecular simulations. First, rigid frameworks were assumed for COFs and MOFs to save a significant amount of computational time. In molecular simulations, chemical and/or mechanical stability of the framework was not considered. COFs and MOFs were assumed to have uniform crystalline structures. However, structural stabilities of MOFs and COFs were checked from their articles which contain their synthesis. Symmetry space group of a framework also checked from its crystal file. Additionally, remaining solvent molecules and defects inside the frameworks can cause blockage for the frameworks' pores. These impurities were cleaned by a python script in the literature. For bio-MOFs, it is assumed that they have non-toxic linkers but to use these MOFs in a biological application, toxicity of these MOFs should be further investigated.

As a conclusion, results obtained from this thesis will be helpful to identify the promising materials for volatile organic compound separation,

## CHAPTER VII: Conclusion

hydrogen storage and air separation. The approaches described in this thesis will be a guide for further experimental and computational studies to investigate various types of materials for gas adsorption and gas separation applications. The biocompatible MOF library created in this thesis will be highly useful for future studies on biomedical applications of MOFs.



## APPENDICES

*APPENDIX A: Supplementary Information for Chapter IV<sup>1</sup>***Table A.1** Structural properties of COFs, IRMOFs, ZIFs

Structure	Name	LCD (Å)	PLD (Å)	$\frac{\text{LCD}}{\text{PLD}}$	Surface Area (m <sup>2</sup> /g)	Pore Volume (cm <sup>3</sup> /g)
COFs	2D-NiPc- BTDA <sup>[1]</sup> COF	12.34	11.96	1.03	1248.84	0.68
	3D-Py <sup>[2]</sup> - COF	24.44	21.57	1.13	7346.88	6.63
	3D-Py-COF- 2P <sup>[3]</sup>	13.47	12.29	1.10	7287.22	3.05
	4PE-1P <sup>[4]</sup>	24.32	23.92	1.02	2332.85	1.39
	4PE-2P <sup>[5]</sup>	32.33	32.02	1.01	2426.71	1.76
	4PE-3P <sup>[6]</sup>	39.21	38.93	1.01	2795.77	2.28
	4PE-TT <sup>[7]</sup>	27.58	27.23	1.01	2203.82	1.42
	AB-COF <sup>[8]</sup>	11.56	11.13	1.04	2010.45	0.96
	ACOF <sup>[9]</sup> -1	11.56	11.13	1.04	2010.45	0.96
	AEM <sup>[10]</sup> - COF-1	29.29	29.11	1.01	1863.62	1.58
	AEM-COF-2	32.26	32.10	1.00	1323.23	1.22
	ATFG <sup>[11]</sup> - COF	10.37	9.90	1.05	1562.20	0.70
	Azo <sup>[12]</sup> -COF	34.48	34.31	1.00	2048.29	2.01
	BDT <sup>[13]</sup> - COF	30.00	29.80	1.01	1809.73	1.54
	BDT- OEt <sup>[14]</sup> -COF	23.47	23.25	1.01	1844.77	1.18
	BF <sup>[15]</sup> -COF- 1	13.26	8.62	1.54	5055.69	1.96
	BF-COF-2	13.28	7.58	1.75	4345.08	1.65
	BLP <sup>[16]</sup> -2H- AA <sup>[17]</sup>	9.50	8.98	1.06	1168.05	0.56
	CC- TAPH <sup>[18]</sup> - COF	9.35	7.17	1.30	4343.24	1.53
	COF-10	31.52	31.34	1.01	1954.35	1.74
COF-102	9.04	7.99	1.13	5086.44	1.86	
COF-103	9.68	8.50	1.14	5294.65	2.05	
COF-105	18.80	16.12	1.17	6661.40	5.17	
COF-108	27.47	19.05	1.44	6378.08	5.38	
COF-11Å	8.39	7.65	1.10	520.44	0.61	
COF-14Å	10.52	9.84	1.07	1397.92	0.75	

<sup>1</sup>The results given in this chapter were published in Journal of Molecular Graphics and Modelling with following reference: Gulcay, E., & Erucar, I. (2019). Molecular simulations of COFs, IRMOFs and ZIFs for adsorption-based separation of carbon tetrachloride from air. *Molecular Graphics and Modelling*, 86, 84-94.

## APPENDICES

COF-16Å	12.73	12.23	1.04	1939.23	0.87
COF-18Å	14.71	14.33	1.03	1759.35	0.89
COF-202	9.87	5.41	1.82	4232.25	1.39
COF-300	9.36	9.26	1.01	3252.49	1.33
COF-320	8.45	8.29	1.02	1793.95	0.89
COF-366	20.46	18.69	1.09	4057.05	2.25
COF-42- bnn <sup>[19]</sup>	17.20	16.81	1.02	2658.96	1.29
COF-42- gra <sup>[20]</sup>	6.14	5.08	1.21	2317.93	1.00
COF-43-bnn	32.50	32.27	1.01	2600.76	2.35
COF-43-gra	13.67	13.35	1.02	3627.01	1.77
COF-5	23.65	23.42	1.01	1716.76	1.24
COF-6	9.15	8.56	1.07	1084.01	0.53
COF-66	27.00	26.66	1.01	4502.56	3.05
COF-8	16.54	16.22	1.02	1554.43	0.93
COF-AA-H	25.69	25.30	1.02	2270.03	1.45
COF <sub>BTA</sub> - PDA <sup>[21]</sup>	17.12	16.83	1.02	2401.63	1.35
COF- JLU2 <sup>[22]</sup>	10.37	9.90	1.05	1331.97	0.67
COF- LZU1 <sup>[23]</sup>	15.99	15.60	1.02	2168.60	1.24
COF-LZU8	13.53	12.98	1.04	839.72	0.81
COF- SDU1 <sup>[24]</sup>	43.27	43.14	1.00	2427.16	2.61
COF- TpAzo <sup>[25]</sup>	26.05	25.82	1.01	2038.03	1.56
CoPc <sup>[26]</sup> - PorDBA	25.52	24.69	1.03	4081.95	2.76
CPF <sup>[27]</sup> -1	23.97	23.07	1.04	5061.17	2.97
CPF-2	22.50	21.58	1.04	5039.69	2.82
CS <sup>[28]</sup> -COF	20.44	20.18	1.01	1600.54	1.01
CTC <sup>[29]</sup> -COF	18.84	18.67	1.01	1496.27	0.90
CTF <sup>[30]</sup> -1	8.94	8.41	1.06	948.99	0.50
CTF-2-AA	10.99	10.56	1.04	1299.70	0.61
CTF-2- AB <sup>[31]</sup>	4.89	3.31	1.47	0.00	0.61
CuP-Ph <sup>[32]</sup> COF	20.10	19.05	1.06	4068.46	2.33
CuP-SQ <sup>[33]</sup> - COF	12.91	11.30	1.14	3245.94	1.47
CuP- TFPh <sup>[34]</sup> COF	19.04	17.93	1.06	4085.32	2.08
DA <sup>[35]</sup> -COF	19.39	19.14	1.01	1608.02	1.08
DAAQ <sup>[36]</sup> - TFP-COF	22.24	22.00	1.01	1732.22	1.19
DAB <sup>[37]</sup> - TFP-COF	22.26	22.00	1.01	1758.50	1.19

## APPENDICES

DBA <sup>[38]</sup> -					
COF 1	29.37	29.18	1.01	1927.03	1.60
DBA-COF 2	34.37	34.20	1.01	2082.70	2.00
DhaTab <sup>[39]</sup>	32.28	32.11	1.01	2121.02	1.99
2,3-DhaTab	29.31	29.12	1.01	2118.19	1.81
2,5-DhaTab	29.61	29.45	1.01	2166.99	1.87
2,3-					
DhaTph <sup>[40]</sup>	19.25	18.20	1.06	4294.81	2.34
2,5-DhaTph	18.47	17.40	1.06	4283.65	2.35
2,3-					
DhaTta <sup>[41]</sup>	29.25	29.22	1.00	2113.35	1.81
2,3-					
DmaTph <sup>[42]</sup>	17.59	16.41	1.07	4115.47	2.15
DTP <sup>[43]</sup> -					
ANDI <sup>[44]</sup> -COF	43.91	43.78	1.00	1840.29	2.20
EB <sup>[45]</sup> -					
COF:Cl	10.55	10.03	1.05	1542.83	0.69
H <sub>2</sub> P-COF	20.26	19.22	1.05	4385.12	2.54
HAT <sup>[46]</sup> -					
COF	9.88	9.12	1.08	1646.33	0.83
HBC <sup>[47]</sup> -					
COF	10.81	10.56	1.02	1545.51	0.74
HCC-H <sub>2</sub> P-					
COF	15.67	14.45	1.08	4090.73	2.06
HO-H <sub>2</sub> P-					
COF	16.31	16.02	1.02	4347.09	2.35
HP <sup>[48]</sup> -COF-					
1	14.79	14.44	1.02	2018.59	1.06
HP-COF-2	17.15	16.84	1.02	2408.04	1.35
HPB <sup>[49]</sup> -COF	7.57	5.77	1.31	2369.36	0.96
ICOF <sup>[50]</sup> -2	17.20	16.60	1.04	2391.86	1.33
ILCOF <sup>[51]</sup> -1-					
AA	21.20	20.79	1.02	3859.18	2.55
ILCOF-1-					
AB	11.09	9.41	1.18	6697.38	2.42
iPrTAPB-					
TFP <sup>[52]</sup>	7.45	6.49	1.15	656.53	0.49
iPrTAPB-					
TFPB <sup>[53]</sup>	15.85	15.35	1.03	1714.68	1.08
MPCOF <sup>[54]</sup>	10.27	9.78	1.05	1392.58	0.66
N3-COF	18.51	18.22	1.02	1923.99	1.24
NPN-1 <sup>[55]</sup>	5.37	4.11	1.31	893.67	0.49
NPN-2	5.27	4.19	1.26	1033.91	0.56
NPN-3	6.14	5.44	1.13	923.19	0.47
NTU <sup>[56]</sup> -					
COF-1	18.69	18.39	1.02	1882.04	1.20
NTU-COF-2	24.83	24.59	1.01	2072.95	1.70
NUS <sup>[57]</sup> -10	12.97	11.98	1.08	1896.70	0.95
NUS-14	40.85	40.70	1.00	2475.42	2.71
NUS-2	10.37	9.90	1.05	1331.97	0.67



## APPENDICES

NUS-3	16.97	16.66	1.02	2031.61	0.99
NUS-9	12.96	12.04	1.08	2377.99	1.24
PC <sup>[58]</sup> -COF	41.12	41.06	1.00	3068.68	3.00
Pc- PBBA <sup>[59]</sup> - COF	16.84	16.55	1.02	1415.46	0.81
PCTF-1 <sup>[60]</sup>	13.75	13.42	1.02	1846.13	1.08
PCTF-2	21.50	21.39	1.01	2208.88	1.57
PCTF-3	27.84	27.70	1.00	2324.71	1.96
Ph-An <sub>CD</sub> - COF <sup>[61]</sup>	23.73	21.05	1.13	5285.83	2.76
Ph-An- COF <sup>[62]</sup>	22.30	22.06	1.01	1722.78	1.16
PI <sup>[63]</sup> -2-COF	23.65	23.43	1.01	2287.74	1.57
PI-3-COF	30.61	30.42	1.01	2289.85	2.03
PI-COF-4	17.52	13.42	1.31	5142.50	3.19
PI-COF-5	26.57	22.38	1.19	6574.27	7.29
PI-COF-5- 2P	13.35	10.52	1.27	6549.49	3.42
PI-COF-4- 2P	8.21	7.60	1.08	5084.00	1.36
POR <sup>[64]</sup> -COF	14.05	12.59	1.12	3128.86	1.53
Por <sup>[65]</sup> -COF	20.45	18.55	1.10	3957.68	2.25
PPy <sup>[66]</sup> -COF	13.71	13.34	1.03	1301.01	0.66
Py-2,2'- BPyPh <sup>[67]</sup> - COF	23.47	23.16	1.01	2275.87	1.63
Py-2,3- BPyPh-COF	22.92	22.67	1.01	2278.77	1.61
Py-2,3- DHPH <sup>[68]</sup> - COF	21.47	20.98	1.02	4481.50	2.69
Py-Azine- COF	13.02	12.51	1.04	2002.94	1.10
Py-DHPH- COF	20.24	19.94	1.02	4799.42	2.70
Star <sup>[69]</sup> -COF- 1	30.61	30.44	1.01	1362.89	1.22
Star-COF-2	37.44	37.30	1.00	1488.42	1.51
Star-COF-3	40.15	40.02	1.00	1610.39	1.72
TAPB <sup>[70]</sup> - PDA <sup>[71]</sup> COF	32.27	32.12	1.00	2386.24	2.21
TAPB- TFP <sup>[72]</sup>	12.01	11.59	1.04	1553.02	0.80
TAPB- TFPB <sup>[73]</sup>	19.29	19.00	1.02	2085.79	1.32
TBFB <sup>[74]</sup> - COF	16.69	16.38	1.02	1679.08	0.98
T <sup>[75]</sup> -COF 1	8.18	7.57	1.08	1017.96	0.48
T-COF 2	14.91	14.57	1.02	1564.85	0.83

## APPENDICES

T-COF 3	12.71	12.36	1.03	1203.20	0.64
TD <sup>[76]</sup> -COF-5	28.37	27.94	1.02	4424.54	3.42
TfpBDH <sup>[77]</sup>	36.31	36.16	1.00	2092.05	2.08
TFPT <sup>[78]</sup> -COF	34.37	34.24	1.00	2081.81	2.02
TH <sup>[79]</sup> -COF-1	12.07	11.68	1.03	1573.49	0.65
Tp-Azo <sup>[80]</sup>	25.67	25.48	1.01	1834.00	1.35
TpBD <sup>[81]</sup>	22.86	22.65	1.01	1727.38	1.19
TpBD-(OMe) <sub>2</sub> <sup>[82]</sup>	20.26	19.93	1.02	2206.69	1.34
TpBD-2NO <sub>2</sub>	21.72	21.48	1.01	1657.98	1.13
TpBDH	22.16	21.93	1.01	1506.86	1.04
TPBD-ME <sub>2</sub> <sup>[83]</sup>	21.64	21.57	1.00	1526.64	1.03
TpBD-NH <sub>2</sub>	22.21	22.05	1.01	1753.91	1.21
TpBD-NHCOCH <sub>3</sub>	18.06	17.74	1.02	1344.33	0.85
TpBD-NO <sub>2</sub>	21.41	21.15	1.01	1500.66	0.98
TP <sup>[84]</sup> -COF	28.71	28.52	1.01	1765.69	1.43
TpPa <sup>[85]</sup> -1	16.14	15.82	1.02	1590.92	0.93
TpPa-1-F2	15.58	15.28	1.02	1354.73	0.77
TpPa-2	13.77	13.38	1.03	1561.67	0.78
TpPa-F <sub>4</sub>	14.90	14.60	1.02	1077.84	0.58
TpPa-NO <sub>2</sub>	11.45	11.10	1.03	1252.24	0.60
TpPa-Py	16.31	16.02	1.02	1591.88	0.95
TpPa-SO <sub>3</sub> H	12.51	12.16	1.03	1275.63	0.63
TpPa-SO <sub>3</sub> H-Py	16.32	16.02	1.02	1518.04	0.84
Tp-Por-COF-AA	41.24	41.08	1.00	1929.60	2.10
Tp-Por-COF-AB	20.14	19.92	1.01	2864.44	1.72
Tp-Stb	22.52	22.28	1.01	1944.86	1.33
TPT <sup>[86]</sup> -COF-1	21.86	21.62	1.01	2076.18	1.39
TPT-COF-2	33.91	33.75	1.00	2392.33	2.18
TRIPTA <sup>[87]</sup>	12.37	11.93	1.04	1447.70	0.78
TT <sup>[88]</sup> -COF	26.31	26.13	1.01	1644.21	1.29
TTF <sup>[89]</sup> -COF	18.56	18.12	1.02	3385.40	1.91
TTF-Py-COF	14.55	14.30	1.02	2031.48	1.10
TThPP <sup>[90]</sup>	17.84	16.66	1.07	3789.60	2.08
TTI <sup>[91]</sup> -COF	18.52	18.22	1.02	1933.40	1.26
ZnPc <sup>[92]</sup> -DPB <sup>[93]</sup>	26.76	26.56	1.01	1820.41	1.39
ZnPc-NDI	27.16	26.97	1.01	1464.70	1.21
ZnPc-COF	19.05	17.93	1.06	3936.35	2.27
ZnPc-PPE	32.24	32.08	1.01	2060.91	1.85

## APPENDICES

	ZnPc-Py	18.53	18.26	1.01	1348.17	0.85
IRMOFs	IRMOF-1	15.07	7.93	1.90	3661.29	1.36
	IRMOF-2	12.93	8.46	1.53	2749.58	1.01
	IRMOF-3	14.99	7.27	2.06	3420.66	1.26
	IRMOF-4	10.10	3.35	3.02	0.00	0.78
	IRMOF-5	10.41	1.72	6.06	0.00	0.60
	IRMOF-6	15.04	6.71	2.24	3164.42	1.20
	IRMOF-7	10.76	4.73	2.27	3303.50	1.07
	IRMOF-8	17.93	9.17	1.96	4375.74	1.88
	IRMOF-9	11.12	8.61	1.29	3428.45	1.16
	IRMOF-10	20.88	12.15	1.72	4902.87	2.64
	IRMOF-11	12.40	6.88	1.80	2659.04	0.94
	IRMOF-12	19.69	9.74	2.02	5062.91	2.26
	IRMOF-13	12.54	6.66	1.88	2616.91	0.92
	IRMOF-14	20.94	10.64	1.97	4826.46	2.32
	IRMOF-15	10.42	7.55	1.38	5941.86	2.03
	IRMOF-16	25.36	17.49	1.45	5935.61	4.48
ZIFs	CO-ZIF-81	10.87	7.80	1.39	1243.80	0.62
	D-ZIF-7	5.18	2.42	2.14	0.00	0.39
	D-ZIF-7 CO <sub>2</sub>	4.64	1.70	2.73	0.00	0.23
	HZIF-1Mo	13.03	3.41	3.82	0.00	0.33
	HZIF-1W	7.33	1.37	5.36	0.00	0.29
	ZIF-1	6.50	2.19	2.96	0.00	0.47
	ZIF-2	6.42	5.29	1.21	1846.22	0.72
	ZIF-3	8.47	5.70	1.49	2016.91	0.78
	ZIF-4	5.14	2.46	2.09	0.00	0.46
	ZIF-5	3.87	2.15	1.80	0.00	0.30
	ZIF-6	9.50	5.74	1.66	2762.12	0.95
	ZIF-7	5.59	2.40	2.32	0.00	0.40
	ZIF-8	11.39	3.41	3.34	0.00	0.69
	ZIF-9	5.64	2.47	2.29	0.00	0.39
	ZIF-10	12.55	7.49	1.68	2395.00	0.98
	ZIF-11	14.79	2.77	5.33	0.00	0.58
	ZIF-12	14.79	2.77	5.33	0.00	0.58
	ZIF-20	15.44	2.87	5.38	0.00	0.60
	ZIF-21	15.92	2.86	5.57	0.00	0.60
	ZIF-22	15.30	2.89	5.29	0.00	0.60
	ZIF-60-MER	12.82	7.61	1.68	1680.65	0.79
	ZIF-64-BCT	7.05	2.15	3.28	0.00	0.47
	ZIF-65-SOD	11.24	3.73	3.01	1173.04	0.55
	ZIF-67-SOD	11.41	3.34	3.41	0.00	0.72
	ZIF-68	10.86	8.04	1.35	1162.30	0.60
	ZIF-69	8.06	5.54	1.45	944.47	0.50
	ZIF-70-GME	15.25	13.38	1.14	2183.72	0.93
	ZIF-71	17.01	5.47	3.11	999.71	0.55
	ZIF-75-GIS	4.46	1.77	2.51	0.00	0.30
	ZIF-76-LTA	15.10	5.11	2.95	1410.82	0.63
ZIF-77	5.05	3.98	1.27	371.99	0.30	
ZIF-77-FRL	5.05	3.98	1.27	375.35	0.30	

APPENDICES

ZIF-80	12.17	10.29	1.18	1234.30	0.59
ZIF-90	11.01	3.49	3.15	0.00	0.65
ZIF-93	16.87	3.51	4.81	0.00	0.60
ZIF-95	21.08	4.61	4.57	1159.52	0.69
ZIF-96	16.66	5.51	3.03	1213.45	0.64
ZIF-97	16.36	3.74	4.37	896.94	0.58
ZIF-100	35.56	4.92	7.22	1853.11	0.93
ZIF-300	7.44	4.55	1.64	415.96	0.40
ZIF-301	7.63	4.58	1.67	452.93	0.44
ZIF-302	7.96	4.38	1.82	735.80	0.51
ZIF-L	4.59	1.64	2.80	0.00	0.31

[1]NiPc-BTDA: nickel(II) phthalocyanine- benzothiadiazole; [2]Py: pyrene-based; [3]2P: biphenyl-4,4'-dicarboxaldehyde; [4]4PE-1P: 1,1,2,2-tetraphenyl-ethene- terephthalaldehyde; [5]4PE-2P: 1,1,2,2-tetraphenyl-ethene- biphenyl-4,4'-dicarboxaldehyde; [6]4PE-3P: 1,1,2,2-tetraphenyl-ethene- *p*-terphenyl-4,4''-dicarboxaldehyde; [7]4PE-TT: 1,1,2,2-tetraphenyl-ethene- thieno[3,2-*b*]thiophene-2,5-dicarboxaldehyde; [8]AB-COF: 1,3,5-triformyl benzene; [9]ACOF-1: azine based COF; [10]AEM: arylene-ethynylene macrocycles; [11]ATFG: 1,3,5-triformylphloroglucinol; [12] Azo: azobenzene [13]BDT: benzodithiophene; [14]OEt: ethoxy [15]BF: base-functionalized; [16]BLP: borazine-linked polymer; [17]AA: eclipsed arrangement with orthorhombic space group Cmm2; [18]TAPH: 5,10,15,20-tetrakis(4-aminophenyl)porphyrin; [19]bnn: boron-nitride topology; [20]gra: staggered topology; [21]BTA-PDA: benzene-1,3,5-tricarbaldehyde- *p*-phenylenediamine; [22]JLU: Jilin University; [23]LZU: Lanzhou University; [24]SDU: Shandong University; [25]TpAzo: 1,3,5- triformylphloroglucinol- 4,4'-Azodianiline; [26]CoPc: cobalt based phthalocyanine; [27] CPF: covalent porphyrinic frameworks; [28]CS: conjugated and stable; [29]CTC: cyclotricatechylene; [30]CTF: covalent triazine-based framework [31]AB: structure with orthorhombic space group Fmm2; [32]CuP: copper 5,10,15,20-tetrakis(ptetraphenylamino)porphyrin; [33]SQ: squaraine; [34]TFPh: tetrafluorophenyl [35]DA: donor and acceptors; [36]DAAQ-TFP: 2,6-diaminoanthraquinone- 1,3,5-triformylphloroglucinol; [37]DAB: *p*-diaminobenzene [38]DBA: dehydrobenzoannulenes [39]DhaTab: dihydroxyterephthalaldehyde- 1,3,5-tris(4-aminophenyl)benzene [40]DhaTph: dihydroxyterephthalaldehyde- 5,10,15,20-tetrakis(4-aminophenyl)-21H,23H-porphine; [41]DhaTta: dihydroxyterephthalaldehyde; [42]DmaTph: dimethoxyterephthalaldehyde -5,10,15,20-tetrakis(4-aminophenyl)-21H,23H-porphine; [43]TP: triphenylene; [44]NDI: naphthalene diimide; [45]EB: ethidium bromide; [46]HAT: hexaazatriphenylene; [47]HBC: hexabenzocoronene; [48]HP: heterogeneous pore structures; [49]HPB: hexaphenylbenzene; [50]ICOF: ionic COF; [51]ILCOF: imine-linked COF; [52]iPrTAPB-TFP: 1,3,5-tris(4'-amino-3',5'-isopropylphenyl)benzene - 1,3,5-triformylphloroglucinol [53]TFPB: 1,3,5-tris(4'-formylphenyl)benzene; [54] MPCOF: super-microporous phosphazene-based COF; [55]NPN: nitroso polymer networks; [56]NTU: Nanyang Technological University; [57]NUS: National University of Singapore; [58] PC: polycationic; [59]Pc-PBBA: Polyfunctional catechols- 1,4-phenylenebis(boronic acid); [60]PCTF: porous covalent triazine-based organic framework; [61]Ph-AnCD: photo responsive anthracene cyclodimer [62]Ph-An: photo responsive anthracene; [63]PI: polyimide; [64]POR: porphyrin; [65]Por: porphyrin; [66]PPy: polypyrene; [67]BPyPh: bipyridine-phenolate; [68]DHPH: dihydroxy-phenolate; [69]STAR: star-shaped; [70]TAPB: 1,3,5-tris(4- aminophenyl)benzene; [71]PDA: terephthalaldehyde; [72]TFP: 1,3,5-triformylphloroglucinol; [73]TFPB: 1,3,5-tris(4'-formylphenyl)benzene ; [74]TBFB: tris(4-bromophenyl)benzene; [75]T: thiophene-based; [76]TD: triptycene-derived; [77] TfpBDH: 1,3,5-tris(4-formylphenyl)benzene - pyromellitic-*N,N'*-bisaminoimide; [78]TFPT: 1,3,5-tris-(4-formyl-phenyl)triazine [79]TH: thiadiazole-functionalized; [80]Tp-Azo: triformylphloroglucinol 4,4'-azodianiline; [81]TpBD: triformylphloroglucinol- benzidine; [82]BD-(OMe)<sub>2</sub>: *o*-dianisidinebenzidine-3,3'-dinitrobenzidine; [83]BD-Me<sub>2</sub>: otolidinebenzidine; [84]TP: triphenylene; [85]TpPa: 1,3,5-triformylphloroglucinol; [86]TPT: triaryloxytriazine; [87]TRIPTA: : rxn between 1,3,5-tris(4-aminophenyl)triazine and 1,3,5-triformylphloroglucinol; [88] TT: thienothiophene based; [89]TTF: tetrathiafulvane based; [90]TThPP: : porphyrin with 4-thiophenophenyl; [91]TTI: triazine triphenyl imine; [92]ZnPc: Zn phthalocyanine; [93]DPB: diphenylbutadiyne

**Table A.2** Data for comparison of our predicted gas uptake data with the experiments[97, 208] and other simulation data[96] available in the literature.

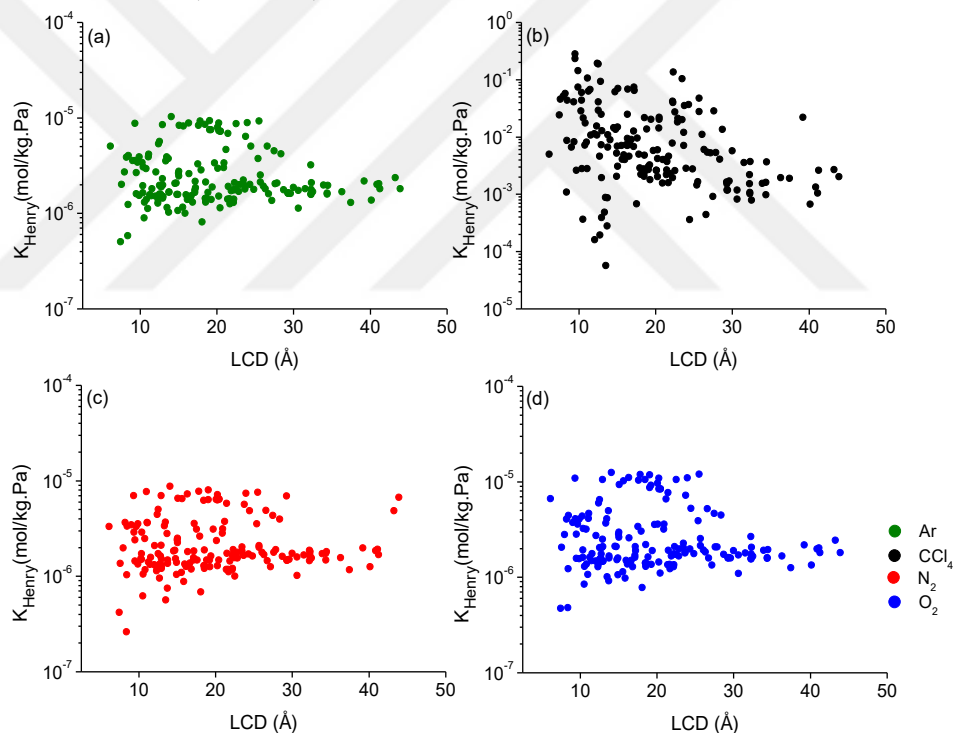
MOF	P (bar)	T (K)	Details	Our Data (mol/kg)	Literature Data (mol/kg)
CPL-11	0.1	298	Saturated CCl <sub>4</sub> <sup>i</sup>	2.39	2.23
Cu-BTC	15	298	Single component	3.62	3.16

APPENDICES

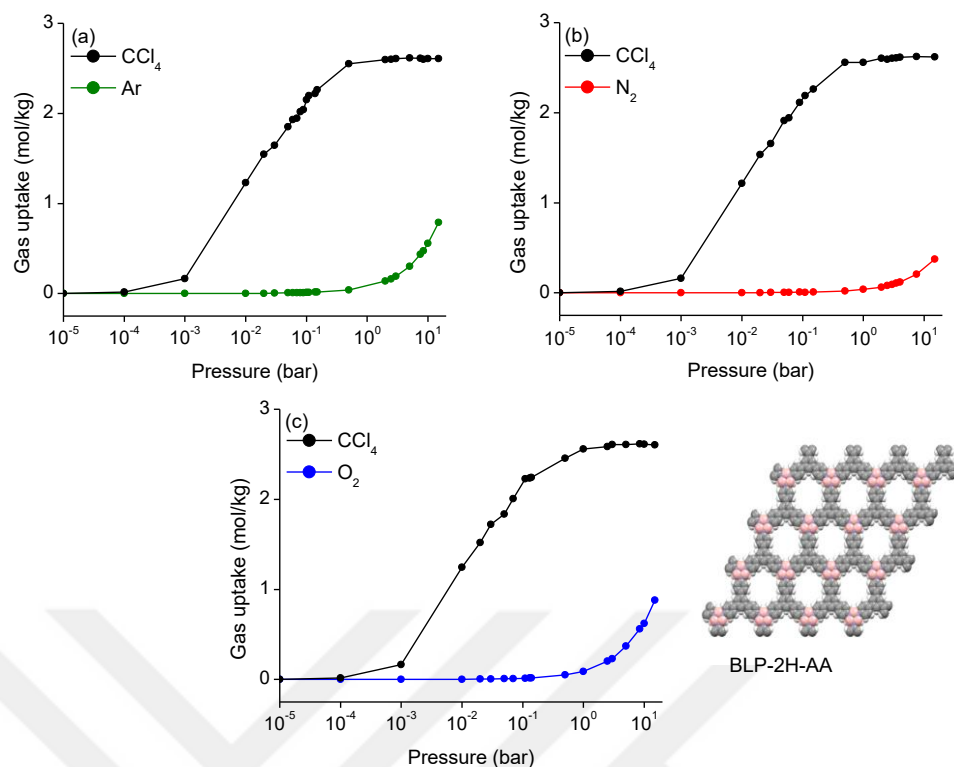
	24.5	298	Ar	5.32	4.58
	34.5	298		6.56	5.55
	0.03	298	Single component CCl <sub>4</sub>	7.00	6.15
	0.07	298		7.12	6.23
	0.1	298		7.18	6.24
	100	298	CCl <sub>4</sub> in air mixture <sup>ii</sup>	7.01	6.21
	21	298	Single component N <sub>2</sub>	3.93	3.06
	100	298		N <sub>2</sub> in air mixture	3.93
		6.3	298	Single component O <sub>2</sub>	1.99
11.05		298	3.02		2.49
22		298	5.02		4.27
	100	298	O <sub>2</sub> in air mixture	0.86	0.53
<b>MIL-101</b>	0.06	303	Single component CCl <sub>4</sub>	12.24	13.00
	0.07	303		12.92	13.14
	0.08	303		13.62	13.21

i: Experimental values for single-component CCl<sub>4</sub> adsorption in CPL-11 were converted to molecules/unit cell by multiplying the reported molecules/ each pore values with 2.5. Then gas uptakes were converted to mol/kg.

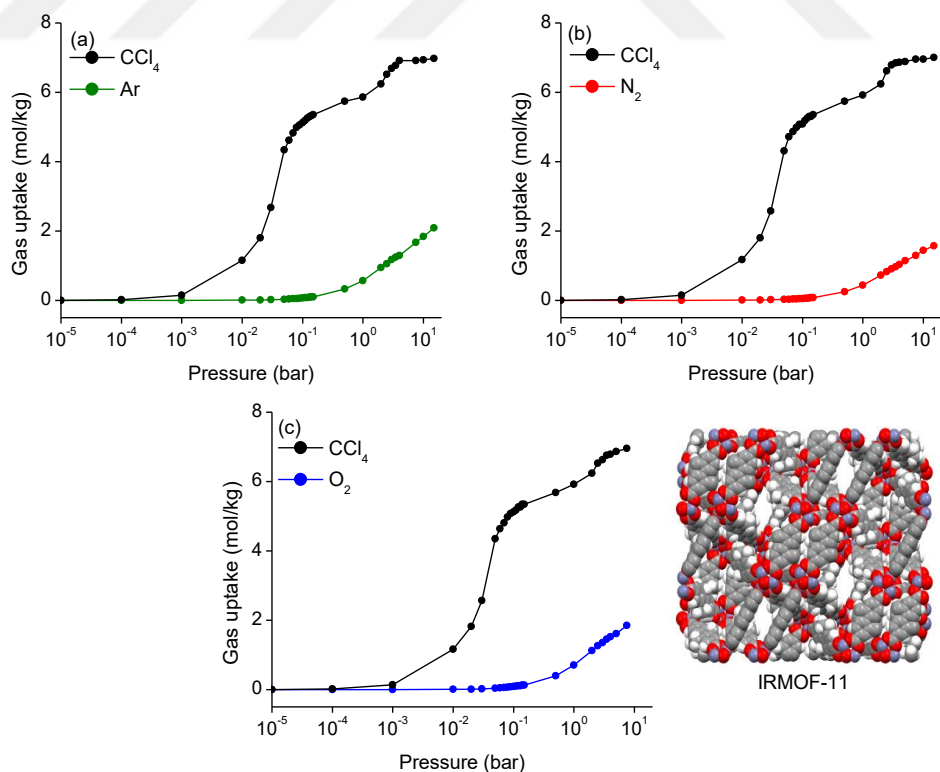
ii: air mixture: 0.999% Ar, 0.1% CCl<sub>4</sub>, 77.922% N<sub>2</sub> and 20.979% O<sub>2</sub>



**Figure A.1** Henry's constants of (a)Ar, (b)CCl<sub>4</sub>, (c)N<sub>2</sub> and (d)O<sub>2</sub> as a function of LCDs of COFs, IRMOFs and ZIFs

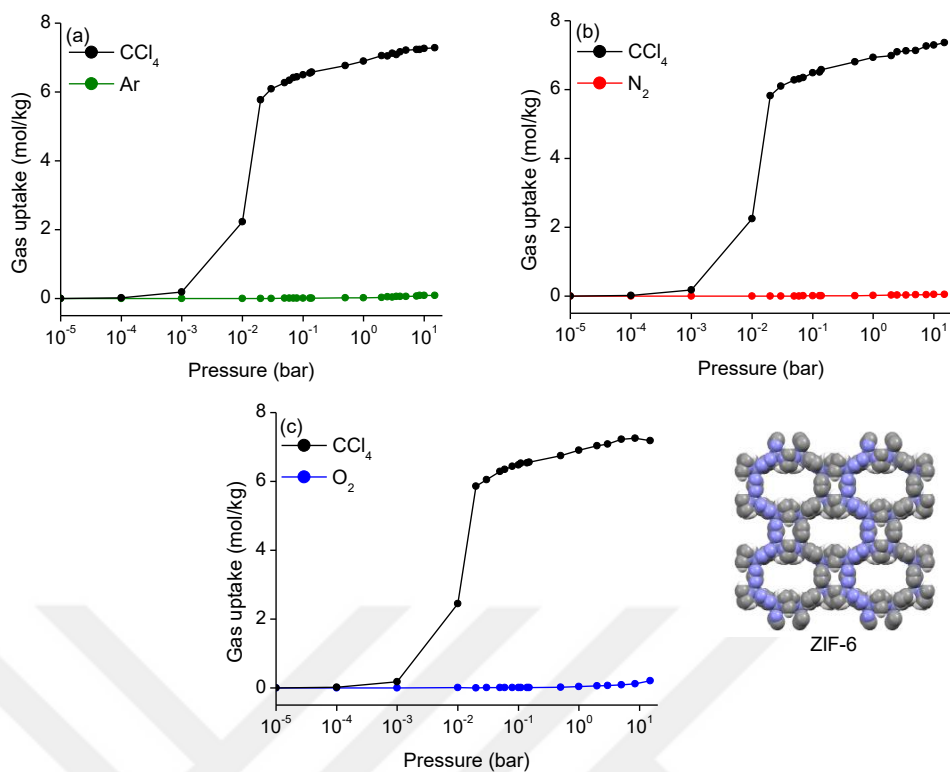


**Figure A.2** Binary mixture adsorption isotherms for (a)  $\text{CCl}_4/\text{Ar}$ , (b)  $\text{CCl}_4/\text{N}_2$  and (c)  $\text{CCl}_4/\text{O}_2$  in BLP-2H-AA at 298 K. The composition of the bulk gas mixtures are  $\text{CCl}_4/\text{Ar}$ : 1/99,  $\text{CCl}_4/\text{N}_2$ : 1/99 and  $\text{CCl}_4/\text{O}_2$ : 1/99.

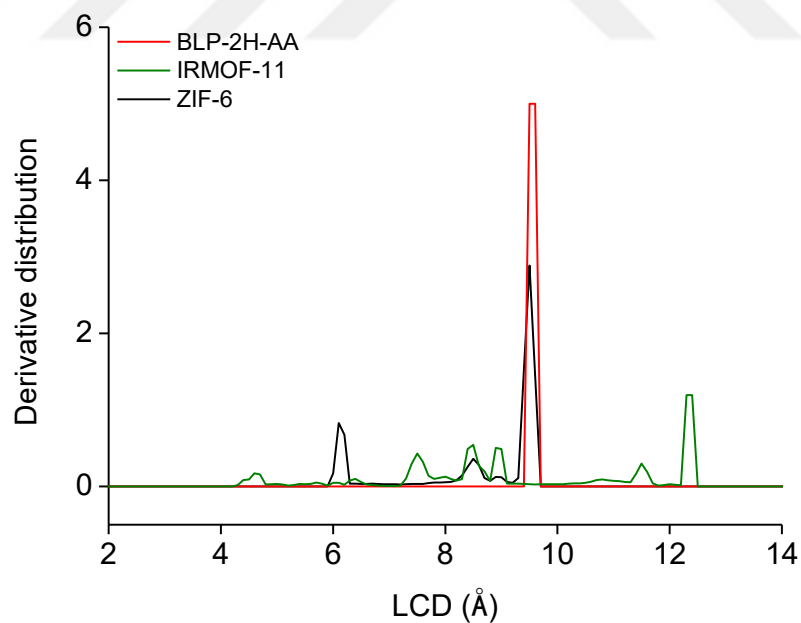


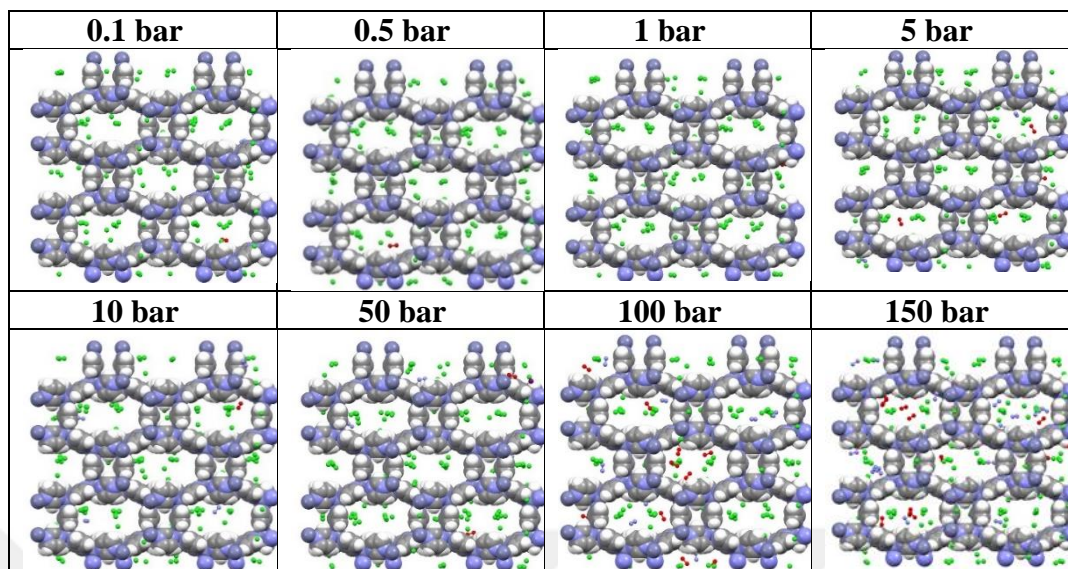
**Figure A.3** Binary mixture adsorption isotherms for (a)  $\text{CCl}_4/\text{Ar}$ , (b)  $\text{CCl}_4/\text{N}_2$  and (c)  $\text{CCl}_4/\text{O}_2$  in IRMOF-11 at 298 K. The composition of the bulk gas mixtures are  $\text{CCl}_4/\text{Ar}$ : 1/99,  $\text{CCl}_4/\text{N}_2$ : 1/99 and  $\text{CCl}_4/\text{O}_2$ : 1/99.

## APPENDICES



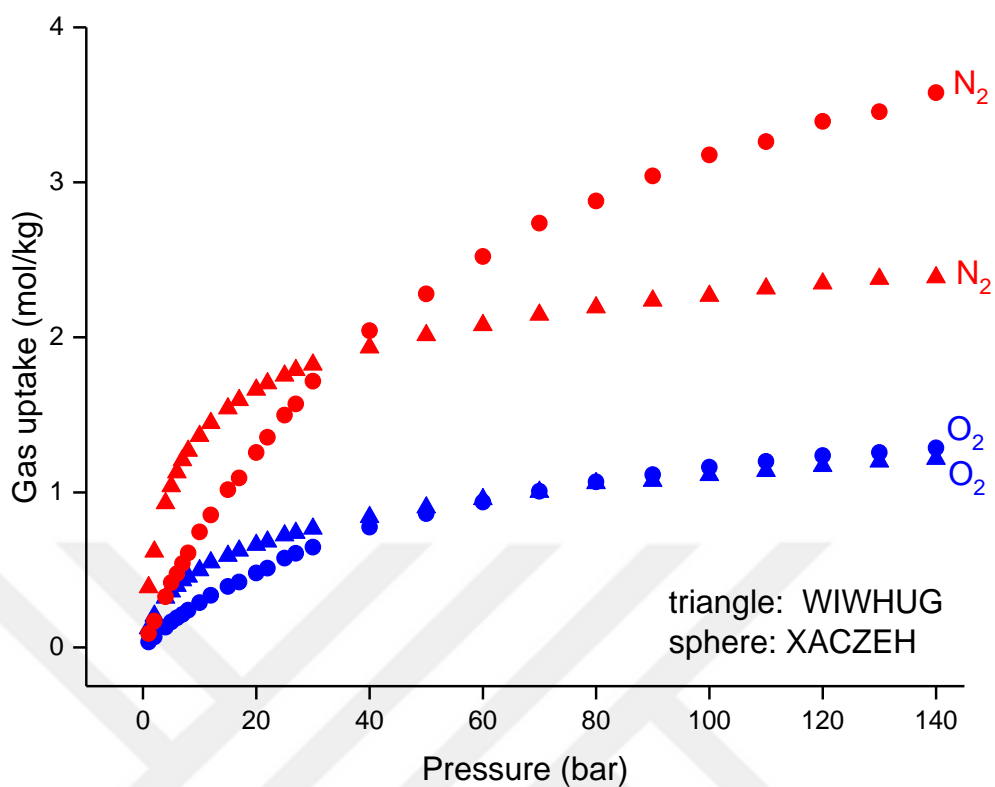
**Figure A.4** Binary mixture adsorption isotherms for (a)CCl<sub>4</sub>/Ar, (b)CCl<sub>4</sub>/N<sub>2</sub> and (c)CCl<sub>4</sub>/O<sub>2</sub> in ZIF-6 at 298 K. The composition of the bulk gas mixtures are CCl<sub>4</sub>/Ar: 1/99, CCl<sub>4</sub>/N<sub>2</sub>: 1/99 and CCl<sub>4</sub>/O<sub>2</sub>: 1/99.



**Figure A.5** Pore size distributions of BLP-2H-AA, IRMOF-11 and ZIF-6.**Figure A.6** GCMC screenshots of Ar (purple spheres), CCl<sub>4</sub> (green), N<sub>2</sub> (blue) and O<sub>2</sub> (red) adsorption in ZIF-6. Dark blue: Zn, blue: N, dark grey: C, white: H**Table A.3** The separation potentials (mol/L) of BLP-2H-AA, IRMOF-11 and ZIF-6 for binary and quaternary mixtures at 10 bar and 298 K.

Material	$\Delta Q_{N_2/CCl_4}$	$\Delta Q_{N_2/(Ar+CCl_4+O_2)}$
BLP-2H-AA	232.22	8.47
IRMOF-11	522.50	17.55
ZIF-6	551.68	18.68

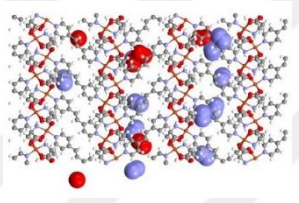
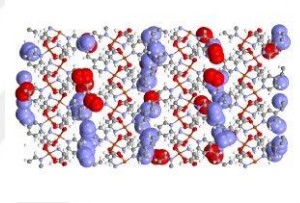
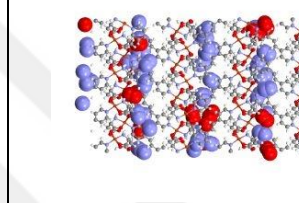
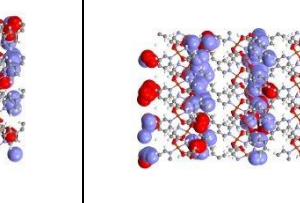
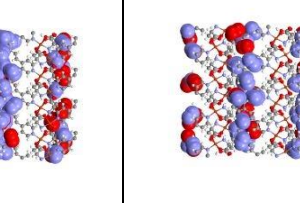
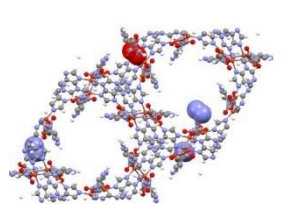
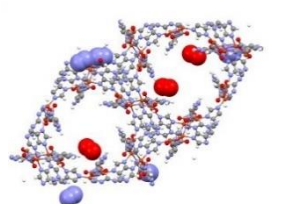
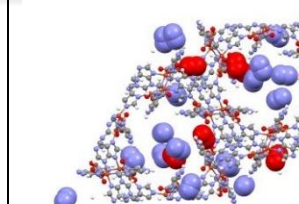
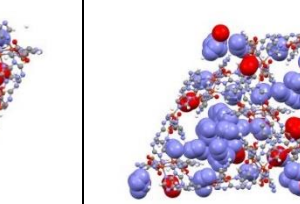
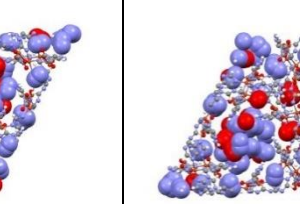


*APPENDIX B: Supplementary Information for Chapter VI<sup>2</sup>*

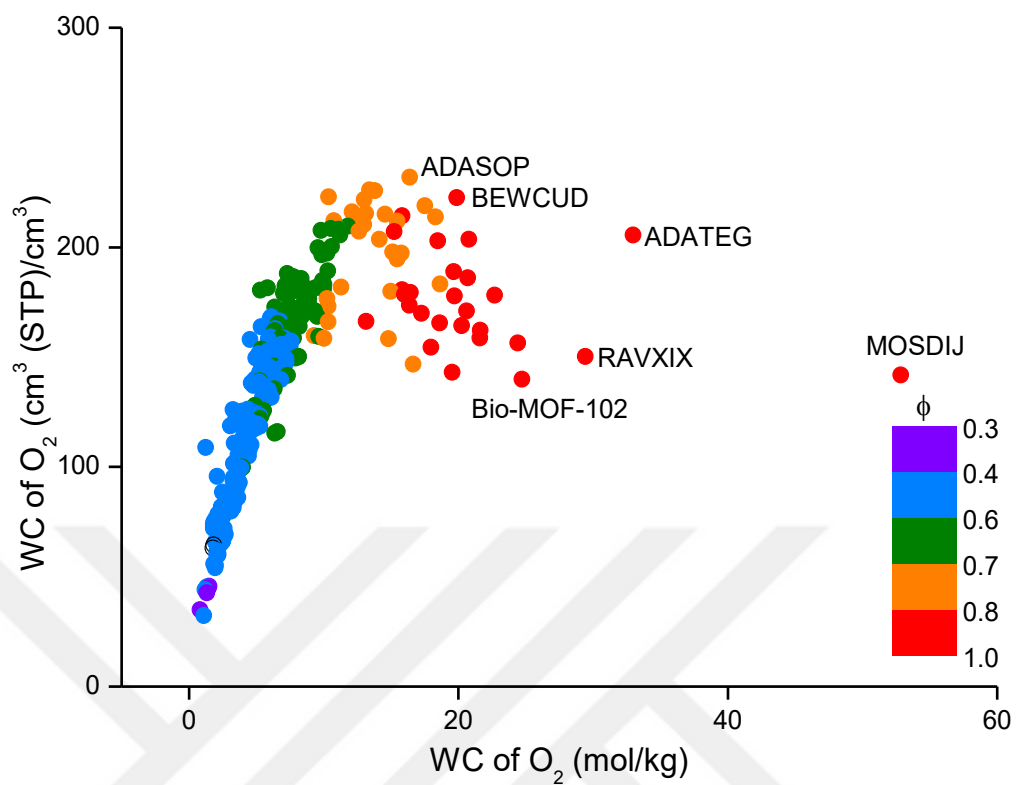
**Figure B.1** Adsorption isotherms of O<sub>2</sub> and N<sub>2</sub> in their binary mixture (O<sub>2</sub>:N<sub>2</sub> is 21:79) in WIWHUG and XACZEH at 298 K up to 140 bar.

<sup>2</sup>The results given in this chapter were published in Industrial & Engineering Chemistry Research with following reference: Gulcay, E., & Erucar, I. (2019). Bio-compatible MOFs for storage and separation of O<sub>2</sub>: A molecular simulation study. Industrial & Engineering Chemistry Research, 58(8), 3225-3237.

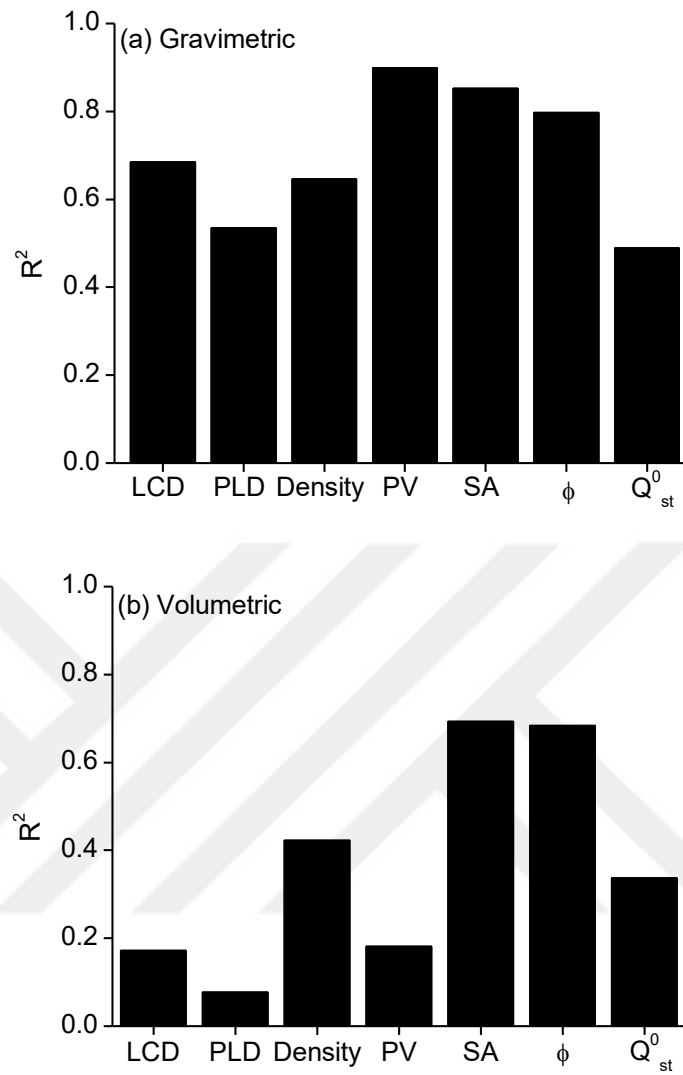
APPENDICES

MOF	1 bar	5 bar	10 bar	100 bar	140 bar
WIWHUG					
XACZEH					

**Figure B.2** GCMC Screenshots of O<sub>2</sub> (red spheres) and N<sub>2</sub> (blue spheres) adsorption in WIWHUG and XACZEH. Red = O, dark blue = N, orange = Cu, dark grey = C, light grey = H



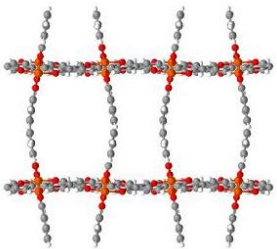
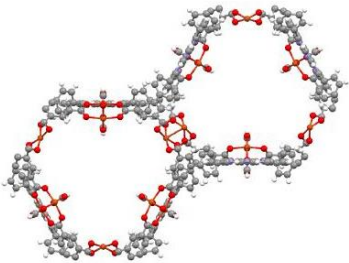
**Figure B.3** Gravimetric and volumetric O<sub>2</sub> working capacities of 315 MOFs at 298 K (at 140 bar storage and 5 bar release pressures). The data points are color mapped by porosities.



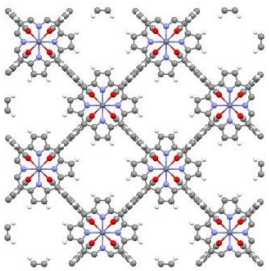
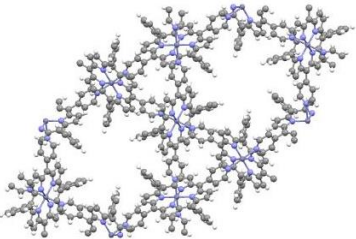
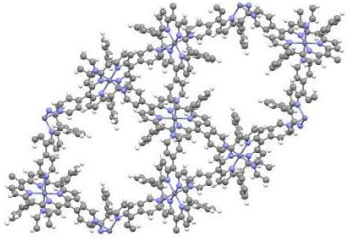
**Figure B.4**  $R^2$  values showing the relations between (a) gravimetric working capacity of  $O_2$  (mol/kg) and several parameters, (b) volumetric working capacity of  $O_2$  ( $cm^3$  (STP)/ $cm^3$ ) and several parameters.

## APPENDICES

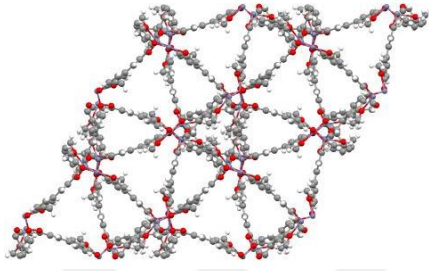
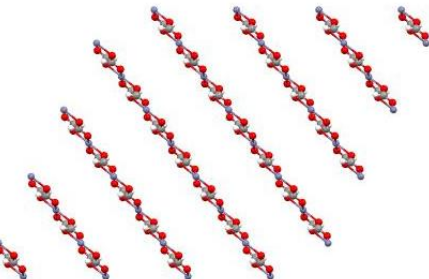
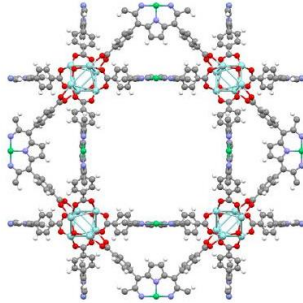
**Table B.1** Crystal properties of the top 17 MOF membranes which surpass the Robeson's 2008 upper bound for O<sub>2</sub>/N<sub>2</sub> separation together with their organic linkers and metals.

MOFs	Organic linker and metals	a (Å)	b (Å)	c (Å)	alpha (°)	beta (°)	gamma (°)	cell
 AGAXIP	Formadide Fe	27.124	15.270	12.0109	90	94.604	90	monoclinic
 BIPSUQ	Porphyrin Cu	33.7831	33.7831	43.456	90	90	120	hexagonal

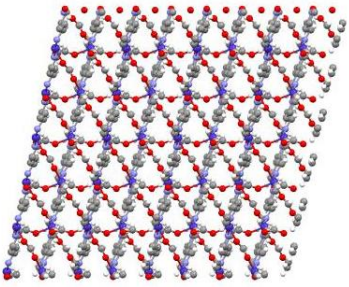
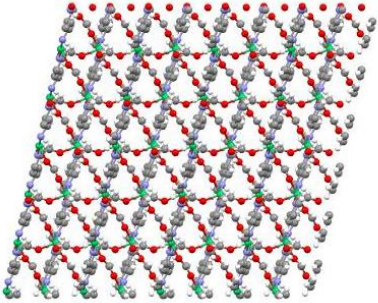
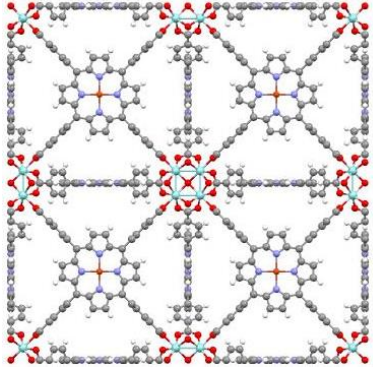
## APPENDICES

 <p>BORYOY</p>	Porphyrin Zn	33.42	33.42	29.89	90	90	90	tetragonal
 <p>CATDIL</p>	Porphyrin Zn	33.0583	33.0583	27.9906	90	90	120	trigonal
 <p>CAYRIE</p>	Porphyrin Zn	33.0866	33.0866	28.308	90	90	120	trigonal

## APPENDICES

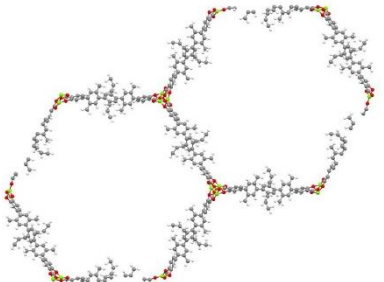
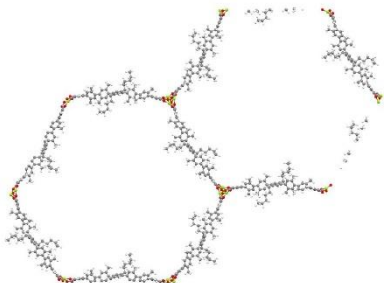
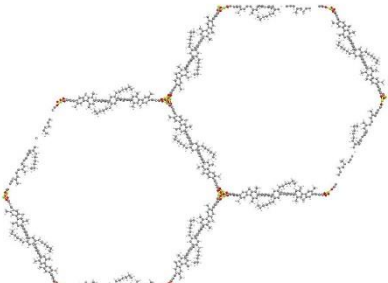
 <p>CUBBEI</p>	2-methoxyphenolate Zn	18.1019	18.1019	24.668	90	90	120	trigonal
 <p>DEPJIR02</p>	Formate Zn	29.782	32.438	33.1	90	116.184	90	monoclinic
 <p>DOGBEI</p>	Porphyrin Zr	38.512	38.512	38.512	90	90	90	cubic

APPENDICES

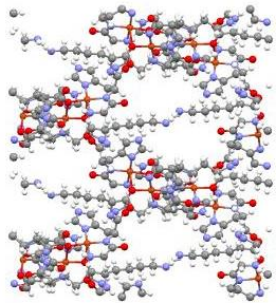
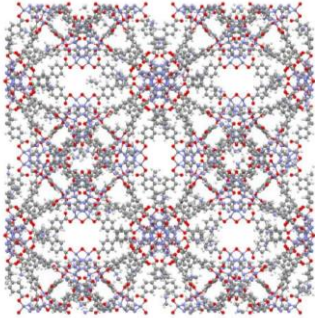
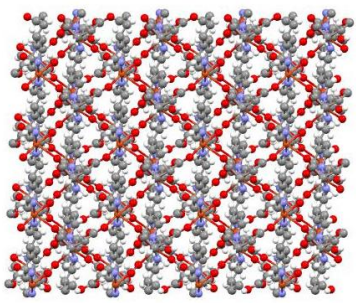
 <p>FIFNUE</p>	<p>Formate Co</p>	<p>31.5324</p>	<p>40.553</p>	<p>32.5236</p>	<p>90</p>	<p>102.223</p>	<p>90</p>	<p>monoclinic</p>
 <p>FIFPAM</p>	<p>Formate Ni</p>	<p>31.4445</p>	<p>40.1202</p>	<p>32.5064</p>	<p>90</p>	<p>102.633</p>	<p>90</p>	<p>monoclinic</p>
 <p>HIKSIF</p>	<p>Porphyrin Zr</p>	<p>19.51</p>	<p>19.51</p>	<p>19.51</p>	<p>90</p>	<p>90</p>	<p>90</p>	<p>cubic</p>



APPENDICES

 <p>RAVWOC</p>	<p>DOT* Mg</p>	<p>68.9586</p>	<p>68.9586</p>	<p>25.8472</p>	<p>90</p>	<p>90</p>	<p>120</p>	<p>triclinic</p>
 <p>RAVXAP</p>	<p>DOT* Mg</p>	<p>91.96</p>	<p>91.96</p>	<p>27.9544</p>	<p>90</p>	<p>90</p>	<p>120</p>	<p>triclinic</p>
 <p>RAVXIX</p>	<p>DOT* Mg</p>	<p>113.774</p>	<p>113.774</p>	<p>27.774</p>	<p>90</p>	<p>90</p>	<p>120</p>	<p>triclinic</p>

APPENDICES

 <p>SADZUV</p>	<p>Peptide Cu</p>	<p>29.2862</p>	<p>29.2862</p>	<p>26.0847</p>	<p>90</p>	<p>90</p>	<p>90</p>	<p>tetragonal</p>
 <p>SAPBIW</p>	<p>Adenine Zn</p>	<p>69.12</p>	<p>69.12</p>	<p>69.12</p>	<p>90</p>	<p>90</p>	<p>90</p>	<p>triclinic</p>
 <p>WIWHUG</p>	<p>Aspartate Cu</p>	<p>26.5776</p>	<p>49.884</p>	<p>31.6016</p>	<p>90</p>	<p>91.713</p>	<p>90</p>	<p>monoclinic</p>

\*DOT: Dioxidoterephthalat

## BIBLIOGRAPHY

- [1] Smith, J.V., *Topochemistry Of Zeolites And Related Materials. 1. Topology And Geometry*. Chem. Rev., 1988. **88**(1): p. 149-182.
- [2] Wilson, S.T., et al., *Aluminophosphate Molecular Sieves: A New Class Of Microporous Crystalline Inorganic Solids*. J. Am. Chem. Soc., 1982. **104**(4): p. 1146-1147.
- [3] Davis, M.E. and R.F. Lobo, *Zeolite And Molecular Sieve Synthesis*. Chem. Mater., 1992. **4**(4): p. 756-768.
- [4] Rouquerol, J., et al., *Adsorption By Powders And Porous Solids: Principles, Methodology And Applications*. 2013: Academic press.
- [5] Martin, C., et al., *Sorption Properties Of AlPO<sub>4</sub>-5 And SAPO-5 Zeolite-like Materials*. Langmuir, 1998. **14**(7): p. 1774-1778.
- [6] Langmi, H., et al., *Hydrogen Adsorption In Zeolites A, X, Y and RHO*. J. Alloys Compd., 2003. **356**: p. 710-715.
- [7] Rioland, G., et al., *Adsorption Of Volatile Organic Compounds In Composite Zeolites Pellets For Space Decontamination*. Adsorption, 2017. **23**(2-3): p. 395-403.
- [8] Malamis, S. and E. Katsou, *A Review On Zinc And Nickel Adsorption On Natural And Modified Zeolite, Bentonite And Vermiculite: Examination Of Process Parameters, Kinetics And Isotherms*. J. Hazard. Mater., 2013. **252**: p. 428-461.
- [9] Smit, B. and T.L.M. Maesen, *Molecular Simulations Of Zeolites: Adsorption, Diffusion, And Shape Selectivity*. Chem. Rev. , 2008. **108**(10): p. 4125-4184.
- [10] Bansal, R.C. and M. Goyal, *Activated Carbon Adsorption*. 1st ed. 2005, Florida: CRC press.
- [11] Lozano-Castello, D., et al., *Influence Of Pore Size Distribution On Methane Storage At Relatively Low Pressure: Preparation Of Activated Carbon With Optimum Pore Size*. Carbon, 2002. **40**(7): p. 989-1002.
- [12] Dąbrowski, A., et al., *Adsorption Of Phenolic Compounds By Activated Carbon—A Critical Review*. Chemosphere, 2005. **58**(8): p. 1049-1070.
- [13] Sircar, S., T. Golden, and M. Rao, *Activated Carbon For Gas Separation And Storage*. Carbon, 1996. **34**(1): p. 1-12.
- [14] Kresge, C., et al., *Ordered Mesoporous Molecular Sieves Synthesized By A Liquid-Crystal Template Mechanism*. Nature, 1992. **359**(6397): p. 710.
- [15] Ying, J.Y., C.P. Mehnert, and M.S. Wong, *Synthesis And Applications Of Supramolecular-Templated Mesoporous Materials*. Angew. Chem., Int. Ed., 1999. **38**(1-2): p. 56-77.
- [16] Kitagawa, S., R. Kitaura, and S.i. Noro, *Functional Porous Coordination Polymers*. Angew. Chem., Int. Ed., 2004. **43**(18): p. 2334-2375.
- [17] Batten, S.R., et al., *Terminology Of Metal–Organic Frameworks And Coordination Polymers (IUPAC Recommendations 2013)*. Pure Appl. Chem., 2013. **85**(8): p. 1715-1724.
- [18] Hijikata, Y., et al., *Pore Design Of Two-Dimensional Coordination Polymers Toward Selective Adsorption*. Inorg. Chem., 2013. **52**(7): p. 3634-3642.
- [19] Li, D. and K. Kaneko, *Molecular Geometry-Sensitive Filling In Semi-Rectangular Micropores Of Organic–Inorganic Hybrid Crystals*. J. Phys. Chem.

## BIBLIOGRAPHY

- B, 2000. **104**(38): p. 8940-8945.
- [20] Kondo, M., et al., *Three-Dimensional Framework With Channeling Cavities For Small Molecules:  $\{[M_2(4, 4'-bpy)_3(NO_3)_4] \cdot xH_2O\}_n$  (M=Co, Ni, Zn)*. *Angew. Chem., Int. Ed.*, 1997. **36**(16): p. 1725-1727.
- [21] Kondo, M., et al., *Microporous Materials Constructed From The Interpenetrated Coordination Networks. Structures And Methane Adsorption Properties*. *Chem. Mater.*, 2000. **12**(5): p. 1288-1299.
- [22] Yaghi, O. and H. Li, *Hydrothermal Synthesis Of A Metal-Organic Framework Containing Large Rectangular Channels*. *J. Am. Chem. Soc.*, 1995. **117**(41): p. 10401-10402.
- [23] Moghadam, P.Z., et al., *Development Of A Cambridge Structural Database Subset: A Collection Of Metal-Organic Frameworks For Past, Present, And Future*. *Chem. Mater.*, 2017. **29**(7): p. 2618-2625.
- [24] Furukawa, H., et al., *The Chemistry And Applications Of Metal-Organic Frameworks*. *Science*, 2013. **341**(6149): p. 1230444.
- [25] Silva, P., et al., *Multifunctional Metal–Organic Frameworks: From Academia To Industrial Applications*. *Chem. Soc. Rev.*, 2015. **44**(19): p. 6774-6803.
- [26] Li, H., et al., *Design And Synthesis Of An Exceptionally Stable And Highly Porous Metal-Organic Framework*. *Nature*, 1999. **402**(6759): p. 276-279.
- [27] Eddaoudi, M., et al., *Systematic Design Of Pore Size And Functionality In Isorecticular MOFs And Their Application In Methane Storage*. *Science*, 2002. **295**(5554): p. 469-472.
- [28] Yaghi, O.M., et al., *Reticular Synthesis And The Design Of New Materials*. *Nature*, 2003. **423**(6941): p. 705-714.
- [29] Zhou, C., et al., *Metal-Organic Framework Glasses With Permanent Accessible Porosity*. *Nat. Commun.*, 2018. **9**(1): p. 5042.
- [30] Bennett, T.D. and A.K. Cheetham, *Amorphous Metal–Organic Frameworks*. *Acc. Chem. Res.*, 2014. **47**(5): p. 1555-1562.
- [31] Allen, F.H., *The Cambridge Structural Database: A Quarter Of A Million Crystal Structures And Rising*. *Acta Crystallogr., Sect. B: Struct. Sci.*, 2002. **58**(3): p. 380-388.
- [32] Altintas, C., I. Erucar, and S. Keskin, *High-Throughput Computational Screening Of The Metal Organic Framework Database For CH<sub>4</sub>/H<sub>2</sub> Separations*. *ACS Appl. Mater. Interfaces*, 2018. **10**(4): p. 3668-3679.
- [33] Rowsell, J.L., et al., *Gas Adsorption Sites In A Large-Pore Metal-Organic Framework*. *Science*, 2005. **309**(5739): p. 1350-1354.
- [34] Vitillo, J.G., B. Smit, and L. Gagliardi, *Introduction: Carbon Capture And Separation*. *Chem. Rev.*, 2017. **117**(14): p. 9521-9523.
- [35] Lee, J., et al., *Metal–Organic Framework Materials As Catalysts*. *Chem. Soc. Rev.*, 2009. **38**(5): p. 1450-1459.
- [36] Vilela, S.M. and P. Horcajada, *MOFs As Supports Of Enzymes In Biocatalysis, in Metal-Organic Frameworks: Applications In Separations And Catalysis*. 2018, Wiley VCH. p. 447-476.
- [37] Erucar, I. and S. Keskin, *Computational Investigation Of Metal Organic Frameworks For Storage And Delivery Of Anticancer Drugs*. *J. Mater. Chem. B*, 2017. **5**(35): p. 7342-7351.
- [38] Gaudin, C., et al., *A Quantitative Structure Activity Relationship Approach To Probe The Influence Of The Functionalization On The Drug Encapsulation Of Porous Metal-Organic Frameworks*. *Microporous Mesoporous Mater.*, 2012. **157**: p. 124-130.

## BIBLIOGRAPHY

- [39] Miller, S.E., et al., *Metal-Organic Frameworks As Biosensors For Luminescence-Based Detection And Imaging*. Interface Focus, 2016. **6**(4): p. 20160027.
- [40] Liu, D., et al., *Metal–Organic Frameworks As Sensory Materials And Imaging Agents*. Inorg. Chem., 2013. **53**(4): p. 1916-1924.
- [41] Wang, H.-S., *Metal–Organic Frameworks For Biosensing And Bioimaging Applications*. Coord. Chem. Rev., 2017. **349**: p. 139-155.
- [42] Chui, S.S.-Y., et al., *A Chemically Functionalizable Nanoporous Material [Cu<sub>3</sub>(TMA)<sub>2</sub>(H<sub>2</sub>O)<sub>3</sub>]<sub>n</sub>*. Science, 1999. **283**(5405): p. 1148-1150.
- [43] Feng, X., X. Ding, and D. Jiang, *Covalent Organic Frameworks*. Chem. Soc. Rev., 2012. **41**(18): p. 6010-6022.
- [44] Cote, A.P., et al., *Porous, Crystalline, Covalent Organic Frameworks*. Science, 2005. **310**(5751): p. 1166-1170.
- [45] El-Kaderi, H.M., et al., *Designed Synthesis Of 3D Covalent Organic Frameworks*. Science, 2007. **316**(5822): p. 268-272.
- [46] Tong, M., et al., *Computation-ready, Experimental Covalent Organic Framework For Methane Delivery: Screening And Material Design*. J. Phys. Chem. C, 2018. **122**(24): p. 13009-13016.
- [47] Furukawa, H. and O.M. Yaghi, *Storage Of Hydrogen, Methane, And Carbon Dioxide In Highly Porous Covalent Organic Frameworks For Clean Energy Applications*. J. Am. Chem. Soc., 2009. **131**(25): p. 8875-8883.
- [48] Tong, M., et al., *Exploring The Structure-Property Relationships Of Covalent Organic Frameworks For Noble Gas Separations*. Chem. Eng. Sci., 2017. **168**: p. 456-464.
- [49] Ding, S.-Y., et al., *Construction Of Covalent Organic Framework For Catalysis: Pd/COF-LZU1 In Suzuki–Miyaura Coupling Reaction*. J. Am. Chem. Soc., 2011. **133**(49): p. 19816-19822.
- [50] Wan, S., et al., *Covalent Organic Frameworks With High Charge Carrier Mobility*. Chem. Mater., 2011. **23**(18): p. 4094-4097.
- [51] Bertrand, G.H., et al., *Thiophene-based Covalent Organic Frameworks*. Proc. Natl. Acad. Sci., 2013. **110**(13): p. 4923-4928.
- [52] Firmino, A.D., et al., *Synthesis Of MOFs At The Industrial Scale*, in *Metal-Organic Frameworks: Applications In Separations And Catalysis*. 2018, Wiley VCH. p. 57-80.
- [53] Siegel, D., B. Hardy, and H. Team, *Engineering An Adsorbent-Based Hydrogen Storage System: What Have We Learned*. 2015.
- [54] García-Holley, P., et al., *Benchmark Study Of Hydrogen Storage In Metal–Organic Frameworks Under Temperature And Pressure Swing Conditions*. ACS Energy Lett., 2018. **3**(3): p. 748-754.
- [55] Rosi, N.L., et al., *Hydrogen Storage In Microporous Metal-Organic Frameworks*. Science, 2003. **300**(5622): p. 1127-1129.
- [56] Zhou, W., et al., *Hydrogen And Methane Adsorption In Metal–Organic Frameworks: A High-Pressure Volumetric Study*. J. Phys. Chem. C, 2007. **111**(44): p. 16131-16137.
- [57] Furukawa, H., M.A. Miller, and O.M. Yaghi, *Independent Verification Of The Saturation Hydrogen Uptake In MOF-177 And Establishment Of A Benchmark For Hydrogen Adsorption In Metal–Organic Frameworks*. J. Mater. Chem., 2007. **17**(30): p. 3197-3204.
- [58] Gómez-Gualdrón, D.A., et al., *Understanding Volumetric And Gravimetric Hydrogen Adsorption Trade-Off In Metal–Organic Frameworks*. ACS Appl.

## BIBLIOGRAPHY

- Mater. Interfaces, 2017. **9**(39): p. 33419-33428.
- [59] Bobbitt, N.S., J. Chen, and R.Q. Snurr, *High-Throughput Screening Of Metal–Organic Frameworks For Hydrogen Storage At Cryogenic Temperature*. J. Phys. Chem. C, 2016. **120**(48): p. 27328-27341.
- [60] Bucior, B.J., et al., *Energy-Based Descriptors To Rapidly Predict Hydrogen Storage In Metal–Organic Frameworks*. Mol. Syst. Des. Eng., 2019. **4**: p. 162-174.
- [61] Han, S.S., et al., *Covalent Organic Frameworks As Exceptional Hydrogen Storage Materials*. J. Am. Chem. Soc., 2008. **130**(35): p. 11580-11581.
- [62] Burchell, T. and M. Rogers, *Low Pressure Storage Of Natural Gas For Vehicular Applications*. SAE Trans., 2000. **109**(4): p. 2242-2246.
- [63] Noro, S.i., et al., *A New, Methane Adsorbent, Porous Coordination Polymer  $[\{CuSiF_6(4,4'$ -bipyridine) $\}_n]$* . Angew. Chem., Int. Ed., 2000. **39**(12): p. 2081-2084.
- [64] Wilmer, C.E., et al., *Large-Scale Screening Of Hypothetical Metal–Organic Frameworks*. Nat. Chem., 2012. **4**(2): p. 83-89.
- [65] Gómez-Gualdrón, D.A., et al., *Exploring The Limits Of Methane Storage And Delivery In Nanoporous Materials*. J. Phys. Chem. C, 2014. **118**(13): p. 6941-6951.
- [66] Bui, M., et al., *Carbon Capture And Storage (CCS): The Way Forward*. Energy Environ. Sci., 2018. **11**(5): p. 1062-1176.
- [67] Dietzel, P.D., V. Besikiotis, and R. Blom, *Application Of Metal–Organic Frameworks With Coordinatively Unsaturated Metal Sites In Storage And Separation Of Methane And Carbon Dioxide*. J. Mater. Chem., 2009. **19**(39): p. 7362-7370.
- [68] Millward, A.R. and O.M. Yaghi, *Metal–Organic Frameworks With Exceptionally High Capacity For Storage Of Carbon Dioxide At Room Temperature*. J. Am. Chem. Soc., 2005. **127**(51): p. 17998-17999.
- [69] Bae, Y.S. and R.Q. Snurr, *Development And Evaluation Of Porous Materials For Carbon Dioxide Separation And Capture*. Angew. Chem., Int. Ed., 2011. **50**(49): p. 11586-11596.
- [70] Gao, S., et al., *Biomimetic O<sub>2</sub>-Evolving Metal-Organic Framework Nanoplatfom For Highly Efficient Photodynamic Therapy Against Hypoxic Tumor*. Biomaterials, 2018. **178**: p. 83-94.
- [71] Wang, Y., et al., *High Pressure Excess Isotherms For Adsorption Of Oxygen And Nitrogen In Zeolites*. Langmuir, 2011. **27**(17): p. 10648-10656.
- [72] Alezi, D., et al., *MOF Crystal Chemistry Paving The Way To Gas Storage Needs: Aluminum-Based soc-MOF For CH<sub>4</sub>, O<sub>2</sub>, And CO<sub>2</sub> Storage*. J. Am. Chem. Soc., 2015. **137**(41): p. 13308-13318.
- [73] Piscopo, C.G., et al., *Positive Effect Of The Fluorine Moiety On The Oxygen Storage Capacity Of UiO-66 Metal–Organic Frameworks*. New J. Chem., 2016. **40**(10): p. 8220-8224.
- [74] Anderson, J.S., et al., *A Five-Coordinate Heme Dioxygen Adduct Isolated within a Metal–Organic Framework*. J. Am. Chem. Soc., 2014. **136**(47): p. 16489-16492.
- [75] Gallagher, A.T., et al., *Dioxygen Binding At A Four-Coordinate Cobaltous Porphyrin Site In A Metal–Organic Framework: Structural, EPR, And O<sub>2</sub> Adsorption Analysis*. Inorg. Chem. Front., 2016. **3**(4): p. 536-540.
- [76] DeCoste, J.B., et al., *Metal–Organic Frameworks For Oxygen Storage*. Angew. Chem., 2014. **126**(51): p. 14316-14319.

## BIBLIOGRAPHY

- [77] Moghadam, P.Z., et al., *Computer-Aided Discovery Of A Metal–Organic Framework With Superior Oxygen Uptake*. Nat. Commun., 2018. **9**(1): p. 1378.
- [78] McIntyre, S.M., et al., *Monte Carlo Simulations To Examine The Role Of Pore Structure On Ambient Air Separation In Metal–Organic Frameworks*. Ind. Eng. Chem. Res., 2018. **57**(28): p. 9240-9253.
- [79] Bobbitt, N.S., et al., *Metal–Organic Frameworks For The Removal Of Toxic Industrial Chemicals And Chemical Warfare Agents*. Chem. Soc. Rev., 2017. **46**(11): p. 3357-3385.
- [80] Glover, T.G., et al., *MOF-74 Building Unit Has A Direct Impact On Toxic Gas Adsorption*. Chem. Eng. Sci., 2011. **66**(2): p. 163-170.
- [81] Katz, M.J., et al., *High Volumetric Uptake Of Ammonia Using Cu-MOF-74/Cu-CPO-27*. Dalton Trans., 2016. **45**(10): p. 4150-4153.
- [82] Hamon, L., et al., *Molecular Insight Into The Adsorption Of H<sub>2</sub>S In The Flexible MIL-53(Cr) And Rigid MIL-47(V) MOFs: Infrared Spectroscopy Combined To Molecular Simulations*. J. Phys. Chem. C, 2011. **115**(5): p. 2047-2056.
- [83] Sánchez-González, E., et al., *Highly Reversible Sorption Of H<sub>2</sub>S and CO<sub>2</sub> By An Environmentally Friendly Mg-based MOF*. J. Mater. Chem. A, 2018. **6**(35): p. 16900-16909.
- [84] DeCoste, J.B. and G.W. Peterson, *Metal–Organic Frameworks For Air Purification Of Toxic Chemicals*. Chem. Rev., 2014. **114**(11): p. 5695-5727.
- [85] Sherry, D., et al., *Current Sources Of Carbon Tetrachloride (CCl<sub>4</sub>) In Our Atmosphere*. Environ. Res. Lett., 2018. **13**(2): p. 024004.
- [86] Anand, K.V., et al., *Protective Effect Of Chrysin On Carbon Tetrachloride (CCl<sub>4</sub>)—Induced Tissue Injury In Male Wistar Rats*. Toxicol. Ind. Health, 2011. **27**(10): p. 923-933.
- [87] Yamamoto, T., et al., *Catalysis-Assisted Plasma Technology For Carbon Tetrachloride Destruction*. IEEE Trans. Ind. Appl., 1996. **32**(1): p. 100-105.
- [88] Urashima, K. and J.-S. Chang, *Removal Of Volatile Organic Compounds From Air Streams And Industrial Flue Gases By Non-Thermal Plasma Technology*. IEEE Trans. Dielectr. Electr. Insul., 2000. **7**(5): p. 602-614.
- [89] Cho, Y., et al., *Visible Light-Induced Degradation Of Carbon Tetrachloride On Dye-Sensitized TiO<sub>2</sub>*. Environ. Sci. Technol., 2001. **35**(5): p. 966-970.
- [90] Ozturk, B. and D. Yilmaz, *Absorptive Removal Of Volatile Organic Compounds From Flue Gas Streams*. Process Saf. Environ. Prot., 2006. **84**(5): p. 391-398.
- [91] Lee, B.D., W.A. Apel, and A.R. Miller, *Removal Of Low Concentrations Of Carbon Tetrachloride In Compost-Based Biofilters Operated Under Methanogenic Conditions*. J. Air Waste Manage. Assoc., 1999. **49**(9): p. 1068-1074.
- [92] Khan, F.I. and A.K. Ghoshal, *Removal Of Volatile Organic Compounds From Polluted Air*. J. Loss Prev. Process Ind., 2000. **13**(6): p. 527-545.
- [93] Do, D. and H. Do, *Adsorption Of Carbon Tetrachloride On Graphitized Thermal Carbon Black And In Slit Graphitic Pores: Five-Site Versus One-Site Potential Models*. J. Phys. Chem. B, 2006. **110**(19): p. 9520-9528.
- [94] Moghadam, P.Z., D. Fairen-Jimenez, and R.Q. Snurr, *Efficient Identification Of Hydrophobic MOFs: Application In The Capture Of Toxic Industrial Chemicals*. J. Mater. Chem. A, 2016. **4**(2): p. 529-536.
- [95] Calero, S., et al., *On The Performance Of Cu-BTC Metal Organic Framework For Carbon Tetrachloride Gas Removal*. Chem. Commun., 2011. **47**(1): p. 508-510.

## BIBLIOGRAPHY

- [96] Martin-Calvo, A., et al., *Effect Of Air Humidity On The Removal Of Carbon Tetrachloride From Air Using Cu-BTC Metal-Organic Framework*. Phys. Chem. Chem. Phys., 2011. **13**(23): p. 11165-74.
- [97] Zheng, Y., et al., *Ultrahigh Adsorption Capacities Of Carbon Tetrachloride On MIL-101 And MIL-101/Graphene Oxide Composites*. Microporous Mesoporous Mater., 2018. **263**: p. 71-76.
- [98] Jafari, S., et al., *Adsorptive Removal Of Toluene And Carbon Tetrachloride From Gas Phase Using Zeolitic Imidazolate Framework-8: Effects Of Synthesis Method, Particle Size, And Pretreatment Of The Adsorbent*. Microporous Mesoporous Mater., 2018. **268**: p. 58-68.
- [99] Barea, E., C.R. Maldonado, and J.A. Navarro, *MOFs for the Capture and Degradation of Chemical Warfare Agents*, in *Metal-Organic Frameworks: Applications in Separations and Catalysis*. 2018, Wiley-VCH: Weinheim, Germany. p. 199-221.
- [100] Khan, N.A., Z. Hasan, and S.H. Jhung, *Adsorptive Removal Of Hazardous Materials Using Metal-Organic Frameworks (MOFs): A Review*. J. Hazard. Mater., 2013. **244**: p. 444-456.
- [101] Kulprathipanja, S., *Zeolites In Industrial Separation And Catalysis*. 2010, Weinheim, Germany: John Wiley & Sons.
- [102] Barea, E., F. Turra, and J.A.R. Navarro, *Separation And Purification of Gases by MOFs*, in *Metal-Organic Frameworks: Applications From Catalysis To Gas Storage*. 2011, John Wiley & Sons.
- [103] Li, J.-R., J. Sculley, and H.-C. Zhou, *Metal-Organic Frameworks For Separations*. Chem. Rev., 2011. **112**(2): p. 869-932.
- [104] García, E.J., et al., *Role Of Structure And Chemistry In Controlling Separations Of CO<sub>2</sub>/CH<sub>4</sub> And CO<sub>2</sub>/CH<sub>4</sub>/CO Mixtures Over Honeycomb MOFs With Coordinatively Unsaturated Metal Sites*. J. Phys. Chem. C, 2012. **116**(50): p. 26636-26648.
- [105] Xian, S., et al., *Highly Enhanced And Weakened Adsorption Properties Of Two MOFs By Water Vapor For Separation Of CO<sub>2</sub>/CH<sub>4</sub> And CO<sub>2</sub>/N<sub>2</sub> Binary Mixtures*. Chem. Eng. J., 2015. **270**: p. 385-392.
- [106] Altintas, C., et al., *Database For CO<sub>2</sub> Separation Performances Of Mofs Based On Computational Materials Screening*. ACS Appl. Mater. Interfaces, 2018. **10**(20): p. 17257-17268.
- [107] Li, J.-R., et al., *Carbon Dioxide Capture-Related Gas Adsorption And Separation In Metal-Organic Frameworks*. Coord. Chem. Rev., 2011. **255**(15-16): p. 1791-1823.
- [108] Erucar, I. and S. Keskin, *High-Throughput Molecular Simulations Of Metal Organic Frameworks for CO<sub>2</sub> Separation: Opportunities And Challenges*. Front. Mater., 2018. **5**: p. 1-6.
- [109] Cengel, Y.A. and M.A. Boles, *Thermodynamics: An Engineering Approach*. 5th ed. 2006, New York: McGraw-Hill.
- [110] Krishna, R., *Methodologies For Evaluation Of Metal-Organic Frameworks In Separation Applications*. RSC Adv., 2015. **5**(64): p. 52269-52295.
- [111] Delavar, M. and N. Nabian, *An Investigation On The Oxygen And Nitrogen Separation From Air Using Carbonaceous Adsorbents*. J. Eng. Sci. Technol., 2015. **10**(11): p. 1394-1403.
- [112] Wang, C.-Y., et al., *Oxygen-Selective Adsorption In RPM3-Zn Metal Organic Framework*. Chem. Eng. Sci., 2017. **165**: p. 122-130.
- [113] Wang, Y., et al., *Computational Study Of Oxygen Adsorption In Metal-*



## BIBLIOGRAPHY

- Organic Frameworks With Exposed Cation Sites: Effect Of Framework Metal Ions.* RSC Adv., 2015. **5**(42): p. 33432-33437.
- [114] Parkes, M.V., et al., *Ab Initio Molecular Dynamics Determination Of Competitive O<sub>2</sub> vs. N<sub>2</sub> Adsorption At Open Metal Sites Of M<sub>2</sub>(dobdc).* Phys. Chem. Chem. Phys., 2016. **18**(16): p. 11528-11538.
- [115] Demir, H., et al., *Metal-Organic Frameworks With Metal Catecholates For O<sub>2</sub>/N<sub>2</sub> Separation.* J. Phys. Chem. C, 2019. **123**(20): p. 12935-12946.
- [116] Banerjee, D., et al., *Xenon Gas Separation And Storage Using Metal-Organic Frameworks.* Chem, 2018. **4**(3): p. 466-494.
- [117] Mueller, U., et al., *Metal-Organic Frameworks Prospective Industrial Applications.* J. Mater. Chem., 2006. **16**(7): p. 626-636.
- [118] Chen, X., et al., *Direct Observation Of Xe And Kr Adsorption In A Xe-selective Microporous Metal Organic Framework.* J. Am. Chem. Soc., 2015. **137**(22): p. 7007-7010.
- [119] Banerjee, D., et al., *Metal-Organic Framework With Optimally Selective Xenon Adsorption And Separation.* Nat. Commun., 2016. **7**: p. 11831.
- [120] Simon, C.M., et al., *What Are The Best Materials To Separate A Xenon/Krypton Mixture?* Chem. Mater., 2015. **27**(12): p. 4459-4475.
- [121] Zhao, Z., et al., *Competitive Adsorption And Selectivity Of Benzene And Water Vapor On The Microporous Metal Organic Frameworks (HKUST-1).* Chem. Eng. J., 2015. **259**: p. 79-89.
- [122] Matito-Martos, I., et al., *Discovery Of An Optimal Porous Crystalline Material For The Capture Of Chemical Warfare Agents.* Chem. Mater., 2018. **30**(14): p. 4571-4579.
- [123] Bernardo, P., E. Drioli, and G. Golemme, *Membrane Gas Separation: A Review/State Of The Art.* Ind. Eng. Chem. Res., 2009. **48**(10): p. 4638-4663.
- [124] Pandey, P. and R. Chauhan, *Membranes For Gas Separation.* Prog. Polym. Sci., 2001. **26**(6): p. 853-893.
- [125] Kärger, J., D.M. Ruthven, and D.N. Theodorou, *Diffusion In Nanoporous Materials.* Vol. 1. 2012, Weinheim, Germany: John Wiley & Sons.
- [126] Robeson, L.M., *The Upper Bound Revisited.* J. Membr. Sci., 2008. **320**(1-2): p. 390-400.
- [127] Murali, R.S., T. Sankarshana, and S. Sridhar, *Air Separation By Polymer-Based Membrane Technology.* Sep. Purif. Rev., 2013. **42**(2): p. 130-186.
- [128] Jeazet, H.B.T., C. Staudt, and C. Janiak, *A Method For Increasing Permeability In O<sub>2</sub>/N<sub>2</sub> Separation With Mixed-Matrix Membranes Made Of Water-Stable MIL-101 And Polysulfone.* Chem. Comm., 2012. **48**(15): p. 2140-2142.
- [129] Rodrigues, M.A., et al., *Nanostructured Membranes Containing UiO-66(Zr) And MIL-101(Cr) For O<sub>2</sub>/N<sub>2</sub> And CO<sub>2</sub>/N<sub>2</sub> Separation.* Sep. Purif. Technol., 2018. **192**: p. 491-500.
- [130] Singh, A. and W. Koros, *Significance Of Entropic Selectivity For Advanced Gas Separation Membranes.* Ind. Eng. Chem. Res., 1996. **35**(4): p. 1231-1234.
- [131] Koresh, J.E. and A. Soffer, *The Carbon Molecular Sieve Membranes. General Properties And The Permeability Of CH<sub>4</sub>/H<sub>2</sub> Mixture.* Sep. Sci. Technol., 1987. **22**(2-3): p. 973-982.
- [132] Koros, W.J. and R. Mahajan, *Pushing The Limits On Possibilities For Large Scale Gas Separation: Which Strategies?* J. Membr. Sci., 2000. **175**(2): p. 181-196.
- [133] Vu, D.Q., W.J. Koros, and S.J. Miller, *Mixed Matrix Membranes Using*

## BIBLIOGRAPHY

- Carbon Molecular Sieves: I. Preparation And Experimental Results*. J. Membr. Sci., 2003. **211**(2): p. 311-334.
- [134] Gascon, J., et al., *Practical Approach To Zeolitic Membranes And Coatings: State Of The Art, Opportunities, Barriers, And Future Perspectives*. Chem. Mater., 2012. **24**(15): p. 2829-2844.
- [135] Zornoza, B., et al., *Combination Of MOFs And Zeolites For Mixed-Matrix Membranes*. ChemPhysChem, 2011. **12**(15): p. 2781-2785.
- [136] Bushell, A.F., et al., *Gas Permeation Parameters Of Mixed Matrix Membranes Based On The Polymer Of Intrinsic Microporosity PIM-1 And The Zeolitic Imidazolate Framework ZIF-8*. J. Membr. Sci., 2013. **427**: p. 48-62.
- [137] Duan, C., et al., *Post-Treatment Effect On Gas Separation Property Of Mixed Matrix Membranes Containing Metal Organic Frameworks*. J. Membr. Sci., 2014. **466**: p. 92-102.
- [138] Huang, A., et al., *A Highly Permeable And Selective Zeolitic Imidazolate Framework ZIF-95 Membrane For H<sub>2</sub>/CO<sub>2</sub> Separation*. Chem. Commun., 2012. **48**(89): p. 10981-10983.
- [139] Bux, H., et al., *Zeolitic Imidazolate Framework Membrane With Molecular Sieving Properties By Microwave-Assisted Solvothermal Synthesis*. J. Am. Chem. Soc., 2009. **131**(44): p. 16000-16001.
- [140] Huang, A., et al., *Molecular-Sieve Membrane With Hydrogen Permselectivity: ZIF-22 In LTA Topology Prepared With 3-Aminopropyltriethoxysilane As Covalent Linker*. Angew. Chem., Int. Ed., 2010. **49**(29): p. 4958-4961.
- [141] Zhao, Z.X., et al., *Gas Separation Properties Of Metal Organic Framework (MOF-5) Membranes*. Ind. Eng. Chem. Res., 2013. **52**(3): p. 1102-1108.
- [142] Altintas, C., et al., *Computer Simulations Of 4240 MOF Membranes For H<sub>2</sub>/CH<sub>4</sub> Separations: Insights Into Structure-Performance Relations*. J. Mater. Chem. A, 2018. **6**(14): p. 5836-5847.
- [143] Dybtsev, D.N., et al., *Microporous Manganese Formate: A Simple Metal-Organic Porous Material With High Framework Stability And Highly Selective Gas Sorption Properties*. J. Am. Chem. Soc., 2004. **126**(1): p. 32-33.
- [144] Adatoz, E., A.K. Avci, and S. Keskin, *Opportunities And Challenges Of MOF-Based Membranes In Gas Separations*. Sep. Purif. Technol., 2015. **152**: p. 207-237.
- [145] Erucar, I. and S. Keskin, *Molecular Modeling Of MOF Membranes For Gas Separations*, in *Membranes For Gas Separations*. 2017. p. 97.
- [146] Erucar, I. and S. Keskin, *Computational Methods For MOF/Polymer Membranes*. Chem. Rec., 2016. **16**(2): p. 703-718.
- [147] Simon-Yarza, T., et al., *The Situation Of Metal-Organic Frameworks In Biomedicine*, in *Comprehensive Biomaterials II*. 2017, Elsevier. p. 720-749.
- [148] Horcajada, P., et al., *Metal-Organic Frameworks In Biomedicine*. Chem. Rev., 2011. **112**(2): p. 1232-1268.
- [149] Rojas, S., T. Devic, and P. Horcajada, *Metal Organic Frameworks Based On Bioactive Components*. J. Mater. Chem. B, 2017. **5**(14): p. 2560-2573.
- [150] An, J., S.J. Geib, and N.L. Rosi, *Cation-Triggered Drug Release From A Porous Zinc-Adeninate Metal-Organic Framework*. J. Am. Chem. Soc., 2009. **131**(24): p. 8376-8377.
- [151] Taylor-Pashow, K.M., et al., *Postsynthetic Modifications Of Iron-Carboxylate Nanoscale Metal-Organic Frameworks For Imaging And Drug Delivery*. J. Am. Chem. Soc., 2009. **131**(40): p. 14261-14263.
- [152] Li, T., et al., *Systematic Modulation And Enhancement Of CO<sub>2</sub>:N<sub>2</sub> Selectivity*

## BIBLIOGRAPHY

- And Water Stability In An Isoreticular Series Of Bio-MOF-11 Analogues.* Chem. Sci., 2013. **4**(4): p. 1746-1755.
- [153] An, J., et al., *Metal-Adeninate Vertices For The Construction Of An Exceptionally Porous Metal-Organic Framework.* Nat. Commun., 2012. **3**: p. 604.
- [154] Li, T., et al., *Stepwise Ligand Exchange For The Preparation Of A Family Of Mesoporous MOFs.* J. Am. Chem. Soc., 2013. **135**(32): p. 11688-11691.
- [155] Smaldone, R.A., et al., *Metal–Organic Frameworks From Edible Natural Products.* Angew. Chem. Int. Ed., 2010. **49**(46): p. 8630-8634.
- [156] Miller, S.R., et al., *Biodegradable Therapeutic MOFs For The Delivery Of Bioactive Molecules.* Chem. Commun., 2010. **46**(25): p. 4526-4528.
- [157] Miller, S.R., et al., *A Rare Example Of A Porous Ca-MOF For The Controlled Release Of Biologically Active NO.* Chem. Commun., 2013. **49**(71): p. 7773-7775.
- [158] Tamames-Tabar, C., et al., *A Zn Azelate MOF: Combining Antibacterial Effect.* CrystEngComm, 2015. **17**(2): p. 456-462.
- [159] Horcajada, P., et al., *Metal-Organic Frameworks As Efficient Materials For Drug Delivery.* Angew. Chem., 2006. **118**(36): p. 6120-6124.
- [160] Giménez-Marqués, M., et al., *Nanostructured Metal–Organic Frameworks And Their Bio-related Applications.* Coord. Chem. Rev., 2016. **307**: p. 342-360.
- [161] Keskin, S. and S. Kızılel, *Biomedical Applications Of Metal Organic Frameworks.* Ind. Eng. Chem. Res., 2011. **50**(4): p. 1799-1812.
- [162] Babarao, R. and J. Jiang, *Unraveling The Energetics And Dynamics Of Ibuprofen In Mesoporous Metal–Organic Frameworks.* J. Phys. Chem. C, 2009. **113**(42): p. 18287-18291.
- [163] Erucar, I. and S. Keskin, *Efficient Storage Of Drug And Cosmetic Molecules In Biocompatible Metal Organic Frameworks: A Molecular Simulation Study.* Ind. Eng. Chem. Res., 2016. **55**(7): p. 1929-1939.
- [164] Kotzabasaki, M. and G.E. Froudakis, *Review Of Computer Simulations On Anti-Cancer Drug Delivery In MOFs.* Inorg. Chem. Front., 2018. **5**(6): p. 1255-1272.
- [165] Katiyar, R.S. and P.K. Jha, *Molecular Simulations In Drug Delivery: Opportunities And Challenges.* Wiley Interdiscip. Rev.: Comput. Mol. Sci., 2018. **8**(4): p. 1358.
- [166] Simagina, A.A., et al., *Towards Rational Design Of Metal-Organic Framework-Based Drug Delivery Systems.* Russ. Chem. Rev., 2018. **87**(9): p. 831-858.
- [167] Miller, M. and I. Megson, *Recent Developments In Nitric Oxide Donor Drugs.* Br. J. Pharmacol., 2007. **151**(3): p. 305-321.
- [168] Hinks, N.J., et al., *Metal Organic Frameworks As NO Delivery Materials For Biological Applications.* Microporous Mesoporous Mater., 2010. **129**(3): p. 330-334.
- [169] Otterbein, L.E., *The Evolution Of Carbon Monoxide Into Medicine.* Respir. Care, 2009. **54**(7): p. 925-932.
- [170] Chavan, S., et al., *CO Adsorption On CPO-27-Ni Coordination Polymer: Spectroscopic Features And Interaction Energy.* J. Phys. Chem. C, 2009. **113**(8): p. 3292-3299.
- [171] Wang, R., *Hydrogen Sulfide: The Third Gasotransmitter In Biology And Medicine.* Antioxid. Redox Signaling, 2010. **12**(9): p. 1061-1064.
- [172] Allan, P.K., et al., *Metal–Organic Frameworks For The Storage And Delivery Of Biologically Active Hydrogen Sulfide.* Dalton Trans., 2012. **41**(14): p. 4060-

## BIBLIOGRAPHY

- 4066.
- [173] Park, K.S., et al., *Exceptional Chemical And Thermal Stability Of Zeolitic Imidazolate Frameworks*. Proc. Natl. Acad. Sci., 2006. **103**(27): p. 10186-10191.
- [174] Cai, H., Y.-L. Huang, and D. Li, *Biological Metal–Organic Frameworks: Structures, Host–Guest Chemistry And Bio-Applications*. Coord. Chem. Rev., 2019. **378**: p. 207-221.
- [175] Horcajada, P., et al., *Flexible Porous Metal–Organic Frameworks For A Controlled Drug Delivery*. J. Am. Chem. Soc., 2008. **130**(21): p. 6774-6780.
- [176] Horcajada, P., et al., *Porous Metal–Organic Framework Nanoscale Carriers As A Potential Platform For Drug Delivery And Imaging*. Nat. Mater., 2010. **9**(2): p. 172-178.
- [177] Hu, Q., et al., *A Low Cytotoxic Cationic Metal–Organic Framework Carrier For Controllable Drug Release*. J. Med. Chem., 2014. **57**(13): p. 5679-5685.
- [178] Willems, T.F., et al., *Algorithms And Tools For High-Throughput Geometry-Based Analysis Of Crystalline Porous Materials*. Microporous Mesoporous Mater., 2012. **149**(1): p. 134-141.
- [179] Blatov, V.A., *Voronoi–Dirichlet Polyhedra In Crystal Chemistry: Theory And Applications*. Crystallogr. Rev., 2004. **10**(4): p. 249-318.
- [180] Alinchenko, M.G., et al., *Morphology Of Voids In Molecular Systems. A Voronoi– Delaunay Analysis Of A Simulated DMPC Membrane*. J. Phys. Chem. B, 2004. **108**(49): p. 19056-19067.
- [181] Nicholson, D. and N.G. Parsonage, *Computer Simulation And The Statistical Mechanics Of Adsorption*. 1982, United States, New York: Academic Press.
- [182] Rappe, A.K., et al., *UFF, A Full Periodic Table Force Field For Molecular Mechanics And Molecular Dynamics Simulations*. J. Am. Chem. Soc., 1992. **114**(25): p. 10024-10035.
- [183] Mayo, S.L., B.D. Olafson, and W.A. Goddard, *Dreiding: A Generic Force Field For Molecular Simulations*. J. Phys. Chem., 1990. **94**(26): p. 8897-8909.
- [184] Lorentz, H., *Ueber Die Anwendung Des Satzes Vom Virial In Der Kinetischen Theorie Der Gase*. Ann. Phys. (Berlin, Ger.), 1881. **248**(1): p. 127-136.
- [185] Berthelot, D., *Sur Le Melange Des Gaz*. C. R. Hebd. Seanc. Acad. Sci. (Paris), 1898. **126**: p. 1703-1855.
- [186] Rappe, A.K. and W.A. Goddard III, *Charge Equilibration For Molecular Dynamics Simulations*. J. Phys. Chem., 1991. **95**(8): p. 3358-3363.
- [187] Ewald, P.P., *Die Berechnung Optischer Und Elektrostatischer Gitterpotentiale*. Ann. Phys., 1921. **369**(3): p. 253-287.
- [188] Frenkel, D. and B. Smit, *Understanding Molecular Simulation: From Algorithms To Applications*. Vol. 1. 2002: Academic press: London.
- [189] Dubbeldam, D., et al., *RASPA: Molecular Simulation Software For Adsorption And Diffusion In Flexible Nanoporous Materials*. Mol. Simul., 2016. **42**(2): p. 81-101.
- [190] Peng, D.-Y. and D.B. Robinson, *A New Two-Constant Equation Of State*. Ind. Eng. Chem. Fundam., 1976. **15**(1): p. 59-64.
- [191] Clark, L.A., A. Gupta, and R.Q. Snurr, *Siting And Segregation Effects Of Simple Molecules In Zeolites MFI, MOR, And BOG*. J. Phys. Chem. B, 1998. **102**(35): p. 6720-6731.
- [192] Mellot, C. and J. Lignieres, *Monte Carlo Simulations Of N<sub>2</sub> And O<sub>2</sub> Adsorption In Silicalite And CaLSX Zeolites*. Mol. Simul., 1997. **18**(6): p. 349-365.
- [193] Makrodimitris, K., G.K. Papadopoulos, and D.N. Theodorou, *Prediction Of Permeation Properties Of CO<sub>2</sub> And N<sub>2</sub> Through Silicalite Via Molecular*

## BIBLIOGRAPHY

- Simulations*. J. Phys. Chem. B, 2001. **105**(4): p. 777-788.
- [194] Buch, V., *Path Integral Simulations Of Mixed Para-D<sub>2</sub> And Ortho-D<sub>2</sub> Clusters: The Orientational Effects*. J. Chem. Phys., 1994. **100**(10): p. 7610-7629.
- [195] Darkrim, F. and D. Levesque, *Monte Carlo Simulations Of Hydrogen Adsorption In Single-Walled Carbon Nanotubes*. J. Chem. Phys., 1998. **109**(12): p. 4981-4984.
- [196] Maxwell, J.C., *II. Illustrations Of The Dynamical Theory Of Gases*. Philos. Mag., 1860. **20**(130): p. 21-37.
- [197] Boltzmann, L., *Lectures On Gas Theory*. 1964, Berkeley: Brush for University of California Press, .
- [198] Nosé, S., *A Unified Formulation Of The Constant Temperature Molecular Dynamics Methods*. J. Chem. Phys., 1984. **81**(1): p. 511-519.
- [199] Hoover, W.G., *Canonical Dynamics: Equilibrium Phase-Space Distributions*. Phys. Rev. A, 1985. **31**(3): p. 1695-1697.
- [200] Einstein, A., *On The Theory Of The Brownian Movement*. Ann. Phys. (Berlin, Ger.), 1906. **4**: p. 371-381.
- [201] Sholl, D.S., *Understanding Macroscopic Diffusion Of Adsorbed Molecules In Crystalline Nanoporous Materials Via Atomistic Simulations*. Acc. Chem. Res., 2006. **39**(6): p. 403-411.
- [202] Basdogan, Y., K.B. Sezginel, and S. Keskin, *Identifying Highly Selective Metal Organic Frameworks For CH<sub>4</sub>/H<sub>2</sub> Separations Using Computational Tools*. Ind. Eng. Chem. Res., 2015. **54**(34): p. 8479-8491.
- [203] Krishna, R., *Methodologies For Screening And Selection Of Crystalline Microporous Materials In Mixture Separations*. Sep. Purif. Technol., 2017. **194**: p. 281-300.
- [204] Krishna, R., *Screening Metal–Organic Frameworks For Mixture Separations In Fixed-Bed Adsorbers Using A Combined Selectivity/Capacity Metric*. RSC Adv., 2017. **7**(57): p. 35724-35737.
- [205] Kesting, R.E. and A.K. Fritzsche, *Polymeric Gas Separation Membranes*. 1993, New York: Wiley&Sons.
- [206] Krishna, R. and J.M. van Baten, *In Silica Screening Of Zeolite Membranes For CO<sub>2</sub> Capture*. J. Membr. Sci., 2010. **360**: p. 323-333.
- [207] Keskin, S. and D.S. Sholl, *Efficient Methods For Screening Of Metal Organic Framework Membranes For Gas Separations Using Atomically Detailed Models*. Langmuir, 2009. **25**(19): p. 11786-11795.
- [208] Matsuda, R., et al., *Temperature Responsive Channel Uniformity Impacts On Highly Guest-Selective Adsorption In A Porous Coordination Polymer*. Chem. Sci., 2010. **1**(3): p. 315-321.
- [209] Férey, G., et al., *A Chromium Terephthalate-Based Solid With Unusually Large Pore Volumes And Surface Area*. Science, 2005. **309**(5743): p. 2040-2042.
- [210] Vega, C., J. Abascal, and I. Nezbeda, *Vapor-Liquid Equilibria From The Triple Point Up To The Critical Point For The New Generation Of Tip4p-Like Models: Tip4p/Ew, Tip4p/2005, And Tip4p/Ice*. J. Chem. Phys., 2006. **125**(3): p. 034503.
- [211] Atci, E. and S. Keskin, *Understanding The Potential Of Zeolite Imidazolate Framework Membranes In Gas Separations Using Atomically Detailed Calculations*. J. Phys. Chem. C, 2012. **116**(29): p. 15525-15537.
- [212] Keskin, S., et al., *Progress, Opportunities, And Challenges For Applying Atomically Detailed Modeling To Molecular Adsorption And Transport In Metal–Organic Framework Materials*. Ind. Eng. Chem. Res., 2008. **48**(5): p.

## BIBLIOGRAPHY

- 2355-2371.
- [213] Hunt, J.R., et al., *Reticular Synthesis Of Covalent Organic Borosilicate Frameworks*. J. Am. Chem. Soc., 2008. **130**(36): p. 11872-11873.
- [214] Du, Y., et al., *Ionic Covalent Organic Frameworks With Spiroborate Linkage*. Angew. Chem., Int. Ed., 2016. **55**(5): p. 1737-1741.
- [215] Greenhow, C. and W.V. Smith, *Molecular Quadrupole Moments Of N<sub>2</sub> And O<sub>2</sub>*. J. Chem. Phys., 1951. **19**(10): p. 1298-1300.
- [216] Jackson, K.T., T.E. Reich, and H.M. El-Kaderi, *Targeted Synthesis Of A Porous Borazine-Linked Covalent Organic Framework*. Chem. Commun., 2012. **48**(70): p. 8823-8825.
- [217] Li, Z., et al., *A 2D Azine-linked Covalent Organic Framework For Gas Storage Applications*. Chem. Commun., 2014. **50**(89): p. 13825-13828.
- [218] Stegbauer, L., et al., *Tunable Water And CO<sub>2</sub> Sorption Properties In Isostructural Azine-Based Covalent Organic Frameworks Through Polarity Engineering*. Chem. Mater., 2015. **27**(23): p. 7874-7881.
- [219] Li, Z., et al., *An Azine-linked Covalent Organic Framework: Synthesis, Characterization And Efficient Gas Storage*. Chem. - Eur. J., 2015. **21**(34): p. 12079-12084.
- [220] Ge, R., et al., *Target Synthesis Of An Azo (N=N) Based Covalent Organic Framework With High CO<sub>2</sub>-over-N<sub>2</sub> Selectivity And Benign Gas Storage Capability*. J. Chem. Eng. Data, 2016. **61**(5): p. 1904-1909.
- [221] Neti, V.S.P.K., et al., *Synthesis Of A Phthalocyanine 2D Covalent Organic Framework*. CrystEngComm, 2013. **15**(36): p. 7157-7160.
- [222] Kaleeswaran, D., P. Vishnoi, and R. Murugavel, *[3+3] Imine And  $\beta$ -ketoenamine Tethered Fluorescent Covalent-Organic Frameworks For CO<sub>2</sub> Uptake And Nitroaromatic Sensing*. J. Mater. Chem. C, 2015. **3**(27): p. 7159-7171.
- [223] Kang, Z., et al., *Mixed Matrix Membranes (MMMs) Comprising Exfoliated 2D Covalent Organic Frameworks (COFs) For Efficient CO<sub>2</sub> Separation*. Chem. Mater., 2016. **28**(5): p. 1277-1285.
- [224] Bhunia, A., V. Vasylyeva, and C. Janiak, *From A Supramolecular Tetranitrile To A Porous Covalent Triazine-Based Framework With High Gas Uptake Capacities*. Chem. Commun., 2013. **49**(38): p. 3961-3963.
- [225] Kahveci, Z., et al., *Targeted Synthesis Of A Mesoporous Triptycene-Derived Covalent Organic Framework*. CrystEngComm, 2013. **15**(8): p. 1524-1527.
- [226] Assfour, B. and G. Seifert, *Adsorption Of Hydrogen In Covalent Organic Frameworks: Comparison Of Simulations And Experiments*. Microporous Mesoporous Mater., 2010. **133**(1-3): p. 59-65.
- [227] McKinlay, A.C., et al., *BioMOFs: Metal–Organic Frameworks For Biological And Medical Applications*. Angew. Chem., Int. Ed., 2010. **49**(36): p. 6260-6266.
- [228] Wilmer, C.E., et al., *Gram-Scale, High-Yield Synthesis Of A Robust Metal–Organic Framework For Storing Methane And Other Gases*. Energy Environ. Sci., 2013. **6**(4): p. 1158-1163.
- [229] Cavka, J.H., et al., *A New Zirconium Inorganic Building Brick Forming Metal Organic Frameworks With Exceptional Stability*. J. Am. Chem. Soc., 2008. **130**(42): p. 13850-13851.
- [230] Siberio-Pérez, D.Y., et al., *Raman Spectroscopic Investigation Of CH<sub>4</sub> And N<sub>2</sub> Adsorption In Metal–Organic Frameworks*. Chem. Mater., 2007. **19**(15): p. 3681-3685.

## BIBLIOGRAPHY

- [231] Karra, J.R. and K.S. Walton, *Molecular Simulations And Experimental Studies Of CO<sub>2</sub>, CO, And N<sub>2</sub> Adsorption In Metal–Organic Frameworks*. J. Phys. Chem. C, 2010. **114**(37): p. 15735-15740.
- [232] Lin, K.J., *SMTF-1: The First Functionalized Metalloporphyrin Molecular Sieves With Large Channels*. Angew. Chem., Int. Ed., 1999. **38**(18): p. 2730-2732.
- [233] Feng, D., et al., *Construction Of Ultrastable Porphyrin Zr Metal–Organic Frameworks Through Linker Elimination*. J. Am. Chem. Soc., 2013. **135**(45): p. 17105-17110.
- [234] Wang, K., et al., *A Series Of Highly Stable Mesoporous Metalloporphyrin Fe-MOFs*. J. Am. Chem. Soc., 2014. **136**(40): p. 13983-13986.
- [235] Deng, H., et al., *Large-Pore Apertures In A Series Of Metal-Organic Frameworks*. Science, 2012. **336**(6084): p. 1018-1023.
- [236] Wang, Y., et al., *Controllable Syntheses Of Porous Metal–Organic Frameworks: Encapsulation Of Ln<sup>III</sup> Cations For Tunable Luminescence And Small Drug Molecules For Efficient Delivery*. Chem. - Eur. J., 2013. **19**(43): p. 14591-14599.
- [237] Gao, W.-Y., L. Wojtas, and S. Ma, *A Porous Metal–Metalloporphyrin Framework Featuring High-Density Active Sites For Chemical Fixation Of CO<sub>2</sub> Under Ambient Conditions*. Chem. Commun., 2014. **50**(40): p. 5316-5318.
- [238] Williams, D.E., et al., *Energy Transfer On Demand: Photoswitch-Directed Behavior Of Metal–Porphyrin Frameworks*. J. Am. Chem. Soc., 2014. **136**(34): p. 11886-11889.
- [239] Cai, H., et al., *Spatial, Hysteretic, And Adaptive Host–Guest Chemistry In A Metal–Organic Framework With Open Watson–Crick Sites*. Angew. Chem., Int. Ed., 2015. **54**(36): p. 10454-10459.
- [240] Wang, Y., et al., *Four Novel Porous Frameworks Constructed By Formate Ligand*. Microporous Mesoporous Mater., 2006. **91**(1): p. 215-220.
- [241] He, W.-L., et al., *Suspending Ionic Single-Atom Catalysts In Porphyrinic Frameworks For Highly Efficient Aerobic Oxidation At Room Temperature*. J. Catal., 2018. **358**: p. 43-49.
- [242] Zou, C., et al., *Four Metalloporphyrinic Frameworks As Heterogeneous Catalysts For Selective Oxidation And Aldol Reaction*. Inorg. Chem., 2013. **52**(7): p. 3620-3626.
- [243] García-Terán, J.P., et al., *An Unusual 3D Coordination Polymer Based On Bridging Interactions Of The Nucleobase Adenine*. Inorg. Chem., 2004. **43**(15): p. 4549-4551.
- [244] Julien, P.A., C. Mottillo, and T. Friščić, *Metal–Organic Frameworks Meet Scalable And Sustainable Synthesis*. Green Chem., 2017. **19**(12): p. 2729-2747.

## VITA

Ezgi Gülçay was born in İstanbul, Turkey on October 7, 1992. In 2015, she graduated from Chemical Engineering Department of İstanbul Technical University. She successfully got her M.Sc. degree from Mechanical Engineering Department at Özyeğin University. Her research interests include molecular simulations of nanoporous materials, molecular dynamics, molecular thermodynamics, adsorption, and diffusion behavior of gas molecules inside adsorbents and membranes. She will continue her Ph.D. work at Institut de Chimie Moléculaire et des Matériaux at Université Montpellier.

### Publications

- 1) Altintas, C., Avci, G, Daglar, H., Gulcay, E. Erucar, I, and Keskin, S., Computer simulations of 4240 MOF membranes for H<sub>2</sub>/CH<sub>4</sub> separations: insights into structure-performance relations. *J. Mater. Chem. A*, 2018. 6(14), p:5836-5847.
- 2) Gulcay, E., and Erucar, I., Molecular simulations of COFs, IRMOFs and ZIFs for Adsorption-based separation of carbon tetrachloride from air. *J. Mol. Graphics Modell.*, 2019. 86, p:84-94.
- 3) Gulcay, E., and Erucar, I., Bio-compatible MOFs for storage and separation of O<sub>2</sub>: A molecular simulation study. *Ind. Eng. Chem. Res.*, 2019. 58(8), p:3225-3237.
- 4) Gulcay, E., and Erucar, I., Computational screening of covalent organic frameworks for hydrogen storage. In revision. *J. Turk. Chem. Soc., Sect. A*. 2019.
- 5) Gulcay, E., and Erucar, I., Metal organic frameworks (MOFs) for biomedical applications. In revision. *Two Dimensional Nanostructures for Biomedical Technology* (Chapter 6), Elsevier. 2019.